Tectonic evolution of the Bayankhongor Ophiolite, Central Mongolia: implications for the Palaeozoic crustal growth of Central Asia

By

A. Craig Buchan BSc (Edinburgh)

A thesis submitted for the degree of
Doctor of Philosophy
at the University of Leicester

Department of Geology
University of Leicester
June 2001

Tectonic Evolution of the Bayankhongor Ophiolite, Central Mongolia: implications for the Palaeozoic crustal growth of Central Asia

A. Craig Buchan

The mechanism of continental growth of Central Asia is currently debated between models invoking continuous subduction-accretion, or punctuated accretion due to closure of multiple ocean basins. Ophiolites in Central Asia may represent offscraped fragments in an accretionary complex or true collisional sutures. The Bayankhongor ophiolite, a NW-SE striking sublinear belt 300 km long and 20 km wide, is the largest ophiolite in Mongolia and possibly Central Asia. The Bayankhongor area is divided into four major lithotectonic units based on interpretation of structural and lithological data from three cross-strike transects: Baidrag complex, Burd Gol, Bayankhongor Ophiolite, and Dzag zones. The Archaean Baidrag complex comprises tonalitic granulites and metasediments. The Burd Gol zone is a metamorphosed sedimentary and igneous mélange. The Bayankhongor zone contains the dismembered ophiolite forming a serpentinite mélange. The Dzag zone consists of asymmetrically folded chlorite-mica schists resembling meta-turbidites. The structure is dominated by steeply dipping, NE directed thrusts and NE-vergent folds. The data suggest the Bayankhongor ophiolite marks the closure of an ocean separating two microcontinents: the Baidrag complex with the Burd Gol accretionary complex to the south, and a northern continent which forms the basement for the Hangai region. Subduction was towards the SW with NE-directed ophiolite obduction onto a passive margin represented by the Dzag zone. Geochemical and Nd isotope studies of the ophiolitic rocks suggest that they were derived from a heterogeneous mantle source composed of a depleted N-MORB and enriched E-MORB component. A model for the tectonic setting of the ophiolitic rocks is presented in which the N-MORB rocks represent melts produced at a mid-ocean ridge, whilst the E-MORB rocks represent off-axis flows or melts produced at transform ridge intersections. Basalts from the Delb Khairkhan mélange have island arc-like chemistry and provide evidence that the ophiolite may have been trapped within a supra-subduction setting prior to obduction. New $^{207}Pb/^{206}Pb$ zircon evaporation ages for granites and rhyolite dykes that intrude the ophiolite and its neighbouring lithotectonic units, suggest that the ophiolite was obducted at *c.* 540 Ma at the beginning of a collisional event that lasted until *c.* 450 Ma. The new data combined with that of previous studies indicate regional correlation of isotopic ages north-westward from Bayankhongor to southern Tuva. These data record oceanic crust formation at *c.* 570 Ma, followed by approximately 30 million years of subduction-accretion that culminated in obduction of ophiolites, collision related metamorphism, and magmatism in the period *c.* 540-450 Ma. Correlation of isotopic-age data for the ophiolites of western Mongolia and southern Tuva suggest that the ophiolites define a major collisional suture in the Central Asian Orogenic Belt which helps define the southern and western margins of the Hangai continental block.

Acknowledgements

This PhD project was mainly funded by an NERC PhD studentship no. GT04/97/145/ES. Collaboration between the University of Leicester and Max-Planck-Institut für Chemie was assisted by grants from the British Council-DAAD Academic Research Collaboration Programme (ARC grant 0964) and INTAS project 95 RUSSIA-0934.

I would like to thank my principal supervisor Dickson Cunningham because without the support of his seemingly endless enthusiasm and encouragement this project would never have been possible. I would also like to thank Brian Windley for his support and also for his money finding skills as without these the isotope section, and therefore, a large chunk of this thesis would never have happened. I would also like to thank Brian for introducing me to the notion of stocking up on miniature's of vodka on the plane on the way to Mongolia.....they can be a lifesaver when you just can't face those never ending bottles and of course save on the duty free costs. I would like to thank Tim Brewer for all of his help and advice on the geochemical side of the project and especially for putting up with my endless questions about things I should have learned years ago.

I would like to thank to all of the staff of the Institute of Geology and Mineral Resources (IGMR) in Ulaanbaatar for their help in organising the field seasons. Special thanks go to Badarch without whom the Leicester Mongolian research projects would never have got off the ground or have ran for this long, but also thank you for being such an instant and good friend throughout the project. Extra special thanks go to Tomurhuu who took me under her wing and didn't let me quit in the second summer season...maybe one day we can go back and pick up my Horse? My eternal gratitude goes to Otgon, Bilge, Sodbayar for the fun times had both in the field and in Ulaanbaatar. Thanks also to Tomurtogoo for the great discussions and for sharing your considerable experience of Bayankhongor and Mongolian ophiolites.

From the Mainz group I owe a lifetimes worth of favours to Jörg Pfänder who taught me all about isotopes for very little return, and showed endless patience....I hope we will continue to work together in the future! Thanks also to Petra, Miranda, and of course Eric who reassured me that sarcasm is alive and well outside of the UK. Thank also to Alfred Kröner for help with zircon dating and also for helping to find funds for visits to Germany as well as fun and jokes in the field. And a hearty thank you to everyone else who was involved with the Mainz collaboration and who made me feel so welcome at the Max-Planck-Institut. I miss the felafel man already!!

I would like to say thanks to all the technicians/ experimental officers, secretarial staff, and general hangers on that have made life in the Leicester Geology department that little bit easier. Thanks also to all of the Academic staff who have at one time or another contributed to the discussion of my research and push the final result forward.

I owe a wealth of gratitude and thanks to my housemates, Pat, Craig, and Matt who have had to put up with an extra grumpy version of me and endless taunts and bad jokes throughout the last months.....of course you could have shown a little more sympathy...I didn't once hear you offer to write it for me...?? Special thanks to Rich for well everything....there are way too many things to write about here......and hey guess what we made it to the end...aren't you glad we didn't decide to run off at the end of second year???

And so to all the other Leicester friends who I am afraid I am just going to thank *en masse* because if I try to name you all I will just offend someone who I forget...you know who you all are and so thanks for the beers and the laughs...they helped a lot!!

Thanks to Stefanja who supplied the seed of thought to start the writing......"There are lots of different kinds of rocks...some are big and some are small...etc." ....and for helping take my mind off the work by showing that there is a world outside geology...sometimes you forget!

Special thanks to go to Joanna for well lots of things...but most of all for staying friends, I know that if you were here you would have helped me get through it and I know you were thinking about me!

And in true Oscar winning speech style I save the biggest and most heartfelt thanks for the people without whom none of this would have been possible, Mum, Dad, and Luann. I couldn't possibly put in to words the amount I would like to thank you....but without your love and support I never would have made it here....and well I think that's everyone.

Contents

List of figures

List of Tables

Chapter 1:

Introduction

The Bayankhongor ophiolite, a NW-SE striking sublinear belt 300 km long and 20 km wide (Fig. 1.1), is the largest ophiolite in Mongolia and possibly Central Asia. This study focuses on the tectonic evolution of the ophiolite, and its implications for the mechanism of Palaeozoic crustal growth in Central Asia. The research was multidisciplinary involving structural and lithological mapping, petrography, geochemistry, Nd isotope analysis, and zircon geochronology. Field research was carried out in Central Mongolia during the summers of 1997-1999. The main objectives of the research were the following: (1) to undertake the first detailed lithological and structural study of the Bayankhongor Ophiolite Zone, in order to establish the tectonic relationship between the ophiolite and its neighbouring lithotectonic units, (2) to carry out geochemical and Nd isotope studies of the ophiolitic rocks to evaluate the possible tectonic settings in which they formed, and evaluate possible mechanisms of ophiolite obduction, (3) to establish geochronological constraints for the duration of subduction, timing of closure of the Bayankhongor ocean and obduction of the ophiolite by dating granite plutons that intrude the ophiolite and neighbouring units, (4) to compare the new data with that of previously published studies of Mongolian ophiolites of similar age along strike to the north-west, and assess regional relationships between the Bayankhongor ophiolite and other ophiolite occurrences (5) to combine the new data in order to produce a model of the tectonic evolution of the Bayankhongor ophiolite, and use this to evaluate the role of the Bayankhongor ophiolite in the Palaeozoic crustal growth of Central Asia. The dissertation is divided into three main chapters, prepared in the form of stand-alone papers suitable for publication. These chapters document the results of the study and address the main objectives described above. These chapters are followed by a summary chapter (5) that synthesises all results into a working model for the tectonic evolution of the Bayankhongor ophiolite.

Chapter 1 presents results from a field study of the lithological and structural characteristics of the Bayankhongor Ophiolite Zone based on research carried out during the summers of 1997-98. Detailed geological maps and structural data are presented for three cross-strike transects through the Bayankhongor Ophiolite and its neighbouring lithotectonic units: the Baidrag block, Burd Gol mélange, and Dzag Zone (Fig. 1.1). The new data suggest that the Bayankhongor ophiolite is a suture marking the position of a Lower Palaeozoic

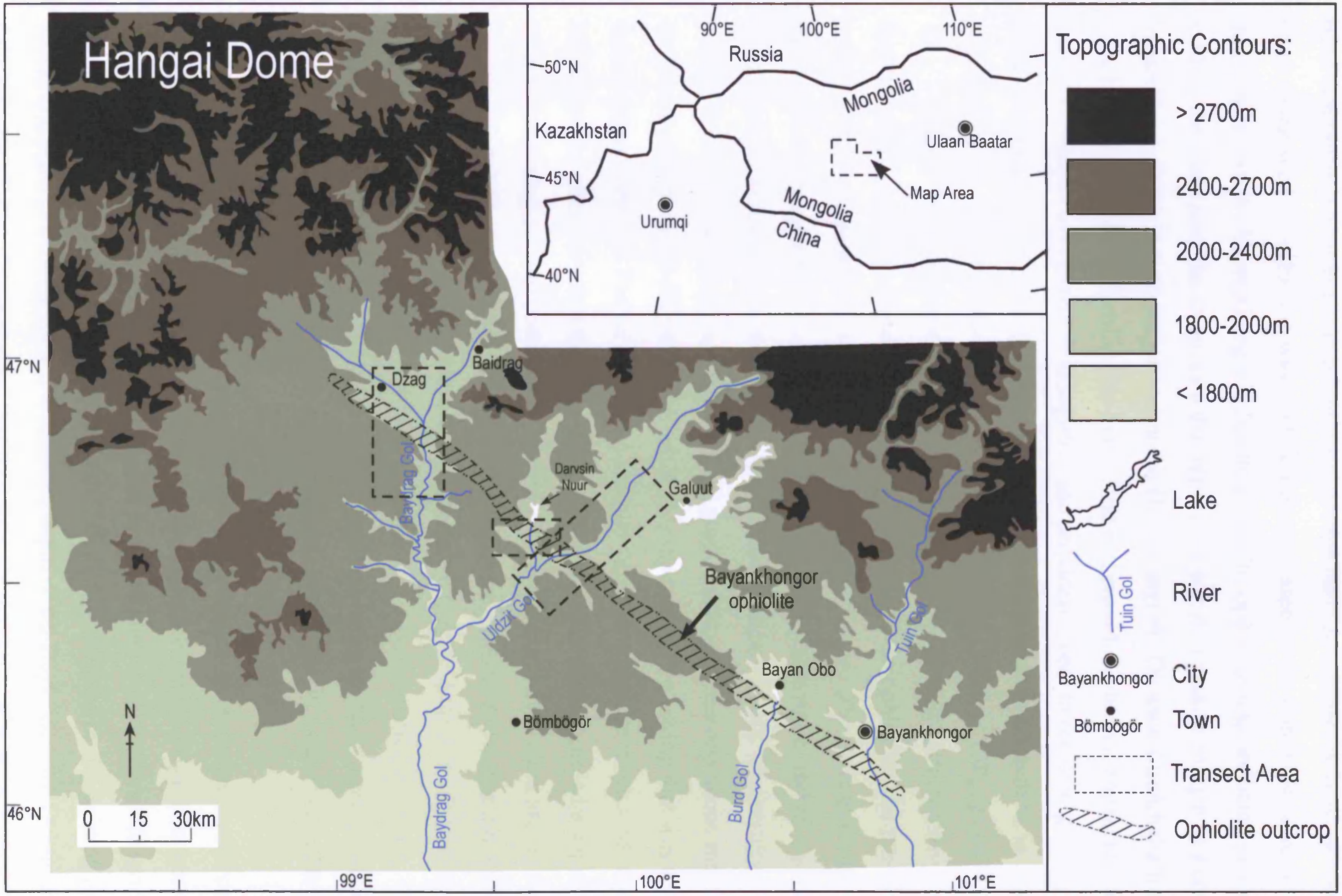

Fig. 1.1: Topographic map of the Bayankhongor area in Central Mongolia. The extent of oucrop of the Bayankhongor Ophiolite is indicated. The location of the three transects mapped during this study along Baidrag Gol, south of Darvsin Nuur, and along Uldzit Gol are shown. In addition to the three transects, reconnaissance studies were carried out along strike as far as Bayankhongor City.

subduction zone between the Baidrag block to the south, and the Dzag zone to the north. The Burd Gol mélange represents an accretionary wedge built up against the Baidrag continental block to the south. Subduction was to the southwest based on the dominant polarity of thrusting within the Bayankhongor ophiolite zone. The ophiolite was obducted in a north-easterly direction over the Dzag zone that represents part of a passive margin to a continent located beneath the sedimentary cover of the Hangai region. Dickson Cunningham and Brian Windley assisted with data collection in the field and provided editorial assistance. Dondov Tomurhuu helped to organise field logistics and provided access to regional geological maps, aerial photographs, and satellite imagery. All three are included as co-authors in a paper published in the *Journal of the Geological Society, London* (2001, v. 158, pp. 445-460).

Chapter 2 is a geochemical and Nd isotope study of samples collected from the Bayankhongor Ophiolite, basalts from a mélange related to the ophiolite, and previously unstudied volcanic rocks which lie to the south of the ophiolite. The main objectives of the study were to determine the possible magma sources of the three units, and to use these to reconstruct the tectonic environment in which the rocks were formed. The results provide new evidence that the ophiolitic magmas were produced from a heterogeneous mantle source composed of depleted N-MORB and E-MORB components, in a setting that was similar to that of the modern East Pacific Rise. The samples from the ophiolite related mélange have island arc-like chemistry that suggests that the ophiolite may have occupied a supra-subduction setting prior to obduction. The volcanic rocks also have island arc-like chemistry, but geochronological constraints suggest that these were generated after the ophiolite was obducted. Jörg Pfänder helped with Nd isotopic analysis at the Max-Planck-Institut für Chemie in Mainz, Germany and provided guidance in the interpretation of results. Tim Brewer advised on sample preparation and provided guidance in the interpretation of geochemical and isotopic data. Both are included as co-authors in a paper submitted to *Chemical Geology*.

Chapter 3 is a study of the geochemistry, Nd isotope concentration, and zircon geochronology of granite plutons and rhyolite dykes that intrude the Bayankhongor Ophiolite and neighbouring lithotectonic units. The data from the granite plutons provide evidence that they represent crustal melts produced at *c.* 540 Ma during collision of the Baidrag and Hangai blocks and provide a minimum age for the obduction of the Bayankhongor Ophiolite. The data from the rhyolite dykes suggest that they were intruded at *c.* 474 Ma and provide a minimum age for generation of the island arc-like volcanic rocks to the south of the ophiolite. The new data, combined with previously published geochronological data, suggest that the ophiolite was obducted onto the Dzag passive margin at *c.* 540 Ma at the beginning of a collision event that lasted until *c.* 450 Ma. Correlation of isotopic-age data for the ophiolites of western Mongolia and southern Tuva suggest that the ophiolites define a major collisional suture in the Central Asian Orogenic Belt which helps define the southern and western margins of the Hangai continental block. Jörg Pfänder and Alfred Kröner assisted with Nd isotope and zircon geochronological analysis at the Max-Planck-Institut für Chemie in Mainz, Germany. Tim Brewer, Dickson Cunningham, and Brian Windley provided critical guidance and editorial assistance. Dondov Tomurhuu and Onongin Tomurtogoo provided logistical help during sample collection in Mongolia. In acknowledgement of their contributions, all of these people are included as co-authors on a paper submitted to *Earth and Planetary Science Letters*.

Chapter 4 summarises the results and conclusions from the preceding chapters and discusses their implications for the tectonic evolution of the Bayankhongor Ophiolite. Three models for the tectonic evolution and obduction of the ophiolite are presented and the merits of each are discussed in terms of the constraints imposed by the presented data. At present, two models appear to be most consistent with data from this study, and constraints for ophiolite obduction suggested by previous studies; supra-subduction entrapment of the Bayankhongor ophiolite above a single subduction zone in which the Burd Gol mélange represents a deformed fore-arc basin, and a double subduction zone model in which the Burd Gol mélange is interpreted as an accretionary complex. Additional work is required in order to resolve the models.

The research presented in this thesis is connected to several ongoing projects that concern orogenic processes in Mongolia and Central Asia. These include Jörg Pfänder's (Max-Planck-Institut für Chemie, Mainz) geochemical and isotopic studies of the Agardagh Tes-Chem ophiolite in southern Tuva, Brian Windley (University of Leicester) and Alfred Kröner's (Mainz University) regional studies of Palaeozoic crustal growth in Central Asia, Dickson Cunningham's (University of Leicester) detailed structural studies of intracontinental mountain building in the Mongolian Altai, and processes of uplift in the Hangai Dome, central Mongolia, Arjan Dijkstra's (University of Leicester) studies of the metamorphic basement of the Altai region, James Howard's (University of Leicester) studies on processes of transpressional basin formation in western Mongolia, Diane Seward's (ETH, Zurich) fission track analyses of uplift and exhumation in the Altai, Larry Snee's (USGS, Denver) Ar-Ar dating of mylonites in the Altai, Lewis Owen's (U. California, Riverside) studies of the geomorphology of the Gobi Altai, and Gombosuren Badarch's (IGMR, UlaanBaatar) terrane synthesis of Mongolia. Together these projects represent a major multidisciplinary effort to understand orogenic processes and the tectonic evolution of Mongolia and Central Asia.

Chapter 2:

Structural and lithological characteristics of the Bayankhongor Ophiolite Zone, Central Mongolia

Introduction

Central Asia is a collage of continental blocks, ancient island arc terranes, subduction complexes and fragments of oceanic crust that amalgamated during the late Precambrian, Palaeozoic and Mesozoic. Şengör *et al.* (1993) produced a regional tectonic synthesis of the basement geology of Western China, Kazakhstan, Mongolia and parts of Russia utilising existing published information, and proposed a mechanism for continuous continental growth through subduction accretion and arc collision. They suggested that a subduction zone existed along the southern margin of the Angara craton (Fig. 2.1 inset) throughout the Palaeozoic era and that a vast complex of arc and subduction-accretion material including offscraped ophiolitic fragments accumulated in front of seaward-migrating magmatic fronts. In contrast, Coleman (1989) and Hsü *et al* (1991) identified distinct ophiolite belts in north-western China, which they interpreted as discrete suture zones separating different Palaeozoic blocks. These models differ in that the former invokes steady state subduction-accretion over a prolonged period of time, whereas the latter favours punctuated accretion by collision and closure of multiple ocean basins now marked by ophiolitic sutures. Mossakovsky *et al.* (1994) proposed a model for Central Asia whereby the early stages of continental growth were dominated by arc development and accretion and the late stages by collision of accreted continents. In order to understand how the bulk of the continent of Asia was formed, it is essential to work out the tectonic significance of the Central Asian ophiolites and their role in the continental accretion process.

Mongolia presents an exceptional opportunity to examine this problem because it lies centrally within this collage (Fig. 2.1 inset) and contains some of the best preserved Palaeozoic ophiolitic rocks in Central Asia with over 60 reported separate occurrences (Fig. 2.2). Despite their abundance, few Mongolian ophiolites have been studied using modern structural techniques and important questions remain regarding their internal structures, mechanism of emplacement and overall tectonic significance. Here we present results of a detailed structural study of the Bayankhongor ophiolite, the longest continuously exposed ophiolite belt in Mongolia and possibly all of Central Asia.

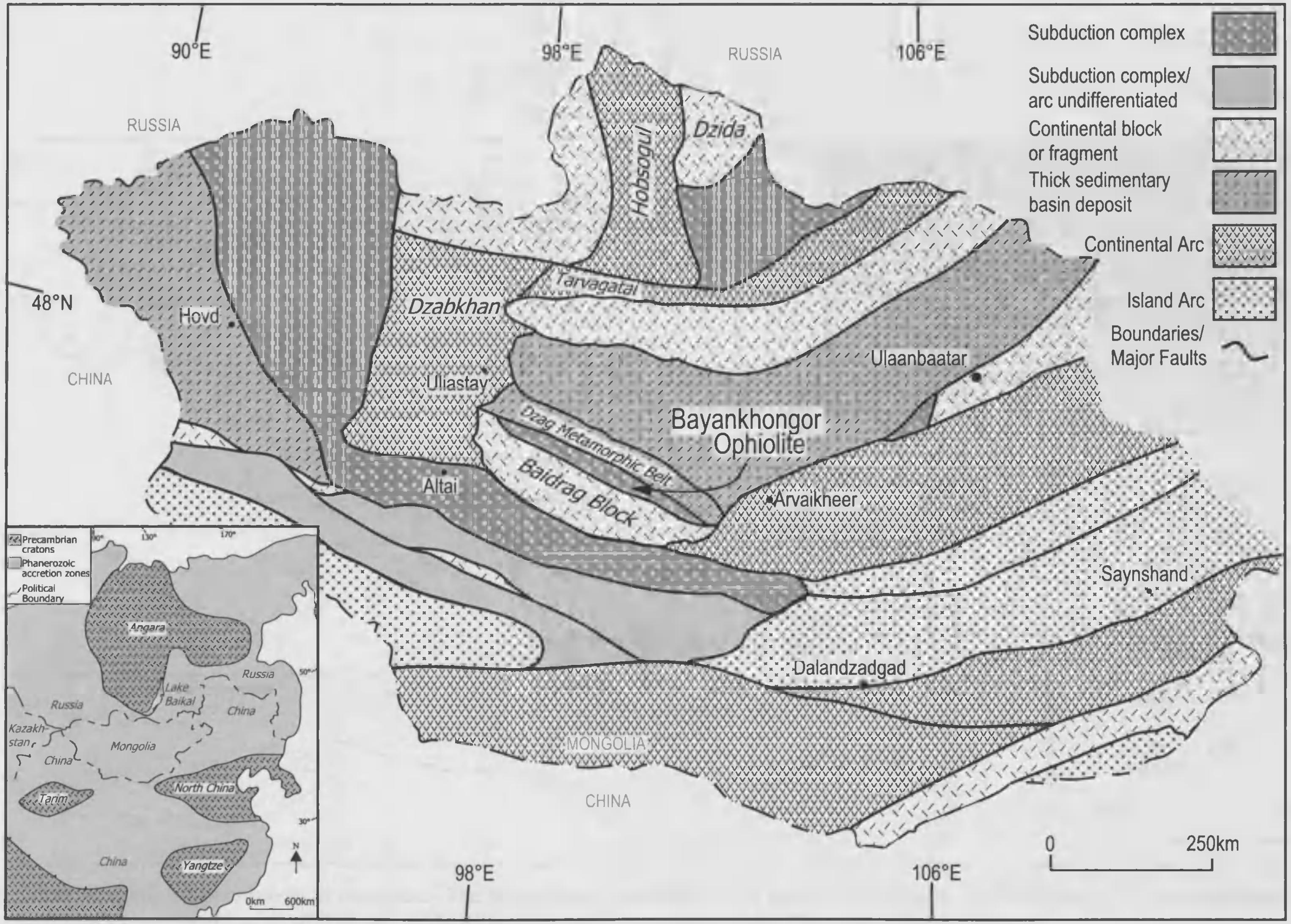

Fig. 2.1: Major terranes of central and western Mongolia from Dorjnamjaa (1998). Position of the Bayankhongor ophiolite zone is indicated. Inset map shows Mongolia's position in Central Asia and locations of major Precambrian cratons.

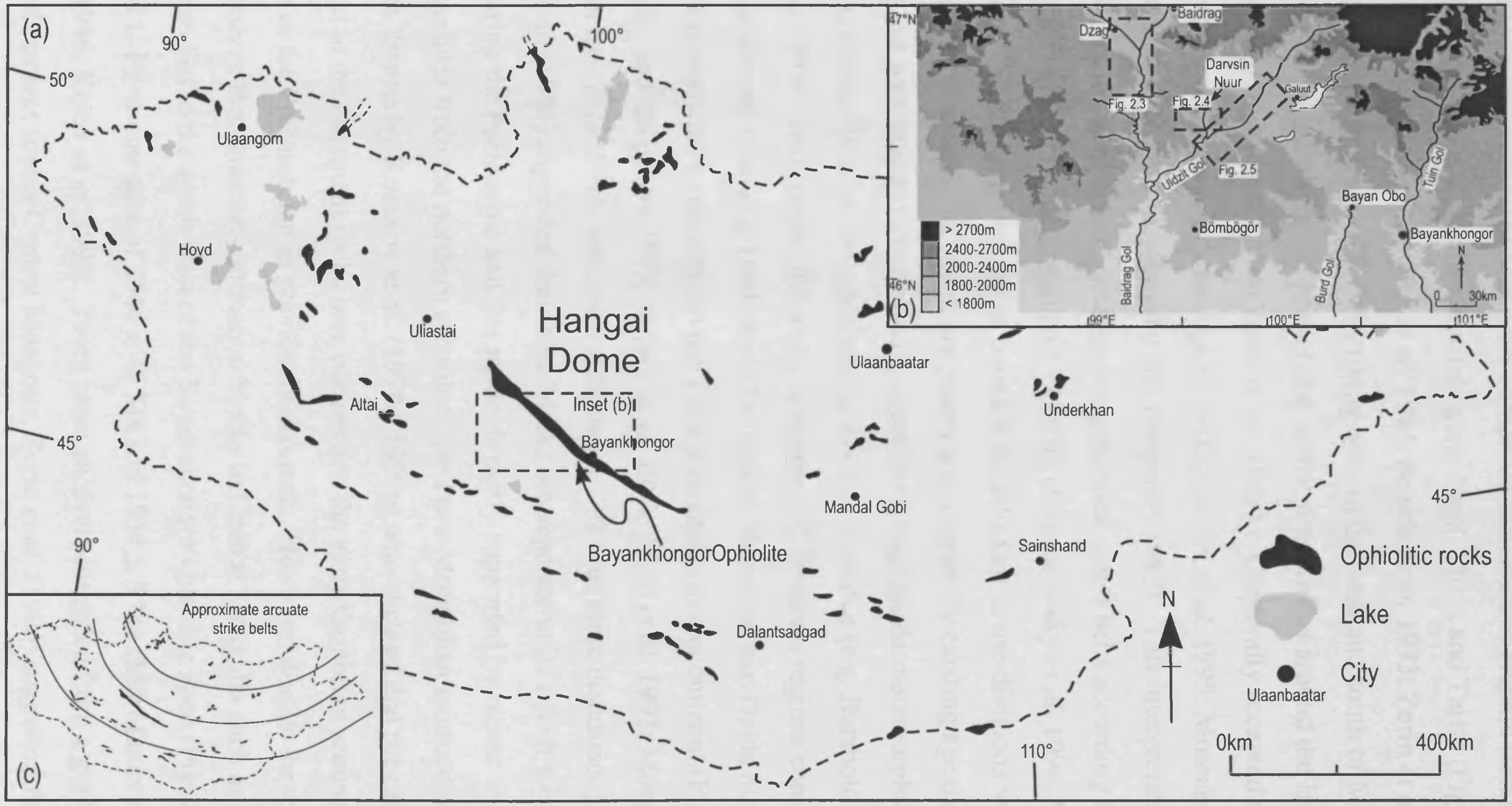

Fig. 2.2: (a) Ophiolite occurrences in Mongolia. The Bayankhongor ophiolite is the largest in the region. (b) Topography of the Bayankhongor area. Locations of transects and Figs. 2.3-2.5 shown. (c) Map showing general structural trends of basement rocks in Mongolia.

Regional Geology

The basement geology of Mongolia comprises tectonostratigraphic terranes between the major Precambrian cratonic blocks of Angara, North China and Tarim (Fig. 2.1; Dobretsov *et al.* 1995; Mossakovsky *et al.* 1994; Şengör *et al.* 1993; Zorin *et al.* 1993). These terranes form gently curving, NW-SE striking belts in the west and south of Mongolia and a less ordered mosaic pattern in the central and northern provinces around the Hangai region (Fig. 2.1; Mossakovsky *et al.* 1994; Zorin *et al.*, 1993). A generally accepted concept is that accretion progressed southwards through time (Dobretsov *et al.* 1995; Mossakovsky *et al.* 1994; Şengör *et al.* 1993; Mossakovsky and Dergunov 1985). This interpretation has traditionally led to the basement geology being divided into 3 belts according to their time of accretion: the Baikalian, Caledonian and Variscan (Mossakovsky *et al.* 1994; Mossakovsky and Dergunov 1985). However, some workers are reluctant to use divisions which refer to European orogenic events and which are poorly constrained by existing age data. Another problem is that past studies have tended to identify all high-grade metamorphic terranes in Mongolia as Precambrian without supporting isotopic evidence (e.g. Barsbold and Dorjnamjaa 1993). Thus some authors have interpreted disparate regions containing crystalline basement (Baidrag, Dzabkhan, Tarvagatai, Hobsogul and Dzida blocks) to be part of a larger Precambrian terrane called the Tuva-Mongolian microcontinent (Fig. 2.1; Mossakovsky and Dergunov 1985; Şengör *et al.* 1993; Zorin *et al.* 1993; Mossakovsky *et al.* 1994; Dobretsov *et al.* 1995; see Lamb & Badarch, 1997 for more discussion). However, Didenko *et al.* (1994) suggested that these blocks are separate units which were brought together during the Palaeozoic and this model is partly supported by recent U-Pb zircon dating of samples from the northern section of the Tuva-Mongolian microcontinent located in Tuva, south Siberia by Kozakov *et al.* (1999a, 1999b) who showed that the earliest deformation in the basement rocks here occurred in the early Cambrian around 536 ± 6 Ma rather than in the Precambrian as previously assumed. However, despite these results, there are some proven Precambrian continental blocks in Central Mongolia such as the Baidrag massif which lies to the south-west of the Bayankhongor ophiolite zone (Fig. 2.1) and which has yielded U-Pb zircon ages of 2646 ± 45 Ma and 1854 ± 5 Ma (Mitrofanov *et al.* 1985; Kozakov 1986; Kotov *et al.* 1995). From cross-sections compiled from a geological and geophysical transect across Central Mongolia, Zorin *et al.* (1993) suggested that continental crust, probably Precambrian in age, is also present below the thick sedimentary cover of the Hangai region to the north-east of the Bayankhongor ophiolite. Kovalenko *et al.* (1996) published an array of Sm-Nd model ages from Phanerozoic granites in the Hangai region, which range from T_{DM}=1058 Ma to T_{DM}=2154 Ma. Because the granites have negative ε_{Nd} values, Kovalenko *et al.* (1996) argue that they are sourced from melting of continental crust below the Hangai region whose minimum age is given by the model ages.

The Bayankhongor ophiolite zone (Figs. 2.1, 2.2) is situated on the southern side of the Hangai mountains which formed during regional Cenozoic doming (Windley and Allen 1993; Barry and Kent 1998; Cunningham 1998). The ophiolite forms a NW-SE striking sub-linear zone approximately 300 km long and up to 20 km wide (Figs. 2.1, 2.2) exposed continuously from just west of the town of Dzag to just east of Bayankhongor City (Fig. 2.2b). Uplift and erosion along the southern flank of the dome has resulted in good exposure of the ophiolite belt. Previous lithological mapping enables a four-fold tectonic subdivision of the region from south to north: the Baidrag complex, Burd Gol mélange, Bayankhongor zone and Dzag zone (Fig. 2.1; Teraoka *et al.* 1996; Tomurtogoo *et al.* 1998).

The Archaean Baidrag complex, composed of tonalitic gneiss, granulite and amphibolite, with minor marble and quartzite, has been interpreted as a microcontinental block (Mitrofanov *et al.* 1985; Kozakov 1986; Kozakov 1997).

The Burd Gol zone is a tectonic mélange containing lenses of sedimentary and igneous rocks cut by abundant quartz veins. From palaeontological dating of stromatolites in limestone lenses, Mitrofanov *et al.* (1981) suggested that the Burd Gol mélange has a late Precambrian age. Within the mélange, metamorphic grade increases towards the north. North of the Burd Gol zone there is a small area of interbedded marine mudstone and limestone which reportedly contain Carboniferous fossils (Dergunov *et al.* 1997).

The Bayankhongor zone contains three sub-units, here named the Delb Khairkhan mélange, ophiolite mélange and Haluut Bulag mélange. The Delb Khairkhan mélange lies to the south of the ophiolite and contains sedimentary and volcanic rocks of Precambrian to Ordovician age (Ryantsev 1994; Dergunov *et al.* 1997). The ophiolite mélange is composed of a complete ophiolite stratigraphy (Moores, 1982), dated at 569 ± 21 Ma (Sm-Nd hornblende and whole rock isochron on gabbro; Kepezhinskas *et al.* 1991) dismembered into blocks enclosed within a serpentinite matrix. The Haluut Bulag mélange is dominantly sedimentary with lenses of bedded limestone, sandstone, siltstone, and locally vesicular basalt, enclosed in a matrix of pelitic schist.

The Dzag zone consists of asymmetrically folded chlorite-mica schists that locally contain relict sedimentary features suggesting they are meta-turbidites.

Transect data

In the summers of 1997 and 1998, three cross-strike geological transects were carried out through the Bayankhongor ophiolite (including Delb Khairkhan and Haluut Bulag mélanges) and adjacent Dzag and Burd Gol zones (Figs. 2.3-2.5). The transects along the Baidrag Gol south of Darvsin Nuur and along the Uldzit Gol, were chosen because of the deep incision and excellent exposure created by these river systems (Fig. 2.2b). Fieldwork focussed on documenting stratigraphic and metamorphic relations, internal structures and structural evolution of the ophiolite and adjacent lithological units. Reconnaissance was also carried out in other areas within the Bayankhongor Zone in order to gain a wider understanding of along-strike variations and to fully characterise the Dzag and Burd Gol zones.

Major lithotectonic units

The study area is divided into six major lithotectonic units: Burd Gol mélange, Carboniferous sedimentary rocks and volcanic sequence, Delb Khairkhan mélange, ophiolitic rocks, Haluut Bulag mélange, and Dzag Zone which are juxtaposed along NE-SW trending, NE vergent thrust faults (Figs. 2.3-2.5). In this section we describe the important lithological characteristics of each unit.

Burd Gol mélange

The contact of the Burd Gol mélange with the Baidrag block to the south is observed south-west of the town of Bömbögör (Fig. 2.2b, N46° 16.962', E99° 32.360'), where granitic gneisses of the Baidrag block are overlain unconformably by a series of thick quartzites and sandstones which comprise the southernmost section of the Burd Gol mélange. The foliation in the Baidrag gneisses dips steeply NW and the Burd Gol mélange rocks dip shallowly NE. Detailed descriptions of the Archaean Baidrag complex can be found in Kozakov (1986) and Kozakov *et al.* (1997). A few kilometres NE of the contact, the Burd Gol mélange becomes more mixed with lenses of sedimentary and igneous lithologies enclosed in a black schist matrix. Andesitic dykes, which cut the foliation are dismembered and surrounded by a matrix of graphitic schists. A more detailed study of the Burd Gol mélange was carried out to the NW of Bömbögör (Fig. 2.2b, N46° 19.785' E99° 36.017') where numerous, variably oriented quartz veins up to 4 m wide cut the mélange. The veins are locally gold-bearing (Komarov *et al.* 1999). Teraoka *et al.* (1996) and Höck *et al.* (2000) obtained a K/Ar ages in the range 699 ± 35 Ma to 533 ± 3 Ma from muscovite from the black schists. To the north of these black schists, many igneous and sedimentary lenses several hundred metres across are enclosed in a black schist matrix. The sedimentary lenses are composed of limestone, sandstone, siltstone,

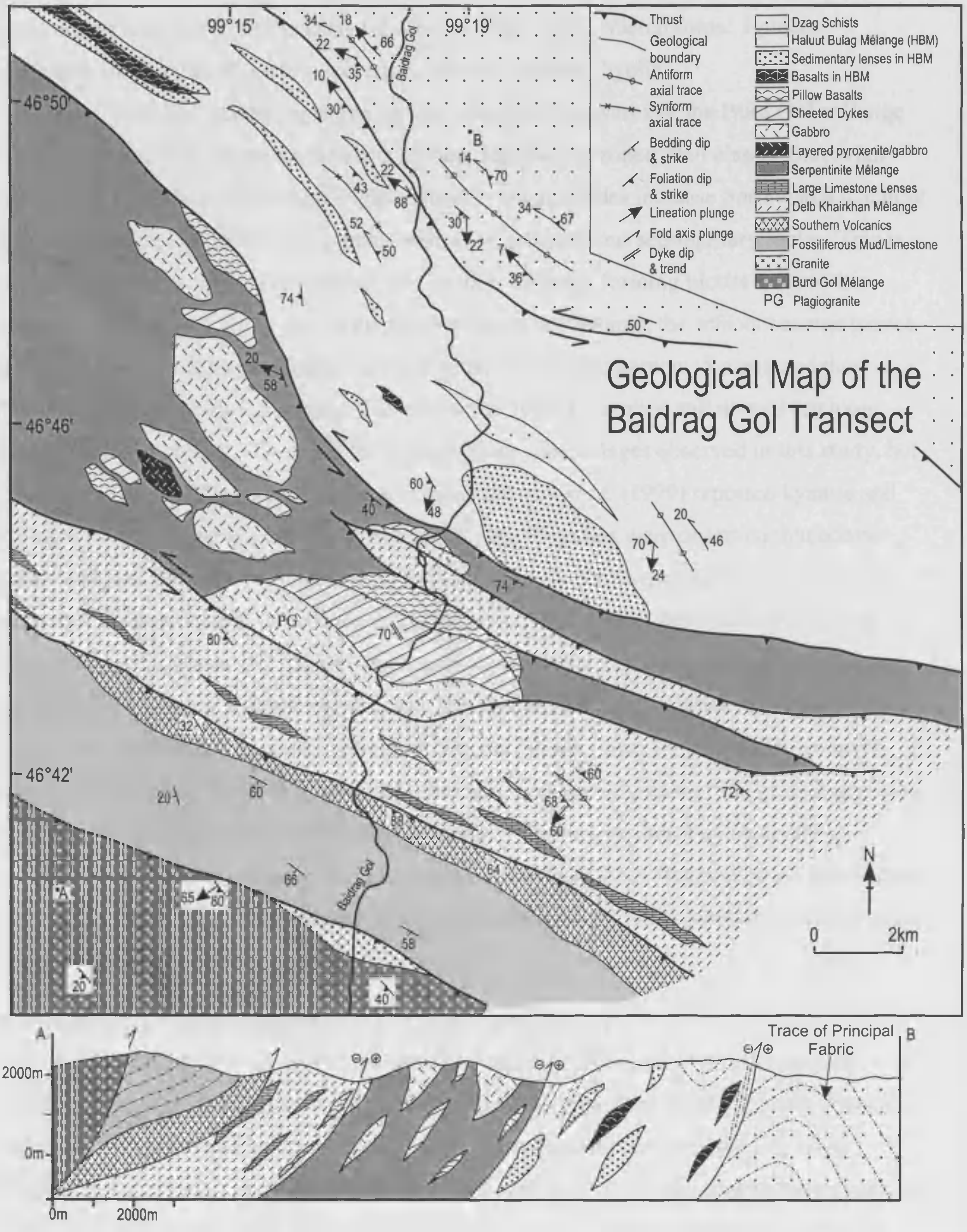

Fig. 2.3: Geological map and cross section of the Baidrag Gol (*River*) transect. See Fig. 2.2b for location.

mudstone, shale, chert and well-bedded calci-turbidite. These lenses contain internal deformation which appears to have formed before incorporation into the mélange matrix, because proximal blocks of the same lithology contain dismembered folds. Igneous lithologies include basalt, gabbro, dolerite, andesite and rare rhyolite.

The Uldzit Gol transect contains particularly good exposures of the Burd Gol mélange that demonstrate that the mélange matrix is metamorphically zoned with classic Barrovian facies (Fig. 2.5). Over a distance of approximately 6 km, grades increase northwards reaching amphibolite facies at the thrusted contact with the Carboniferous sedimentary rocks. This is indicated by metamorphic assemblages that contain cleavage forming biotite and biotite porphyroblasts up to 1 cm in size in the south whereas northwards, the schists become garnet-biotite-muscovite-bearing with abundant euhedral, syntectonic garnets (5 mm), and then staurolite–muscovite-biotite schists. The staurolites form 1 cm wide and up to 3 cm long euhedral porphyroblasts. These are the highest-grade assemblages observed in this study, but Dergunov *et al.* (1997) reported sillimanite and Komarov *et al.* (1999) reported kyanite and sillimanite from the same unit. Possible kyanite pseudomorphs were observed, but contact metamorphism, caused by a local granite intrusion, may have overprinted any higher-grade metamorphic assemblage. Takahashi and Oyungerel (1997, 1998) determined K-Ar ages ranging from 551 Ma to 467 Ma on biotite and muscovite from granite plutons in the Uldzit Gol area, which they interpreted to represent the crystallisation age. However, because these granites are tectonically foliated, we suggest that the younger ages may be due to younger metamorphic events. Local amphibolite bodies and mélange schists near the granite intrusion, contain a contact overprint texture with 5-10 cm acicular bow-tie hornblende crystals overprinting the primary schistosity. The amphibolites form sheet-like bodies but it is unclear whether they were originally lava flows or dykes since they are dismembered and surrounded by the pelitic schists of the mélange.

Carboniferous Sedimentary Rocks & Southern Volcanics

To the north and north-east of the Burd Gol mélange, there are interbedded green Carboniferous fossiliferous marine mudstones and limestones (Fig. 2.3-2.5), which contain abundant, well preserved brachiopods, bryozoans, crinoids and corals (Tungalag 1996; Dergunov *et al.* 1997). The sedimentary rocks are well bedded and dominated by mudstones with beds 2 to 5 metres thick. The limestone beds vary from a few centimetres to about 3 metres thick and occur locally and discontinuously. These are the youngest known rocks in the study area.

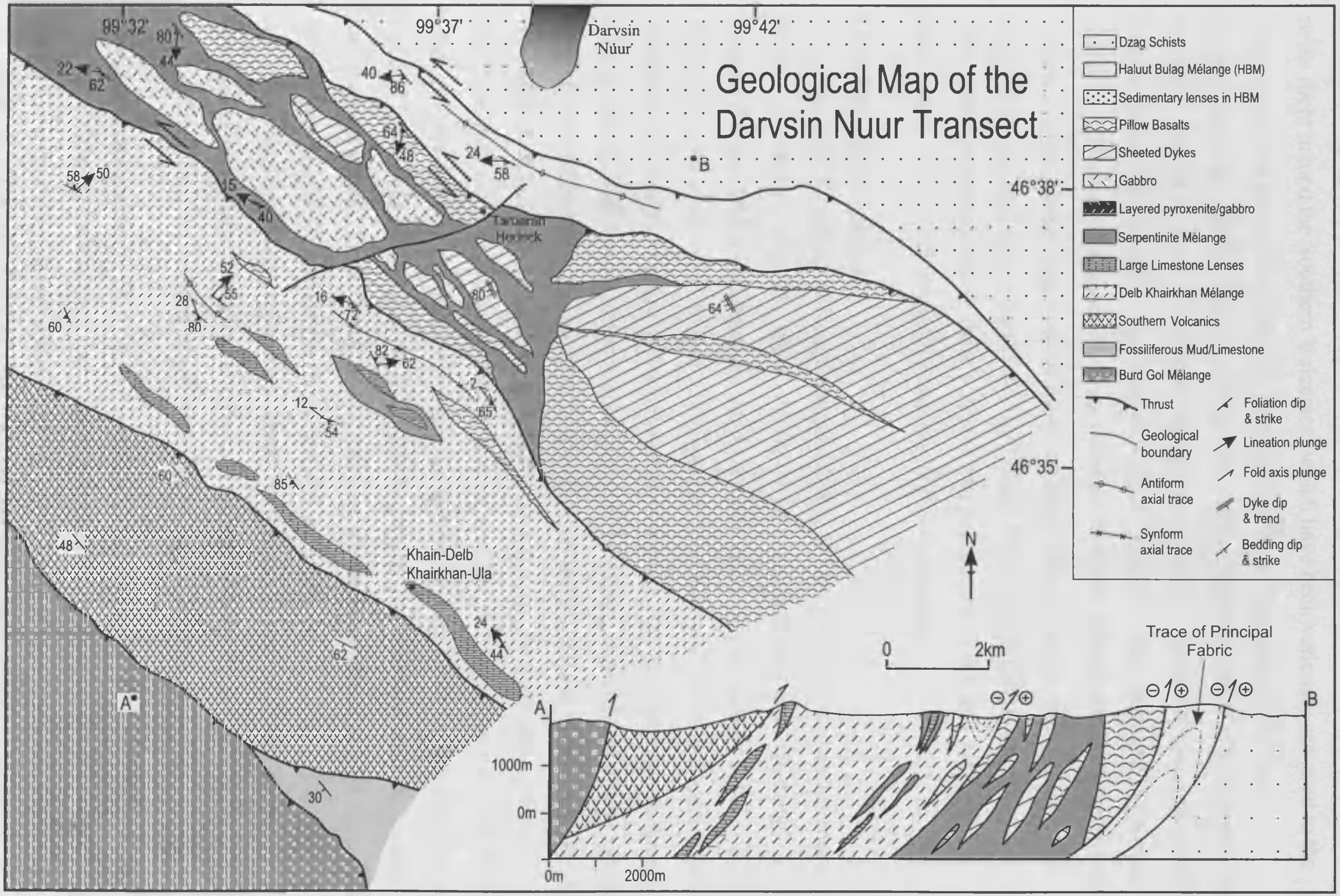

Fig. 2.4: Geological map and cross section of the Darvsin Nuur (*Lake*) transect. See Fig. 2.2b for location.

The Carboniferous sedimentary rocks lie unconformably on (Fig. 2.3), or in thrust contact with (Figs. 2.4, 2.5), a sequence of extrusive volcanic rocks and minor sedimentary rocks (here named the Southern Volcanics) which have been variously assigned to the Ordovician (Dergunov *et al.* 1997) or Devonian periods (Tungalag, 1996) based on palaeontological evidence and correlation with similar units elsewhere. The volcanic strata consist of sheet-like flows of andesite, dacite, basalts, and trachybasalts that are interbedded with agglomerates and tuffs. There are also small intrusive bodies of quartz-plagioclase porphyry. Dacites and agglomerates are the most abundant lithologies. The agglomerates contain 2-5 cm angular fragments of nearly all other volcanic rocks, enclosed in a fine groundmass dominated by plagioclase. Individual flows vary in thickness from about 1m to 15m. Stratigraphically above these volcanic and plutonic rocks is a thin conformable sequence (5-10m) of volcanogenic conglomerate and sandstone.

Delb Khairkhan mélange

The Delb Khairkhan mélange contains mixed lenses of igneous and sedimentary rocks enclosed in a matrix of pelitic schist. Along the southern boundary of the mélange in the Baidrag Gol and Uldzit Gol transects, igneous rocks seemingly derived from the volcanogenic sequence to the south, consisting of quartz-plagioclase porphyry, dacite and volcanogenic conglomerates and sandstones are included in the mélange. On the north side of the mélange near its contact with the ophiolitic sequence, lenses of gabbro, dolerite and pillow basalts several hundred metres long and 20 to 30 metres wide resemble those in the ophiolite (Figs. 2.3, 2.4). In addition to the volcanogenic sedimentary rocks, there are lenses of limestone, quartzite, shale and sandstone. Along the contact with the volcanic rocks there is a prominent ridge of limestone that continues in en-echelon segments along strike to the east for several hundred kilometres (Figs. 2.3-2.5). The ridge limestone is interbedded with shales and mudstones, bedding dips SW and the unit has a maximum thickness of around 1 km.. Similar limestones occur as smaller lenses throughout the mélange.

The ridge limestones contain abundant well-preserved stromatolites. These stromatolites have been identified as *conofiton gargantuous* by Boishenko (1979) and interpreted as late Precambrian in age (Riphean stage in Russian terminology).

Ophiolitic Rocks

The ophiolitic rocks comprise a complete ophiolite stratigraphy (Moores, 1982); i.e. ultramafic cumulates, gabbro, sheeted dykes, pillow lava and local chert and limestone. However, the ophiolite is dismembered into blocks, which vary in the completeness of their internal stratigraphy (Figs. 2.3-2.5). These blocks are enclosed in a matrix of sheared,

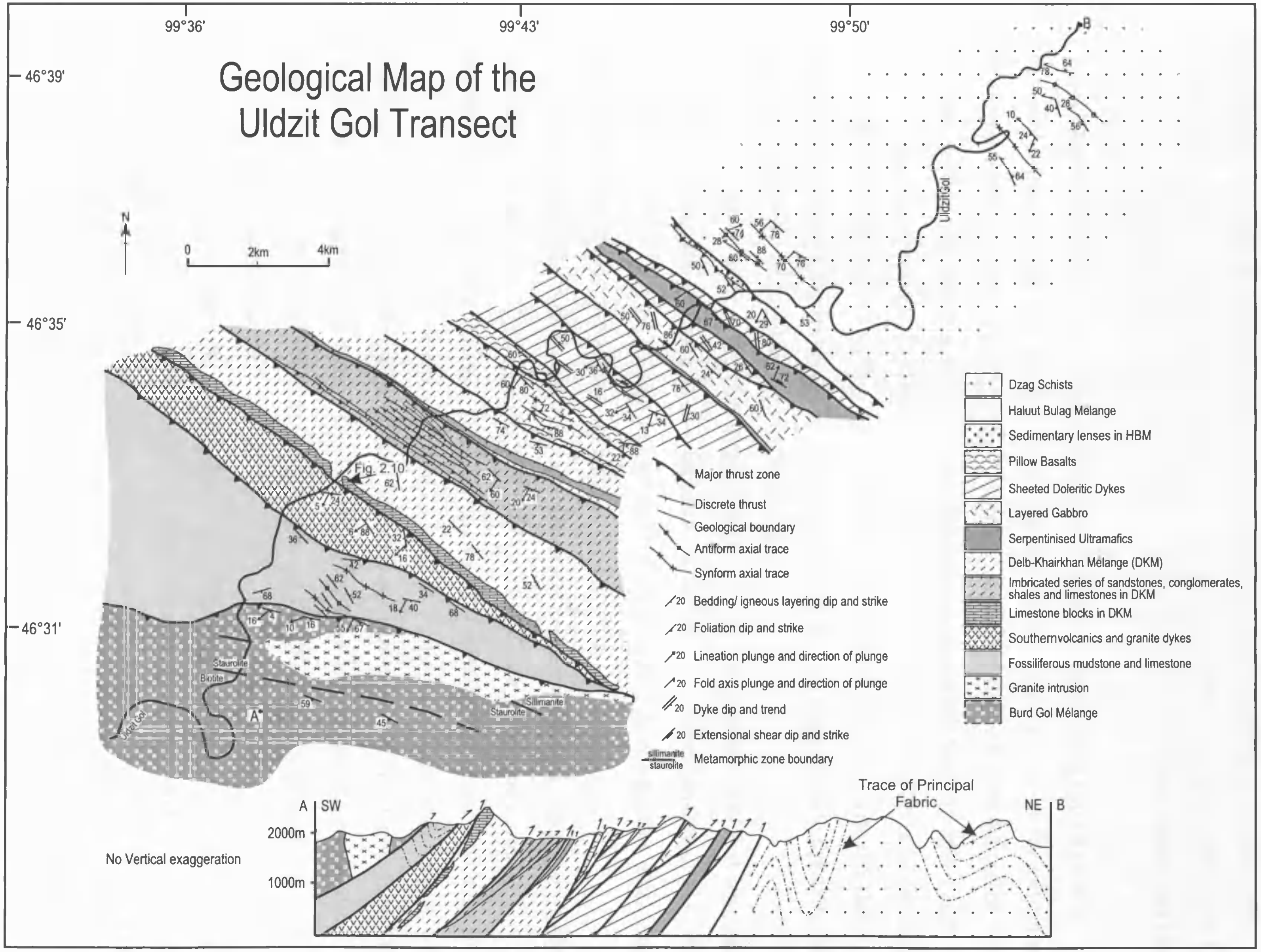

Fig. 2.5: Geological map of the Uldzit Gol transect. See Fig. 2.2b for location. Note that the Delb Khairkhan mélange is subdivided into smaller lithological groups to highlight the imbricate structure that occurs where mechanically weak matrix is subordinate to rigid coherent blocks. This structural relationship is unique to this transect.

serpentinised ultramafic rocks and thus the entire sequence constitutes another mélange. The composition of the mélange varies along strike. In the north-west, the sequence is dominated by blocks of gabbro, poorly preserved pyroxenite and pillow basalt surrounded by serpentinite, whereas in the south-east it is dominated by pillow basalt and sheeted dyke lenses (Figs. 2.3-2.5). In the east of the Darvsin Nuur transect and throughout the Uldzit Gol section, the mélange has less serpentinite matrix and is dominated by thrust imbricated blocks of upper ophiolite stratigraphy (Figs. 2.4, 2.5).

Gabbro blocks (Fig. 2.6a) have metre-scale compositional layering (pyroxenite to leucogabbro) and crystal size layering on tens of metre scale. Generally (with the exception of local pyroxenite-dominated bodies; Fig. 2.3) gabbro lenses are derived from the top of the cumulate section near the sheeted dyke transition because numerous doleritic dykes and sills crosscut cumulate layering. The dykes consistently strike between 280°-300° and dip steeply NE. One gabbro block (PG on Fig. 2.3) located on the southern boundary with the Delb Khairkhan mélange in the Baydrag Gol transect contains several plagiogranite dykes 1-1.5 m thick discordant to the cumulate layering of the gabbro.

On the eastern bank of the Uldzit Gol, a gabbro block has graded layers that become particularly leucocratic reaching near-anorthositic compositions. Kepezhinskas *et al.* (1991) produced a Sm-Nd whole rock and mineral isochron age of 569 ± 21 Ma for this unit, which they interpreted to be the crystallisation age.

The sheeted dyke complex is very well preserved and demonstrates clear dyke-in-dyke relationships (Fig. 2.6b). There are two different types of dykes in the study area, plagiophyric and aphyric (Ryantsev 1994, Dergunov *et al.* 1997). The plagiophyric dykes are on average 2-3m wide and are characterised by large (3-5 cm) plagioclase phenocrysts, which are concentrated in the centre of the dykes. The aphyric variety are around 1m wide and have a more typical doleritic composition and texture. In addition, the aphyric dykes are often slightly discordant to the plagiophyric ones suggesting that they may be derived from a different generation of magma.

The boundary between the sheeted dykes and pillow lavas is tectonic (Figs. 2.3-2.5), and because of shearing, the pillow basalts are locally poorly preserved. Aphyric (Fig. 2.6c) and plagiophyric pillow basalts are present and are mineralogically and texturally similar to the sheeted dykes. These similarities suggest that dykes intruding the pillow section represent the feeding conduits for successive flows. Multiple flows are separated by zones of pillow breccia. The pillow lavas show considerable hydrothermal alteration with epidote veining and epidotisation of some pillows.

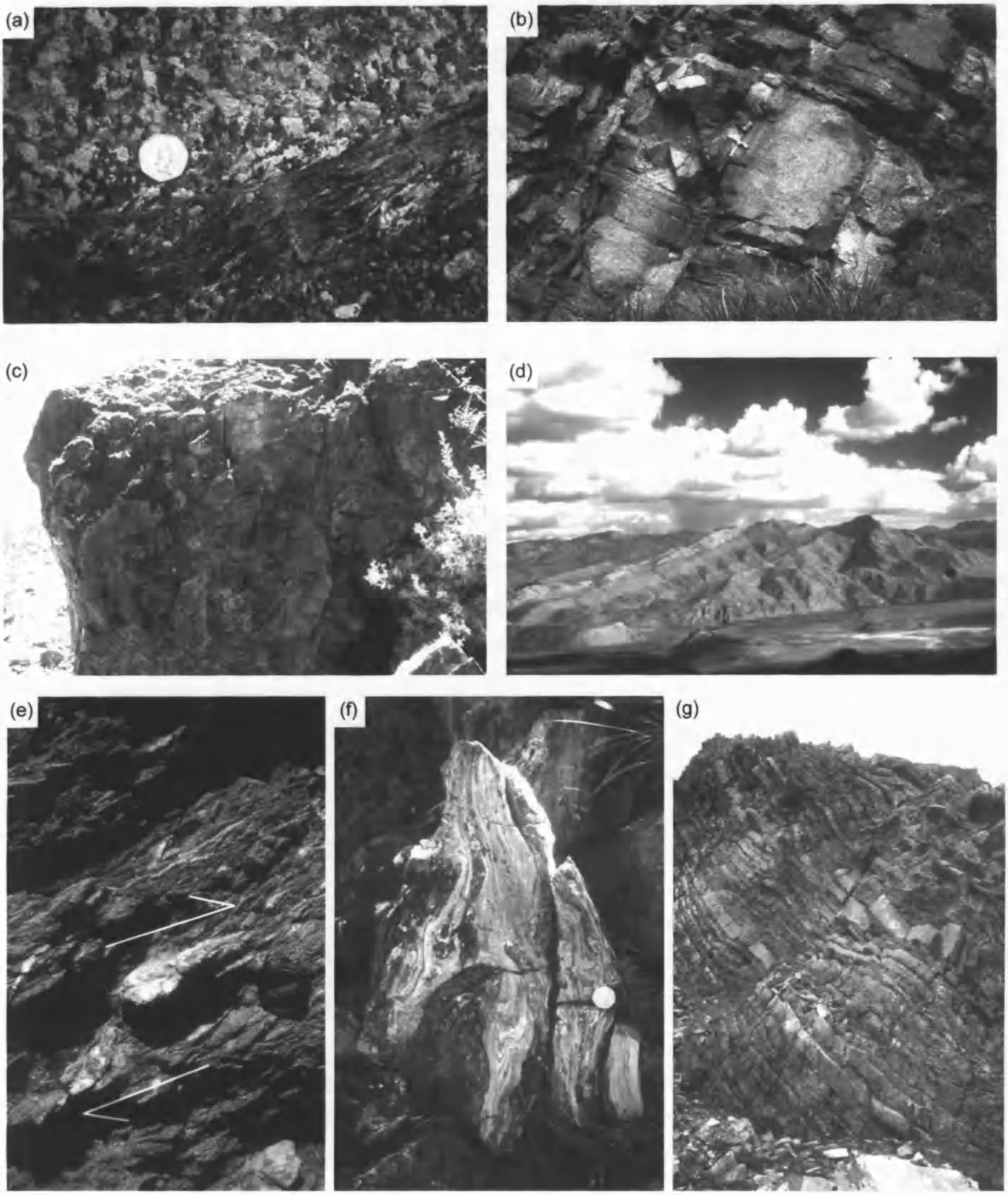

Fig. 2.6:. Photographs illustrating typical lithologies of major tectonic units. (a-c) Ophiolitic rocks: (a) Gabbro with a small ductile shear zone, (b) Sheeted dykes (c) Aphyric pillow basalt, (d) View looking east of bedded sedimentary rocks in the Haluut Bulag mélange. The darker rocks in the centre are interbedded basaltic lavas, (e) View looking NW of asymmetric calcite boudin in the Dzag zone suggesting top-to-the NE shear, (f-g) Burd Gol mélange: (f) SE view of deformed limestone surrounding fragments of basalt, (g) Calc-turbidite beds looking SE. (See also Appendix A)

On the western bank of the Uldzit Gol (Fig. 2.5; N46° 33.640', E99° 43.625') outcrops of well-preserved pillow basalts contain inter-pillow limestone and chert, and are locally overlain by bedded black chert and limestone. This is the only location where bedded sedimentary rocks were observed to be in direct contact with the pillow basalts. Neither the cherts nor the limestones were found to contain fossils, but Ryantsev (1994) reported lower Cambrian sponge spicules from the same unit.

Haluut Bulag mélange

The Haluut Bulag mélange is dominated by sedimentary lithologies. However, these lithologies are different from those of the Delb Khairkhan mélange, suggesting that the constituent lithologies of the two mélanges formed in different environments. The Haluut Bulag mélange contains lenses of limestone, sandstone, chert, tuff, minor acid volcanic material, and vesicular basalt. The basalts have a different composition to that of the ophiolite pillow basalts, that are enclosed in a pelitic matrix, which is itself lithologically heterogeneous. The matrix varies in composition from black shale to carbonate mudstone and quartzose siltstone. The matrix is metamorphosed to low-grade phyllite that surrounds coherent lenses that are commonly intensely fractured and internally brecciated.

Some very large km-scale blocks within the mélange in the Baidrag Gol transect, contain interbedded basalt, mudstone and limestone, with a shallow NE dip (Fig. 2.6d). These large blocks dominate the NW margin of the mélange for 12 km along strike at the contact zone with the Dzag zone.

Dzag Zone

the Dzag zone is composed of highly deformed pelitic and psammitic schists of lower greenschist grade containing rare 0.5 m wide layers of limestone. The composition of the schists varies slightly with higher muscovite contents occurring in the south immediately below the thrusted contact with the Haluut Bulag mélange.

Less metamorphosed fine-grained interbedded siltstones, sandstones and shales contain rounded quartz grains and preserved sedimentary structures (e.g. Bouma sequences and dewatering structures) and resemble slightly metamorphosed turbidites. Cleavage generally overprints and obscures primary bedding. However, approximately 5 km to the north of the town of Dzag (Fig. 2.2b), outcrops of the Dzag schists contain reasonably preserved pebbles of sandstone and siltstone despite penetrative cleavage development. Reconnaissance to the north of Dzag showed that the Dzag schists continue northeastwards over a cross-strike width of at least 10 km consisting of chlorite-muscovite-schists in which the amount of chlorite relative to muscovite increases, in a northwards direction, away from the thrust contact to the south.

Kurimoto *et al.* (1998) obtained a K/Ar date of 453.9 ± 9.1 Ma on white mica from a locality on the east side of the Baidrag Gol (N46°45.93', E99°26.98') close to the contact between the Dzag zone and the Haluut Bulag mélange and produced a second date of 447.4 ± 9.0 Ma from a second sample of Dzag schists near Bayan Obo village (N46°19.88', E100°14.50'). They interpreted these dates to represent an Ordovician regional metamorphic event.

Structural Characteristics

Despite the general continuity of lithotectonic units in the study area, the structural architecture of the Bayankhongor zone is complex and changes along strike. In this section we describe detailed structural observations from each of the three transects from west to east followed by observations made during reconnaissance mapping in areas to the east near Bayankhongor City.

Baidrag Gol Transect

Burd Gol mélange

The foliation in the matrix of the Burd Gol mélange dominantly dips shallowly (between 20° and 40°) south to south-west but is locally folded into gentle NE-vergent asymmetric folds. The folding becomes more intense and foliation in the matrix dips more steeply (80°) towards the unit's northern contact which is a thrust fault that places the mélange over Carboniferous marine mudstones to the north (Fig. 2.3)

Carboniferous sedimentary rocks & Southern Volcanics

Bedding in the Carboniferous rocks dips moderately to the SW (40° to 60°; Fig. 2.3) and contains evidence of brittle fracturing and brecciation. In this transect, the contact between the Carboniferous strata and the volcanic sequence appears to be an unconformable sedimentary contact (Fig. 2.3)

The dip of flows in the Southern Volcanics varies from about 60° SW to sub-vertical close to the contact with the Delb Khairkhan mélange to the north (Fig. 2.3). A weak shear fabric occurs preferentially along the chilled margins between successive flows and is most strongly developed near the thrusted contact between the volcanic rocks and the Delb Khairkhan mélange to the north. The foliation dips steeply to the SW, has a down-dip lineation, and C-S fabrics suggest top-to-the-NE shearing i.e. the volcanic sequence has been transported over the Delb Khairkhan mélange to the north (see cross section in Fig. 2.3).

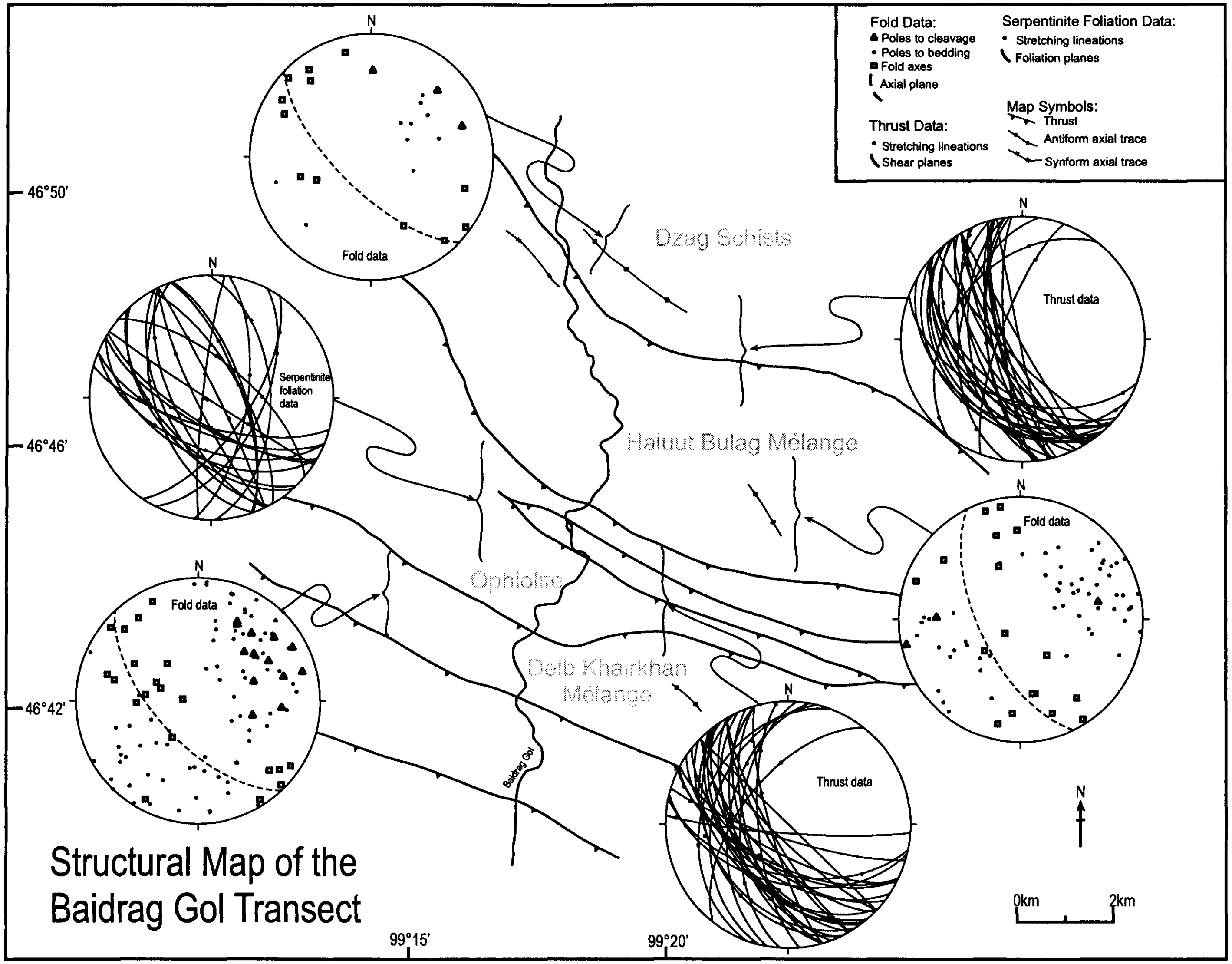

Fig. 2.7: Structural data from the Baidrag Gol transect. Fold data indicate SW-dipping axial planes consistent with NE-vergent thrusting. Shallow stretching lineations to WNW or NW, shown on thrust data plots, are consistent with shear sense criteria which suggest a sinistral strike slip component to the deformation. Foliation in the serpentinite mélange dips SW and ENE dips about a vertical axis due to fabric divergence around rigid lenses in the mélange, rather than folding. Lower hemisphere, equal area stereoplots. Refer to Fig. 2.3 for lithological relations.

Delb Khairkhan mélange

The structure of the Delb Khairkhan mélange is very complex. Foliation in the matrix generally dips between 40°-80° SW, but locally is vertical or dips steeply NE. Foliation generally strikes NW-SE but is locally deflected around more competent lenses that are elongate parallel to strike. Small-scale folds of the foliation with fold axes trending NW and axial planes dipping SW occur locally (Figs. 2.3, 2.7).

Quartz and chlorite stretching lineations show two major trends, either down dip to the SW or sub-horizontal plunge to the west or north-west, i.e. along strike (Fig. 2.7). SW lineations are most common. Asymmetric quartz boudins and rotated lithic clasts observed parallel to SW-trending lineations suggest top-to-the-NE movement, whereas shear sense where sub-horizontal lineations predominate is top-to-the-south-east or sinistral sense. Within the pervasively sheared mélange matrix, there are discrete zones of more concentrated shearing and brittle crushing. These high strain zones are marked by 20 to 30m-wide belts in which the matrix rocks have been fractured to form gouge-like clay, which contains a sub-vertical fabric. Slickensides trend around 285° with a near horizontal plunge. C-S fabrics parallel to the slickensides again suggest top-to-ENE movement. The boundary of the Delb Khairkhan mélange with the ophiolite is complex in this transect; it has an 'S' shaped map view (Fig. 2.3), reflecting repetition caused by thrust imbrication.

Ophiolitic Rocks

The ophiolitic mélange in the Burd Gol transect contains many large blocks and some near complete sections of ophiolite stratigraphy (Fig. 2.3). The largest blocks are at least 4 km long, and 2 km wide (Fig. 2.3) and the smallest are centimetre scale. Most of the larger blocks are composed of gabbro with cumulate layering dipping gently to the SW, but the dip direction is inconsistent in smaller blocks suggesting that these have been rotated during shearing.

A more complete ophiolite section crosses the Baidrag Gol (Fig. 2.3), the lowest unit is gabbro which contains an increasing number of doleritic dykes towards the north, culminating in local occurrences of sheeted dykes. However, the boundary between the gabbro-dyke unit and the sheeted dyke complex is tectonic (dipping SW) with the gabbro thrust over the sheeted dykes (Fig. 2.3). Although the general stratigraphic sequence has remained intact, the boundaries between units are sheared.

The sheeted dykes have trends consistent with dykes in the gabbro of between 280° and 300°, and dip to the SW (Fig. 2.3). Local shearing, with a SW dipping foliation, along the chilled margins of some individual dykes has produced internal breccias distorting the dyke-in-dyke relationships.

The serpentinite matrix forms low-lying easily eroded topography. The foliation in the serpentinite matrix dips steeply (60°-90°) to the SW or NE fanning around a vertical axis along strike. We interpret this to be due to the foliation diverging around rigid lenses as no evidence for folding was observed (Figs. 2.3, 2.7). Lineations are difficult to detect; the few that were observed are generally expressed by chlorite accumulations on shear surfaces and record variable directions (Fig. 2.7).

The overall width of the serpentinite mélange is variable along strike in the Baidrag Gol transect. Towards the west, the width of the belt increases to more than 15 km (Fig. 2.3). However, to the east the width narrows to about 1–2 km.

The contact between the serpentinite mélange and the Haluut Bulag mélange to the north is not well exposed due to low topography and grass cover. However, it is probably tectonic because foliation intensity increases towards the contact.

Haluut Bulag mélange

The matrix structure of the Haluut Bulag mélange is dominated by a well-developed SW-dipping shear fabric (Figs. 2.7) that is locally folded into NE-vergent asymmetric folds (Fig. 2.7), and a second weak cleavage is developed axial planar to these folds. Locally, the fold hinges become rotated due to development of minor orthogonal shears in the matrix causing it to be broken into blocks. Chlorite and biotite stretching lineations on the foliation planes trend either down-dip to the south-west or oblique to the west and north-west. C-S fabrics, rotated quartz clasts and asymmetric boudins in shear zones suggest top-to-the-NE shear sense consistent with that documented previously in the Delb Khairkhan mélange.

Dzag Zone

The contact between the Haluut Bulag mélange and the Dzag zone to the north is exposed in only one locality on the western bank of the Baidrag Gol near its junction with the Dzag Gol (Fig. 2.3, N46° 49.688', E99° 16.989'). There, the rocks of the Haluut Bulag mélange are thrust over the Dzag zone along a thrust fault which dips between 50° and 80° to the SW (Figs. 2.3, 2.7). The fault zone is about 20m thick and contains internally imbricated slices of the Dzag schists. The cleavage is deformed into asymmetric NE-vergent folds (Fig. 2.7). Minor fold axes have consistent shallow plunges to the NW, and a weak SW-dipping second cleavage is axial planar to the hinge zones. Abundant thin calcite and quartz veins cut the schists, and have been boudinaged and rotated parallel to the first cleavage. Lineations are not well developed in the contact thrust zone with the Haluut Bulag mélange, but those that are detectable suggest slightly oblique slip in a WSW-ENE direction. Shear sense indicators such as boudinaged veins (Fig. 2.6e) suggest top-to-the-NE shearing which is consistent with the NE vergence of folds of the first cleavage. Immediately to the north of this locality, outcrop exposure ends and grass covered plains obscure the geology around the town of Dzag (Fig 2.2b).

Darvsin Nuur Transect

Burd Gol mélange

The Darvsin Nuur transect is located approximately 40 km SE along strike from the Baidrag Gol transect (Fig. 2.2). In the Darvsin Nuur transect, the Burd Gol mélange is poorly exposed due to grass cover. However, the rocks that are exposed are dominated by pelitic schists with a penetrative schistose foliation that dips SW at approximately 40°-60°. The northern margin of the mélange is marked by a thrust contact with both the Carboniferous sedimentary rocks and extrusive volcanic sequence (Fig. 2.4).

Carboniferous sedimentary rocks &Southern Volcanics

The Carboniferous sedimentary rocks crop out in the SW of the transect area and increase in thickness towards the SW (Fig. 2.8). Bedding dips about 30° SW. The contact between the Carboniferous rocks and the Southern Volcanics is unexposed.

The Southern Volcanics are poorly exposed over a 5 km width but extends along strike to the NW and SE. Flows of basalt and dacite strike NW-SE and have a variable dip between 40° and 60° S or SW (Fig. 2.4). Locally developed sub-vertical ENE-WSW striking shear zones record dextral shear sense based on asymmetry of boudinaged calcite veins. These shear zones have a maximum width of 10 cm and are confined to the volcanic units. Near the contact of the volcanic series with the Delb Khairkhan mélange, to the north, a pervasive shear fabric is developed in the volcanic units with shear zones dipping approximately 50° to the SW. Quartz stretching lineations in the shear zones are down-dip and rotated clasts in the agglomerates suggest top-to-the-NE shearing or thrusting of the volcanic series over the Delb Khairkhan mélange (Figs. 2.4).

Delb Khairkhan mélange

The principal fabric in the Delb Khairkhan mélange becomes gradually steeper from 50° at the thrust contact to approximately 80° near the limestone at the summit of the Khain-Delb Khairkhan-Ula ridge (Fig. 2.4). The limestone is highly fractured and contains abundant calcite and quartz veins. Thin interbeds of shale dipping approximately 60° SW within the limestone have accommodated local shearing. On the north side of the ridge, there is a 300m wide zone of shale that is deformed into NE vergent open folds with minor fold axes plunging consistently 10°-30° NW (Fig. 2.4, 2.8). The area to the south of the contact with the ophiolitic rocks is a broad valley with only a few small isolated hills providing exposure of the mélange.

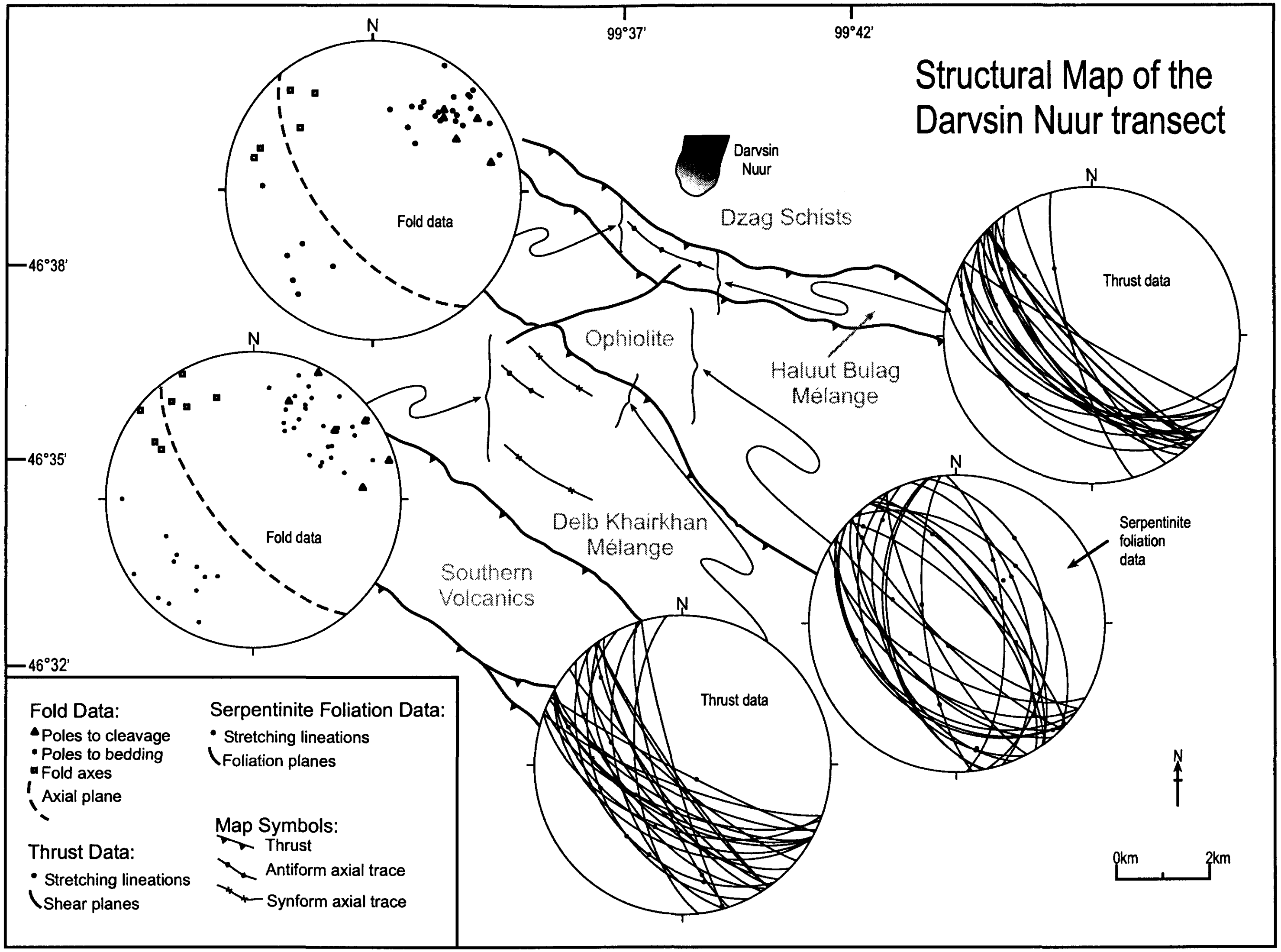

Fig. 2.8: Structural data from the Darvsin Nuur transect. SW-dipping thrust fabric and axial planes of folds are consistent with NE-vergence. Foliation in the serpentinite mélange is steep and fans about a NW-SE vertical axis. Lower hemisphere, equal area stereoplots. Refer to Fig. 2.4 for lithological relations.

On the north side of the mélange there is a small block of brecciated dolomite surrounded by foliated serpentinite forming a broadly sigmoidal outcrop pattern (Fig. 2.4). As well as the serpentinite outcrops, there are also some pillow basalt blocks in variable states of preservation near the contact of the Delb Khairkhan mélange with the ophiolitic rocks (Fig. 2.4) which contain a heavily sheared phacoidal texture, with individual phacoids forming rod-like structures. The long axes of the rods have variable orientations in individual blocks suggesting rotation between blocks. The matrix schists around these blocks have a more consistent foliation that dips approximately 70°-85° to the SW and in some places locally to the NE (Fig. 2.8). Amphibole and calcite stretching lineations on the foliation planes plunge shallowly WNW and asymmetric minor folds suggest thrust movement with a sinistral component. The contact of the Delb Khairkhan mélange with the ophiolitic sequence is not exposed, but is assumed to be tectonic due to well developed shear fabric close to the contact zone in both the pillow lava blocks and the matrix schists.

Ophiolitic Rocks

The large gabbro block on the west side of the area in figure 2.4 (N46° 37.000' E99° 35.000'), has well developed reticulate vein networks associated with local normal-sense shear zones. Other small shear zones with ductile characteristics (Fig. 2.6a) are not associated with veining but are also normal-sense. The normal-sense shears are confined to the gabbro block and may represent relict ocean floor faulting.

In the easternmost section, there is a very large block of pillow basalt and sheeted dyke rocks that extends into the Uldzit Gol section and has a more thrust-imbricate style of deformation (Fig. 2.4). The contact between the pillow basalt block and the sheeted dykes is sheared and is almost vertical but reliable indicators of shear sense were not found. The strike and dip of the dykes in this transect, and in the Baidrag Gol transect are similar, i.e. they strike NW-SE and dip 60°-80° SW (Figs. 2.3, 2.4). Flows in the pillow basalts dip steeply to the SW at around 60° to 80°.

Within the serpentinite matrix, small sheeted dyke lenses approximately 5m in length have their long axes orientated NW-SE parallel to the strike of the serpentinite foliation, which clearly diverges around and envelops the blocks. The dominant foliation dip is to the SW consistent with that observed throughout the transect (Figs. 2.4, 2.8). Serpentine and talc stretching lineations are either down-dip, or plunge shallowly to the NE or SW. Deviations from south-westerly dips occur in zones where there are large expanses of serpentinite without coherent blocks. The foliation in such areas generally has a near vertical to NE dip, possibly related to foliation fanning around vertical (Fig. 2.8). Generally, it is difficult to measure foliation planes because the serpentinite contains small phacoidal bodies rather than parallel cleavage planes.

At the contact zone between the serpentinite mélange and the Haluut Bulag mélange (Fig. 2.4), there are highly sheared pillow basalts on the south side and highly sheared limestones and pelitic rocks on the north side. On both sides of the contact a strong penetrative foliation dips 30°-50° to the SW (Fig. 2.8). Chlorite and quartz stretching lineations plunge in a SW or WSW direction. C-S fabrics and asymmetric quartz boudins parallel to these lineations suggest top-to-the-NE or top-to-the-east directed shear consistent with the general directions observed in the Baidrag Gol Transect.

Haluut Bulag mélange

The Haluut Bulag mélange is significantly thinner in the area of Darvsin Nuur than in the Baidrag Gol transect, reaching less than 2 km maximum outcrop thickness.

Cleavage planes in the mudstone, dip shallowly SW near the contact with the serpentinite mélange, but steeply NE towards the Dzag zone in the north. It appears therefore that the foliation is folded into a large NE-vergent open fold (Figs. 2.4, 2.8). Foliation is more strongly developed in the mudstones near the contact with the Dzag zone, suggesting a tectonic contact (Figs. 2.4, 2.8) but the actual contact is unexposed.

Dzag Zone

There is very poor exposure of the Dzag lithologies in this transect area due to low topography around Darvsin Lake.

Uldzit Gol Transect

Burd Gol mélange

The overall structure of the Burd Gol mélange is extremely complex with variable foliation strike and dip. As well as pervasive shearing within the matrix there are local areas of more concentrated shear. In the high strain zones, a near vertical penetrative foliation strikes NW-SE, and rocks have suffered intense brittle deformation and internal brecciation producing 5 m wide zones of clay gouge material. In one high strain zone, shearing has produced ductile mylonitic fabrics in limestone surrounding fragments of basalt (Fig. 2.6f). Away from the high strain zones large lenses of undeformed sedimentary rocks (Fig. 2.6g) are enclosed within the pelitic schist matrix. Near to the contact with the Carboniferous rocks to the north, the foliation in the mélange matrix becomes more uniform dipping to the SW. The contact is a thrust fault (Fig. 2.5) marked by a clear topographic break striking NE-SW. The pelitic schists and amphibolites in the Burd Gol mélange above the fault have a well developed cleavage dipping 4°-20° SW (Figs. 2.5, 2.9). Biotite and amphibole lineations on

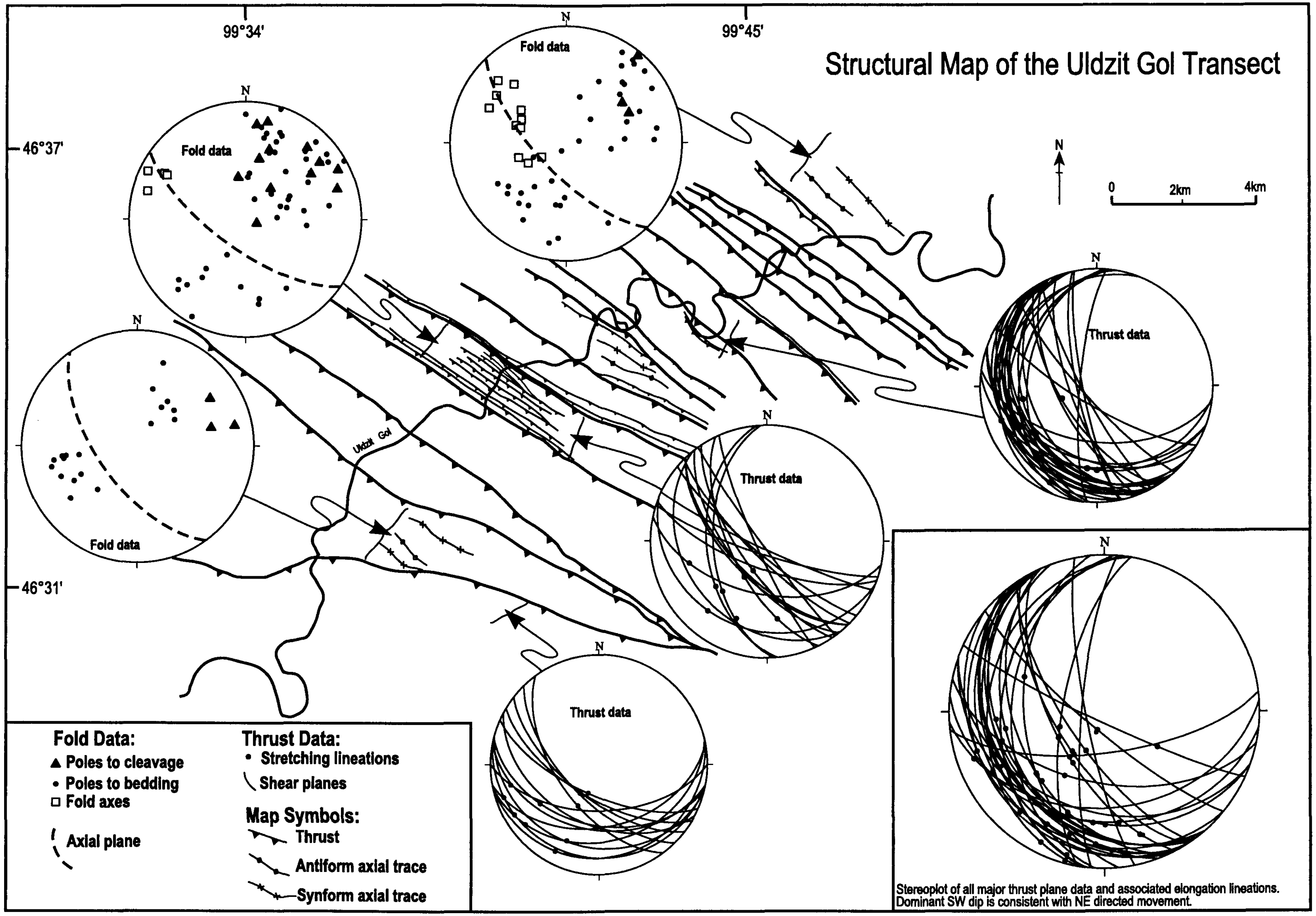

Fig. 2.9: Structural data from the Uldzit Gol transect. SW-dipping axial planes of folds and dominant SW-dipping thrust fabric suggest NE-vergent thrusting in the area. Lower hemisphere, equal area stereoplots. Refer to Fig. 2.5 for lithological relations.

the cleavage plane plunge consistently SW or WSW (Figs. 2.5, 2.9). C-S fabrics and rotated staurolite porphyroblasts within the matrix schists suggest top to the NE movement.

Carboniferous sedimentary rocks & Southern Volcanics

Directly beneath the thrust contact with the Burd Gol mélange in the footwall, Carboniferous limestones are mylonitised and the mylonitic fabric is folded into tight isoclinal folds inclined slightly to the NE. Fold axes plunge shallowly NW. The degree of mylonitisation diminishes to the north of the contact, where after 30 m the rocks lack shear fabrics and folds are more open in character (Figs. 2.5, 2.9).

Near the northern contact with the Southern Volcanics, the Carboniferous sedimentary rocks have a weak cleavage that dips steeply SW and is accompanied by brecciation of the mudstones. The volcanic rocks immediately on the north side of the contact are also foliated with the same dip and strike. The actual contact is not exposed and there are no reliable shear sense indicators, but it appears likely that the Carboniferous rocks have been thrust over the volcanic units based on the evidence for NE transport of the Burd Gol mélange and the NE-vergent folding within the Carboniferous rocks (Figs. 2.5, 2.9).

On the northern side of the Southern Volcanics, the rocks are weakly foliated with foliation dipping to the south or south-west (Fig. 2.5). Down-dip quartz stretching lineations and C-S fabrics suggest top-to-the-north or north-east, or thrusting of the volcanic and Carboniferous rocks over the Delb Khairkhan mélange to the north (see cross section Fig. 2.5).

Delb Khairkhan mélange

In this transect, the mélange is divided into two compositional and structural zones. The southern zone is lens-dominated and highly imbricated by thrusting with very little pelitic matrix (Fig. 2.5, cross section), whereas the northern section near the ophiolite is dominated by a pelitic matrix. Figure 2.10 shows a view across the imbricate zone looking NW. The northern and southern zones are separated by a zone of concentrated shearing (Fig. 2.5, N46° 34.000', E99° 39.000'), in which the matrix rocks have suffered intense brittle deformation and internal brecciation. This shear zone marks a metamorphic divide because the matrix rocks on the north side are more recrystallised with a greater abundance of muscovite and sericite defining the principal foliation. The dominant dip of the foliation is to the SW and there are some minor folds with axial planes that dip SW and quartz stretching lineations also plunge SW consistent with overall NE transport (Figs. 2.5, 2.9). Near the contact between the Delb Khairkhan mélange and the ophiolite, the foliation is more strongly developed suggesting a non-exposed tectonic contact.

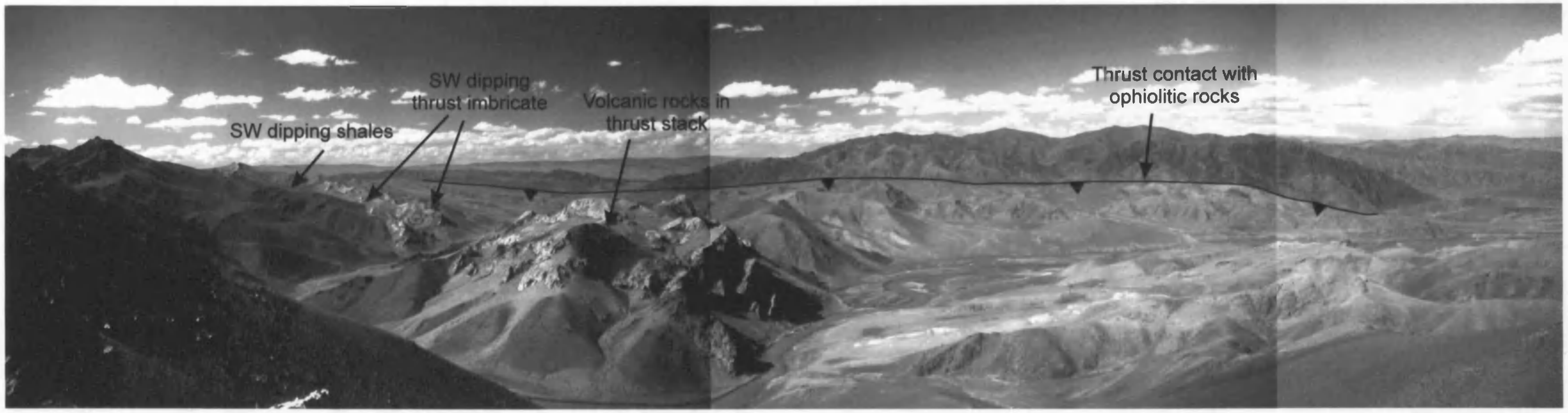

Fig. 2.10: Composite panoramic photograph looking NW across the Delb Khairkhan mélange to the thrust contact with the ophiolitic rocks in the Uldzit Gol Transect. Note that topography at the thrust contact with the ophiolitic rocks does not reflect resistance to erosion (see Fig. 2.3 for viewpoint location).

Ophiolitic Rocks

Immediately to the north of the Delb Khairkhan mélange is a block of aphyric pillow basalt that has pervasive SW dipping foliation. Small, locally developed shears dip N and contain C-S fabrics and offset veins that suggest normal shear sense. Surrounding these shears are zones of carbonate alteration and copper mineralisation. Since the normal-sense shears are confined to the pillow basalts we suggest that these structures may be relicts of ocean floor faulting.

SW dipping foliation becomes more pervasive to the north, close to the contact with a block of sheeted dykes, suggesting a sheared contact. Sub-horizontal chlorite stretching lineations plunge WSW or ESE, and rotated plagioclase phenocrysts parallel to the WSW lineation suggest top-to-ENE shearing. The sheeted dyke complex to the north has a total thickness of approximately 2.5 km but is actually composed of two sheeted dyke blocks juxtaposed along a large thrust fault which has caused the dyke rocks to have a strong shear fabric throughout an area 100m wide (Fig. 2.5). The dykes strike NW, consistent with those observed in the other two transects, but in contrast they dip NE.

A large gabbro body to the north contains several dykes intruded along NNE dipping shears in the gabbro body. The dykes have been boudinaged into a series of sigmoidal lenses enclosed in mylonitised gabbro. Rotation of phenocrysts in the gabbro and C-S fabrics in the dykes suggests that the shears are normal sense. Locally dykes form complex reticulate networks, which end abruptly in shear zones that offset the dykes suggesting normal shear sense. The normal shears are confined to the gabbro block and do not extend into the surrounding serpentinite mélange.

The northernmost section of sheeted dykes at the contact with the Haluut Bulag mélange has a prominent foliation which dips steeply to the SW

Haluut Bulag mélange

On the west side of the Uldzit Gol, the Haluut Bulag mélange is very thin and is composed of only a single massive limestone block. On the eastern side of the Uldzit Gol, the mélange widens and is dominated by pelitic schists with small lenses of sandstone and siltstone. Foliation in the schists dips variably to the SW (Fig. 2.9). Near the contact with the Dzag zone, schistosity becomes steeper (up to 80° to the SW) and more pervasive (Fig. 2.9).

Dzag Zone

The foliation of the schists in the Dzag zone immediately north of the contact, is folded and kinked into open, NE vergent asymmetric folds (Fig. 2.5, 2.9). Chlorite stretching lineations on the foliation plane plunge SW (Figs. 2.5, 2.9) and asymmetric boudinaged calcite veins viewed parallel to the lineation direction suggest top-to-the-NE shearing,

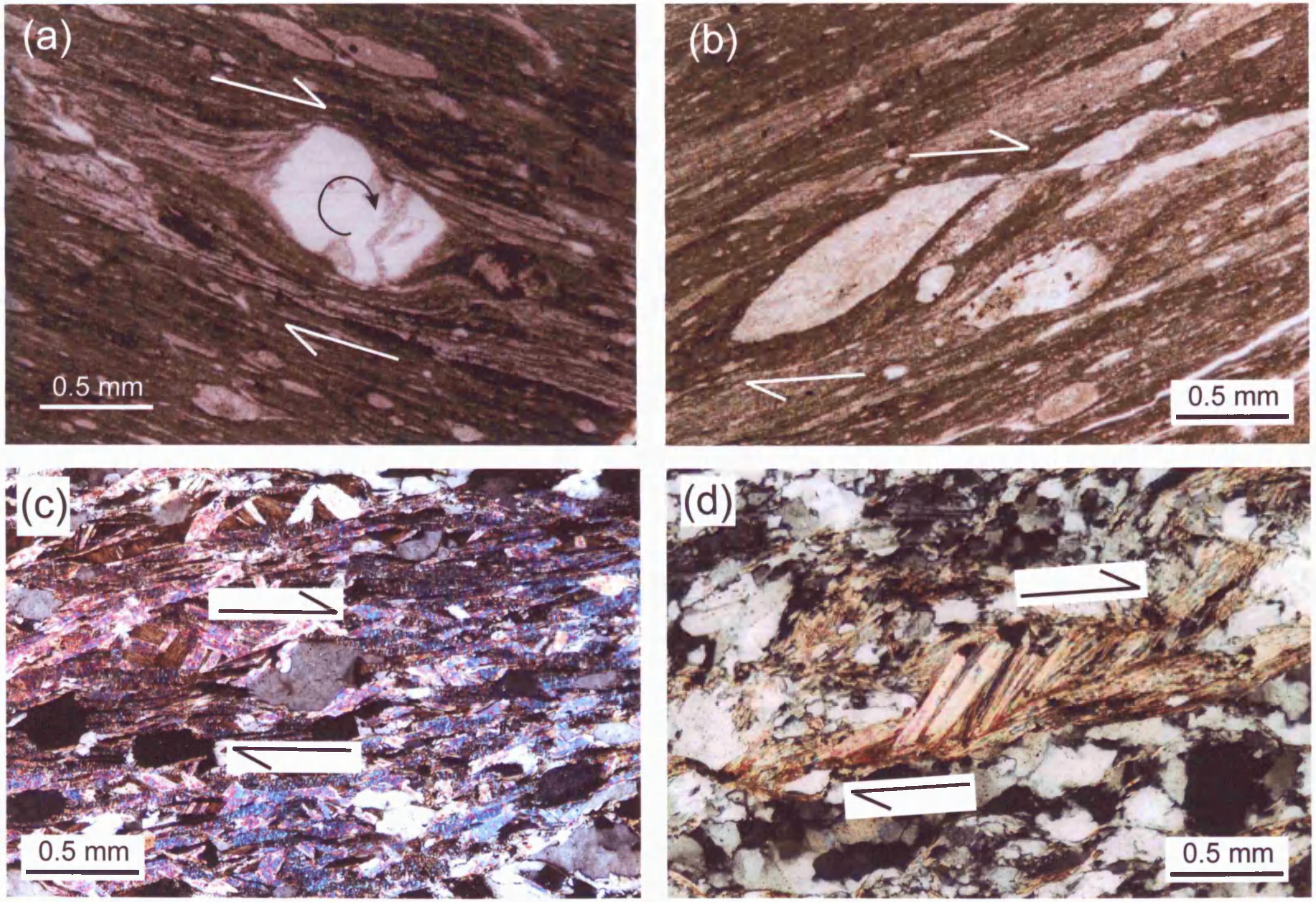

Fig. 2.11: NE vergent microstructural kinematic indicators. (a)-(b) Sheared basalt samples from thrust contact between ophiolite mélange and Haluut Bulag mélange. (a) Clockwise rotated (NE vergent) plagioclase crystal displacing cleavage fabric. (b) Boudinaged sericite epidote pseudomorph after plagioclase, forming σ-type top-to-NE shear sense indicator. (c) Quartz-mica schist from Delb Khairkhan mélange collected near to thrust contact with ophiolitic mélange. σ-type quartz porphyroblasts and mica fish indicate top-to-NE shearing. (d) Quartz-muscovite-chlorite schist from the Dzag Zone collected near to thrust contact with Haluut Bulag mélange. Rotated mica plates indicate top-to-NE shear sense.

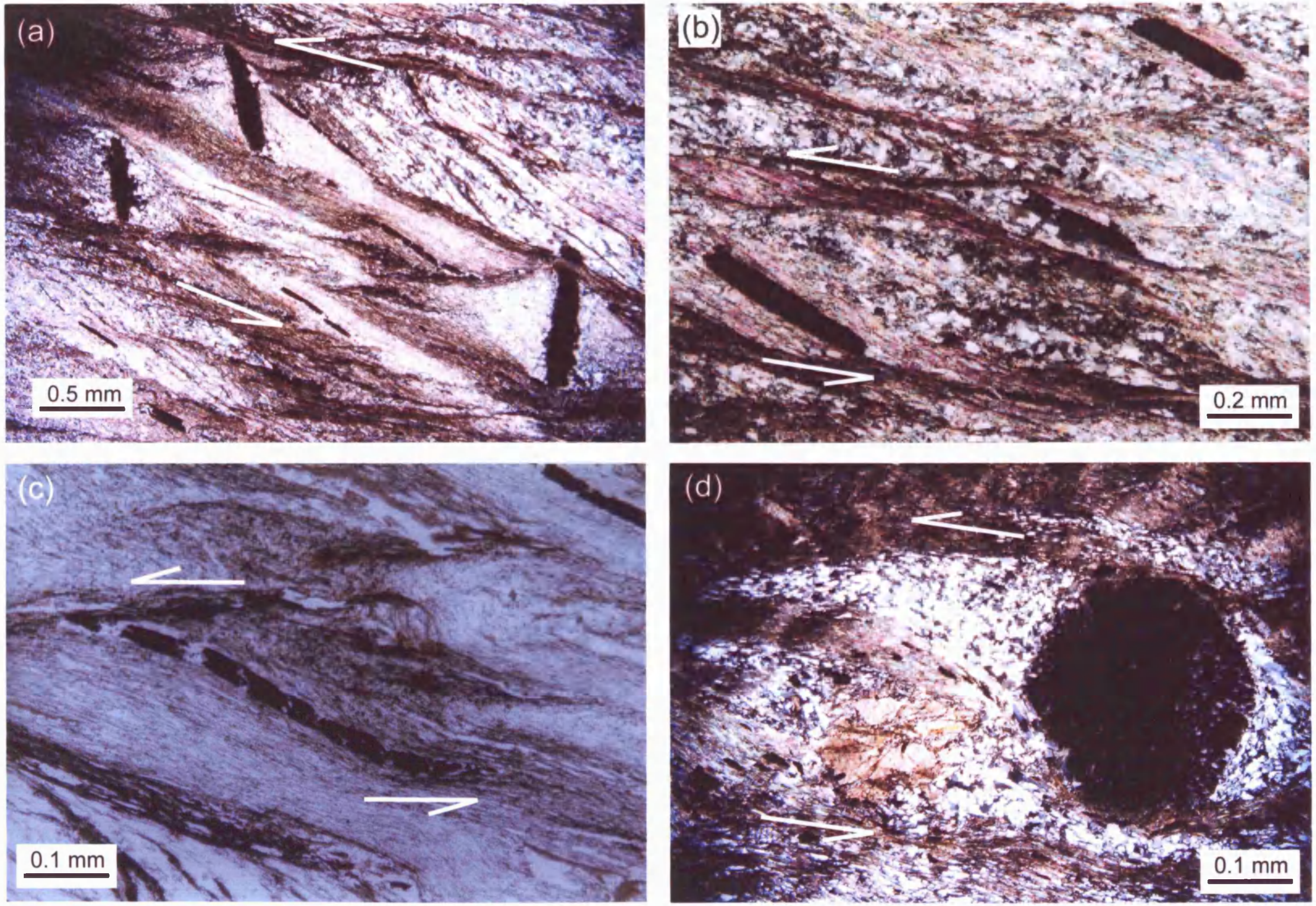

Fig. 2.12: NE vergent microstructural kinematic indicators. (a)-(c) Quarts mica schists from the Burd Gol mélange, collected near to contact with Delb Khairkhan mélange east of Uldzit Gol transect. Opaque (graphite ?) porphyroblasts are rotated and extended in direction of shear. Quartz σ-type mantles and mica fish indicate top-to-NE sense of shear. (d) Garnet-biotite-mica schist from the Burd Gol mélange, collected near to thrust contact with Carboniferous mudstones in Uldzit Gol transect (see Fig. 2.5). σ-type quartz mantles around rotated garnet porphyroblast and biotite porphyroblast indicate top-to-NE sense of shear.

consistent with the general shear directions recorded throughout the transect (see cross section Fig. 2.5).

Microstructural kinematic indicators

In order to confirm the sense of shear suggested by macro-scale shear sense indicators in the field, orientated samples were collected for microstructural analysis. The samples were collected from the shear zones along major thrust contacts between the ophiolite mélange and Haluut Bulag mélange (Figs. 2.11a & 2.11b), Delb Khairkhan mélange and ophiolite mélange (Fig. 2.11c), Dzag schists and Haluut Bulag mélange (Fig. 2.11d), the Burd Gol mélange and Delb Khairkhan mélange (Figs. 2.11a-c), and the Burd Gol mélange and Carboniferous sediments (Fig. 2.11d). All of the samples collected have shear sense indicators that suggest top-to-the-NE shearing, consistent with that observed in the field.

Reconnaissance observations near Bayan Obo and Bayankhongor City

Reconnaissance studies were carried out to assess whether the structural observations made in the three transect areas continue along strike to the SE.

Near Bayan Obo village (Fig. 2.2b) the same lithotectonic units of the Delb Khairkhan mélange, ophiolite zone and Haluut Bulag mélange were found but without the Carboniferous sedimentary rocks or volcanic sequence. The structures in the three mélange units are consistent with those observed in the transect zones i.e. a SW-dipping foliation and top-to-the-NE shear sense. However, the sub-linear arrangement of units breaks down near Bayankhongor City, where it becomes difficult to discern individual mélange units. Sporadic outcrops of ophiolite lithologies are surrounded by shale and limestone. Unfortunately, the degree of exposure is very poor making it impossible to carry out detailed structural investigations. Delor (1999) produced an Ar-Ar age of 484 ± 5.9 Ma of hornblende from a foliated pillow basalt collected just SW of Bayankhongor City which was interpreted as the age of metamorphism.

The Dzag schists to the north of Bayankhongor City have slightly different structural characteristics with foliation commonly dipping steeply NE. However this is variable along strike and because the average dip value is approximately 80° this variation could simply be the result of steep cleavage fanning.

Discussion

The above data show that all three transects share structural and lithological similarities that can be extrapolated over the entire 300 km strike length of the ophiolite zone. The main

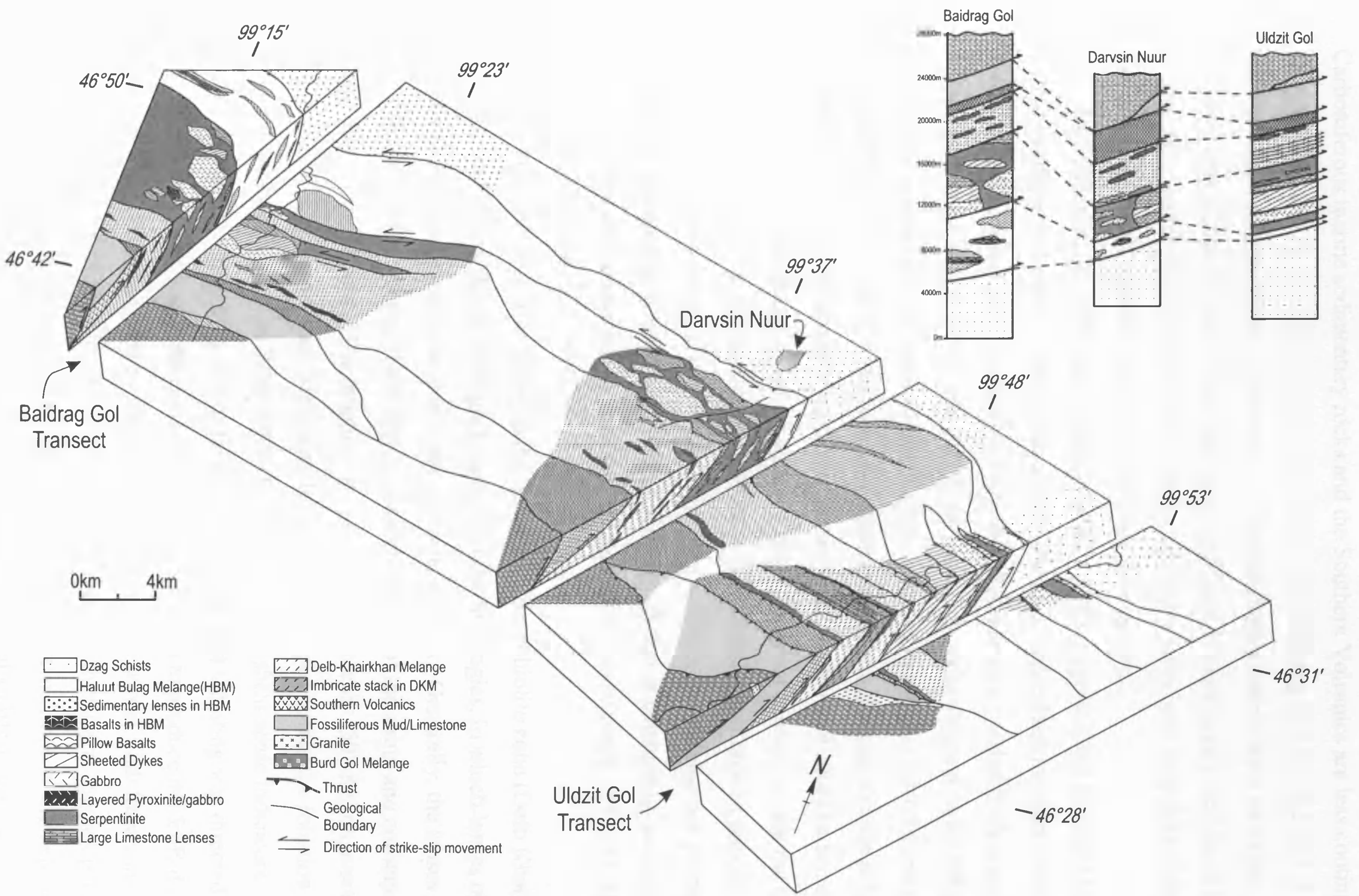

Fig. 2.13. Block diagram illustrating interpreted along-strike linkage of lithological units and major faults within the Bayankhongor ophiolite belt. Continuity of units and structures in unmapped areas is interpreted from geomorphic relations and aerial photograph analysis. Schematic columns represent correlation of tectonic stratigraphy between transect areas. Dotted tie lines represent interpreted correlation between boundaries along strike. Note discontinuous nature of the Carboniferous mudstones and the changes in thickness of other units.

subdivisions of the Burd Gol and Delb Khairkhan mélanges, ophiolitic rocks, Haluut Bulag mélange and Dzag zone can be traced continuously along strike (Fig. 2.13). In contrast, the Carboniferous marine sedimentary rocks and the Southern Volcanics are less continuous and occur only locally in the transect areas (Fig. 2.13), but not along strike to the east as shown by reconnaissance investigations. Moreover, the Carboniferous sedimentary rocks are discontinuous within the individual transect areas (Fig. 2.13) and have experienced less intense deformation than the other lithological units as the beds have only been tilted to the SW or gently folded without penetrative cleavage development.

Mitrofanov *et al.* (1985) and Komarov *et al.* (1999) suggested that the Burd Gol mélange represents a passive margin sequence. Although bedded sedimentary rocks in unconformable contact with the Baidrag block could constitute a passive margin environment, we believe that the highly mixed and structurally complex rocks adjacent to the ophiolite zone constitutes a subduction accretion complex. The Burd Gol mélange is also the most highly metamorphosed unit locally containing amphibolite grade staurolite and kyanite schists. The increase in metamorphic grade towards the contact with the ophiolite could be because deeper sections of the accretionary wedge are exposed along the thrust contact, or that the contact itself represents the site of the original subduction zone and locus of highest pressure metamorphic assemblages. The abundant quartz veins within the mélange are probably products of dewatering of sedimentary rocks and dehydration of subducting oceanic crust similar to those described from modern accretionary environments such as Nankai in Japan (Agar 1990; Maltman *et al.* 1992).

All three mélanges that make up the Bayankhongor ophiolite zone (Delb Khairkhan, ophiolite, and Haluut Bulag mélanges) contain similar lithologies, in which lenses of competent rocks are enclosed within a less competent matrix. Generally, the lenses are largely undeformed, whereas the matrix has absorbed most of the strain and consequently has a well-developed foliation. The foliation consistently dips steeply (50°-80° on average) to the SW (Figs. 2.7-2.9). In addition, stretching lineations developed within the foliation plane trend uniformly to the SW or WSW-ESE (Figs 2.7-2.9), and shear sense indicators consistently suggest top-to-the-NE or ESE. It is possible that thrusting was directed first to the NE and then there was a change in stress field conditions to produce the ESE-directed strike-slip movement indicated by the shallow lineations. However, both lineation orientations are defined by chlorite and quartz which deform ductiley at low temperatures (<400°C), thus both directions of movement may have been synchronous and deformation may have been partitioned between NE-directed thrusting and sinistral strike-slip displacements in an overall transpressional regime. However, with the present data it is impossible to conclude definitively whether this is the case or if deformation was partitioned in time. The fact that folding in the Dzag zone is consistently NE-vergent might suggest that the ENE strike-slip zones are a more localised feature within the ophiolite zone. We suggest that combining the overall thrust movement with a strike-slip component is a mechanism by which mélanges can be created that have complexly mixed lithological lenses, but within clearly defined boundaries i.e. only ophiolitic rocks in the serpentinite mélange. Thus internal divisions are mixed, but original facies boundaries are commonly retained (Fig. 2.13). An exception to this is within the Delb Khairkhan mélange where ophiolitic lenses such as pillow basalts and serpentinite (Figs. 2.3, 2.4) are included in the sediment-dominated mélange, presumably due to localised mixing along the contact where a sinistral strike-slip component of deformation has occurred. There are some slight differences in the style of deformation of the mélange units along strike. The most notable example is in the Uldzit Gol Transect where the Delb Khairkhan and serpentinite mélanges contain an imbricate thrust stack instead of a pervasively sheared mélange (Fig. 2.5). This is probably because where imbrication has occurred, the mélanges contain less mechanically weak matrix and accommodate shortening by discrete thrust motion between more rigid lenses.

Lithological variations within the Delb Khairkhan mélange suggest that the mélange is derived from different tectonic environments. The large limestone lenses that locally contain stromatolites, and sandstone and conglomerates suggest a shallow water environment, whereas the fine muds and siltstones which comprise the protolith for the matrix schists suggest deeper water environments. Together, these rocks may represent sediments from the trench of a subduction zone with the limestones and sandstones being shed from the top of the accretionary wedge and the pelitic rocks of the mélange matrix representing pelagic mudstone scraped from the ocean floor.

The Dzag schists to the north of the ophiolite zone have previously been interpreted as part of an accretionary wedge (Dergunov *et al.* 1997). We believe that thick and lithologically monotonous chlorite mica schists, may have once been clastic turbidites and more likely represent a deep-water passive margin or more specifically continental rise sequence than an accretionary wedge. In addition, the Haluut Bulag mélange which is composed dominantly of limestone lenses in a pelagic matrix also contains vesicular basalts suggesting subaerial eruption. These rocks may have been shed from a continental margin to the north onto the continental rise as debris flows and subsequently incorporated into the mélange during obduction of the ophiolite.

Previously, there has been disagreement over the direction of obduction of the ophiolite and the vergence of structures. Tomurtogoo (1989, 1997) suggested that the ophiolite was thrust to the SW based mostly on inferred dip of stratigraphic units, whereas Kopteva *et al.* (1984), Ryantsev (1994) and Dergunov *et al.* (1997) recognised SW-dipping faults and suggested NE-directed thrusting based on the palaeontological age of the units available. We agree with the latter opinion based on the evidence presented here of consistent SW-dipping structures and shear sense indicators which suggest NE or ENE movement.

The ophiolite contains a complete igneous stratigraphy of serpentinised ultramafics, gabbro, sheeted dykes, and pillow lavas, as described by Moores (1982). We interpret the rocks to have formed at a spreading centre based on the stratigraphic relations, presence of sheeted dykes, and relict normal faults that presumably formed during sea-floor spreading. What remains unclear is whether the rocks formed in an open ocean or a marginal back-arc basin associated with a subduction zone. The discovery of limestone in spaces between pillow basalts suggests that the ophiolite formed in an environment above the carbonate compensation depth, but conversely, local occurrences of chert suggest a deeper water environment. As there are no other sedimentary rocks in direct contact with the ophiolite and since dismemberment makes it difficult to determine how thick the ocean crust was, we cannot draw any more substantive conclusions. The only current published geochemical data available on the ophiolitic lithologies are in Kepezhinskas *et al.* (1991) which ambiguously show some MORB characteristics together with indications of a modified source, possibly a plume. The evidence for a shallow water environment shown by the interpillow limestones suggests that this was not a normal Atlantic-type ocean basin. A more detailed environmental model requires a better geochemical database.

The chronology of deformation in the area is complex and the age of obduction of the ophiolite remains controversial. Deformation occurred in the Burd Gol mélange as early as 699 Ma (Teraoka *et al.* 1996) which implies that subduction was occurring from at least this time, well before the obducted ophiolitic rocks were formed at 569 ± 21 Ma (Sm-Nd mineral and whole rock isochron; Kepezhinskas *et al.* 1991). Dates relating to metamorphism of the Dzag schists cluster around 450 Ma (K-Ar method on white micas; Kurimoto *et al.* 1998) and combined with the Ar-Ar age of 484 Ma (Delor, 2000) from the ophiolite itself suggests that obduction may have occurred around this time. However, this age could equally relate to post obduction metamorphism. The inclusion of the Carboniferous sedimentary rocks within the thrust imbricated succession may suggest that deformation was continuous until post Carboniferous times. However, since the sediments are less penetratively deformed than the other units, we suggest that these represent an overlap assemblage, deposited after major deformation associated with ophiolite obduction and mélange deformation in the Bayankhongor area. Post-Carboniferous reactivation of the Bayankhongor zone may be related to late Palaeozoic tectonic events in southern Mongolia (Hendrix *et al.* 1996; Lamb and Badarch 1997; Höck 2000), but the actual extent of these deformational events in the Southern Hangay region is poorly resolved. Work in progress will hopefully lead to more precise dating and will allow a more detailed evolutionary history to be developed

Because the area is dominated by sedimentary mélanges, it could be suggested that Şengör *et al.*'s (1993) model of a vast accretion complex applies to this area. Moreover, the occurrence of andesitic dykes intruding the Burd Gol mélange and the intermediate volcanic sequence to the north (Fig. 2.13), could be interpreted to represent incipient arc formation, with the arc built on top of the accretionary wedge. This architecture is a prominent feature of the Şengör *et al.* (1993) model. However, an implicit part of their model is that the accretion zone has a continuous history, therefore ophiolites represent offscraped fragments within the complex rather than discrete sutures. It seems unlikely that an ophiolite fragment 300 km long would remain intact and unmixed with the rest of the rocks in an accretionary wedge. In addition, other small ophiolite occurrences less than 300 km to the east and west suggest that the ophiolite extends further along-strike (Fig. 2.2). Moreover, current work in Tuva (southern Siberia) by Pfänder *et al.* (1999) has identified ophiolite occurrences also dated at 569 ± 1.0 Ma (Pb-Pb on single zircon) suggesting that these ophiolites may be genetically related to the Bayankhongor ophiolitic rocks. Also, growing evidence for a continental block beneath Hangai (e.g. Sm-Nd model ages of Kovalenko *et al.* 1996) suggests that the Bayankhongor ophiolite marks a collisional suture between the Baidrag and Hangai continents.

Our preferred interpretation is that the Bayankhongor ophiolite represents a suture marking the position of a now inactive subduction zone between the Baidrag block to the south, and the Dzag zone to the north. Subduction was to the SW based on the dominant polarity of thrusting with the Burd Gol mélange representing an accretionary wedge built up against the Baidrag continental block to the south. The ophiolite was obducted in a north-easterly direction over the Dzag zone which may have been part of a passive margin of a continent located beneath the sedimentary cover of the Hangai region. Future work along strike is needed to establish whether the ophiolite belt can be traced into neighbouring regions and therefore constitutes one of the major suture belts of Central Asia.

Published in the Journal of the Geological Society, London, ***158**, 2001, pp. 445-460.*

Co-authors: Dickson Cunningham, Brian F. Windley & D. Tomurhuu

Chapter 3:

Tectonic environment of formation of the Bayankhongor Ophiolite, Central Mongolia: geochemical and Nd isotopic constraints.

Introduction

The Central Asian Orogenic Belt (CAOB) is a complex collage of continental blocks, island arc terranes and fragments of oceanic crust that was amalgamated during the Palaeozoic to Mesozoic. Growing evidence supports a mechanism of continental growth by subduction-accretion with punctuated collisions forming ophiolitic sutures between accreted blocks (Coleman 1989, Hsü *et al.* 1991, Mossakovsky *et al.* 1994, Buchan *et al.* 2001). Despite an improved understanding of the crustal growth mechanism, there is disagreement about the pre-accretion architecture of the orogen and demarcation of individual blocks. Ophiolites are of great importance in understanding the pre-accretion history of orogenic belts because in most cases they define the collisional suture line between accreted terranes and hence the position of the ocean basin that once separated them. Therefore, in order to understand the subduction-accretion history of the CAOB it is important to define the tectonic environment in which the ophiolites, and hence former ocean basins, of Central Asia were formed. Mongolia presents an exceptional opportunity to examine this problem because it occupies a central position within the CAOB (Fig. 3.1) and contains some of the best preserved ophiolites in Central Asia with over 60 reported occurrences (Fig. 3.1). Despite their abundance, few Mongolian ophiolites have been studied using modern geochemical and isotopic techniques and therefore petrogenetic models for their creation are rare. The Bayankhongor ophiolite is the largest continuously exposed ophiolite in Mongolia and possibly all of Central Asia (Fig. 3.1). This paper presents the results of the first comprehensive geochemical and Nd isotope study of the Bayankhongor ophiolitic rocks. The data are used to define the possible source(s) from which the ophiolitic magmas were extracted and hence gain a better understanding of the tectonic setting in which the oceanic crust was produced. In addition to the ophiolitic rocks, geochemical and isotopic data are presented for a previously unstudied suite of younger volcanic rocks, which lie to the south of the ophiolite (Southern Volcanics in Fig. 3.2). The data for the Southern Volcanics is used in combination with previously studied field relations and geochronological data (Chapter 4;

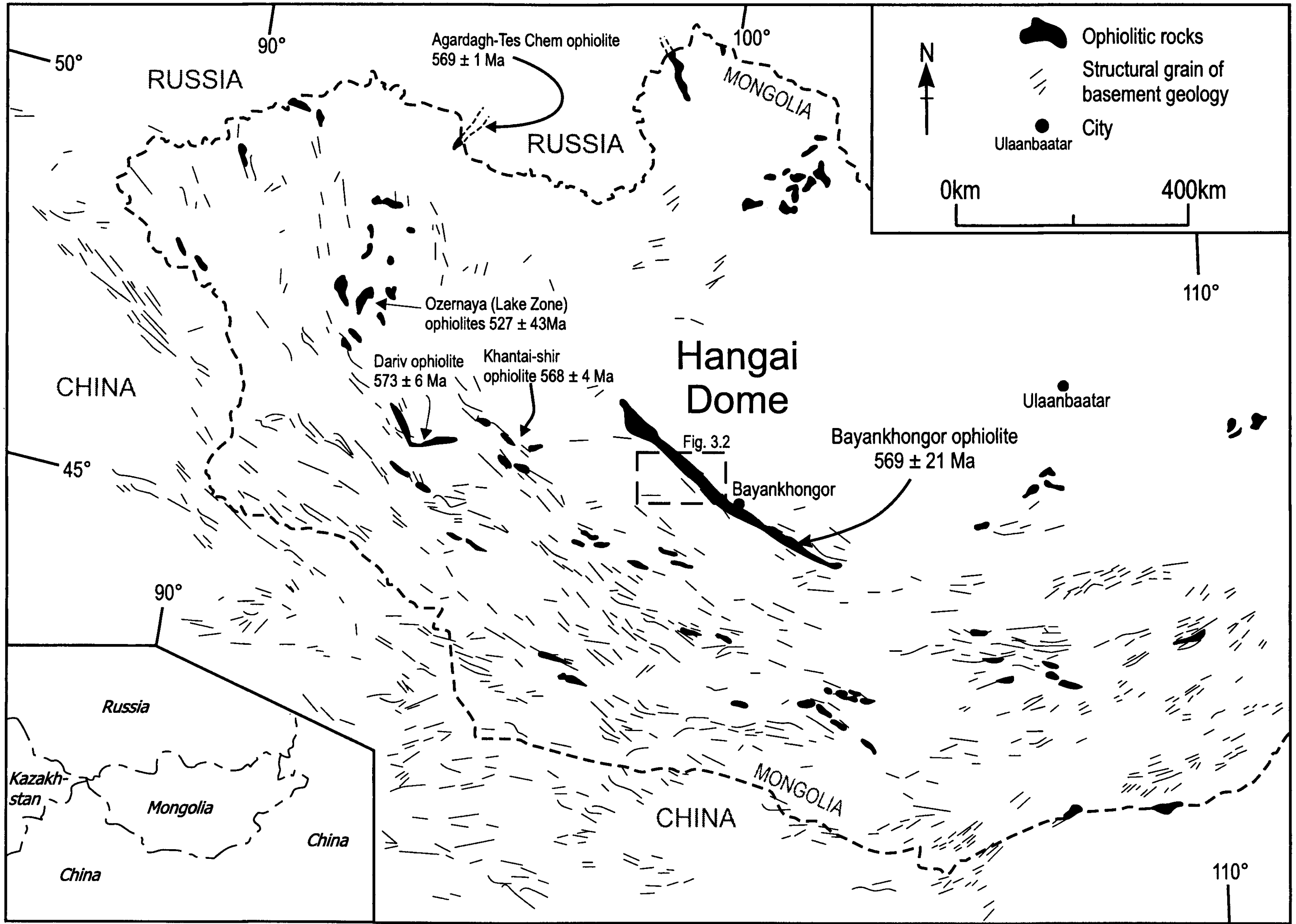

Fig. 3.1: Ophiolite occurrences in Mongolia. The Bayankhongor ophiolite is the largest. Isotopic age data for the highlighted ophiolites shows that they were created at around 570 Ma. The trace of basement structural grain indicates that these ophiolites occur along a gently curving semi-continuous belt. Sources of age data: Bayankhongor (Kepezhinskas et al. 1991), Khantaishir and Dariv (Salnikova *pers comm.*), Ozernaya (Kovalenko et al. 1996a) and Agardagh Tes-Chem (Pfänder et al. 1999).

Buchan *et al.* submitted), to suggest possible tectonic environments in which the rocks could have formed in relation to the subduction-accretion system which led to the obduction of the Bayankhongor ophiolite.

The tectonic models suggested here for the creation of the Bayankhongor oceanic crust are intended only as a working hypothesis, because the geochemical data alone do not point towards a unique interpretation. Nevertheless, the data provide important constraints on the evolution of the ophiolitic rocks and the subduction-accretion system that led to their eventual obduction.

Geological Setting

The Bayankhongor ophiolite zone (Fig. 3.1) is situated on the southern side of the Hangai dome that was regionally uplifted during the mid-late Cenozoic (Windley and Allen 1993; Barry and Kent 1998; Cunningham 1998, Cunningham 2001). The ophiolite forms a NW-SE striking sub-linear zone approximately 300 km long and up to 20 km wide (Figs. 3.1, 2). Previous lithological mapping enables a four-fold tectonic subdivision of the region from south to north: the Baidrag complex, Burd Gol mélange, Bayankhongor zone and Dzag zone (Fig. 3.2; Buchan *et al.* 2001; Teraoka *et al.* 1996; Tomurtogoo *et al.* 1998).

The Archaean Baidrag complex dated at 2650 ± 30 Ma (U-Pb zircon, Mitrofanov *et al.* 1985), is composed of tonalitic gneiss, granulite and amphibolite, with minor marble and quartzite; it is interpreted as a microcontinental block (Mitrofanov *et al.* 1985; Kozakov 1986; Kozakov 1997).

The Burd Gol mélange (Fig. 3.2) consists of lenses of sedimentary and igneous rocks enclosed in a matrix of pelite and graphite schists, which are cut by abundant quartz veins. From palaeontological interpretation of stromatolites in limestone lenses, Mitrofanov *et al.* (1981) suggested that the Burd Gol mélange is Neoproterozoic in age. Within the mélange, the metamorphic grade increases from greenschist to amphibolite facies towards the north (Chapter 2; Buchan *et al.* 2001). Metamorphic white-micas within the mélange have K-Ar ages ranging from 699 ± 35 Ma to 533 ± 3 Ma (Teraoka *et al.* 1996, Höck *et al.* 2000).

North of the Burd Gol mélange, there is a small area of interbedded marine mudstone and limestone which contain Carboniferous fossils (Fig. 3.2; Dergunov *et al.* 1997). Between the Carboniferous sedimentary rocks and the Bayankhongor ophiolite zone, there is a thrust-sliver of volcanic rocks, here named the Southern Volcanics (Fig. 3.2). The Southern Volcanics consist of multiple sheet flows of intermediate basalts, andesite, dacite, volcanic breccia, and local tuffs. The volcanic rocks are occasionally overlain by volcanogenic conglomerates and sandstone and are locally cross-cut by rhyolite dykes that have a crystallisation age of 474 ± 8 Ma ($^{207}Pb/^{206}Pb$ zircon evaporation Chapter 4; Buchan *et al.* submitted), which is taken as the

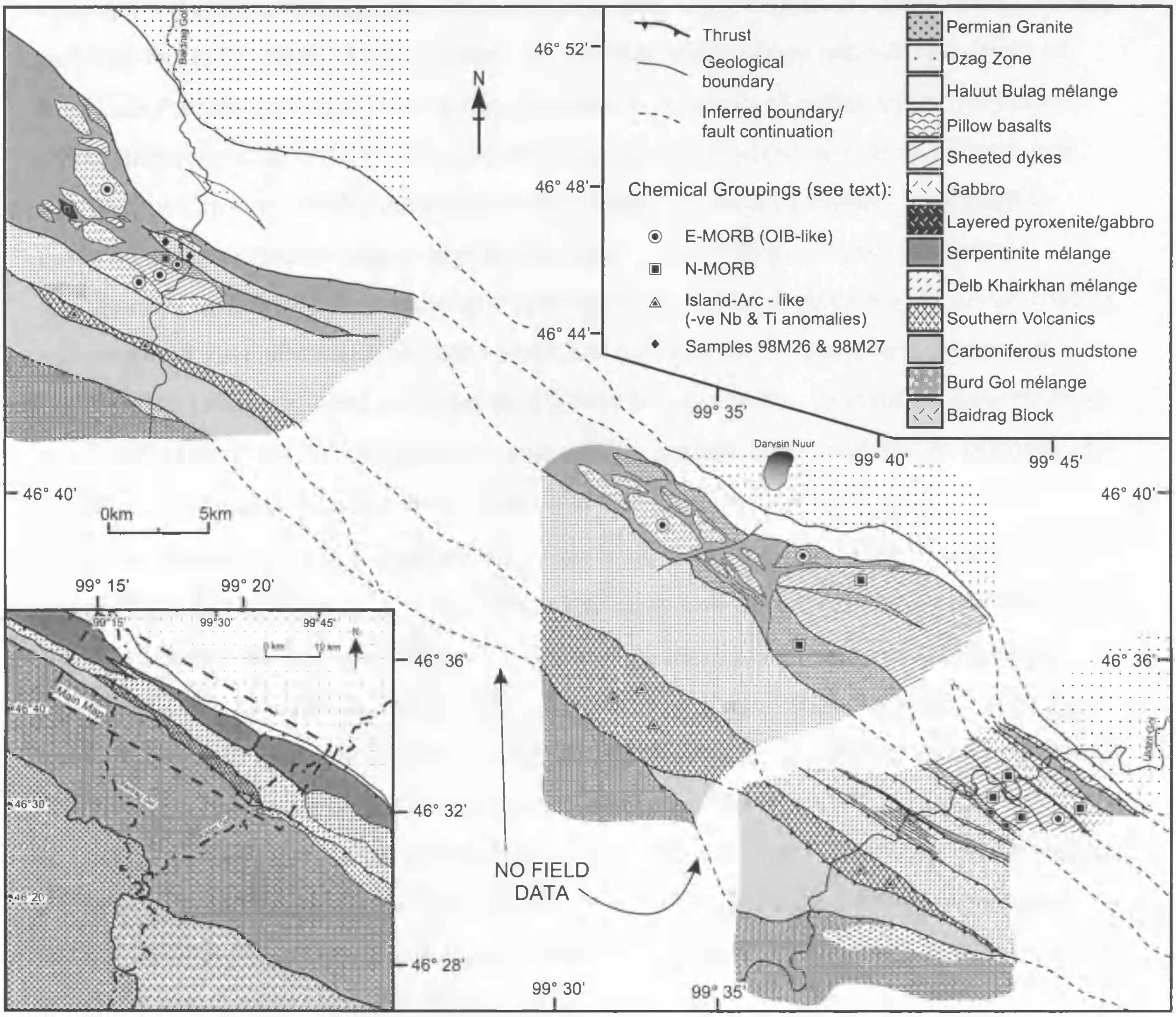

Fig. 3.2: Geological map of the transect areas studied for within the Bayankhongor Ophiolite Zone. Transects were located along well exposed river sections from west to east: Baidrag Gol, Darvsin Nuur, and Uldzit Gol. The approximate distribution of geochemical groupings discussed in the text is marked. Inset map shows larger-scale regional geology.

minimum age of formation for this volcanic sequence. The Southern volcanics and Carboniferous rocks have experienced less intense deformation than the rest of the major lithotectonic units in the Bayankhongor Ophiolite zone and as a result, are only locally brecciated in association with gentle folding.

The Bayankhongor zone is divided into three sub-units: the Delb Khairkhan mélange, ophiolite mélange, and the Haluut Bulag mélange (Fig. 3.2, Chapter 2). The Delb Khairkhan mélange lies to the south of the ophiolite and contains sedimentary and volcanic rocks of Mid-Late Precambrian to Ordovician age enclosed in a matrix of pelitic schists (Ryantsev 1994; Dergunov *et al.* 1997). The ophiolite mélange is composed of a complete ophiolite stratigraphy (Moores, 1982), dismembered into blocks of varying internal stratigraphic completeness, enclosed within a serpentinite matrix. The only previously published geochemical data for the Bayankhongor ophiolite rocks is that of Kepezhinskas *et al.* (1991), who reported trace element data from basalts and gabbros within the ophiolite mélange highlighting LREE enriched characteristics for the pillow basalts. In addition Kepezhinskas *et al.* (1991) analysed Nd isotopes for a leucogabbro sample, and calculated an isochron age of 569 ± 21 Ma (Sm-Nd hornblende-whole rock isochron) and initial $\varepsilon_{Nd(569)} = +11.9$, indicating an extremely depleted mantle source for the gabbro compared to a depleted mantle value of approximately $\varepsilon_{Nd(569)} = +8.7$ at this time (determined using models of De Paolo *et al.* 1988 and Stein and Hofmann 1994). To explain the chemical and isotopic nature of the ophiolitic rocks Kepizhinskas *et al.* (1991) suggested an origin by the ophiolitic rocks being produced by melting at a plume influenced mid oceanic ridge segment associated with major transform faults, similar to that documented in sections of the Mid-Atlantic ridge (Schilling *et al.* 1983). Kepezhinskas *et al.*'s (1991) Nd isochron age, compares well with more precise U-Pb ages for ophiolites along strike to the west (Fig. 3.1). The predominantly sedimentary Haluut Bulag mélange contains lenses of bedded limestone, sandstone, siltstone, and locally vesicular basalt, enclosed in a matrix of pelitic schist.

The Dzag zone (Fig. 3.2) consists of asymmetrically folded chlorite-mica schists that contain relict sedimentary features that suggest they were originally turbidites (Chapter 2; Buchan *et al.* 2001). K-Ar dates of white-micas associated with the thrust separating the ophiolite zone and Dzag zone range from 395 ± 20 Ma to 453.9 ± 9.1 Ma (Teraoka *et al.* 1996, Kurimoto *et al.* 1998) and are interpreted to reflect the time of collision and obduction of the ophiolite (Chapter 4; Buchan *et al.* submitted).

The structure of the Bayankhongor area is dominated by NW-SE striking, NE directed thrusts, which have juxtaposed the different litho-tectonic units. In addition the litho-tectonic units have been internally dismembered by sinistral strike-slip displacements, which have contributed to mélange formation. It is unclear whether the strike-slip deformation was a separate event from thrusting, but based on field observations presented in Chapter 2, it is suggested that the two were coeval in a NE directed transpressive regime.

The Bayankhongor ophiolite is interpreted as a suture marking the position of a Lower Palaeozoic subduction zone between the Baidrag block to the south, and the Dzag zone to the north. The Burd Gol mélange represents an accretionary wedge built up against the Baidrag continental block to the south. Subduction was to the southwest based on the dominant polarity of thrusting within the Bayankhongor ophiolite zone. The ophiolite was obducted in a north-easterly direction over the Dzag zone that represents part of a passive margin to a continent located beneath the sedimentary cover of the Hangai region (Chapter 2; Buchan *et al.* 2001).

Petrography of Bayankhongor ophiolitic rocks

The field characteristics of the Bayankhongor ophiolitic rocks, including large scale lithological and structural relations, are discussed in detail in Chapter 2 and so are not repeated here. A geological map of the study area is presented in Fig. 3.2. In this section the hand specimen and thin-section petrography of the ophiolitic rocks is presented. The stratigraphy is described from bottom to top beginning with the ultramafic section.

Ultramafic rocks

Dergunov *et al.* (1997) reported that the mantle section of the Bayankhongor ophiolite contains dunite and harzburgite tectonites, but in the areas examined for this study only serpentinised peridotites were observed. However, several 100m-scale mélange blocks were located which contain sections of layered cumulate pyroxenites (Fig. 3.2). The pyroxenites exhibit modal layering grading into mafic gabbros within 3-5m thick zones, where plagioclase content increases from approximately 5% to 30%. Clinopyroxene and orthopyroxene are dominant (approximately 60-80%) forming 5-15 mm anhedral crystals in an interlocking granular texture (Fig. 3.3a) with subordinate plagioclase. Some orthopyroxenes contain inclusions of small clinopyroxene crystals and a small percentage exhibit exsolution lamellae of clinopyroxene. The majority of the clinopyroxene crystals contain exsolution lamellae, which are also composed of clinopyroxene. Opaque minerals are the only apparent accessory phases. No olivine is preserved due to serpentinisation and mesh-like serpentinite makes up approximately 30% of the rock (Fig. 3.3b). Some clinopyroxenes are also serpentinised around their edges with resultant coronas of opaque minerals.

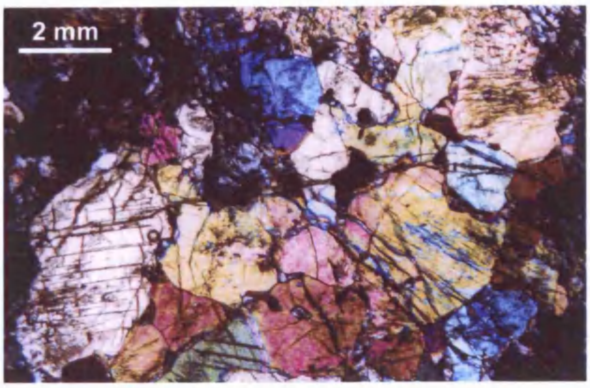

Fig. 3.3a: Pyroxenite sample 98M79. Example of typical granular texture of the Pyroxenites of the bayankhongor ophiolite. Large-interlocking anhedral clynopyroxene crystals dominate the field of view. A single orthopyroxene crystal exhibits first order grey birefringence colours in the bottom left corner of the picture. The top left corner contains serpentine and aggregates of opaque minerals after clinopyroxene.

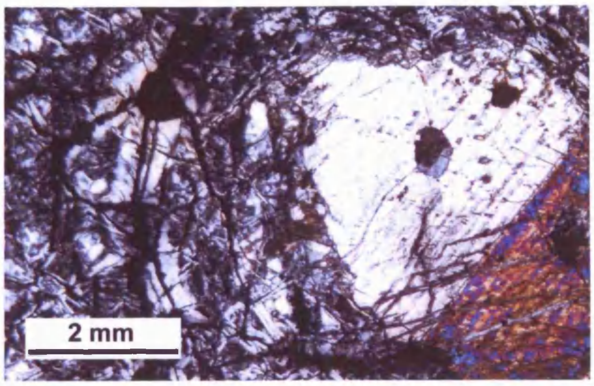

Fig. 3.3b: Pyroxenite. Left of picture is dominated by a large twinned augite crystal. The augite crystal is completely surrounded by and partially corroded by serpentine. The mesh textured serpentine typically comprises around 30% of the volume of pyroxenite samples and has possibly replaced olivine as well as clinopyroxene. Aggregates of secondary opaque minerals help to define the mesh texture.

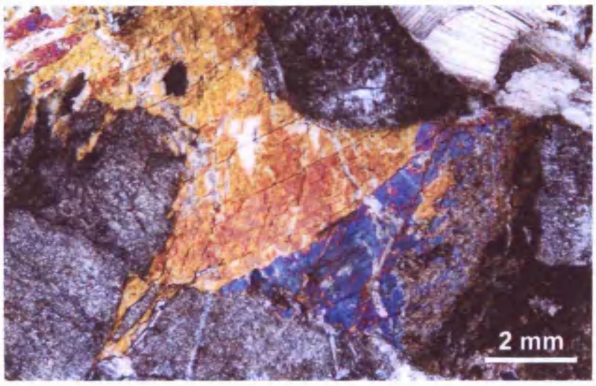

Fig. 3.3c: Gabbro. This picture illustrates the typical nature of the gabbros of the Bayankhongor ophiolite. The centre of the field is occupied by a large interstitial anhedral clinopyroxene crystal which is exsolving pigeonite in the top left corner. The interstitial site lies between 3 large plagioclase phenocrysts that are completely pseudomorphed by aggregates of sericite and epidote.

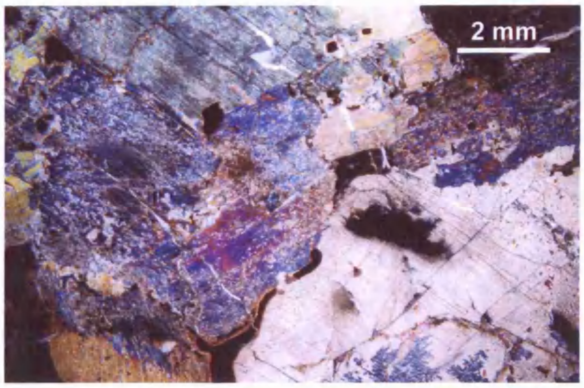

Fig. 3.3d: Gabbro. Example of one of the freshest gabbro samples collected. The field of view is dominated by 3 large clinopyroxene crystals and 1 orthopyroxene that is exsolving clinopyroxene in blebby clots. In the bottom centre of the view the edges of the orthopyroxene and clinopyroxene crystals have been partially replaced by brown amphibole and it is unclear if the clot of opaque minerals are secondary also.

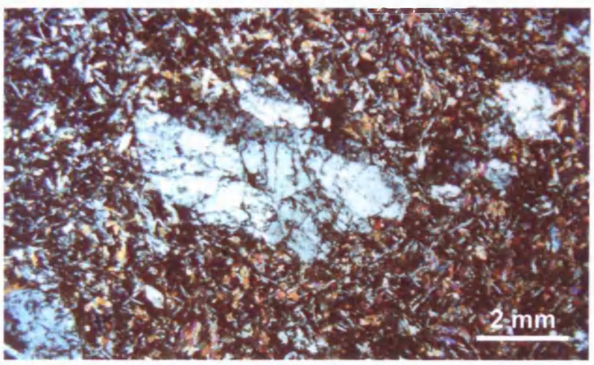

Fig. 3.3e: Porphyritic Sheeted Dyke. This sample is rare in that it contains fresh plagioclase phenocrysts. The phenocryst in the centre of the view is small compared to the majority of the porphyritic dykes in which phenocrysts are generally 20-30 mm in length. The groundmass in the sample above is composed of randomly oriented plagioclase with interstitial clinopyroxene and opaque minerals.

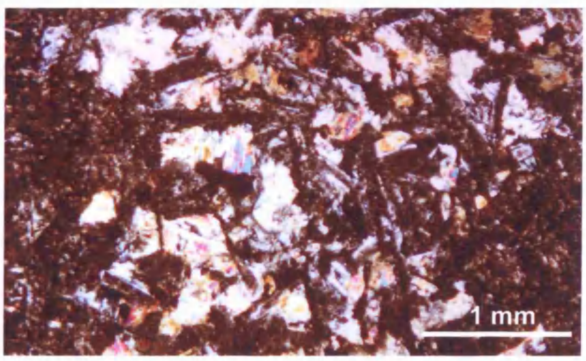

Fig. 3.3f: Porphyritic Sheeted Dyke. A more typical example of the nature of the porphyritic sheeted dykes. The left and right of the picture contain the edges of two large plagioclase phenocrysts that have been completely replaced by aggregates of sericite and epidote. The ground mass plagioclase has also been replaced and has a common muddy brown colouration. Interstitial clinopyroxene is reasonably fresh but in places is

Gabbro

The ophiolite mélange contains blocks of both layered and isotropic gabbro, but layered gabbro is the dominant type (Fig. 3.2). The layered gabbros grade modally over a thickness of 2-5m from dominantly ferromagnesian minerals up to dominantly plagioclase and locally near anorthositic composition at the top of some layers. The gabbros are heavily altered and primary mineralogy is commonly difficult to discern. However, despite alteration, most samples contain fresh anhedral clinopyroxene that contains exsolution lamellae of pigeonite, but the dominant phase is altered plagioclase (Fig. 3.3c). A few samples contain rare orthopyroxene phenocrysts that contain blebby exsolution of clinopyroxene (Fig. 3.3d). Plagioclase and some clinopyroxene form a dominantly interlocking granular texture. However, most of the clinopyroxene occupies the interstices between plagioclase laths (Fig. 3.3c). Some samples have plagioclase poikilitically enclosed within clinopyroxene, but this is rare. Clots of opaque minerals also occupy interstitial sites (Fig. 3.3d). Accessory phases are apatite, sphene, opaque minerals and rare zircons. Alteration has dominantly affected plagioclase by completely replacing the crystals with aggregates of white-mica (sericite) and epidote (Fig. 3.3c). However, clinopyroxene is also replaced by aggregates of tremolite, actinolite, and chlorite fringed by opaque minerals, or occasionally by hornblende psuedomorphs. Pseudomorphed clinopyroxene is almost always associated with or crosscut by veins filled with chlorite, calcite, and epidote. Similar alteration characteristics are described for the cumulate sections of the Troodos (Gillis & Robinson 1985; Richardson *et al.* 1987; Schiffman & Smith 1988; Malpas 1990), Oman (Nehlig & Juteau 1998a; 1998b) and Josephine ophiolites (Alexander & Harper 1992), and are suggested to relate to ocean floor hydrothermal alteration. Crystallisation order is difficult to determine due to the affects of alteration, but appears to have been plagioclase followed closely by, or coevally with clinopyroxene, and lastly opaque minerals.

Sheeted Dykes

The sheeted dyke complex (Fig. 3.2) of the Bayankhongor ophiolite contains porphyritic and aphyric dolerite dykes. The dykes are on average 2-3 m wide and both porphyritic and aphyric types appear coeval because they mutually intrude each other. The petrography of each will now be described separately:

Porphyritic Dolerite Dykes

The porphyritic sheeted dykes contain 20-30 mm randomly orientated phenocrysts of plagioclase (Fig. 3.3e), which are concentrated in the centre of individual dykes and were presumably transported from a magma chamber suspended within the rising melt (Moores &

Vine 1971; Ernst 1999). The phenocrysts are set in a ground mass of finer grained plagioclase, clinopyroxene, and opaque minerals (Fig. 3.3e). The groundmass plagioclase (60 % mod. prop.) forms randomly orientated subhedral laths (3-4 mm) that are occasionally partially enclosed within clinopyroxene (4-6 mm) forming a subophitic doleritic texture (Figs. 3.3e & 3.3f). However, clinopyroxene (30 % mod. prop., 1-2 mm) is generally an interstitial phase between plagioclase laths (Fig. 3.3f). Opaque minerals (10 % mod. prop.) are interstitial forming small anhedral clots (0.5-1 mm) between plagioclase laths and interstitial clinopyroxene. All of porphyritic dolerite samples have suffered extensive alteration (Fig. 3.3f). Plagioclase phenocrysts in almost all samples are completely replaced by pseudomorphs of white-mica and accumulations of epidote (Fig. 3.3f). The plagioclase in the groundmass is also rarely preserved and is similarly replaced by white-mica aggregates (Fig. 3.3f). The small interstitial clinopyroxenes are generally fresh, but larger oikocrysts are often replaced by green/brown amphibole and chlorite pseudomorphs (Fig. 3.3f). Both interstitial clinopyroxene and clinopyroxene oikocrysts are replaced by aggregates of tremolite/actinolite and serpentine where veins cross-cut the samples (Fig. 3.4a). The veins are also filled with tremolite/actinolite, in addition to chlorite, epidote, and very rarely quartz (Fig. 3.4a). Tremolite/actinolite pseudomorphs of clinopyroxene are often surrounded by coronas of opaque minerals.

Aphyric Dolerite Dykes

The aphyric sheeted dykes are much finer grained (<1 mm) than the groundmass of the porphyritic dykes, but their mineralogy is the same. Randomly orientated, subhedral plagioclase laths (0.5-1mm) dominate making up approximately 60 % modal proportion (Fig. 3.4a). Clinopyroxene (30 % mod. prop.) subophitically encloses plagioclase or occupies interstitial sites between plagioclase laths forming a doleritic texture. Opaque minerals (10 % mod. prop.) form small concentrations or anhedral clots (< 0.5 mm) in interstitial sites. The aphyric dykes are generally less altered than the porphyritic type. However, plagioclase is rarely preserved and is replaced by clay mineral aggregates and epidote accumulations. Clinopyroxene is reasonably fresh but often contains alteration rims of chlorite and occasionally green amphibole. Where clinopyroxene is completely replaced it is pseudomorphed by amphibole or chlorite (Fig. 3.4a). The strongest alteration is concentrated in zones around crosscutting veins filled with tremolite/actinolite and chlorite (Fig. 3.4a).

Additional alteration

In a few locations, some of the sheeted dyke complex contain reticulate vein networks but samples were not collected from these areas. The veins are filled with epidote and iron oxide accumulations. In a region up to 10 cm around the veins, the dolerite is completely epidotised and/or has a rusty appearance due the accumulation of iron-oxide. In addition dyke margins are locally silicified suggesting that these also acted as conduits for hydrothermal fluids. Similar features have been described within stockwork systems within the Troodos ophiolite, associated with hydrothermal alteration and massive sulphide mineralisation (Schiffman & Smith 1988).

Pillow Basalts

The pillow basalt section of the ophiolite (Fig. 3.2) also contains porphyritic and aphyric types. Aphyric pillows are dominant forming small (< 1.5 m) rounded to lobate pillows with classic pinch and swell morphology. The areas between the pillows are filled with altered glass, hyaloclastite, pillow breccia and occasionally carbonate. Some of the carbonate may have formed due to alteration of the pillow basalts and glassy margins, but Ryazentsev (1994) reported fossil sponge spicules from interpillow limestone in the Bayankhongor ophiolite. Porphyritic pillows are generally larger (0.5-2 m) and form local accumulations surrounded by aphyric pillows. The petrography of the two varieties is discussed separately below:

Porphyritic Pillow Basalts

The porphyritic pillows contain 5-20 mm phenocrysts of plagioclase and clinopyroxene (Fig. 3.4b). The clinopyroxene crystals are composed of subhedral twinned augite that occasionally are rimmed by chlorite. Plagioclase phenocrysts have all been replaced by clay aggregate pseudomorphs. The phenocrysts are enclosed in a very fine grained (< 0.5 mm) groundmass of plagioclase, clinopyroxene, opaque minerals, and devitrified glass (Fig. 3.4b). Plagioclase is the dominant ground mass phase forming small (< 0.5 mm) randomly orientated microlites (Fig. 3.4b). Clinopyroxene and opaque minerals are interstitial. The porphyritic pillows all show signs of alteration similar to that in the sheeted dykes; plagioclase is replaced with white-mica and epidote and many clinopyroxenes have been replaced by amphibole and chlorite pseudomorphs.

Aphyric Pillow Basalts

The aphyric pillows have a very similar character to that of the porphyritic pillow ground mass. Fine grained (< 0.5 mm), randomly orientated plagioclase laths are dominant (60 % mod. prop.), with anhedral clinopyroxene (20 % mod. prop.) occupying interstitial sites between plagioclase laths. Interstitial areas not filled by clinopyroxene (20 % mod. prop.) contain devitrified glass and/or chlorite (Fig. 3.4c). The aphyric pillows are generally less altered than the porphyritic type. Plagioclase is most affected by alteration and few samples contain any fresh crystals. Clinopyroxene is usually fresh but occasionally is replaced by chlorite (Fig. 3.4c). A few of the aphyric pillows contain vesicles < 10 mm in size filled with calcite and zeolites (Fig. 3.4d). Vesicular samples are rare and contain the same bulk mineralogy and textural characteristics as the rest of the aphyric pillow basalts (Fig. 3.4d).

Additional alteration

As was the case for the sheeted dyke complex, local areas of the pillow basalt section are cross-cut by reticulate vein networks. The veins are usually filled with epidote, calcite and iron oxide. Pillows which are cut by these veins have a rotted gossan-like appearance and contain sulphide mineralisation in the form of pyrite and chalcopyrite, but this is usually concentrated in the immediate vicinity of the veins. In addition some pillows contain copper sulphide mineralisation and these pillows have a bleached appearance and their margins may be partially silicified. No samples were collected in regions affected by such extreme alteration. Similar alteration features are well documented in the Troodos (Gillis & Robinson 1985; Richardson *et al.* 1987; Schiffman & Smith 1988; Malpas 1990) and Oman ophiolites (Nehlig & Juteau 1998a; 1998b), and are thought to be associated with massive sulphide mineralisation and hydrothermal alteration in black-smoker systems,.

Petrography of the Southern Volcanics

The Southern Volcanics (Fig. 3.2) are composed of a mix of dominantly intermediate igneous extrusive rocks ranging from basalts to dacites (Fig. 3.5). The detailed structural and lithological field relations of the volcanic rocks and their neighbouring units are presented in Chapter 2 (Buchan *et al.* 2001) and will not be repeated here. However, it is important to note that the Southern Volcanics form a separate thrust sliver from the ophiolitic rocks and thus their pre-allochtonous relationship with the ophiolitic rocks is unclear. The petrography of the range of volcanic extrusive rocks is presented in order of abundance in the following section. The geochemistry and petrography of rhyolite dykes that intrude the Southern Volcanics is discussed in detail in Chapter 4 (Buchan *et al.* 2001, submitted to Tectonophysics). The Southern Volcanics also contain rare local occurrences of tuffs and volcanogenic sediments, that were not sampled in this study.

Dacite

Dacite is the dominant lithology in the Southern Volcanics (approximately 80 % of complex) forming 5-10 m thick purple to red coloured massive sheet flows. The dacites contain large (10-20 mm) phenocrysts and glomerocrysts of plagioclase (10 % mod. prop.) enclosed in a fine-grained (< 5 mm) groundmass composed of plagioclase (50 % vol.), quartz (20 % vol.), and alkali feldspar (10 % vol.; Fig. 3.4e). Accessory phases include opaque minerals, apatite, zircon and epidote. The plagioclase in the groundmass forms an interlocking granular texture and quartz and alkali feldspar form anhedral crystals in the interstices between plagioclase

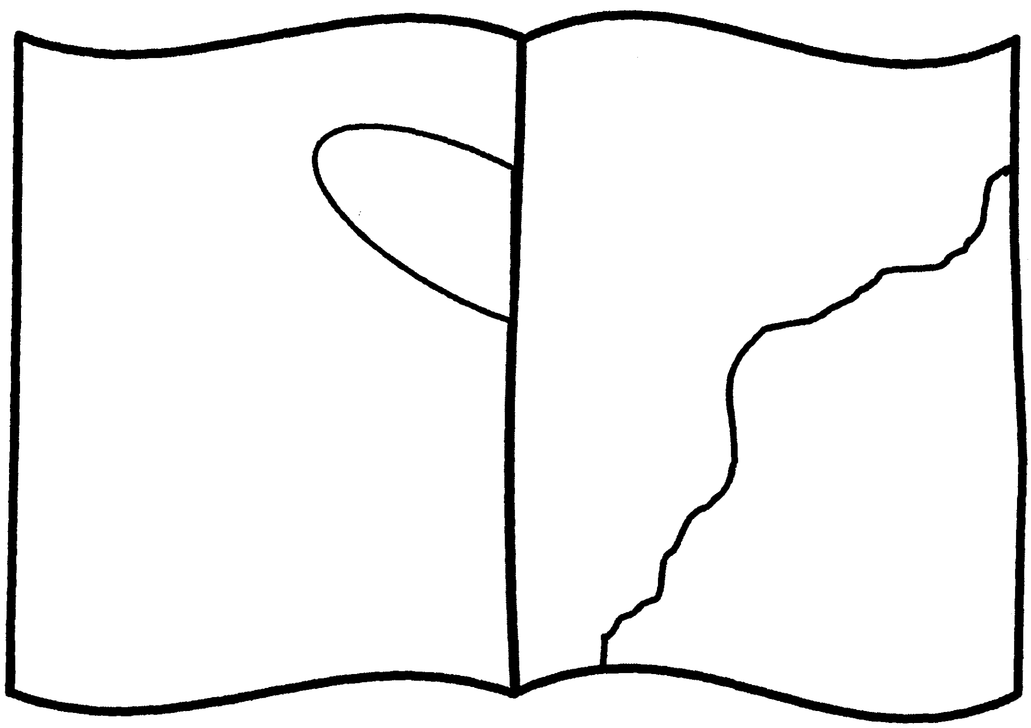

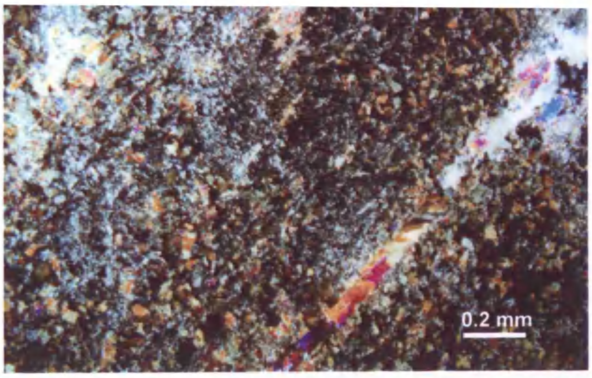

Fig. 3.4a: Aphyric Dolerite Dyke. This is a typical example of an aphyric dolerite dyke from the Bayankhongor ophiolite. Plagioclase forms the bulk of the rock as randomly orientated laths which are mostly replaced by sericite and epidote alteration. Clinopyroxene occupies the interstices between the plagioclase laths and is sometimes replaced by chlorite, amphibole and actinolite. The vein crosscutting the right of the picture is filled with tremolite/actinolite and chlorite.

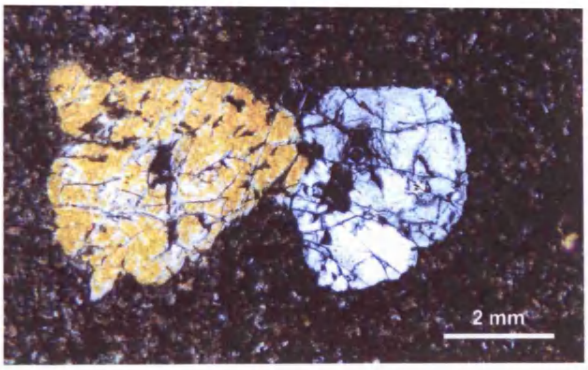

Fig. 3.4b: Porphyritic Pillow Basalt. This porphyritic basalt sample contains dominantly phenocrysts of clinopyroxene but many other samples contain plagioclase. The pyroxenes are enclosed in a fine grained (<0.5mm) groundmass of randomly orientated plagioclase microlites and interstitial clinopyroxene. Plagioclase is occasionally sub-ophitically enclosed by clinopyroxene, but this is rare. The bulk of the groundmass plagioclase has been replaced by white-

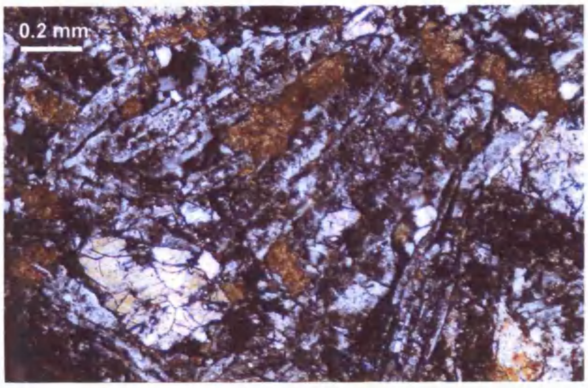

Fig. 3.4c: Aphyric Pillow Basalt. This is a fairly coarse aphyric pillow basalt with plagioclase crystals <1 mm in length. The plagioclase is fairly fresh but patches of sericite and epidote alteration are visible as brightly coloured spots. A large interstitial clinopyroxene crystal is visible in the bottom left of the picture, but has weak colours as it is partially chloritised. This sample also contains devitrified glass (brown material) occupying the interstices between plagioclase crystals.

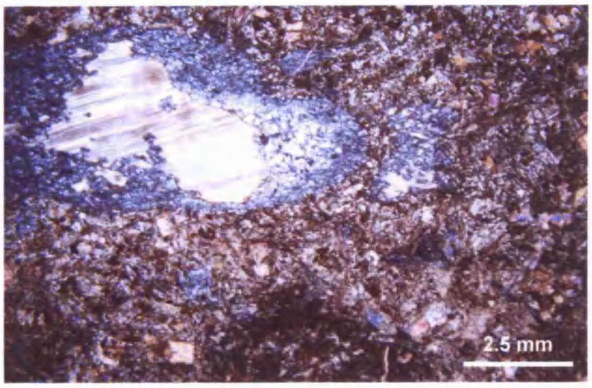

Fig. 3.4d: Vesicular Pillow Basalt. Vesicular basalts are rare in the Bayankhongor ophiolite rocks. They typically contain large ellipsoid vesicles which are filled with zeolites and/or calcite as is the case for the sample pictured. The vesicular basalts are typically strongly altered and contain little or no fresh plagioclase and few fresh clinopyroxenes. Some fresh clinopyroxene and amphibole pseudomorphs can be picked out in the right of the field of view.

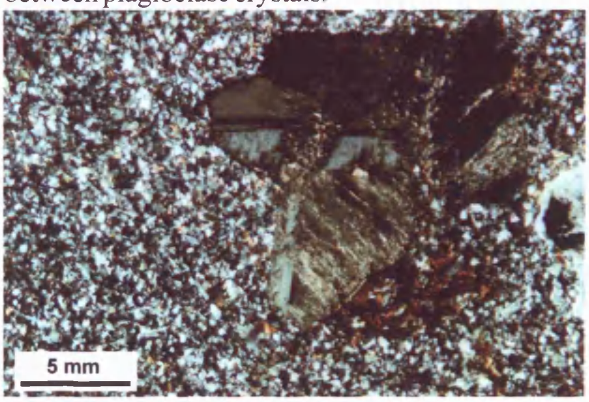

Fig. 3.4e: Dacite. This is a typical example of a dacite from the Southern Volcanic group. The field of view is dominated by a large plagioclase glomerocryst. The plagioclase is partially altered to sericite and epidote, but hints of magmatic zonation can still be made out around the rim of the lowest crystal in the group. The groundmass is composed of plagioclase, alkali feldspar, rare quartz and opaque

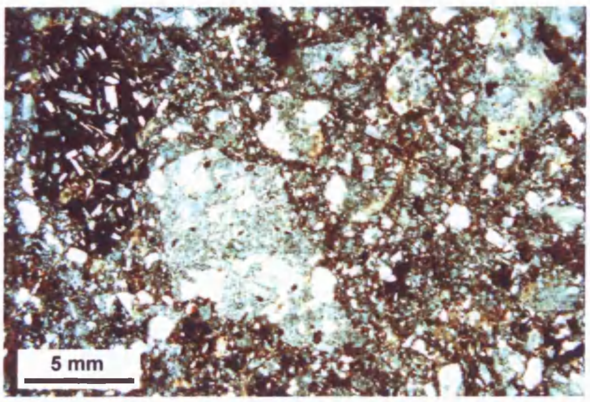

Fig. 3.4f: Volcanic Breccia. This is an example of a typical volcanic breccia from the Southern Volcanic group (see Fig. 2). The breccias contain angular fragments of most of the other lithologies found within the Southern Volcanics. The sample pictured above contains mostly fragments of dacite but also rhyolite in the centre of the view. The groundmass surrounding the fragments is also dacitic.

Special Note

Page 50 missing from the original

crystals. The dacites are on the whole fresh with only mild alteration of plagioclase to sericite and epidote. However, some sheets have a deep red colouration caused by accumulations of iron oxide mineralisation associated with crosscutting hematite veins. In these red coloured flows the mineralogy and texture of the rock is difficult to identify as the plagioclase is nearly all replaced by sericite and epidote which obscure previous crystal boundaries.

Volcanic Breccias

The volcanic breccias contain angular clasts of dominantly dacite, but also nearly all of the lithologies contained within the Southern Volcanics. Clasts are angular (Fig. 3.4f) and range in size from < 1 mm to approximately 100 mm. The clasts are enclosed in fine a grained (< 0.5 mm) matrix of granular plagioclase, potassium feldspar, quartz, and rare biotite. Accessory phases are opaque minerals, zircon, and epidote. The breccias are reasonably fresh although some of the plagioclase in the matrix is altered to sericite and epidote aggregates in the vicinity of calcite veins.

Andesite

The andesites contain phenocrysts (10-20 mm) of zoned plagioclase and subordinate amphibole. The phenocrysts are enclosed in a very fine-grained (< 0.1 mm) groundmass composed dominantly of plagioclase microlites, but also contains interstitial clinopyroxene and opaque minerals. The andesites are generally fresh although some of the plagioclase phenocrysts are partially replaced by sericite and epidote and the groundmass contains chlorite in places presumably replacing clinopyroxene.

Basalts

The basalts in the Southern Volcanics are dominantly porphyritc. Clinopyroxene and forms 5-10 mm subhedral to anhedral phenocrysts. Many of the clinopyroxene phenocrysts contain rims of brown amphibole, that may be related to late stage alteration. The phenocrysts are enclosed in a microcrystalline groundmass of plagioclase, clinopyroxene, opaque minerals, and devitrified glass. Many of the clinopyroxene crystals in the groundmass are replaced by chlorite and plagioclase is often altered to sericite and epidote.

Analytical Techniques

Sampling procedure and processing

Samples were chosen from the ophiolitic rocks and the Southern Volcanics in order to cover the whole compositional and lithological range observed during field mapping. Samples were collected from each of three transect areas shown in Figure 3.2. In addition, ophiolitic samples were collected during reconnaissance investigations of ophiolite exposures along-strike as far as Bayankhongor City (Fig. 3.1). Outcrops affected by vein networks or highly altered regions were avoided. To ensure the freshest possible samples were analysed, weathered and altered surfaces of samples were carefully removed by hand before rocks were crushed using a fly-press (to allow further elimination of altered sections within samples) and powdered using an agate Tema Mill.

Major and trace element geochemistry

Major and trace elements (Tables 3.1 & 3.2) were analysed by XRF at the University of Leicester, using conventional techniques described by Tarney and Marsh (1991). Major elements were measured on fused glass discs using a lithium tetraborate-metaborate flux; trace elements were measured on pressed powder pellets using a Moviol binding agent. Only major element totals between 98.5-101.5% were accepted. For major elements the typical lower limit of detection (LLD) is 0.01% and precision is better than 0.5% at 100 times LLD. XRF major and trace element reproducibility for international reference materials is shown in Appendix B, and is on average within 5%.

Samples used for REE analysis were digested using microwave digestion in a combined solution of HF-HNO_3. The REE were separated from the bulk sample using Dowex AG 50W-8X cation-exchange resin. After separation, REE concentrations (Tables 3.1 & 2) were determined using an ICP-Optical Emission Spectrometer at the University of Leicester, following the methods described by Harvey et al. (1996). Reproducibility of repeated measurements on the international standard JB-1a was within 5 % of recommended values (Appendix B).

Nd isotope analysis

Nd isotopic compositions (Tables 3.3 & 3.4) were determined using a Finnigan MAT 261 multicollector thermal ion mass spectrometer in static mode at the Max-Planck-Institut für Chemie in Mainz, Germany. Nd isotopic ratios and Nd, Sm concentrations were analysed by isotope dilution using a mixed ^{150}Nd-^{149}Sm spike. The spike was added prior to sample digestion in HF-HNO_3 within closed Teflon beakers for >48 hours at 200 °C. The REE fraction was separated from the bulk sample using Biorad AG 50W-X12 cation-exchange

Table 3.1a: *Major, Trace, and Rare Earth Element concentrations of Bayankhongor ophiolite rocks.*

Sample	97M76	97M74	97M110C	97M109	98M109B	98M114B	97M48	98M123	97M43	97M115B	97M74B	97M67	98M28	98M88C	98M40	98M38	98M20	98M41	98M89B	98M30
Lithology	Dol aph	basalt	basalt	basalt	basalt	Dolerite	Dol porph	basalt	basalt	basalt	basalt	Dol porph	basalt	basalt	basalt	basalt	basalt	basalt	basalt	basalt
Location	N46°30.630' E99°56.479'	N46°30.840' E99°56.971'	N46°33.604' E99°43.684'	N46°33.604' E99°43.684	N46°37.308' E99°41.081'	N46°36.537' E99°41.223'	N46°35.373' E99°41.010'	N46°29.779' E99°56.232'	N46°35.867' E99°45.964'	N46°34.505' E99°43.204'	N46°30.840' E99°56.971'	N46°35.867' E99°45.964'	N46°43.684' E99°18.189'	N46°12.788' E100°26.680'	N46°43.378' E99°17.987'	N46°43.378' E99°17.987'	N46°45.814' E99°17.211'	N46°43.378' E99°17.987'	N46°12.788' E100°26.680	N46°43.684' E99°18.189'
SiO_2	47.45	47.37	51.43	48.61	49.88	49.05	47.65	46.31	47.69	46.89	44.79	47.98	47.68	47.76	47.37	48.62	47.82	48.49	49.31	47.12
TiO_2	2.43	2.10	1.94	1.68	2.02	1.69	1.27	1.07	0.57	0.69	0.35	1.33	1.53	1.74	1.74	2.22	1.29	2.27	1.16	0.79
Al_2O_3	13.75	14.28	14.85	17.42	14.05	15.03	15.79	16.56	22.66	21.49	21.43	14.75	14.85	14.28	15.05	13.63	15.04	13.78	15.19	21.90
Fe_2O_3	14.50	13.87	9.52	10.50	13.13	12.42	10.79	9.56	5.76	6.48	5.98	9.69	12.32	12.78	11.62	14.79	10.04	14.96	9.99	6.30
MnO	0.20	0.22	0.23	0.22	0.16	0.20	0.17	0.13	0.10	0.10	0.10	0.16	0.17	0.19	0.19	0.23	0.17	0.22	0.16	0.10
MgO	5.57	5.17	6.11	8.93	5.00	6.17	6.84	6.93	3.93	4.17	6.00	9.04	6.60	5.66	6.71	4.75	8.02	4.78	6.82	4.25
CaO	9.17	10.62	7.39	3.08	9.98	10.28	8.56	11.32	9.99	12.68	11.85	11.02	11.22	10.70	11.27	8.57	11.42	8.36	10.52	12.10
Na2O	3.32	2.13	5.16	5.16	3.85	3.30	2.80	3.68	3.37	2.93	2.57	2.40	2.82	2.57	2.95	2.99	2.53	3.13	3.79	3.24
K2O	0.16	0.15	0.10	0.12	0.03	0.31	0.27	0.05	1.66	0.64	1.15	0.36	0.04	0.03	0.15	0.11	0.21	0.09	0.20	0.46
P2O5	0.28	0.28	0.17	0.15	0.25	0.18	0.15	0.12	0.08	0.08	0.04	0.21	0.19	0.26	0.19	0.25	0.13	0.27	0.20	0.11
L.O.I.	2.32	2.54	2.42	4.49	2.42	1.55	5.31	3.75	3.97	3.22	4.61	2.52	2.92	2.45	2.41	2.57	1.75	2.56	2.92	3.36
Total	99.16	98.72	99.32	100.37	100.78	100.18	99.60	99.48	99.78	99.38	98.87	99.45	100.35	98.41	99.65	98.75	98.42	98.92	100.28	99.73
Mg#	46.3	45.6	59.1	65.7	46.1	52.8	58.7	62.0	60.5	59.1	69.3	67.7	54.6	49.9	56.5	42.0	64.2	41.8	60.6	60.3
Ni	41	37	70	60	43	30	75	85	42	41	98	152	32	28	41	15	85	18	54	27
Cr	62	64	217	194	70	48	165	263	136	71	562	304	14	43	54	4	334	0.4	108	61
Ba	45	49	50	43	37	88	69	33	441	124	154	127	17	23	87	150	81	131	169	155
Rb	1.4	1.4	1.4		0.9	4.6	2.8	0.8	29.9	11.8	16.2	3.8	1.0	1.0	2.5	2.1	4.4	1.6	3.8	8.5
Sr	183.9	250.9	133.0	96.1	64.3	179.4	119.7	91.8	220.6	261.2	366.4	210.4	81.5	318.4	184	148.5	152.8	153.3	129.7	381.8
Th	3.3	1.8	2.5	1.5	4.3	2.6	1.6	2.3	2.8	1.6	2.0	2.4	3.3	1.4	3.8	3.0	2.1	4.4	3.6	2.6
U	< 0.5	< 0.5	< 0.5	< 0.5	0.2	0.3	< 0.5	0.8	< 0.5	< 0.5	< 0.5	< 0.5	0.3	< 0.5	< 0.5	0.7	< 0.5	0.2	0.9	0.2
Pb	< 0.5	< 0.5	< 0.5	< 0.5	< 0.5	1.6	< 0.5	1.3	< 0.5	< 0.5	< 0.5	< 0.5	0.5	1.2	1.1	< 0.5	< 0.5	0.3	< 0.5	< 0.5
Nb	14.7	16.2	4.5	3.9	15.2	9.5	9.6	5.8	6.2	4.4	2.7	19.4	22.0	24.9	22.3	32.0	12.1	33.1	18.7	13.3
Zr	165.0	153.0	149.2	113.6	138.5	102.3	86.0	88.3	40.8	44.8	26.1	101.7	110.4	148	116.6	154.9	87.1	163.4	108.4	68.2
Y	43.9	39.1	39.4	33.1	42.9	35.7	30.3	24.4	15.0	18.7	10.9	20.2	26.5	31	29.5	41.5	24.7	44	23.8	17.9
La	11.0	10.8	4.6	4.2	8.8	7.8	6.4	4.6	2.3	2.9	1.8	11.4	12.9	17.8	14.1	18.5	7.6	19.0	11.4	7.3
Ce	29.9	28.1	16.7	13.4	21.6	21.7	17.2	11.2	5.6	7.1	4.4	27.3	26.0	47.4	31.8	41.0	16.8	40.9	23.5	14.7
Pr	4.2	3.9	2.7	2.2	3.0	3.2	3.1	1.6	0.8	1.0	0.7	3.6	3.5	7.2	4.4	5.0	2.2	5.3	3.0	1.8
Nd	18.8	18.2	13.9	11.4	15.2	16.0	13.0	8.5	4.2	5.3	3.6	14.4	14.4	39.6	18.6	22.3	10.4	22.6	12.9	8.0
Sm	5.7	5.4	4.3	3.7	4.5	4.6	3.6	2.7	1.3	1.6	1.1	4.5	3.9	9.8	5.0	5.6	3.0	5.6	3.4	2.2
Eu	2.0	1.9	1.6	1.5	1.5	1.5	1.3	1.2	0.6	0.7	0.6	1.3	1.4	2.0	1.6	1.8	1.2	2.0	1.3	0.8
Gd	7.2	6.8	6.0	5.2	5.3	5.8	4.6	4.0	1.9	2.2	1.7	4.2	4.6	8.3	5.4	6.6	4.0	6.9	4.2	2.2
Dy	7.4	6.9	6.3	5.6	5.0	5.5	4.5	3.6	2.3	2.6	2.0	4.2	4.0	7.1	4.7	6.7	4.2	5.7	3.5	2.7
Er	4.7	4.7	3.8	3.4	3.1	3.5	2.9	2.7	1.4	1.7	1.1	2.9	3.0	4.2	2.9	3.9	2.3	3.9	2.4	1.4
Yb	3.9	3.5	3.1	2.8	3.4	3.5	2.7	2.2	1.4	1.5	1.0	1.9	2.6	3.1	2.7	3.5	2.0	3.8	1.9	1.2
Lu	0.5	0.5	0.4	0.4	0.5	0.5	0.4	0.3	0.2	0.2	0.1	0.3	0.4	0.5	0.4	0.5	0.3	0.6	0.3	0.2
Nb/Y	0.33	0.41	0.11	0.12	0.35	0.27	0.32	0.24	0.41	0.24	0.25	0.96	0.83	0.80	0.76	0.77	0.49	0.75	0.79	0.74
Zr/Y	3.76	3.91	3.79	3.43	3.23	2.87	2.84	3.62	2.72	2.40	2.39	5.03	4.17	4.77	3.95	3.73	3.53	3.71	4.55	3.81
Δ-Nb	0.16	0.22	-0.31	-0.22	0.31	0.29	0.37	0.04	0.52	0.38	0.41	0.37	0.47	0.34	0.47	0.53	0.38	0.52	0.37	0.50
$(Nb/La)_{PRIMA}$	1.32	1.49	0.97	0.91	1.72	1.21	1.48	1.26	2.74	1.53	1.53	1.70	1.70	1.39	1.57	1.72	1.58	1.73	1.64	1.81
$(La/Sm)_{Chnd}$	1.25	1.28	0.69	0.75	1.26	1.09	1.14	1.11	1.09	1.17	0.99	1.64	2.16	1.17	1.81	2.15	1.65	2.18	2.18	2.20
$(Sm/Yb)_{Chnd}$	1.62	1.74	1.57	1.47	1.45	1.48	1.49	1.32	1.09	1.18	1.29	2.61	1.66	3.54	2.09	1.76	1.64	1.65	1.94	1.93
$(La/Yb)_{Chnd}$	2.03	2.23	1.09	1.10	1.83	1.62	1.69	1.46	1.19	1.38	1.28	4.30	3.60	4.14	3.78	3.79	2.71	3.60	4.23	4.23

Major elements in wt. %; trace elements and REE in ppm.
Major and trace elements determined by XRF; REE determined by ICP-OES.

PRIMA: Primitive mantle normalised (Hofmann 1988); Chnd: Chondrite normalised (Sun & McDonough 1989).
Δ-Nb relative displacement from the lower limit of the Iceland array in Figure 3.22

Lithological abbreviations: Dol aph = aphyric dolerite; Dol porph = porphyritic dolerite

Table 3.1b: *Major, trace, and Rare Earth element concentration of cumulate rocks of the Bayankhongor ophiolite*

Sample	**98M79**	**97M50**	**97M53B**	**98M51**	**98M97**	**98M022B†**	**98M058†**	**98M080†**	**98M096†**
Lithology	Pyroxenite	Gabbro	Gabbro	Gabbro	Gabbro	Gabbro	Gabbro	Gabbro	pyroxenite
Location	N46°45.684' E99°13.143'	N46°33.871' E99°47.039'	N46°34.656' E99°45.637'	N46°43.055' E99°17.312'	N46°38.464' E99°36.093'	N46°45.314' E99°15.389'	N46°43.086' E99°16.937'	N46°45.684' E99°13.143'	N46°38.464' E99°36.093'
SiO2	41.41	48.81	49.66	47.55	44.84	45.31	58.11	46.90	43.54
TiO2	0.42	0.33	0.35	0.61	0.32	0.30	1.33	2.22	0.23
Al2O3	2.15	18.53	16.79	15.79	19.47	17.98	17.49	10.17	2.25
Fe2O3	15.52	5.31	7.48	4.83	4.38	6.69	6.73	13.18	9.57
MnO	0.23	0.10	0.15	0.10	0.08	0.12	0.11	0.26	0.13
MgO	28.53	7.61	7.23	8.58	8.94	11.25	2.61	12.31	29.62
CaO	7.22	12.49	7.10	17.30	14.80	12.14	4.34	10.33	8.50
Na2O	0.04	2.87	3.90	1.55	1.70	1.99	5.43	2.40	0.06
K2O	0.01	0.26	2.04	0.17	0.25	0.14	1.15	0.46	0.00
P2O5	0.02	0.02	0.03	0.02	0.02	0.02	0.15	0.16	0.01
L.O.I.	5.05	2.58	5.40	2.82	3.87	3.67	2.36	1.27	7.27
Total	100.59	98.91	100.14	99.32	98.65	99.60	99.79	99.66	101.07
Mg#	80.5	76.3	68.5	80.0	82.1	79.1	46.6	67.7	87.4
Ba	12	57	266	62	56	61	219	117	12
Rb	0.5	3.1	32.8	4.1	2.9	3.8	30.4	3.6	0.2
Sr	17.6	278.1	121.4	308.5	841.1	242	536	68.2	5.8
Th	1.8	2.5	1.2	2.6	1.8	2.3	4.4	3.1	1.5
U	0.1	< 0.5	< 0.5	0.3	< 0.5	< 0.5	< 0.5	0.8	1
Pb	2.8	< 0.5	< 0.5	0.8	1.8	< 0.5	5.5	< 0.5	< 0.5
Nb	1.4	1.7	1.2	3.3	1.4	0.6	5.3	130.6	0.3
Zr	21.4	21.4	15.9	38.8	18.8	14.3	135.9	251.2	9.2
Y	7.6	9.0	8.9	9.2	4.8	5.2	23.1	180.2	2.5
La	2.4	2.1	1.8	3.9	2.9	1.2	10.9	47.9	1.3
Ce	9.0	5.8	5.6	10.3	7.5	3.9	23.2	157.3	6.3
Pr	1.5	0.9	1.0	1.7	1.2	NA	NA	NA	NA
Nd	7.6	5.4	6.1	8.7	6.2	3.9	15.8	105.8	0.2
Sm	2.4	1.8	1.9	2.5	1.7	NA	NA	NA	NA
Eu	0.7	0.7	0.6	0.9	0.6	NA	NA	NA	NA
Gd	2.7	2.3	2.0	2.8	1.8	NA	NA	NA	NA
Dy	2.4	2.7	1.8	2.4	1.5	NA	NA	NA	NA
Er	1.5	2.0	1.1	1.5	1.0	NA	NA	NA	NA
Yb	0.9	1.1	0.7	0.8	0.5	NA	NA	NA	NA
Lu	0.2	0.2	0.1	0.1	0.1	NA	NA	NA	NA
Nb/Y	0.18	0.19	0.13	0.36	0.29	0.12	0.23	0.72	0.12
Zr/Y	2.82	2.38	1.79	4.22	3.92	2.75	5.88	1.39	3.68
Δ-Nb	0.14	0.29	0.39	0.09	0.07	-0.04	-0.38	1.32	-0.27
(Nb/La)PRIMA	0.58	0.81	0.66	0.85	0.47				
(La/Sm)Chnd	0.65	0.74	0.62	1.01	1.15				
(Sm/Yb)Chnd	2.85	1.86	2.87	3.63	3.71				
(La/Yb)Chnd	1.86	1.37	1.79	3.64	4.25				

Major elements in wt. %; trace elements and REE in ppm.
Major and trace elements determined by XRF; REE determined by ICP-OES.
PRIMA: Primitive mantle normalised (Hofmann 1988).
Chnd: Chondrite normalised (Sun & McDonough 1989).
Δ-Nb relative displacement from the lower limit of the Iceland array in Figure 3.22
†: La, Ce, and Nd measured by XRF.

Table 3.1c: *Major and Trace element concentrations of Bayankhongor ophiolite samples analysed by XRF only.*

Sample	97M110	97M75	97M51	97M68B	97M113	97M112B	97M112A	97M114	97M78	97M115	97M38	98M011	98M018	98M019	98M034	98M035	98M036	98M037	98M042	98M043
Lithology	Basalt	Basalt	Dol aph	Dol porph	Dol aph	Dol aph	Dol aph	Dol aph	Dol porph	Dol porph	Dol porph	Basalt	basalt	Basalt	Basalt	Basalt	Basalt	Basalt	Basalt	Basalt
Location	N46°33.604' E99°43.684'	N46°30.840' E99°56.971'	N46°34.156' E99°44.911'	N46°35.867' E99°45.964'	N46°34.000' E99°43.354'	N46°33.604' E99°43.684'	N46°33.604' E99°43.684'	N46°34.505' E99°43.246'	N46°34.737' E99°43.080'	N46°34.505' E99°43.204'	N46°35.867' E99°45.964'	N46°51.418' E99°10.720'	N46°45.755' E99°17.296'	N46°45.755' E99°17.296'	N46°45.699' E99°18.796'	N46°43.526' E99°18.031'	N46°43.526' E99°18.031'	N46°43.378' E99°17.987'	N46°43.378' E99°17.987'	N46°43.378' E99°17.987'
SiO2	55.16	50.11	49.66	49.60	47.20	46.97	49.76	48.47	46.89	49.87	48.08	47.74	45.99	66.23	46.77	47.76	47.60	48.26	47.72	47.16
TiO2	1.57	1.90	1.44	1.65	1.67	3.01	1.02	1.45	0.69	1.49	1.00	0.64	2.02	0.67	1.35	0.86	0.82	1.03	1.72	2.12
Al2O3	14.35	14.51	14.13	14.66	14.62	14.75	18.92	14.18	21.49	13.68	16.87	22.00	16.07	10.94	13.72	13.72	14.01	17.94	14.76	14.33
Fe2O3	7.83	11.23	12.51	10.54	13.45	14.02	9.26	12.02	6.48	11.56	9.12	6.33	13.69	4.83	13.76	9.36	9.17	9.85	11.74	12.71
MnO	0.20	0.15	0.22	0.17	0.21	0.28	0.33	0.17	0.10	0.18	0.15	0.09	0.16	0.06	0.25	0.16	0.15	0.18	0.20	0.21
MgO	6.23	5.75	7.48	7.65	6.16	6.68	7.18	6.48	4.17	7.86	6.11	4.09	7.59	3.56	7.33	10.25	10.37	6.42	6.80	5.94
CaO	8.43	8.30	8.51	9.88	11.16	9.30	7.69	10.88	12.68	10.05	10.99	12.66	7.27	3.79	12.18	11.76	11.67	10.19	10.96	9.82
Na2O	5.36	5.19	3.48	3.44	2.27	3.69	4.09	3.10	2.93	3.09	3.02	3.25	3.46	1.82	0.31	2.26	1.86	3.54	2.76	3.02
K2O	0.09	0.11	0.62	0.41	0.08	0.09	0.44	0.37	0.64	0.38	0.62	0.50	0.02	1.49	0.01	0.61	1.07	0.54	0.14	0.12
P2O5	0.15	0.25	0.17	0.33	0.19	0.33	0.09	0.18	0.08	0.20	0.12	0.08	0.15	0.15	0.13	0.08	0.08	0.12	0.19	0.24
L.O.I.	2.01	3.44	2.29	2.15	3.59	2.75	3.48	2.08	3.22	2.08	2.55	3.16	4.67	5.41	5.43	2.65	2.75	2.63	2.41	2.47
Total	101.37	100.95	100.49	100.50	100.59	101.87	102.27	99.37	99.38	100.44	98.64	100.54	101.08	98.93	101.24	99.45	99.55	100.71	99.40	98.13
Mg#	64.2	53.5	57.3	62.0	50.7	51.7	63.6	54.8	59.1	60.5	60.1	59.2	55.5	62.3	54.5	71.1	71.8	59.4	56.6	51.2
Ni	65	71	39	122	39	59	59	42	135	50	41	163	32	NA	74	150	151	69	55	32
Cr	110	178	39	301	63	103	186	29	188	122	70	319	84	NA	148	444	446	176	59	32
Ba	47	30	242	149	42	55	39	130	97	144	102	16.9	274.7	NA	19	228	350	190	93	71
Rb	< 0.5	< 0.5	12.1	5.3	< 0.5	< 0.5	4.0	6.7	6.4	11.4	8.1	0.3	65.4	NA	0.6	16.5	29.8	9.9	2.7	1.9
Sr	144.3	88.8	150.6	205.2	74.7	104.3	188.9	179.3	163.2	225.2	247.3	242.8	117.1	23.2	323.5	128	115.3	255.4	220.6	178.5
Th	1.5	3.6	2.5	4.4	3.6	3.2	0.7	1.8	1.8	2.0	1.1	1.8	10	3.2	3.2	2.4	3.2	2.2	4.4	4
U	< 0.5	< 0.5	< 0.5	< 0.5	< 0.5	< 0.5	< 0.5	< 0.5	< 0.5	< 0.5	< 0.5	0.6	1.5	0.3	< 0.5	0.6	0.6	< 0.5	0.9	< 0.5
Pb													8.3		0.8					
Nb	3.9	16.6	10.7	34.5	13.7	12.2	2.0	13.1	15.6	8.1	3.8	7.3	11.5	1.1	4.8	9.4	9.1	11.9	22.3	28
Zr	116.7	141.6	92.7	161.8	115.5	233.5	68.8	103.2	106.4	68.6	45.8	82.1	193	12	98	53.2	54	69.7	112.3	142.4
Y	32.2	33.0	34.1	32.3	38.1	60.8	22.9	35.8	29.1	27.0	17.6	23.4	25.8	1.1	27.4	20.4	19.5	24.9	29.6	35.3
Nb/Y	0.12	0.50	0.31	1.07	0.36	0.20	0.09	0.37	0.54	0.30	0.22	0.31	0.45	1.00	0.18	0.46	0.47	0.48	0.75	0.79
Zr/Y	3.62	4.29	2.72	5.01	3.03	3.84	3.00	2.88	3.66	2.54	2.60	3.51	7.48	10.91	3.58	2.61	2.77	2.80	3.79	4.03
Δ-Nb	-0.25	0.23	0.40	0.43	0.37	-0.08	-0.24	0.42	0.39	0.44	0.28	0.19	-0.29	-0.25	-0.08	0.60	0.56	0.56	0.51	0.48

Major elements in wt. %; trace elements and REE in ppm.
Major and trace elements determined by XRF; REE determined by ICP-OES.
Δ-Nb relative displacement from the lower limit of the Iceland array in Figure 3.22

Table 3.1c: *continued.*

Sample	98M054	98M088A	98M088B	98M089A	98M098	98M108A	98M108B	98M109A	98M111A	98M111B	98M111C	98M112	98M114A	98M121A	98M121B	98M122	98M124	98M125
Lithology	Basalt	Basalt	Basalt	Basalt	Dolerite	Basalt	Basalt	Basalt	Basalt	Basalt	Basalt	Basalt	Dolerite	Dolerite	Dolerite	Basalt	Dolerite	Dolerite
Location	N46°42.828' E99°16.664'	N46°12.788' E100°26.680'	N46 12.788 E100 26.680	N46°12.788' E100°26.680'	N46°38.309' E99°34.874'	N46°37.308' E99°41.081'	N46°37.308' E99°41.081'	N46°37.308' E99°41.081'	N46°36.537' E99°41.223'	N46°36.537' E99°41.223'	N46°36.537' E99°41.223'	N46°36.537' E99°41.223'	N46°36.537' E99°41.223'	N46°29.779' E99°56.232'	N46°29.779' E99°56.232'	N46°29.779' E99°56.232'	N46°29.779' E99°56.232'	N46°29.779' E99°56.232'
SiO2	45.40	47.81	47.81	47.59	47.25	49.95	50.87	49.60	49.58	49.82	48.19	94.04	49.57	46.72	46.80	51.22	46.92	48.37
TiO2	3.38	1.73	1.73	1.42	2.33	1.98	1.97	2.10	1.20	1.34	1.25	0.09	1.39	1.70	1.99	1.07	1.57	1.11
Al2O3	16.82	14.53	14.47	15.23	15.25	13.95	13.46	14.03	16.67	16.16	16.19	0.59	15.24	14.67	15.64	15.11	15.16	14.97
Fe2O3	13.22	12.77	12.85	11.05	12.92	10.41	10.64	12.70	9.51	10.41	9.44	4.84	11.52	12.86	12.29	8.06	12.42	11.51
MnO	0.17	0.19	0.19	0.18	0.20	0.17	0.16	0.15	0.14	0.14	0.16	0.02	0.18	0.16	0.16	0.14	0.18	0.17
MgO	4.98	5.66	5.64	7.25	5.92	5.98	6.02	4.83	5.98	6.94	6.92	0.15	7.09	6.49	6.98	7.18	6.64	8.05
CaO	9.25	10.79	10.81	10.51	10.25	9.01	8.01	9.81	10.67	9.51	10.83	0.34	10.35	9.63	9.55	11.56	11.48	11.02
Na2O	3.64	2.55	2.49	3.54	3.20	4.36	4.36	3.88	2.95	3.15	3.45	0.05	3.42	3.28	3.47	2.87	2.19	2.94
K2O	0.77	0.04	0.03	0.14	0.42	0.71	0.58	0.03	0.71	0.40	0.35	0.03	0.50	0.81	0.74	0.12	0.51	0.16
P2O5	0.14	0.26	0.26	0.23	0.28	0.29	0.28	0.27	0.15	0.16	0.16	0.01	0.17	0.20	0.24	0.16	0.19	0.14
L.O.I.	2.47	2.47	2.45	2.87	2.20	3.88	2.91	2.39	3.42	2.65	3.62	0.36	1.98	2.67	2.73	3.51	2.80	1.91
Total	100.24	98.79	98.72	100.01	100.21	100.69	99.26	99.78	100.96	100.69	100.56	100.53	101.41	99.19	100.60	100.99	100.07	100.34
Mg#	45.9	49.9	49.7	59.6	50.7	56.4	56.0	46.1	58.6	60.0	62.3	6.5	58.0	53.2	56.1	66.7	54.6	61.1
Ni	28	27	27	56	33	95	85	43	43	46	58	NA	42	NA	NA	NA	NA	NA
Cr	4	43	41	119	22	279	267	70	169	177	170	NA	21	NA	NA	NA	NA	NA
Ba	188	38	20	117	282	174	141	29	122	151	175	1.4	116.7	128.2	125.1	44.6	131.3	44.7
Rb	26.7	0.4	0.8	3.2	6.5	12.9	9.6	0.7	13	7	6	0.1	7.2	11.1	10.1	0.4	5.6	1.6
Sr	355.7	311.6	316.5	147.3	276.8	156.6	157.6	62.4	164.4	166.9	188.3	4.3	181.5	306.9	887.9	163.1	368.9	120.6
Th	3.2	3.6	2.9	3.4	4.6	2.4	2.9	4	1.9	4.6	1.6	2.2	2.6	2.5	4.7	3.8	3.4	3.7
U	0.1	< 0.5	2	< 0.5	1	< 0.5	0.7	0.4	< 0.5	< 0.5	0.3	0.8	< 0.5	< 0.5	< 0.5	0.9	< 0.5	< 0.5
Pb	0.4	0.2	0.4	< 0.5	< 0.5	< 0.5	1.8	< 0.5	< 0.5	< 0.5	< 0.5	< 0.5	< 0.5	< 0.5	< 0.5	< 0.5	< 0.5	< 0.5
Nb	5.1	25.3	25.2	21.6	25.9	26.9	27.1	15.9	7.6	7.6	7.2	1	9.2	11.6	12.7	5.7	10.1	6.9
Zr	115.2	146.9	148.8	122.7	160.1	157	157.9	144.8	92.5	92.4	92.1	17.5	95.3	155.7	136.6	84.2	110.1	87.9
Y	28	31.4	31.4	26.3	33.3	31	31.2	45.7	30.4	31.5	32.1	0.6	33.9	42.9	43.2	23.8	34.6	27.8
Nb/Y	0.18	0.81	0.80	0.82	0.78	0.87	0.87	0.35	0.25	0.24	0.22	1.67	0.27	0.27	0.29	0.24	0.29	0.25
Zr/Y	4.11	4.68	4.74	4.67	4.81	5.06	5.06	3.17	3.04	2.93	2.87	29.17	2.81	3.63	3.16	3.54	3.18	3.16
Δ-Nb	-0.18	0.36	0.35	0.37	0.32	0.33	0.33	0.32	0.21	0.23	0.21	-0.85	0.31	0.10	0.25	0.07	0.24	0.17

Major elements in wt. %; trace elements and REE in ppm.
Major and trace elements determined by XRF; REE determined by ICP-OES.
Δ-Nb relative displacement from the lower limit of the Iceland array in Figure 3.22

Table 3.2: *Major, Trace, and Rare Earth element concentrations of Southern Volcanics and samples 98M26 and 98M27 from the Delb Khairkhan mélange.*

Sample	**98M26**	**98M27**	**98M60**	**98M62**	**98M9**	**98M56**	**98M72**	**98M105**	**97M126B**	**97M129**	**98M46**	**98M55**	**97M101†**	**97M119†**	**97M126A†**	**98M45†**	**98M73†**	**98M74†**	**98M103†**	**98M104†**
Lithology	basalt	basalt	dacite	dacite	dacite	dacite	andesite	andesite	dacite	basalt	dacite	dacite	dacite	volcanic breccia	dacite	dacite	andesite	andesite	dacite	dacite
Location	N46°44.261' E99°17.932'	N46°44.261' E99°17.932'	N46°42.904' E99°16.143'	N46°42.904' E99°16.143'	N46°42.904' E99°16.143'	N46°43.086' E99°16.937'	N46°42.236' E99°16.357'	N46°35.167' E99°32.325'	N46°31.538' E99°38.739'	N46°31.583' E99°38.739'	N46°42.798' E99°16.971'	N46°42.798' E99°16.971	N46°33.008' E99°40.262'	N46°31.738' E99°37.789'	N46°31.583' E99°38.739'	N46°45.755' E99°17.296'	N46°42.236' E99°16.357'	N46°42.603' E99°15.047'	N46°42.671' E99°14.736'	N46°34.963' E99°31.151'
SiO2	68.34	62.75	56.96	54.61	60.75	63.13	60.82	62.27	61.96	51.12	51.65	65.69	62.08	63.12	58.47	52.05	63.19	52.44	57.48	65.88
TiO2	0.76	0.85	1.15	0.75	0.86	1.07	1.04	0.98	0.84	1.45	0.25	0.71	0.76	0.77	1.48	0.26	0.57	1.38	0.97	0.57
Al2O3	12.73	15.00	17.86	16.57	15.09	13.57	16.26	15.99	14.96	17.90	19.21	13.08	15.92	17.16	13.90	19.36	15.44	15.91	16.69	13.72
Fe2O3	6.85	7.06	6.67	7.25	8.08	6.97	7.31	5.31	5.90	8.59	2.73	4.70	5.11	4.99	8.64	2.75	4.21	9.11	5.52	4.24
MnO	0.09	0.07	0.08	0.09	0.15	0.11	0.08	0.10	0.10	0.10	0.04	0.07	0.04	0.05	0.09	0.05	0.07	0.12	0.07	0.06
MgO	2.70	4.11	2.94	3.31	3.30	4.04	1.00	1.29	3.57	4.16	0.91	2.36	3.24	3.13	1.77	0.91	1.43	3.74	1.43	2.33
CaO	0.81	1.74	3.45	6.36	3.51	2.54	2.22	4.92	3.18	6.93	18.07	2.63	2.01	1.16	4.66	18.21	3.72	5.16	2.62	4.44
Na2O	2.96	2.22	5.46	3.86	5.65	4.44	8.68	5.58	5.63	3.77	4.38	3.49	6.47	8.29	6.21	4.42	5.91	7.50	9.24	4.40
K2O	1.13	2.12	0.89	1.53	0.03	0.42	1.00	0.65	1.39	0.70	0.53	2.56	1.13	0.81	1.15	0.53	1.16	0.27	0.33	0.77
P2O5	0.12	0.16	0.15	0.15	0.13	0.14	0.28	0.17	0.11	0.17	0.11	0.18	0.13	0.12	0.17	0.11	0.12	0.19	0.15	0.15
L.O.I.	2.93	4.53	5.03	5.83	1.98	3.96	2.75	3.70	3.74	4.80	2.61	3.71	3.13	1.87	3.84	1.84	4.43	5.45	3.91	3.79
Total	99.42	100.59	100.66	100.31	99.53	100.39	101.45	100.95	101.38	99.68	100.48	99.17	100.02	101.47	100.38	100.48	100.26	101.27	98.42	100.35
Mg#	47.0	56.7	49.8	50.6	47.9	56.6	23.5	35.4	57.6	52.1	42.8	53.0	58.8	58.5	31.5	42.8	43.3	48.0	36.9	55.2
Ni	33	59	14	52	48	31	2.3	17	50	48	7.2	26	27	42	47	8	14	45	11	20
Cr	106	125	13	136	28	136	6.7	19	114	32	16	72	73	93	108	18	29	13	22	39
Ba	215	470	374	315	13	218	143	144	294	87	159	899	100	175	378	143	171	125	134	100
Rb	42.1	97.1	30	63.4		14.8	23.8	9.2	23.5	10.5	13.1	71.2	25.9	13.0	16.3	13.4	36.6	5.1	8.3	18.4
Sr	56.3	82.8	433.3	409.3	125.3	388.9	134.0	336.5	304.8	325.1	442.5	271.1	252.2	578.8	247.2	355.4	332.6	209.0	494.0	314.5
Th	11.3	11.8	4.2	13.0	3.3	7.1	6.0	4.6	2.5	3.5	2.6	13.0	3.4	2.5	2.7	3.5	3.4	3.6	2.5	1.9
U	2.2	2.8	0.5	2.8	1.0	1.4	1.5	0.6	< 0.5	< 0.5	< 0.5	2.0	< 0.5	< 0.5	< 0.5	0.6	0.9	0.1	< 0.5	0.8
Pb	9.4	9.7	2.0	13.2	< 0.5	4.2	6.6	5.5	< 0.5	5.4	0.2	13.1	4.7	2.8	3.9	0.3	4.5	4.7	0.3	0.9
Nb	10.1	13.9	4.6	13.7	17.2	6.2	7.8	4.5	2.7	4.1	1.8	10.2	4.1	3.0	6.3	2.3	3.6	5.3	4.0	2.3
Zr	235.9	194.9	133.2	171.2	292.1	141.3	228.2	167.7	110.2	146.3	93.0	190.3	148.9	125.1	174.1	93.7	133.9	158.9	149.7	81.9
Y	24.7	27.6	25.3	29.2	46.4	24.3	42.8	25.5	18.6	30.6	9.2	18.2	22.1	17.8	29.8	9.2	20.4	32.1	24.8	16.9
La	17.37	29.26	6.20	38.64	18.83	11.54	13.44	10.40	5.58	8.75	3.70	44.40	10.8	8.3	9.2	4.3	8.4	9.6	13.0	8.3
Ce	40.60	77.40	18.76	71.20	45.79	26.88	35.99	28.11	15.07	23.27	9.20	84.08	14	8	17	6.2	4.7	24.4	81.6	8.1
Pr	5.38	11.19	2.80	8.47	5.03	2.61	4.02	2.93	2.07	2.94	1.07	7.70	NA	NA	NA	NA	NA	NA	NA	
Nd	21.40	53.90	14.00	29.16	22.28	10.46	18.85	12.61	10.13	13.13	5.03	24.87	12.6	10.4	12.4	4.1	11.0	16.9	2.6	11.4
Sm	5.52	10.03	3.90	6.05	5.56	2.88	4.98	3.83	2.72	4.16	1.49	4.46	NA	NA	NA	NA	NA	NA	NA	NA
Eu	0.99	1.61	1.06	1.41	1.69	0.95	1.54	1.22	0.94	1.52	0.51	1.50	NA	NA	NA	NA	NA	NA	NA	NA
Gd	3.83	8.87	3.74	5.16	6.76	3.58	5.75	4.00	3.11	4.79	2.07	4.72	NA	NA	NA	NA	NA	NA	NA	NA
Dy	3.10	6.63	3.20	3.93	6.98	3.34	5.34	3.61	2.86	4.47	1.88	3.63	NA	NA	NA	NA	NA	NA	NA	NA
Er	1.70	3.48	1.88	2.76	4.18	1.89	3.27	2.13	1.52	2.70	0.95	2.40	NA	NA	NA	NA	NA	NA	NA	NA
Yb	1.78	2.69	1.83	2.36	4.73	1.96	3.40	2.06	1.50	2.75	0.69	1.48	NA	NA	NA	NA	NA	NA	NA	NA
Lu	0.29	0.52	0.29	0.36	0.71	0.30	0.53	0.32	0.23	0.41	0.13	0.24	NA	NA	NA	NA	NA	NA	NA	NA
Nb/Y	0.41	0.50	0.18	0.47	0.37	0.26	0.18	0.18	0.15	0.13	0.20	0.56	0.19	0.17	0.21	0.25	0.18	0.17	0.16	0.14
Zr/Y	9.55	7.06	5.26	5.86	6.30	5.81	5.33	6.58	5.92	4.78	10.11	10.46	6.74	7.03	5.84	10.18	6.56	4.95	6.04	4.85
Δ-Nb	-0.53	-0.19	-0.39	-0.06	-0.23	-0.32	-0.39	-0.58	-0.58	-0.44	-0.90	-0.47	-0.58	-0.66	-0.41	-0.80	-0.58	-0.38	-0.55	-0.44
(Nb/La)PRIMA	0.58	0.47	0.74	0.35	0.91	0.53	0.58	0.43	0.48	0.47	0.48	0.23								
(La/Sm)Chnd	2.03	1.88	1.03	4.12	2.19	2.59	1.74	1.75	1.33	1.36	1.60	6.43								
(Sm/Yb)Chnd	3.44	4.14	2.36	2.85	1.31	1.63	1.63	2.07	2.01	1.68	2.39	3.35								
(La/Yb)Chnd	6.99	7.80	2.43	11.73	2.85	4.23	2.84	3.63	2.67	2.28	3.82	21.54								

Major elements in wt. %; trace elements and REE in ppm.
Major and trace elements determined by XRF; REE determined by ICP-OES. †: La, Ce, and Nd determined using XRF.

PRIMA: Primitive mantle normalised (Hofmann 1988); Chnd: Chondrite normalised (Sun & McDonough 1989).
Δ-Nb relative displacement from the lower limit of the Iceland array in Figure 3.22

Table 3.3: *Sm-Nd concentrations and isotope ratios of ophiolitic rocks and samples 98M26 and 98M27 from the Delb Khairkhan mélange.*

Sample	Lithology	Sm (ppm)	Nd (ppm)	$^{147}Sm/^{144}Nd$	$^{143}Nd/^{144}Nd$ (measured)	$^{143}Nd/^{144}Nd$ (569 Ma)	ε_{Nd} (569 Ma)	Model Age (Ma)
97M74B	Basalt	1.00	3.39	0.1781	0.513024 ± 30	0.512360	+8.9	539
97M109	Basalt	4.15	12.17	0.2061	0.513080 ± 05	0.512312	+7.9	1367
98M109B	Basalt	4.83	16.28	0.1793	0.512984 ± 05	0.512316	+8.0	733
98M114B	Dolerite	3.81	12.11	0.1901	0.513046 ± 09	0.512337	+8.4	671
97M76	Dolerite	5.69	19.55	0.1759	0.513011 ± 06	0.512355	+8.8	562
97M110C	Basalt	5.09	15.04	0.2047	0.513074 ± 04	0.512311	+7.9	1252
97M74	Basalt	5.17	17.96	0.1741	0.512920 ± 08	0.512271	+7.1	883
98M20	Basalt	3.07	11.10	0.1671	0.512884 ± 10	0.512261	+7.0	868
98M40	Basalt	4.17	16.35	0.1541	0.512769 ± 08	0.512195	+5.7	972
97M67	Dolerite	3.64	15.41	0.1429	0.512725 ± 07	0.512192	+5.6	913
98M88C	Basalt	4.93	19.56	0.1526	0.512777 ± 13	0.512208	+5.9	929
98M28	Basalt	4.90	14.29	0.2073	0.512802 ± 09	0.512029	+2.4	7764
98M38	Basalt	5.88	23.29	0.1528	0.512793 ± 09	0.512223	+6.2	892
97M50	Gabbro	1.58	4.39	0.2175	0.513125 ± 11	0.512314	+8.0	-1128
98M51	Gabbro	1.81	6.15	0.1777	0.512764 ± 05	0.512101	+3.8	1622
98M97	Gabbro	1.41	5.29	0.1615	0.512619 ± 09	0.512017	+2.2	1540
98M79	Pyroxenite	1.03	5.88	0.1062	0.512783 ± 20	0.512387	+9.4	521
98M26†	Basalt	4.67	21.23	0.1329	0.512141 ± 09	0.511646	-5.1	1892
97M27†	Basalt	5.57	28.79	0.1169	0.511847 ± 15	0.511411	-9.6	2039

Uncertainties for the $^{143}Nd/^{144}Nd$ ratios are 2σ (mean) errors in the last two digits.

ε_{Nd} and initial $^{143}Nd/^{144}Nd$ values are calculated for a crystallisation age of 569 Ma (Kepizhinskas *et al.* 1991) relative to CHUR with present day values of $^{143}Nd/^{144}Nd = 0.512638$ and $^{147}Sm/^{144}Nd = 0.1966$ (Jacobsen & Wasserberg, 1980).

†: Samples from Delb Khairkhan Melange, ε_{Nd} and initial $^{143}Nd/^{144}Nd$ calculated using age of ophiolite as estimate

Table 3.4: *Sm-Nd concentrations and isotope ratios of Southern Volcanics.*

Sample	Lithology	Sm (ppm)	Nd (ppm)	$^{147}Sm/^{144}Nd$	$^{143}Nd/^{144}Nd$ (measured)	$^{143}Nd/^{144}Nd$ (500 Ma)	ε_{Nd} (500 Ma)	Model Age (Ma)
98M72	Andesite	5.20	19.94	0.1578	0.512751 ± 15	0.512234	+4.7	1083
98M62	Dacite	5.91	32.85	0.1087	0.511582 ± 10	0.511226	-15.0	2260
98M60	Dacite	3.26	12.08	0.1629	0.512828 ± 11	0.512294	+5.9	965
98M56	Dacite	3.29	13.82	0.1439	0.512503 ± 11	0.512032	+0.7	1406

Uncertainties for the $^{143}Nd/^{144}Nd$ ratios are 2σ (mean) errors in the last two digits.

ε_{Nd} and initial $^{143}Nd/^{144}Nd$ values are calculated for a crystallisation age of 500 Ma estimated from age of rhyolite dykes (474 Ma, Buchan *et al.* under peer review) that crosscut the Southern Volcanics relative to CHUR with present day values of $^{143}Nd/^{144}Nd = 0.512638$ and $^{147}Sm/^{144}Nd = 0.1966$ (Jacobsen & Wasserberg, 1980).

resin. Sm and Nd were separated from the other rare earth elements using HDEHP-coated Teflon powder. Total procedural blanks were <30 pg for Nd. Nd isotopic ratios were normalised to $^{146}Nd/^{144}Nd = 0.7219$. Repeated measurements of the La Jolla standard gave $^{143}Nd/^{144}Nd = 0.511837 \pm 0.000036$, $^{145}Nd/^{144}Nd = 0.348405 \pm 0.000022$ and $^{150}Nd/^{144}Nd = 0.236493 \pm 0.000081$ (2σ, n = 38; see Table B5).

Geochemical and Nd Isotopic concentrations of ophiolitic rocks

Major and trace element analysis of the Bayankhongor ophiolite rocks focussed on samples from the pillow basalt and sheeted dolerite dyke sections in order to minimise the contribution of crystal fractionation to any observed patterns in the data. In addition, the gabbros and pyroxenites of the cumulate section are more pervasively altered than the basalts and dolerites, and this may complicate interpretation of their geochemical characteristics. The pillow basalts and dolerite dykes of the Bayankhongor ophiolite exhibit similar mineralogy and essentially the same petrographic texture, although the dolerites are slightly coarser grained. Therefore, their chemical and isotopic characteristics are presented together.

Pillow Basalts and sheeted dykes

Major element concentrations

A selection of 58 samples of pillow basalts and dolerite dykes were analysed for major element chemistry (Tables 3.1a and 3.1c). The pillow basalts and dolerite dykes of the Bayankhongor ophiolite have a restricted range of SiO_2 (43-55 wt. %) but more variable total alkalis ($Na_2O + K_2O$ = 0.32-5.45 wt. %) concentrations. Using the classification of Le Maitre *et al.* (1989) these correspond to the field for basalts (Fig. 3.5). A few samples plot on the margin of the trachy basalt field (Fig. 3.5), which may be a result of ocean floor hydrothermal alteration. The basalts and dolerites have a wider range of MgO (10.4-3.9 wt. %) concentrations as expected for mafic rocks (Tables 3.1a & 3.1c, Fig. 3.6a), and a range in Mg# between 72 and 42. Other major element concentrations, such as TiO_2 (0.4-3.4 wt. %), Fe_2O_3 (5.8-16.2 wt. %), Al_2O_3 (13.0-22.7 wt. %), and CaO (3.1-12.7 wt. %), show greater variation. Plots of MgO (Figs. 3.6a & 3.6b) and more clearly Mg# (Figs. 3.6e & 3.6f) versus TiO_2 and Fe_2O_3, show a positive correlation of TiO_2 and Fe_2O_3 with decreasing MgO and Mg# indicative of combined fractional crystallisation of clinopyroxene and plagioclase (Schilling *et al.* 1983, Helz 1987), which is consistent with the observed phenocryst phases in the basalts and dolerites. A less pronounced positive correlation is apparent for MgO versus Al_2O_3 (Fig. 3.6c) which may relate plagioclase accumulation (Schilling *et al.* 1983, Helz 1987), but may also be affected by alteration. Plots of CaO versus MgO and Mg# (Figs. 3.6d & 3.6h) indicate a weak positive to horizontal correlation of CaO with increasing MgO and

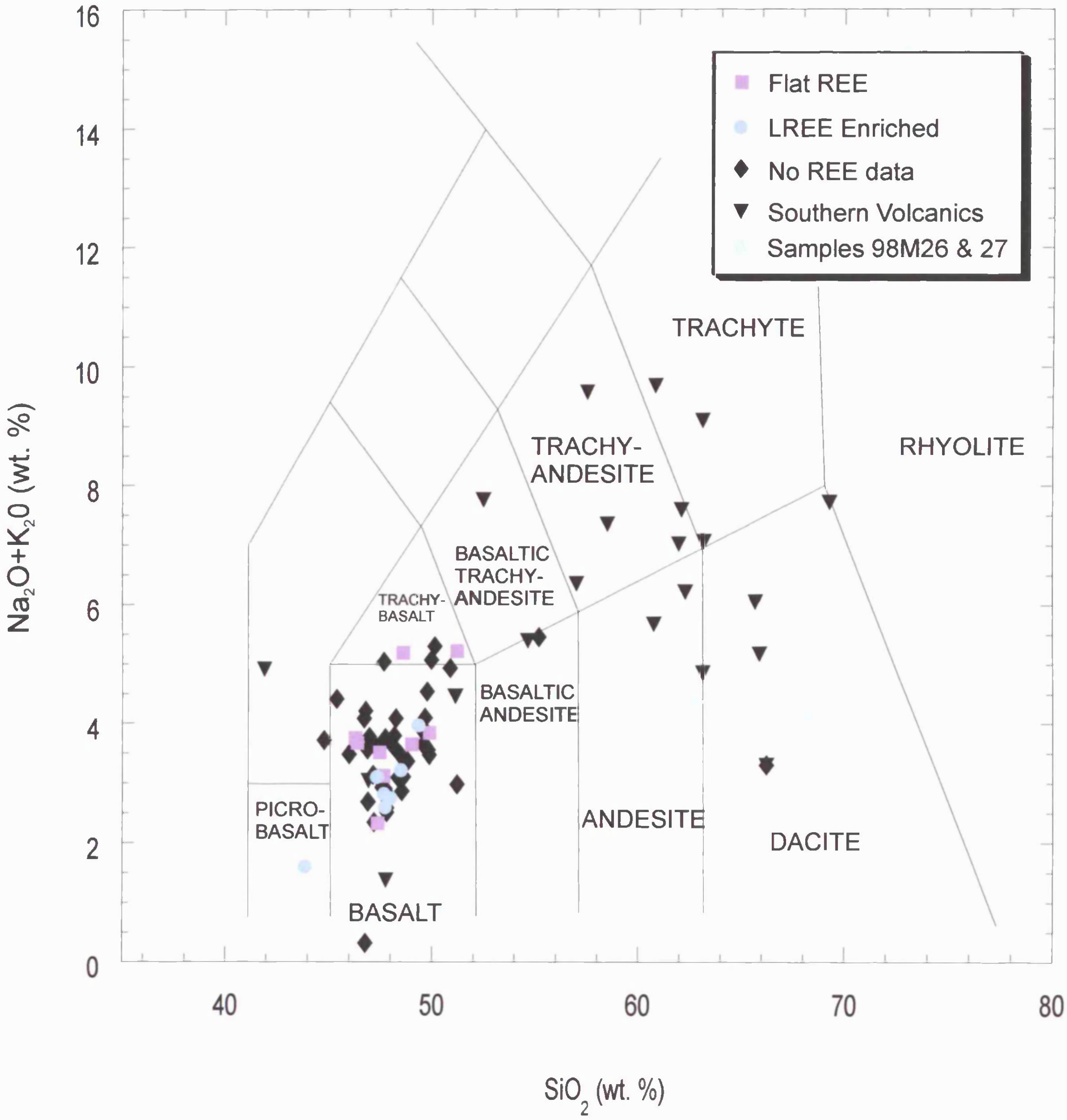

Fig. 3.5: Plot of SiO_2 vs. total alkalis for the Bayankhongor ophiolite rocks and Southern Volcanics. Classification fields are those of Le Maitre *et al.* (1989).

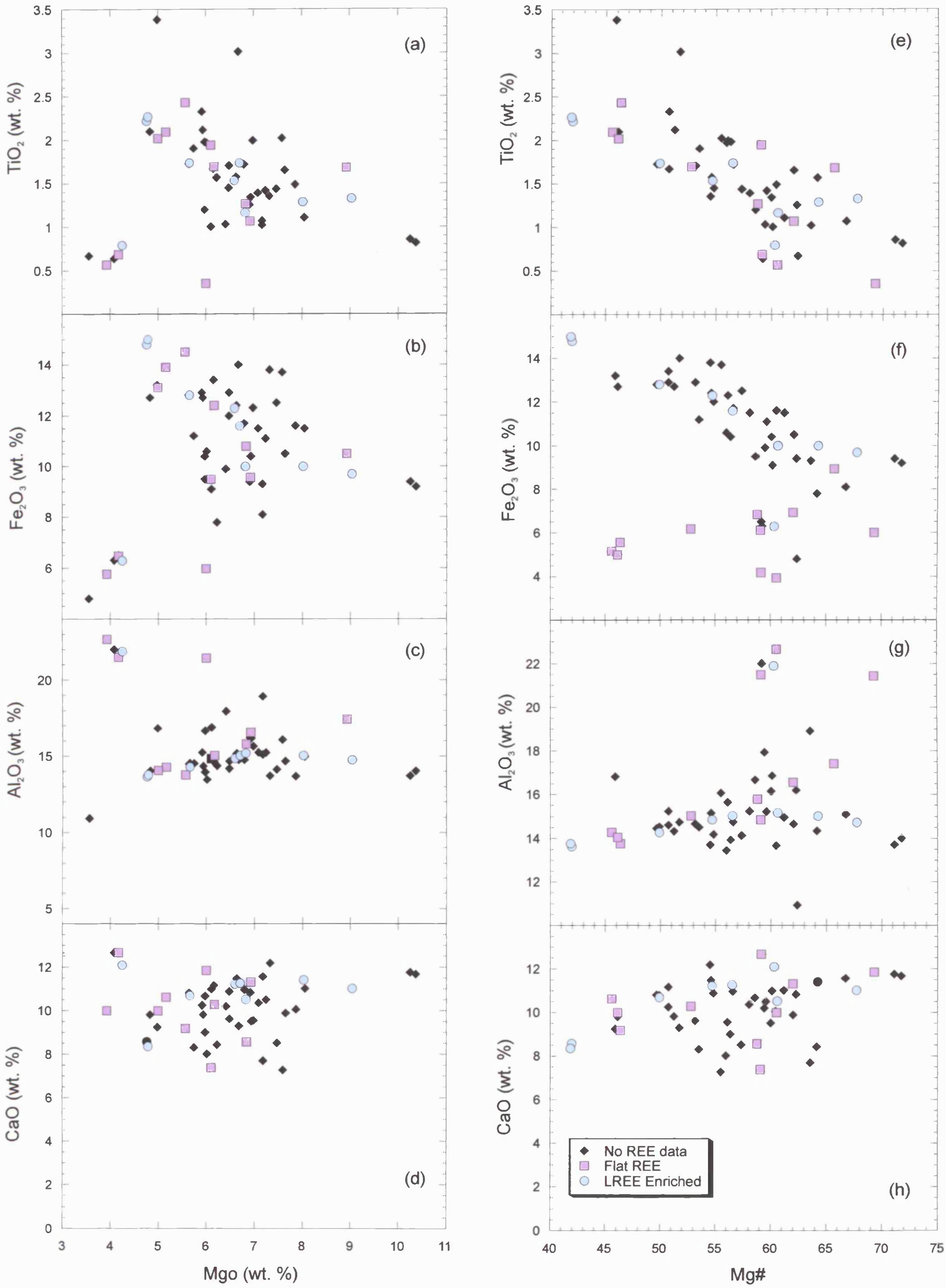

Fig. 3.6: Bivariate plots of major element compositional variation of the Bayankhongor ophiolitic basalts and dolerites.

Mg# and may be caused by plagioclase buffering of the melt (Cox & Hawkesworth 1985), which is consistent with the petrographic observation of plagioclase as the dominant phenocryst and groundmass phase in both the basalts and dolerites.

Trace and Rare Earth element concentrations

A selection of 20 of the freshest basalt and dolerite samples were analysed for trace and Rare Earth (REE) element concentrations, which are listed in Table 3.1a. In all samples Ba (17-441 ppm), Rb (0.8-29.9 ppm), and Sr (64.3-876.4 ppm) are the most variable elements and do not correlate with any partial melting or crystal fractionation indicators, suggesting that they may be affected by late stage alteration effects and so will not be considered further.

The Bayankhongor pillow basalts and sheeted dyke dolerites exhibit a large variation of trace element concentration from 10-100 times that of Primitive Mantle (Table 3.1a, Figs. 3.7a & 3.7b) and a similarly for the REE with 10-100 times Chondrite across the range of elements (Table 3.1a, Figs. 3.8a & 3.8b). Primitive mantle normalised (PRIMA) trace element patterns show that the basalts and dolerites fall into two groups. The first group is enriched in the Large Ion Lithophile Elements (LILE) and High Field Strength Elements (HFSE) compared to more compatible elements e.g. $(Nb/Yb)_{PRIMA}$ = 4.0-13.1 (Fig. 3.7a). The second group has almost flat trace element patterns with $(Nb/Yb)_{PRIMA}$ = 1.7-3.1, to mildly depleted LILE and HFSE patterns with $(Nb/Sm)_{PRIMA}$ = 0.64 (Fig. 3.7b).

REE concentrations for the pillow basalts and sheeted dykes are also variably enriched with element concentrations varying from 10-100 times chondrite across the range (Table 3.1a, Figs. 3.8a & 3.8b). Chondrite normalised (Chnd) REE patterns also identify two groups corresponding to those of the PRIMA patterns. The first group has enriched LREE relative to HREE with $(La/Yb)_{Chnd}$ = 2.7-10 (Table 3.1a, Fig. 3.8a), and the second group has essentially flat patterns $(La/Yb)_{Chnd}$ = 1.1-2.2, to slightly LREE depleted patterns indicated by $(La/Sm)_{Chnd}$ = 0.68 (Table 3.1a, Fig. 3.8b). Both the LREE enriched and flat REE groups have approximately the same HREE concentrations at around 10 times chondrite (Er = 6.8-28.5 ppm, Yb = 23.0-5.8 ppm, Lu = 5.2-22.0 ppm; Table 3.1a).

Nd isotope concentrations

A selection of 13 samples (10 basalt and 3 dolerite) were analysed to determine their Nd isotope concentrations. Samples were chosen to cover the whole of the range of trace element and REE concentrations described above. The analysed samples have measured $^{147}Sm/^{144}Nd$ = 0.1429-0.2073 and $^{143}Nd/^{144}Nd$ = 0.152725-0.153080 (Table 3.2). Initial ratios calculated for Kepizhinskas *et al.*'s (1991) suggested ophiolite age of 569 Ma, gives $^{143}Nd/^{144}Nd$ (569) = 0.512029-0.512355 (Table 3.2) and a total range of initial epsilon Nd values of $\varepsilon_{Nd(569)}$ = +2.4 to +8.8 (Table 3.2, Fig. 3.9). The groups identified by trace element and REE concentrations

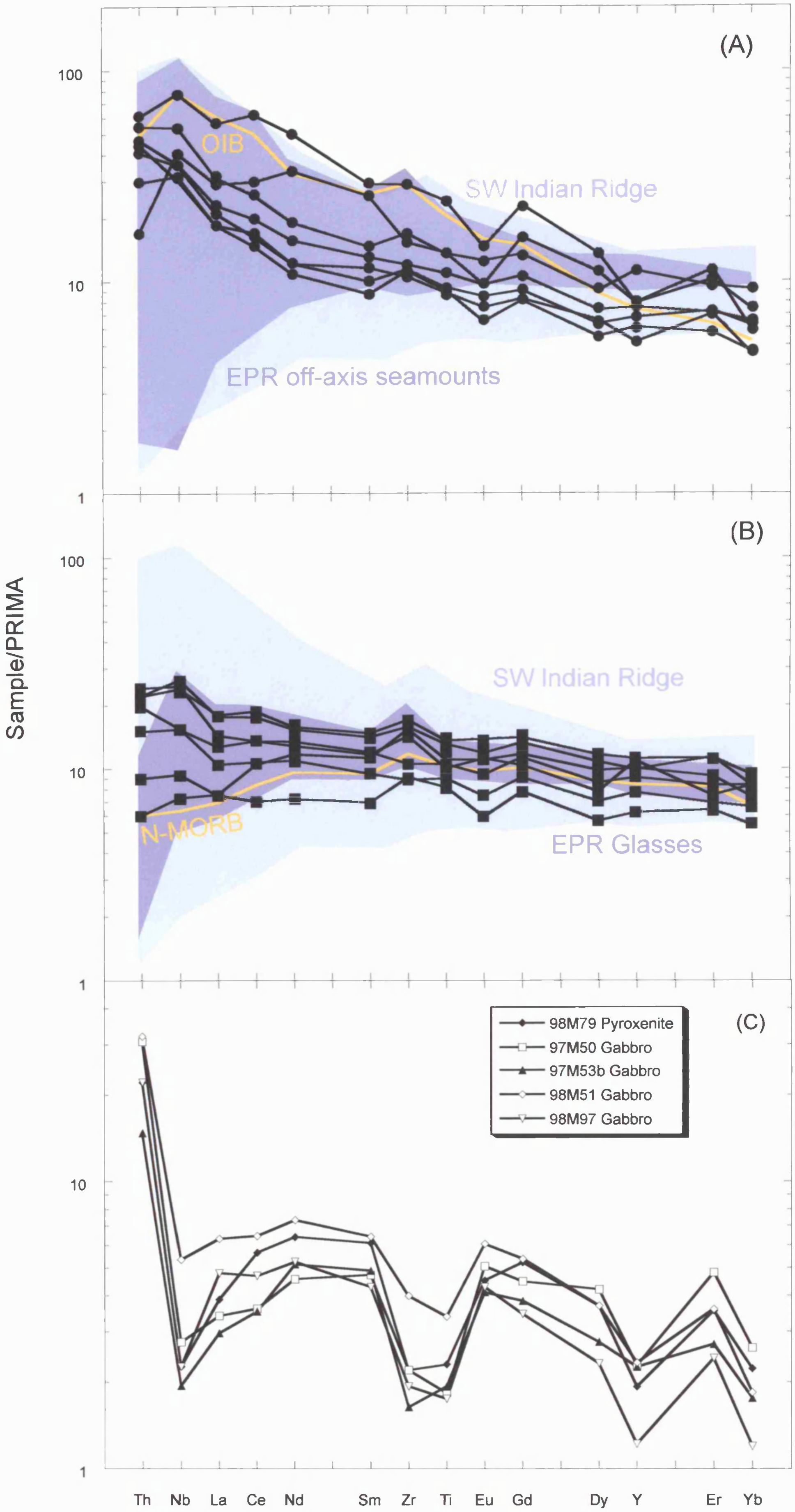

Fig. 3.7: Primitive mantle (PRIMA; Hofmann 1988) normalised trace element patterns for the Bayankhongor ophiolitic rocks. (A) & (B) Basalts and dolerites; (C) Cumulate rocks. For distribution of lithologies see Fig. 3.2. East Pacific Rise (EPR) ridge and off-axis, non-plume related seamount field is based on data taken from Niu *et al.* (1999), Cousens (1996), and Niu & Batiza (1997). Field of SW Indian ridge is based on data from Mahoney *et al.* (1998).

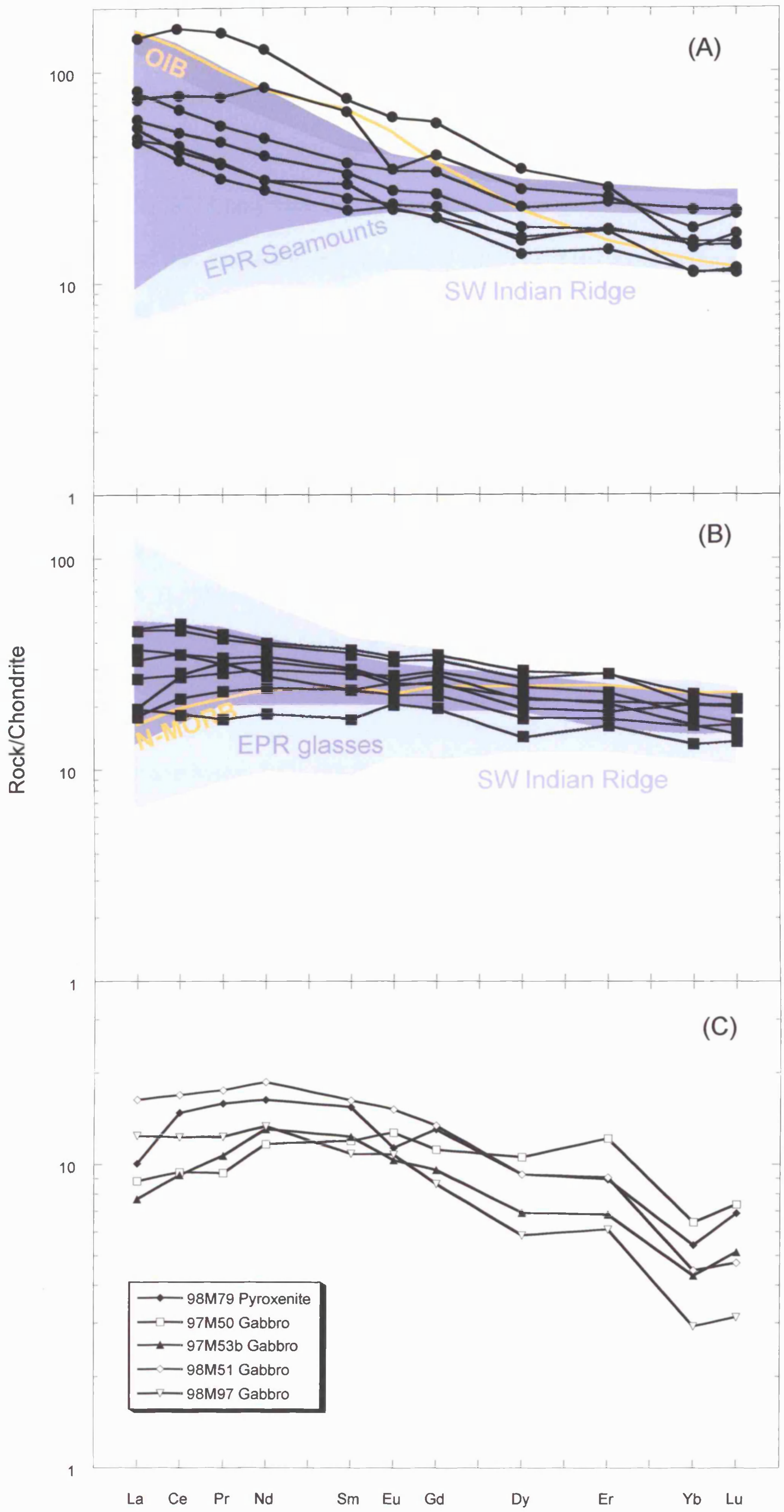

Fig. 3.8: Chondrite (Chnd; Sun & McDonough 1989) normalised REE patterns for the Bayankhongor ophiolitic rocks. (A) & (B) Basalts and dolerites; (C) Cumulate rocks. For distribution of lithologies see Fig. 3.2. East Pacific Rise (EPR) ridge and off-axis, non-plume related seamount field is based on data taken from Niu *et al.* (1999), Cousens (1996), and Niu & Batiza (1997). Field of SW Indian ridge is based on data from Mahoney *et al.* (1998).

also have different initial epsilon Nd values. The LREE enriched group have slightly enriched $\varepsilon_{Nd(569)}$ = +2.4 to +6.2 with the bulk concentrated around $\varepsilon_{Nd(569)} \approx +5.5$ (Fig. 3.10). The group with flat REE and trace element patterns have more depleted $\varepsilon_{Nd(569)}$ = +7.0 to +8.9 (Fig. 3.10) and the maximum value of $\varepsilon_{Nd(569)}$ = +8.9 is approximately the same as that of depleted mantle at the time (Fig. 3.9).

Gabbro and pyroxenite

Major element concentrations

A selection of 7 gabbro samples and 2 pyroxenite samples were analysed to determine their major element concentrations, which are given in Table 3.3. The gabbros have a very similar range of SiO_2 (44.8-58.1 wt.%) and Fe_2O_3 (4.4-13.2 wt. %) concentrations to the basalt and dolerites (Table 3.3). However they have a larger range of MgO (2.6-12.3 wt. %), Mg#(46.5-82.1), TiO_2(0.3-2.2), Al_2O_3 (10.2-19.5 wt. %), and total alkalis (Na_2O+K_2O = 1.6-5.4 wt. %, Table 3.3). No trends are identified on bivariant plots of MgO or Mg# versus other major elements and may reflect the greater degree of alteration of the gabbros.

The pyroxenites have lower SiO_2 (41.4-43.5 wt. %), TiO_2 (0.23-0.42 wt. %), Al_2O_3 (2.15-2.25 wt. %), and total alkalis (Na_2O+K_2O = 0.06-0.55 wt. %) than the other ophiolitic rocks. However, they have the highest MgO (28.5-29.6 wt. %), Mg# (100.6-101.1), and Fe_2O_3 (9.6-15.5 wt. %) concentrations.

Trace and Rare Earth element concentrations

The freshest gabbro (4 samples) and pyroxenite (1 sample) samples collected, were analysed to determine their trace element and REE concentrations, which are presented in Table 3.3. The gabbro and pyroxenite samples have very similar overall trace element and REE concentrations (Table 3.3). The apparent enrichment of Th (Fig. 3.7) relative to the rest of the trace elements, (e.g. $(Th/Sm)_{PRIMA}$ = 3.0-6.5, $(Th/Yb)_{PRIMA}$ = 8.4-18.5) for the gabbros and pyroxenites may be an artefact of XRF measurement, because the concentrations are close to the lower level of detection (2 ppm) by this method. PRIMA normalised trace element pattern for the gabbros and pyroxenites (Fig. 3.7) have pronounced negative Zr, Ti, Y, and Yb anomalies with respect to the other trace elements ($(Zr/Sm)_{PRIMA}$ = 0.34-0.62, $(Ti/Eu)_{PRIMA}$ = 0.36-0.56, $(Y/Er)_{PRIMA}$ = 0.47-0.83, $(Yb/Er)_{PRIMA}$ = 0.51-0.65; Fig. 3.7c). The gabbro and pyroxenite samples also have very similar chondrite normalised REE patterns (Fig. 8c). All samples are enriched in LREE with respect to HREE with $(La/Yb)_{Chnd}$ = 1.29-3.99 (Table 3.3, Fig. 3.8c).

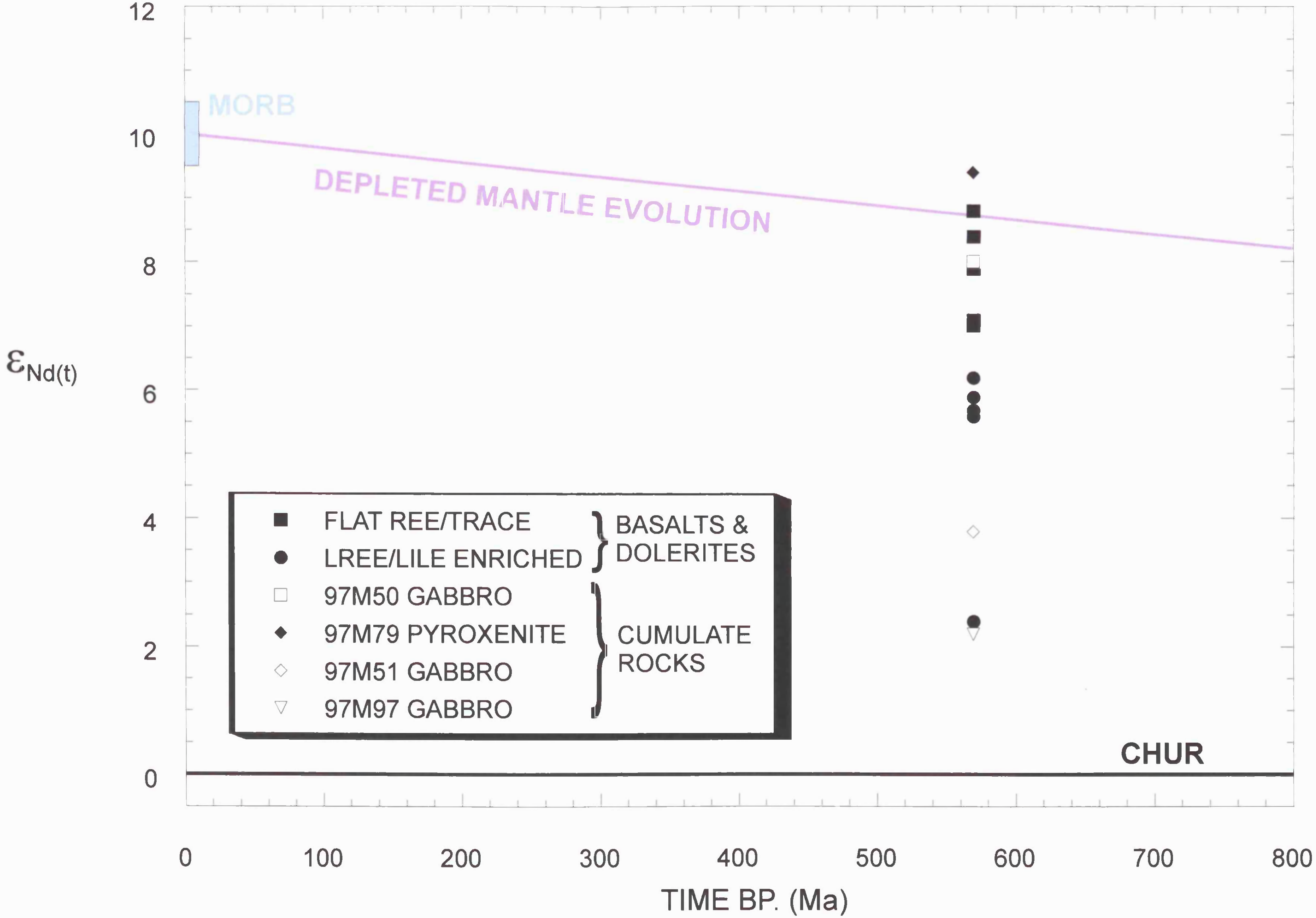

Fig. 3.9: Initial ε_{Nd} values for the Bayankhongor ophiolite rocks. For description of geochemical groupings see text and Figures 3.7 & 3.8. Depleted mantle evolution calculated using the model of De Paolo (1981). CHUR = Chondritic Universal Reservoir.

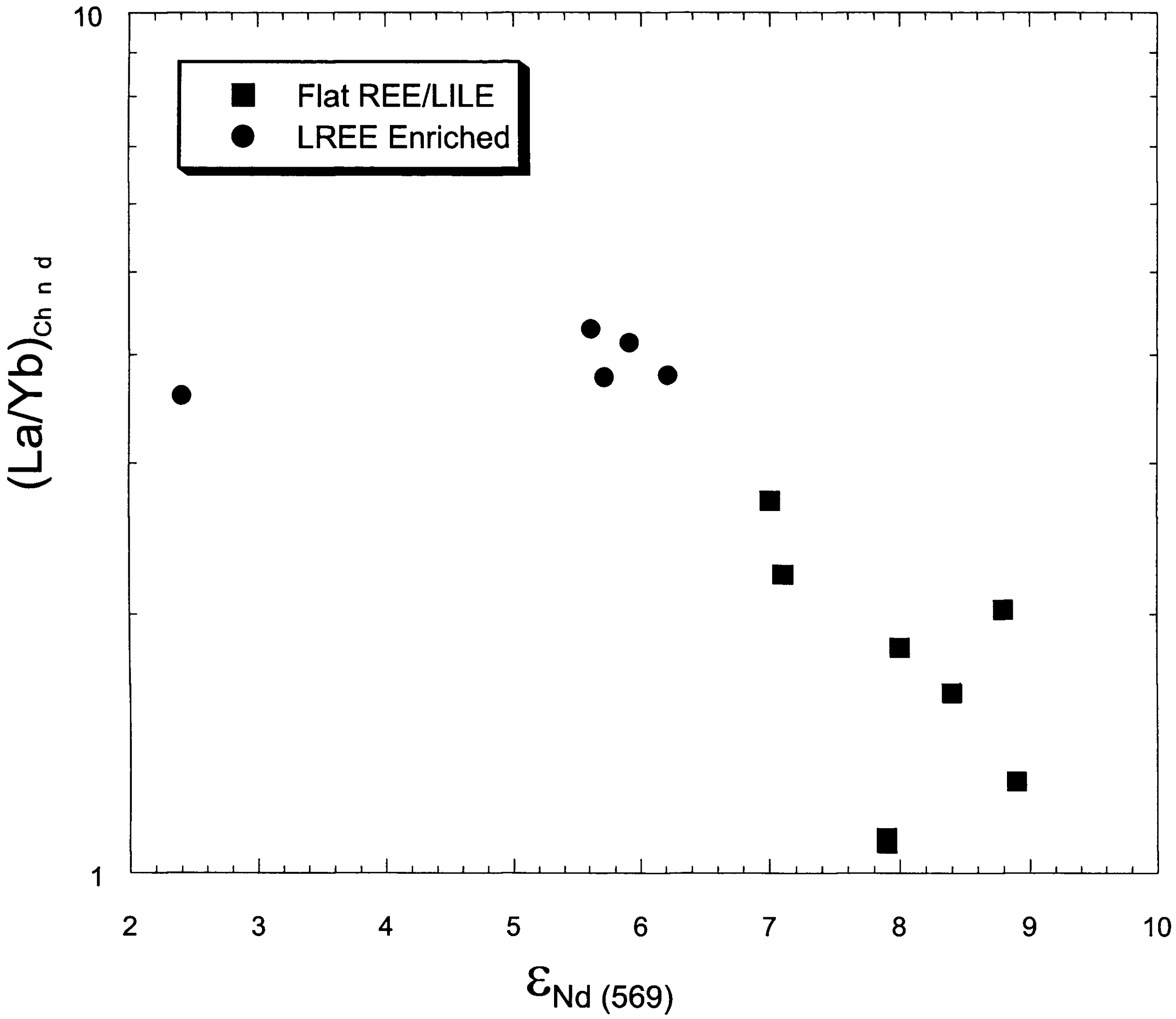

Fig. 3.10: Plot of chondrite normalised (Sun & McDonough, 1985) La/Yb ratio vs. initial ε_{Nd} of the Bayankhongor ophiolite basalts and dolerites. For description of geochemical groupings see text and Figures 3.7 & 3.8.

Nd isotope concentrations

Three gabbro and one pyroxenite samples were analysed to determine their Nd isotope concentrations, which are given in Table 3.2. The pyroxenite sample 98M79 has measured $^{147}Sm/^{144}Nd = 0.1062$ and $^{143}Nd/^{144}Nd = 0.512783$ (Table 3.2). Its calculated initial ratio at 569 Ma is $^{143}Nd/^{144}Nd\ (569) = 0.512387$ and it has an initial $\varepsilon_{Nd(569)} = +9.4$ making it the most depleted sample analysed during this study (Table 3.2, Fig. 3.9). The gabbros have a range of measured $^{147}Sm/^{144}Nd = 0.1062\text{-}0.2175$ and $^{143}Nd/^{144}Nd = 0.512619\text{-}0.513125$ (Table 3.2). Their calculated initial ratios have a range of $^{143}Nd/^{144}Nd\ (569) = 0.512101\text{-}0.512314$ and initial $\varepsilon_{Nd(569)} = +2.2$ to $+8.0$. The initial ε_{Nd} values of the gabbro samples correspond to the LREE enriched ($\varepsilon_{Nd(569)} = +2.2$ and $+3.8$) and flat REE ($\varepsilon_{Nd(569)} = +8.0$) basalt and dolerite groups with the gabbro ranges, but the restricted sample population of this study it is not certain if this would be true for all of the gabbro blocks in the ophiolite mélange. Note that there is no evidence from any of the ophiolitic samples for initial ε_{Nd} values as depleted as Kepezhinskas *et al.*'s (1991) gabbro value of $\varepsilon_{Nd(569)} = +11.9$.

Geochemical and Nd Isotopic concentrations of the Delb Khairkhan Mélange basalts

Buchan *et al.* (2001; Chapter 2) suggested that blocks of pillow basalt within the Delb Khairkhan mélange, may have been derived from the ophiolite, because the mélange also contains metaliferous and deep ocean sediments. To test this theory, samples of sheared basalts (98M26 and 98M27) were collected from the Delb Khairkhan mélange near to its thrusted contact with the ophiolite mélange (see Fig. 3.2 for location), in order to compare their chemical and isotopic characteristics with those of the ophiolite rocks.

Major element concentrations

Samples 98M26 and 98M27 have higher SiO_2 (62.7-68.3 wt. %) concentrations than the ophiolite basalts (Table 3.3). On the SiO_2 vs. total alkalis classification diagram of La Maitre *et al.* (1989) they fall in the andesite and dacite fields indicating that they are more evolved than the ophiolite rocks (Fig. 3.5), which is consistent with their lower MgO (2.7-4.1 wt. %) concentration. However the rest of their major element concentrations are broadly similar to those of the ophiolite basalts (e.g. Al_2O_3 = 12.7-15.0, TiO_2 = 0.7-0.8, and Fe_2O_3 = 6.9-7.1 wt. %; Table 3.3).

Trace and Rare Earth element concentrations

The trace element and REE concentrations of samples 98M26 and 98M27 are very different to those of the ophiolite basalts and are listed in Table 3.3. Plots of PRIMA normalised trace

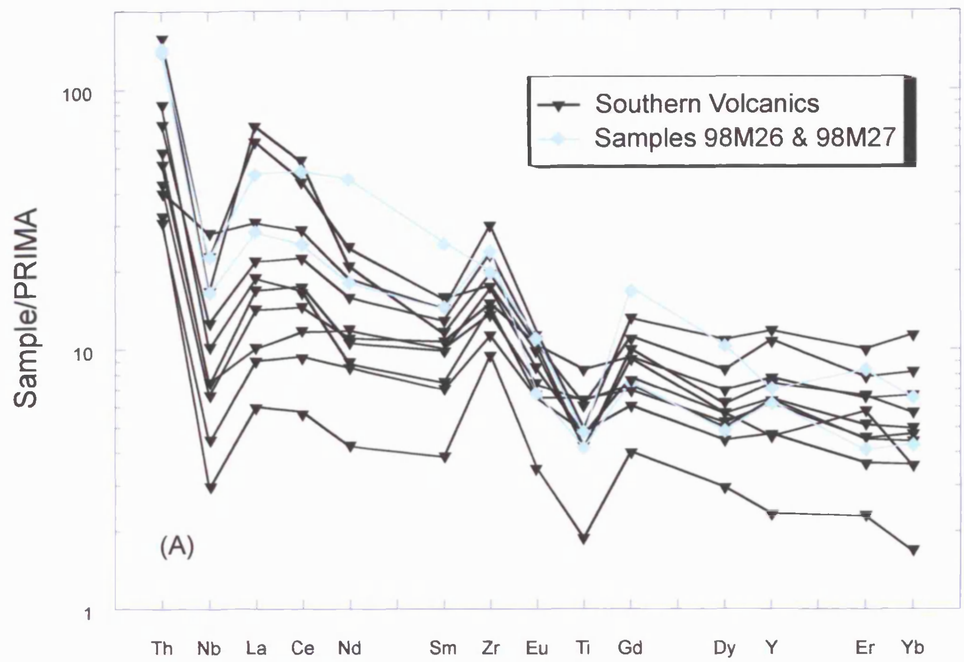

Fig. 3.11: Primitive mantle (PRIMA; Hofmann 1988) normalised trace element patterns for the Southern Volcanics and samples 98M26 & 98M27 from the Delb Khairkhan mélange (see Fig. 3.2 for location).

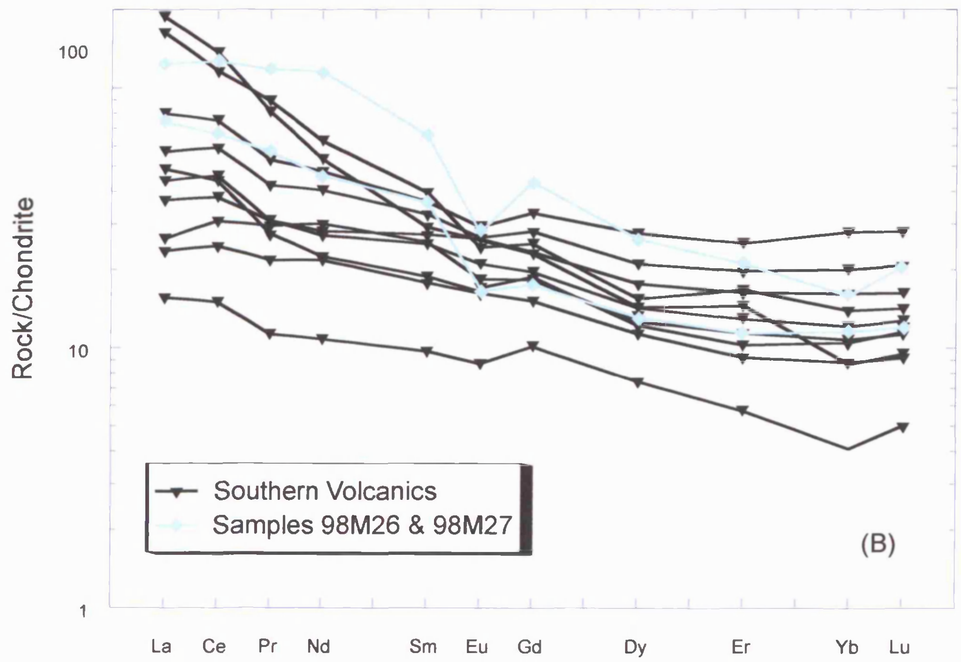

Fig. 3.12: Chondrite (Chnd; Sun & McDonough 1989) normalised REE patterns for the Southern Volcanics and samples 98M26 & 98M27 from the Delb Khairkhan mélange (see Fig. 3.2 for location).

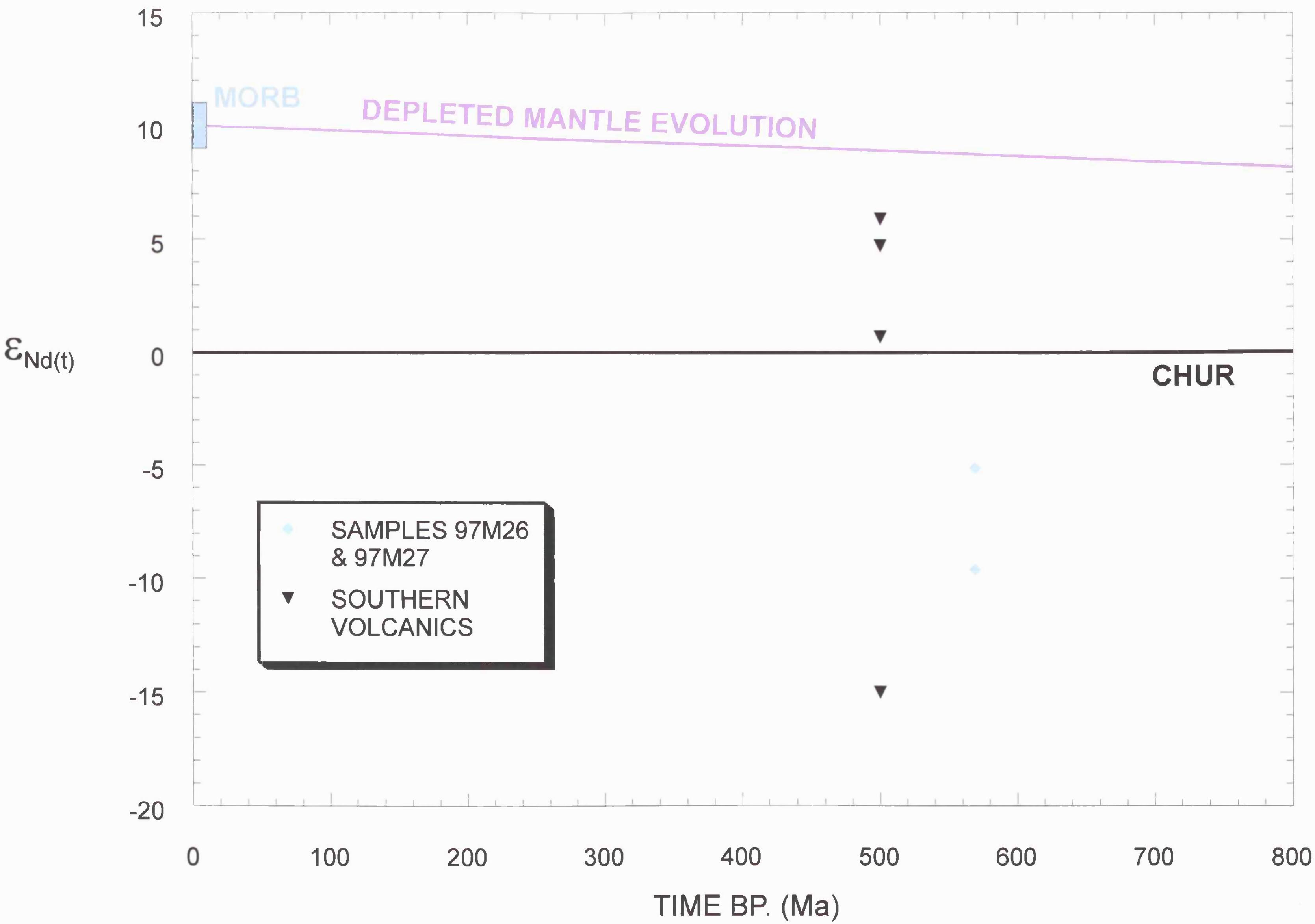

Fig. 3.13: Initial ε_{Nd} values for the Southern Volcanic rocks and samples 98M26 & 98M27 from the Delb Khairkhan mélange (see Fig. 3.2 for location). Depleted mantle evolution calculated using the model of De Paolo (1981). CHUR = Chondritic Universal Reservoir.

elements for samples 98M26 and 98M27, show that they are enriched in LILE relative to more compatible elements ($(Th/Sm)_{PRIMA}$ = 5.75-9.74; Fig. 3.11). However, they have marked negative Nb and Ti anomalies indicated by ratios of $(Nb/La)_{PRIMA}$ = 0.47-0.58, and $(Ti/Gd)_{PRIMA}$ = 0.27-0.56 (Fig. 3.11) which are not observed in the ophiolitic basalts. Chondrite normalised REE patterns of samples 98M26 and 98M27 (Fig. 3.12), indicate enrichment of LREE relative to HREE ($(La/Yb)_{Chnd}$ = 7.0-7.8) and are similar to those of the ophiolite basalts.

Nd isotope concentrations

Samples 98M26 and 98M27 have measured $^{147}Sm/^{144}Nd$ = 0.1169-0.1329 and $^{143}Nd/^{144}Nd$ = 0.511847-0.512141. The exact age of these basalts is unknown but in order to compare them with the ophiolitic basalts initial ratios and epsilon Nd values were calculated at 569 Ma giving initial $^{143}Nd/^{144}Nd$ (569) = 0.511411-0.511646 and initial $\varepsilon_{Nd(569)}$ = -5.1 and -9.6 (Fig. 3.13) which indicate that the source of samples 98M26 and 98M27 was much more evolved than that of the ophiolite.

Geochemical and Nd isotope concentrations of Southern Volcanics

Samples from the Southern Volcanic unit of the Bayankhongor zone (Fig. 3.2) were selected to represent the full range of lithologies that were identified in the field. More dacites were analysed because they are the dominant lithology in the Southern Volcanics.

Major element concentrations

A total of 18 samples were analysed to determine major element compositions, which are listed in Table 3.3. The Southern Volcanic rocks have a large range in SiO_2 (51.1-70.1 wt. %) and total alkalis (Na_2O+K_2O = 3.3-9.7) concentrations which reflects the variety of lithologies present in the unit from basalts to dacites and even trachytes (Fig 3.5; Table 3.3). The volcanics have a more restricted range of MgO (0.9-4.1 wt. %) concentrations than the ophiolitic rocks, but a larger range of Mg# (23.5-62.3; Table 3.3). They have a range of Al_2O_3 = 10.9-19.4, Fe_2O_3 = 2.7-9.1, CaO = 1.2-18.2, and TiO2 = 0.3-1.5 wt. % (Table 3.3). Bivariant plots of SiO_2 and vs. Al_2O_3, Fe_2O_3, CaO, and TiO_2 (Fig. 3.14) indicate negative trends with increasing SiO_2 consistent with fractionation of plagioclase and possibly magnetite as phenocryst and major groundmass phases (Wilson 1989). However, no correlation is apparent in bivariate plots of major elements vs. MgO or Mg# (Fig. 3.15).

Trace and Rare Earth element concentrations

Ten samples of the freshest samples were analysed to determine their trace element and REE concentrations which are listed in Table 3.3. The Southern Volcanics are all enriched in LILE

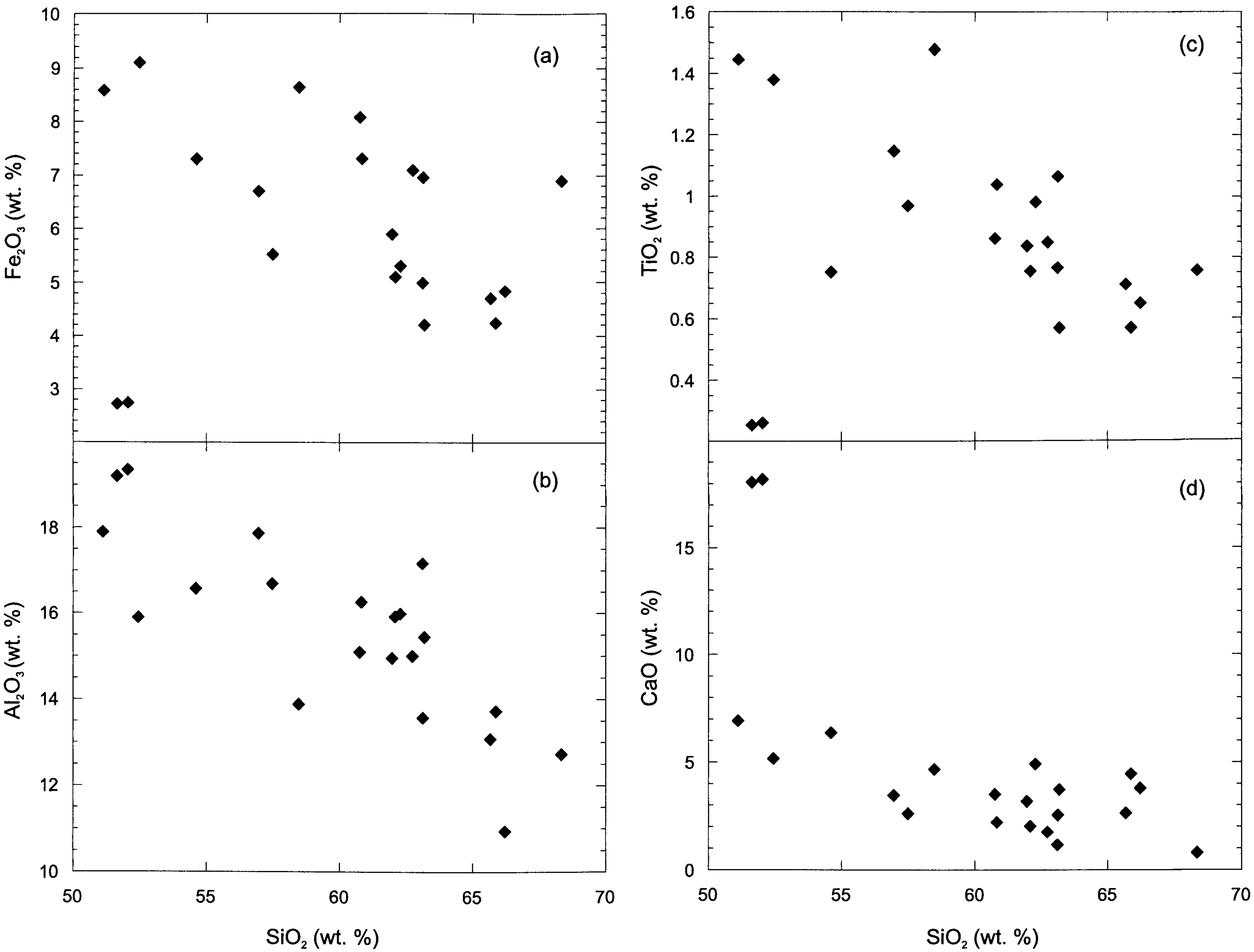

Fig. 3.14: Bivariate plots of major element compositional variation of the Southern Volcanic rocks.

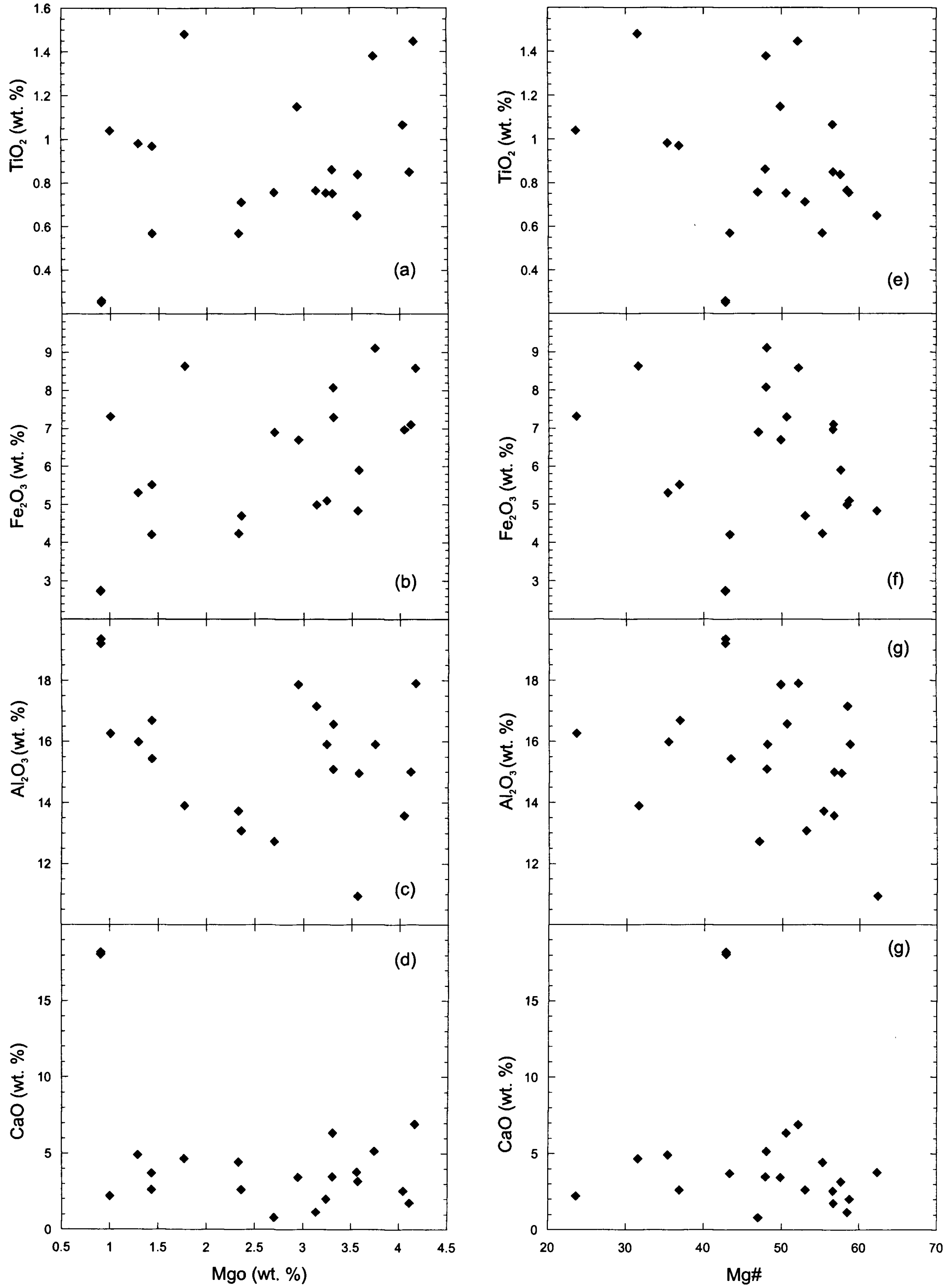

Fig. 3.15: Bivariate plots of major element compositional variation of the Southern Volcanic rocks.

(e.g. Ba = 13.8-899.2 ppm, Rb = 9.2-71.2 ppm; Table 3.3) and some of the HFSE (e.g. $(Th/Yb)_{PRIMA}$ = 3.6-44.8; Table 3.3). However, primitive mantle normalised trace element patterns (Fig. 3.11) indicate selective depletion of Nb and Ti relative to the rest of the trace element range with $(Nb/La)_{PRIMA}$ = 0.2-0.9 and $(Ti/Gd)_{PRIMA}$ = 0.3-0.9. Chondrite normalised REE patterns (Fig. 3.12) for the Southern Volcanics, show that all of the samples have enriched LREE relative to HREE indicated by $(La/Yb)_{Chnd}$ = 2.1-20.3. The southern volcanic samples have a larger range than the ophiolite rocks in HREE concentration with levels varying from 5 to 30 times chondritic (Fig. 3.12).

Nd isotope concentrations

Four samples from the Southern Volcanics were analysed to determine their Nd isotope concentrations which are listed in Table 3.4. The Southern Volcanic samples have a range of measured $^{147}Sm/^{144}Nd$ = 0.1087-0.1629 and measured $^{143}Nd/^{144}Nd$ = 0.51182-0.512828 (Table 3.4). The actual age of the Southern Volcanic rocks is unknown, but rhyolite dykes that intrude the volcanics have a crystallisation age of 474 Ma ($^{207}Pb/^{206}Pb$ zircon evaporation, see discussion in Chapter 4), which can be taken as an estimate of the minimum age of the volcanic rocks. In order to calculate initial Nd isotope ratios and initial epsilon Nd values a crystallisation age was estimated at approximately 500 Ma based on the age of the rhyolite dykes. This is a reasonable estimate since the Nd isotope ratios will not change significantly over 50 Ma. The calculated initial $^{143}Nd/^{144}Nd$ (500) = 0.511226-0.512294 and calculated $\varepsilon_{Nd(500)}$ = +4.7 to –15.0 (Table 3.4, Fig. 3.13).

Petrogenesis of the Bayankhongor ophiolite rocks

Whilst the stratigraphy of the Bayankhongor ophiolite and in particular the existence of an extensive sheeted dyke sequence, suggests that the rocks were produced by melting at a mid ocean ridge, the available field data do not uniquely indicate the type of oceanic basin within which the ophiolitic rocks were produced (e.g. a large Atlantic/Pacific type, or a supra-subduction marginal basin). Geochemical and isotopic characteristics of ophiolitic rocks provide insights into the type of magma sources from which the ophiolite partial melts were produced. Because source composition is affected by processes operating within a specific tectonic environment, identification of the ophiolitic magma source thus constrains the possible tectonic environments of ophiolite formation.

The data presented here for basalt and dolerite samples from the Bayankhongor ophiolite, demonstrate a high degree of chemical variability from relatively depleted high MgO (10.4 wt. %) and Mg# = 72 to more enriched compositions. However despite such variability, it is evident that the pillow basalts and dolerite dykes can be divided into two groups based on their trace element and REE characteristics. One group exhibits enrichment of LREE and LILE (Figs. 3.7a & 3.8a), whilst the other contains generally flat REE and trace elements patterns (Figs. 3.7b & 3.8b). The geographic distribution of the geochemical groups is shown on Figure 3.2, and despite a slight zonation, both groups are found across the whole mélange and within the same mélange blocks and so were probably formed within the same tectonic environment and not tectonically juxtaposed at a later time. In addition, the groups are not defined by differences in petrography because both porphyritic and aphyric basalts and dolerites are contained in the groups (Table 3.1).

It is important to constrain whether the two groups represent differences in source composition or are the result of varying degrees of partial melting and/or crystal fractionation effects on melts from a homogeneous source.

Partial melting effects

Because trace elements exhibit varying degrees of compatibility between a melt and residual solid, their abundance in an igneous rock is greatly influenced by the degree of partial melting that takes place (Sun & McDonough 1989). The general result is that low degree melts tend to concentrate highly incompatible elements such as LREE, whereas high degree partial melts tend to display more equal relative distributions of trace elements (Sun & McDonough 1989). This effect could produce the observed trace element groupings for the Bayankhongor basalts and dolerites, with small degree partial melts producing the LREE enriched group (Fig. 3.8a) and larger degree melts resulting in the flat REE patterns (Fig. 3.8b). One way of testing whether this is the case is to compare ratio pairs of highly incompatible elements whose bulk partition coefficients are very similar and will therefore vary little during partial melting (Bougault *et al.* 1980; Sun and McDonough 1989). Thus the slope of a correlation line on a bivariate plot of two such highly incompatible elements corresponds to the ratio of the concentration of the elements in the source and any variation in the ratio reflects heterogeneity in the source (Bougault *et al.* 1980). Figure 3.16 shows bivariate plots of elements considered to have very similar bulk partition coefficients during mantle melting for both of the trace element groups. Both of the groups define an approximately constant Nb/La ratio suggesting that variations in the concentration of these elements may be the result of partial melting. However, the other ratio pairs show that whilst the flat REE group tend to always form a correlation with constant slope, the LREE enriched group vary markedly from this trend. The variation of the LREE enriched group relative to the flat REE group suggests that for the bulk of the trace element concentrations, the relative differences in enrichment between the groups cannot be explained by partial melting.

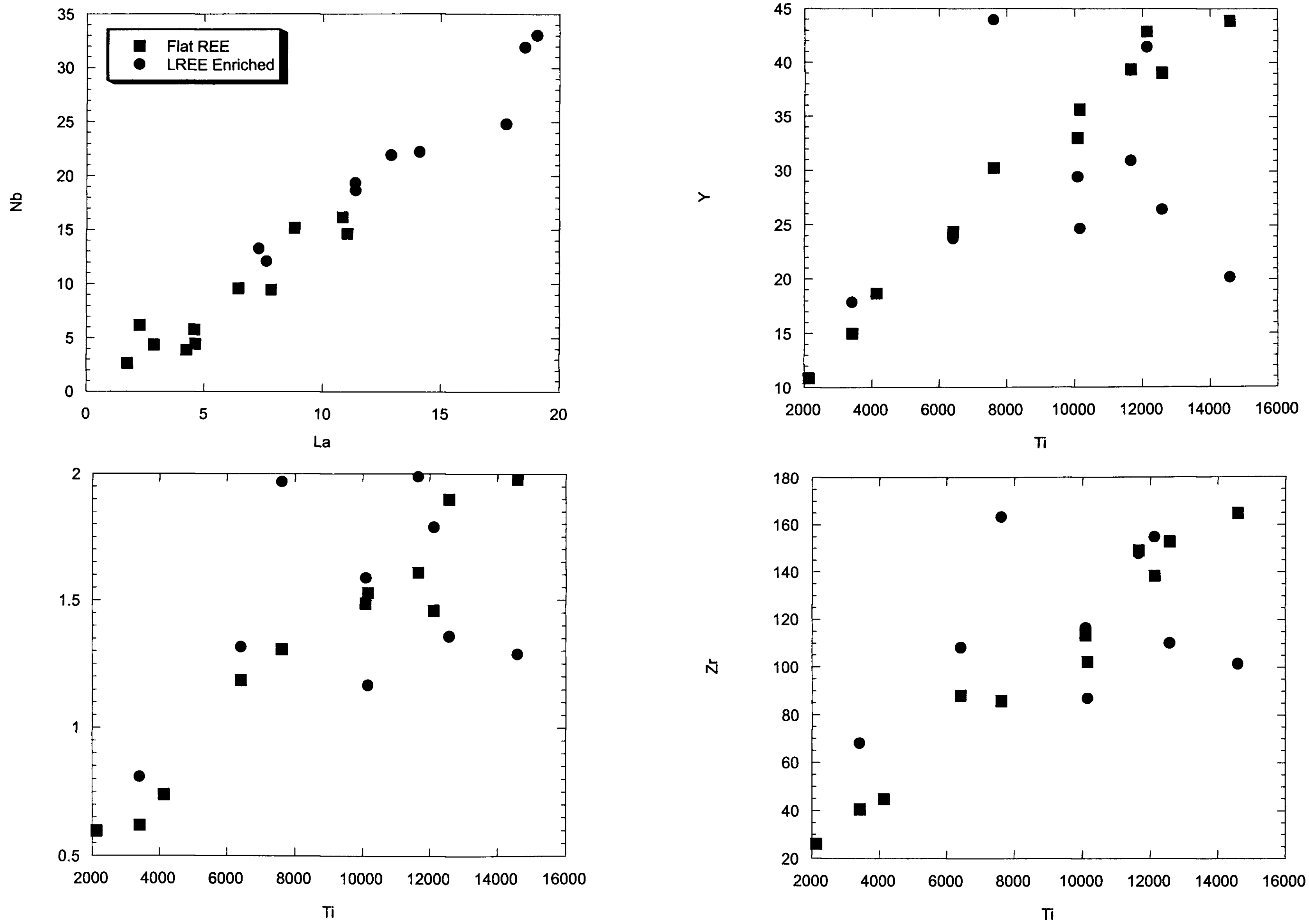

Fig. 3.16: Bivariate plots of variation in concentration of trace elements with very similar partition coefficients for the basalts and dolerites of the Bayankhongor ophiolite.

Fractional crystallisation effects

The correlation of major element concentrations illustrated in Figure 3.6, provides evidence that fractional crystallisation of plagioclase and clinopyroxene played a role in the evolution of the ophiolitic magmas. Fractional crystallisation can also affect the trace element evolution of melts and thus their concentrations in the resultant rock, because more compatible elements will be preferentially partitioned into mineral phases, whilst incompatible element will remain in the melt (Rollinson 1993). Because the concentrations of highly compatible elements in a liquid are most strongly affected by fractional crystallisation, bivariate plots of compatible elements against an index of fractionation can be used to test for its effects (Rollinson 1993). Plots of the highly incompatible elements Ni and Cr vs. MgO for the Bayankhongor ophiolitic rocks (Fig. 3.17), indicate that there is no clear correlation between these elements that can be attributed to crystallisation dependency.

Nd Isotope and trace element constraints for magma source composition

Because initial Nd isotope ratios of igneous rocks are directly related to those of their source and are not affected by crystal fractionation or alteration, they can be used to make direct inferences on the composition of the magma source. The initial ε_{Nd} values of the basalts and dolerites of the Bayankhongor ophiolite define two groups that correspond to those defined by trace elements and REE (Fig. 3.10).

The trace element and REE patterns of the Flat REE group resemble those of N-MORB to T-MORB and are similar to patterns for N-MORB basaltic glasses from the East Pacific Rise (EPR; Figs. 3.7b & 3.8b). All of the samples from this group plot consistently within the MORB field on trace element tectonic environment discrimination diagrams (Figs. 3.18 & 3.19). Initial epsilon Nd values of the N-MORB group fall in the range $\varepsilon_{Nd(569)} = +7.0$ to $+8.9$ and are close to the modelled value for the depleted mantle at 569 Ma of $\varepsilon_{NdDM\,(569)} = +8.8$ (De Paolo 1988; Stein & Hofmann 1994). The ε_{Nd} values and MORB-like trace element patterns (Fig. 3.8b), suggest that this group represents melts produced by partial melting of a depleted mantle source at a mid-ocean ridge.

Trace element and REE patterns of the LREE enriched group resemble those of OIB or E-MORB and are similar to patterns for off-axis seamounts associated with the EPR and E-MORB basalts from the SW Indian Ridge (Fig. 3.8a). The samples from this group plot within the E-MORB to within-plate tholeiite to alkali basalt fields on tectonic environment discrimination diagrams (Figs. 3.18 & 3.19). Initial epsilon Nd values of samples in the enriched group have a range of $\varepsilon_{Nd(569)} = +2.4$ to $+6.2$ (Fig. 3.10), which suggests that they were produced by melting of a more enriched mantle source than those of the N-MORB

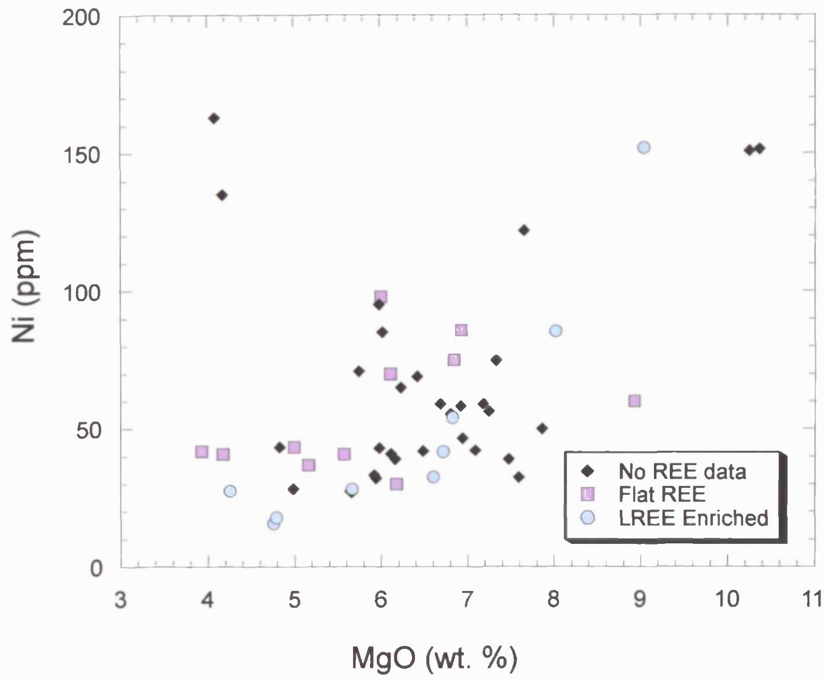

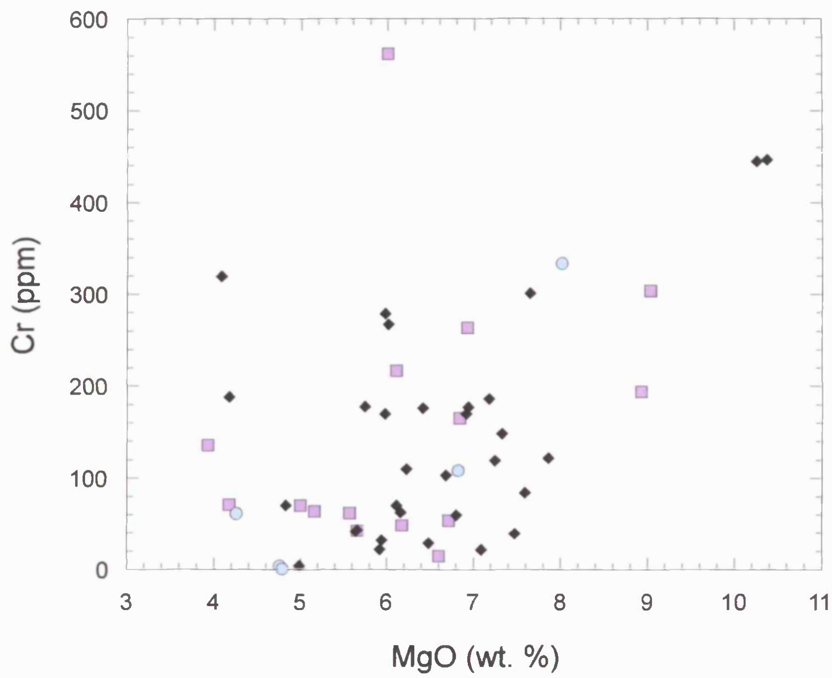

Fig. 3.17: Bivariate plots of the variation of the strongly incompatible elements Ni and Cr vs. MgO for the basalts and dolerites of the Bayankhongor ophiolite (See text and Figures 3.7 & 3.8 for descriptions of geochemical groups.

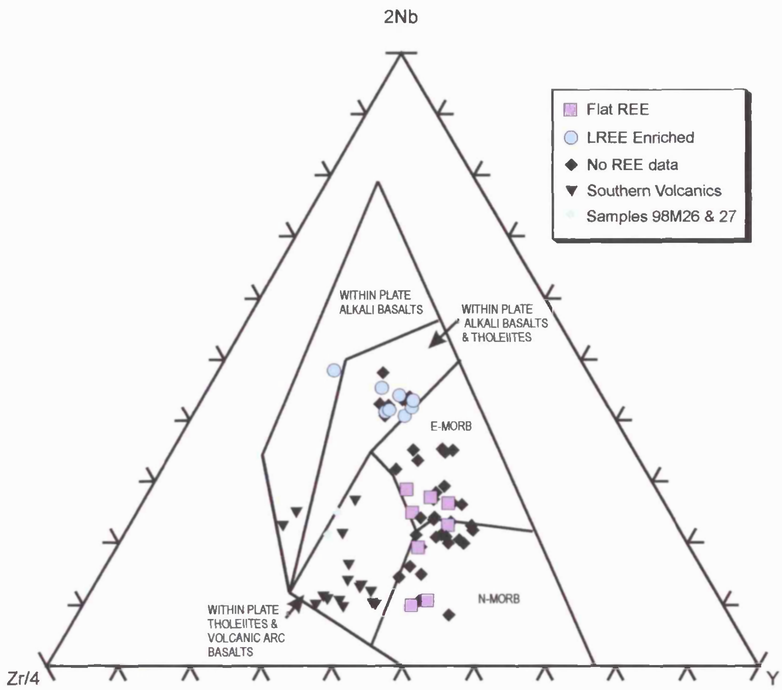

Fig. 3.18: Plot showing trace element discrimination of tectonic environment (Meschede 1986) for the basalts and dolerites of the Bayankhongor ophiolite, Southern Volcanic rocks, and samples 98M26 & 98M27 from the Delb Khairkhan mélange (See Fig. 3.2 for location).

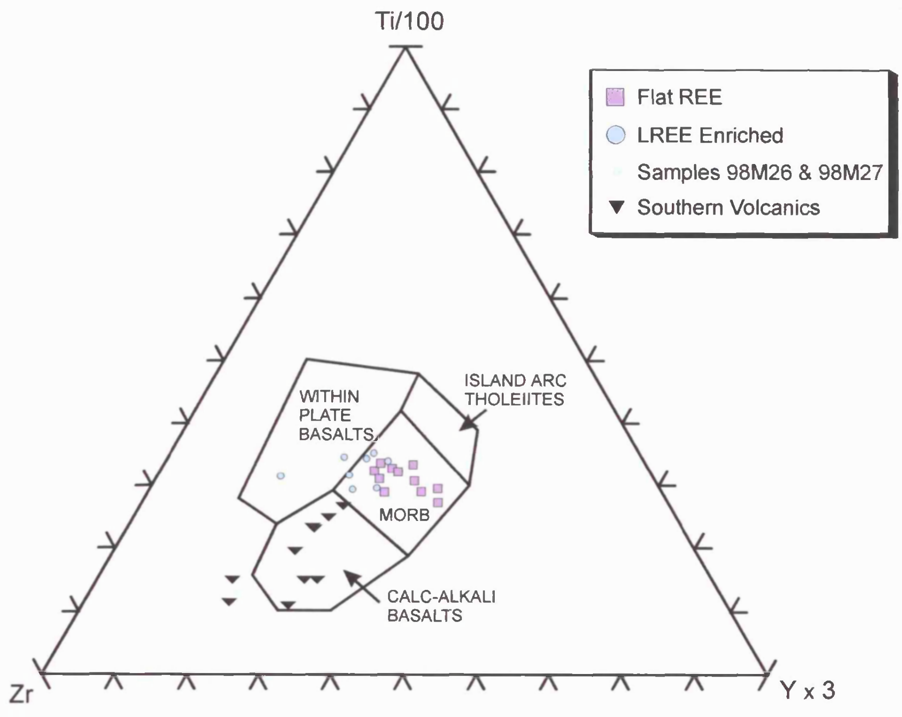

Fig. 3.19: Plot showing trace element discrimination of tectonic environment (Pearce & Cann 1973) for the basalts and dolerites of the Bayankhongor ophiolite, Southern Volcanic rocks, and samples 98M26 & 98M27 from the Delb Khairkhan mélange (See Fig. 3.2 for location).

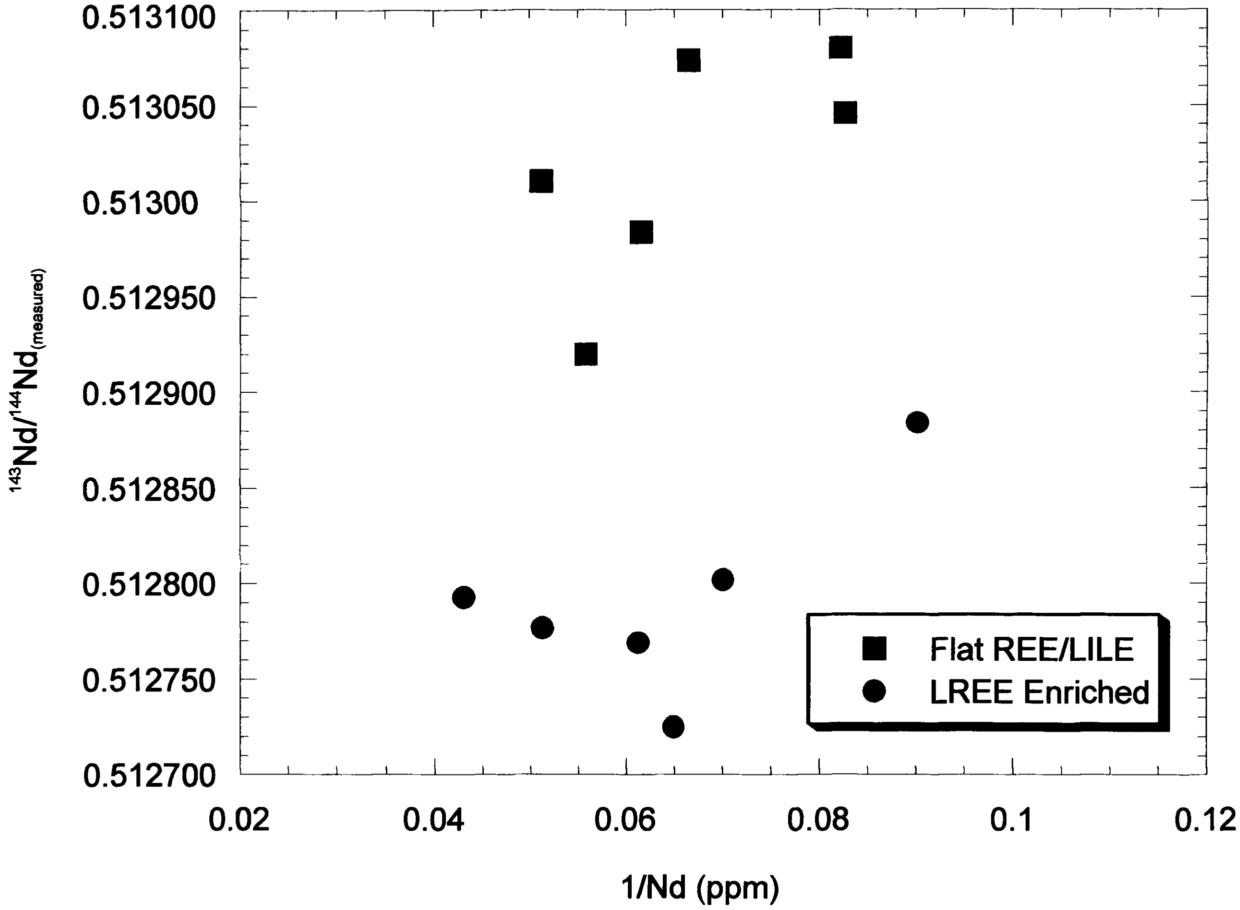

Fig. 3.20: Plot of variation of measured $^{143}Nd/^{144}Nd$ ratios vs. Nd concentration in ppm for the basalts and dolerites of the Bayankhongor ophiolite. For descriptions of the geochemical groupings see text and Figures 3.7 & 3.8.

group. However, the composition of the E-MORB basalts does not necessarily represent the actual composition of the enriched source, but instead may reflect an intermediary composition produced by mixing of an enriched source, with the depleted mantle N-MORB source. However, Figure 3.20 shows that there is no apparent simple two component mixing trend between the two groups. Therefore, it is suggested that the isotope ratios and trace element patterns of the Bayankhongor pillow basalts and sheeted dyke dolerites define two separate mantle sources for the ophiolite magmas.

Based on their initial ε_{Nd} values (Fig. 3.9), the gabbro and pyroxenite samples can also be divided into the depleted and enriched groups, despite having trace element and REE concentrations that are generally the same (Figs. 3.7c & 3.8c). The pyroxenite sample (98M79) has the most depleted initial $\varepsilon_{Nd(569)}$ = +9.4 (Table. 3.2) and may represent a part of the residual depleted mantle of the ophiolite, rather than a part of the cumulate section. Kepizhinskas *et al.* (1991) produced an initial $\varepsilon_{Nd(569)}$ = +11.9 for a gabbro sample from the Bayankhongor ophiolite, which is much higher than the modelled depleted mantle values of $\varepsilon_{NdDM\ (569)}$ = +8.8, and would suggest the presence of an ultra-depleted mantle source.

However, none of the samples analysed in this study produced ε_{Nd} values that were as depleted as those of Kepezhinskas *et al.* (1991), or that were significantly more depleted than values for depleted mantle at 569 Ma suggesting that there is no evidence for an ultra-depleted source.

Petrogenesis of the Delb Khairkhan Mélange basalts

Basalt samples 98M26 and 98M27 collected from the Delb Khairkhan mélange (Fig. 3.2), are petrographically similar to the basalts of the ophiolite mélange, but are geochemically very different. The trace element concentrations of the Delb Khairkhan mélange basalts show that they have LILE enrichment, but are depleted in the high field strength elements Ti and Nb relative to N-MORB patterns (Figs. 3.11 & 3.12). These characteristics are thought to result from processes that are unique to, or enhanced by melting in supra-subduction environments ('subduction signature') where fluids and melts expelled from the subducting oceanic crust preferentially enrich the mantle, which has been depleted by MORB extraction, with mobile elements such as LILE, whilst the relative depletion in immobile elements such as HFSE is increased since these are retained in the subducting crust (Pearce and Norry 1979; Wood 1980; Saunders *et al.* 1980; Pearce 1982; Shervais 1982; Pearce *et al.* 1984; Saunders & Tarney 1984). In addition, samples 98M26 and 98M27 plot within the calc-alkaline and volcanic arc fields on trace element tectonic discrimination diagrams (Figs. 3.18 & 3.19).

The Nd isotope systematics of samples the Delb Khairkhan mélange basalts also differ from those of the ophiolite rocks. Samples 98M26 and 98M27 have initial $\varepsilon_{Nd(569)}$ = -5.1 and -9.6 which require a considerably more enriched magma source than that of the ophiolite rocks. A subduction zone environment provides many possible candidates for such an enriched source by melting of subducted sediments and/or assimilation of continental crust or accreted sediments if the arc was located on a continental margin or on top of the accretionary prism. Assimilation of subducted sediment has been suggested to account for similar geochemical and isotopic characteristics for basalts from the Agardagh Tes-Chem ophiolite (Pfänder *et al.* submitted), which lies along strike to the north-west of Bayankhongor in southern Tuva (Fig. 3.1). The depleted mantle model ages of samples 98M26 and 98M27 of T_{DM} = 1892 Ma and T_{DM} = 2039 Ma are consistent with assimilation of older continental crust or crustal sediments.

The trace element and Nd isotope characteristics of the Delb Khairkhan mélange basalts suggest that their melts were extracted from different sources to those of the ophiolite and thus may have been produced within a different tectonic environment.

Petrogenesis of the Southern Volcanics

The Southern Volcanic rocks exhibit a larger variety of lithologies (Fig. 3.5) and more evolved compositions than those of the ophiolite mélange. It has been demonstrated that variations in the SiO_2 and total alkalis composition of the Southern Volcanic rocks reflects their lithological diversity (Figs. 5) but correlation of SiO_2 against other major elements suggest that their origin may be cogenetic (Fig. 13.4). The correlation of the highly incompatible elements Ni and Cr with MgO (Fig. 3.21), coupled with the observed major element trends (Fig. 3.14), suggests that fractional crystallisation may have played an important role in producing the diversity of lithologies observed in the Southern Volcanics.

Nd Isotope and trace element constraints for magma source composition

Despite the lithological diversity of the Southern Volcanics, their normalised trace element and REE patterns are essentially the same, and vary only in their bulk enrichment relative to PRIMA or chondrite (Figs. 3.11 & 3.12). The trace element concentrations of the volcanics indicate that they have a 'subduction signature' demonstrated by LILE enrichment, accompanied by depletion of Nb and Ti (Figs. 3.11 & 3.12), suggesting that the Southern Volcanics were formed within a supra-subduction zone environment. A supra-subduction interpretation for the origin of the volcanic rocks is consistent with tectonic environment discrimination diagrams, because the volcanic samples plot consistently within the volcanic arc or calc-alkaline basalt fields (Figs. 3.18 and 3.19).

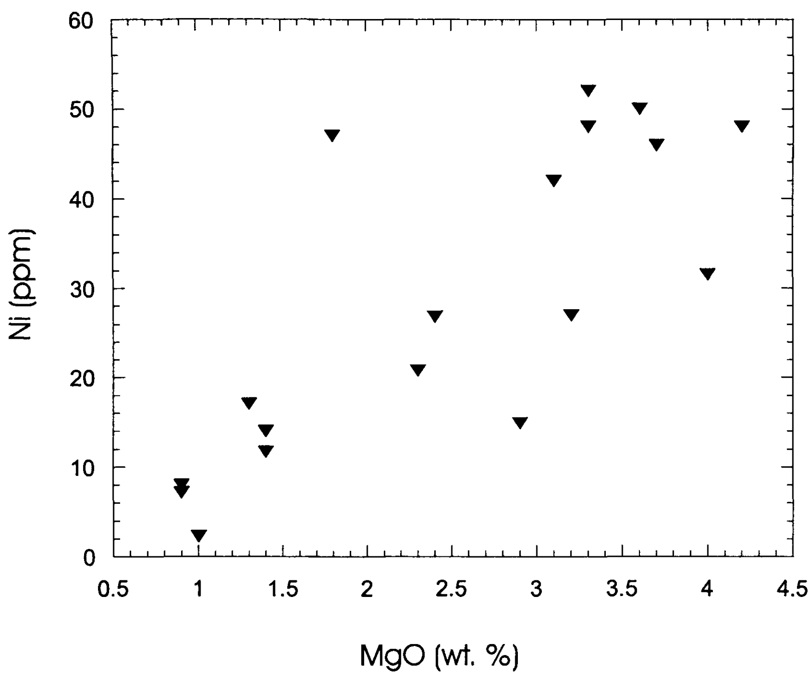

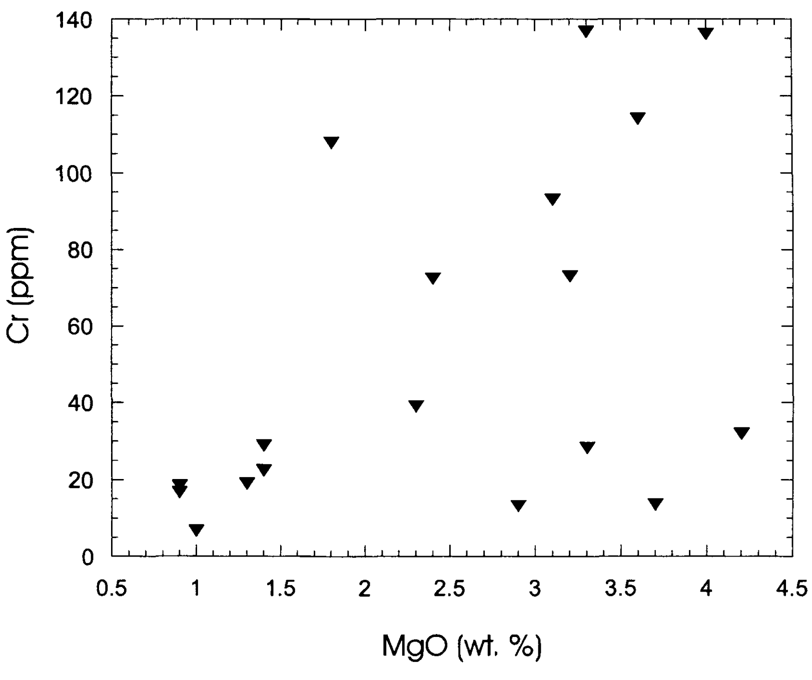

Fig. 3.21: Bivariate plots of the strongly compatible elements Ni and Cr vs. MgO. Correlation of Ni and Cr with falling MgO indicate that fractional crystallisation may have played an important role in the genesis of the Southern Volcanic rocks.

The Nd isotope systematics of the Southern Volcanics are highly variable with initial $\varepsilon_{Nd(500)}$ = +4.7 to –15.0 and depleted mantle model ages that range from T_{DM} = 965 Ma to T_{DM} = 2260 Ma. These factors suggest that the volcanic magmas were derived from a combination of a moderately enriched mantle source (compared to a depleted mantle with $\varepsilon_{NdDM(500)}$ = +8.9; DePaolo 1988) and a strongly enriched older crustal source. The original composition of the end member sources, and the processes by which they interacted to make the range of compositions observed is unclear and more extensive sampling is required in order to resolve these questions.

The evolved lithologies (trachytes and dacites), calc-alkaline nature and 'subduction signature' of the Southern Volcanics suggests that they may have formed in an island arc type setting. Chemically the Southern Volcanics are similar to the Delb Khairkhan mélange basalts (98M26 and 98M27), but because the age of the Delb Khairkhan rocks is unknown, their tectonic relationship with the Southern Volcanics is unclear.

Magma source constraints on the tectonic environment of formation of the Bayankhongor Ophiolite rocks

The identification of multiple source components for the Bayankhongor ophiolite rocks has implications for the tectonic environment in which they were created, because it must contain a mechanism by which melts can be produced that preserve evidence of distinct mantle sources. Several different modern ocean environments exist that could account for either a single heterogeneous mantle, or the existence of distinct mantle sources that interact to produce oceanic crust with variable geochemical and isotopic characteristics. This section examines some of these possible environments and discusses their validity as tectonic environments in which the Bayankhongor ophiolite could have formed with respect to the constraints provided by field relations and geochemical characteristics.

Mantle plume as the enriched source component of the Bayankhongor ophiolite

One of the simplest mechanisms to produce oceanic crust with both depleted and enriched source signatures is by the interaction of an enriched mantle plume with depleted upper mantle. Mantle plumes or 'hot-spots' in an oceanic intra-plate setting result in chains of large oceanic islands that can contain both enriched and depleted mantle signatures such as the Emperor seamounts containing the volcanically active Hawaiian islands (Leeman *et al.* 1994; Norman and Garcia *et al.* 1999), or the Galapagos islands created by the Galapagos plume (White *et al.* 1993; Geist *et al.* 1998 Hoernle *et al.* 2000). Alternatively enriched mantle plumes that impinge on a mid-oceanic ridge can produce enriched OIB and E-MORB basalts from melting of the plume, or N-MORB to T-MORB basalts through entrainment of the depleted upper mantle surrounding the plume. A plume-ridge interaction model has been suggested to explain the basalt chemistry and topographic expression of Iceland (Fitton *et al.* 1997; Kempton *et al.* 2000; Hards *et al.* 2000; Hanan *et al.* 2000), parts of the Mid-Atlantic ridge (Yu *et al.* 1997; Cannat *et al.* 1999; Hannigan *et al.* 2000), and the Pacific-Antarctic ridge (Hekinian *et al.* 1999). A third possible environment for producing basalts more enriched than MORB is as part of an oceanic plateau such as the Ontong Java, Kerguelan and Caribbean-Colombian plateaus (Kerr *et al.* 2000, Frey *et al.* 2000, Lapierre *et al.* 2000). However, basalts produced in these environments tend to have exclusively flat REE patterns (Kerr *et al.* 2000) and so cannot explain the OIB-like patterns of the Bayankhongor rocks.

On plots of Zr/Y vs. Nb/Y (Fig. 3.22), the basalts and dolerites of the Bayankhongor ophiolite plot largely within the Iceland array of Fitton *et al.* (1997), but form two distinct groups with one concentrated towards the depleted end of the array whilst the other plots at the more enriched end. The ophiolite samples which plot below the lower limit of the array are those which have chondrite normalised LREE depleted N-MORB-like REE patterns and correspondingly plot within the range of MORB basaltic glasses from the East Pacific Rise (EPR; Fig. 3.22). Fitton *et al.* (1991) suggested that the resultant array could be used to discriminate plume related basalts from those formed at mid ocean ridges and within island arcs, because basalts produced by melting of depleted mantle have lower Nb/Y ratios and higher Zr/Y ratios than plume basalts and so will plot below the lower limit of the array. This has been shown to be true for the Ontong Java and Caribbean-Colombian oceanic plateau basalts (Kerr *et al.* 2000) and also most ophiolites which are suggested to be plume related (Fig. 3.23). In addition, MORB ophiolites such as the Internal Liguride ophiolite plot below the lower limit of the array close to the EPR MORB field (Fig. 3.23). However, it can be shown that enriched non-plume related basalts also plot within the Iceland array, such as those from slow spreading SW Indian mid-ocean ridge and non-plume related seamounts and off-axis basalts from the EPR (Fig. 3.23b). Also, ophiolites that are interpreted to have formed within supra-subduction zone settings, such as in Oman (Searle 1999; Shervais 2001) and Troodos (Robertson & Xenophontos 1993), also plot within or cross the lower boundary of the array (Fig. 3.23b) and yet these bodies were not formed by plume related magmatism, but do contain some basalts with enriched trace element chemistry (Shervais 2001). Therefore, it appears that caution must be exercised when interpreting samples which plot within the Iceland array as necessarily plume related. Nevertheless, the array does help to identify the existence of possible enriched mantle components.

On the basis of geochemistry and Nd isotope concentrations alone, it is possible that the Bayankhongor basalts were sourced from a mantle plume as suggested by Kepizhinskas *et al.* (1991) and by the fact that they plot within the Iceland array (Fig. 3.22). However, there is no

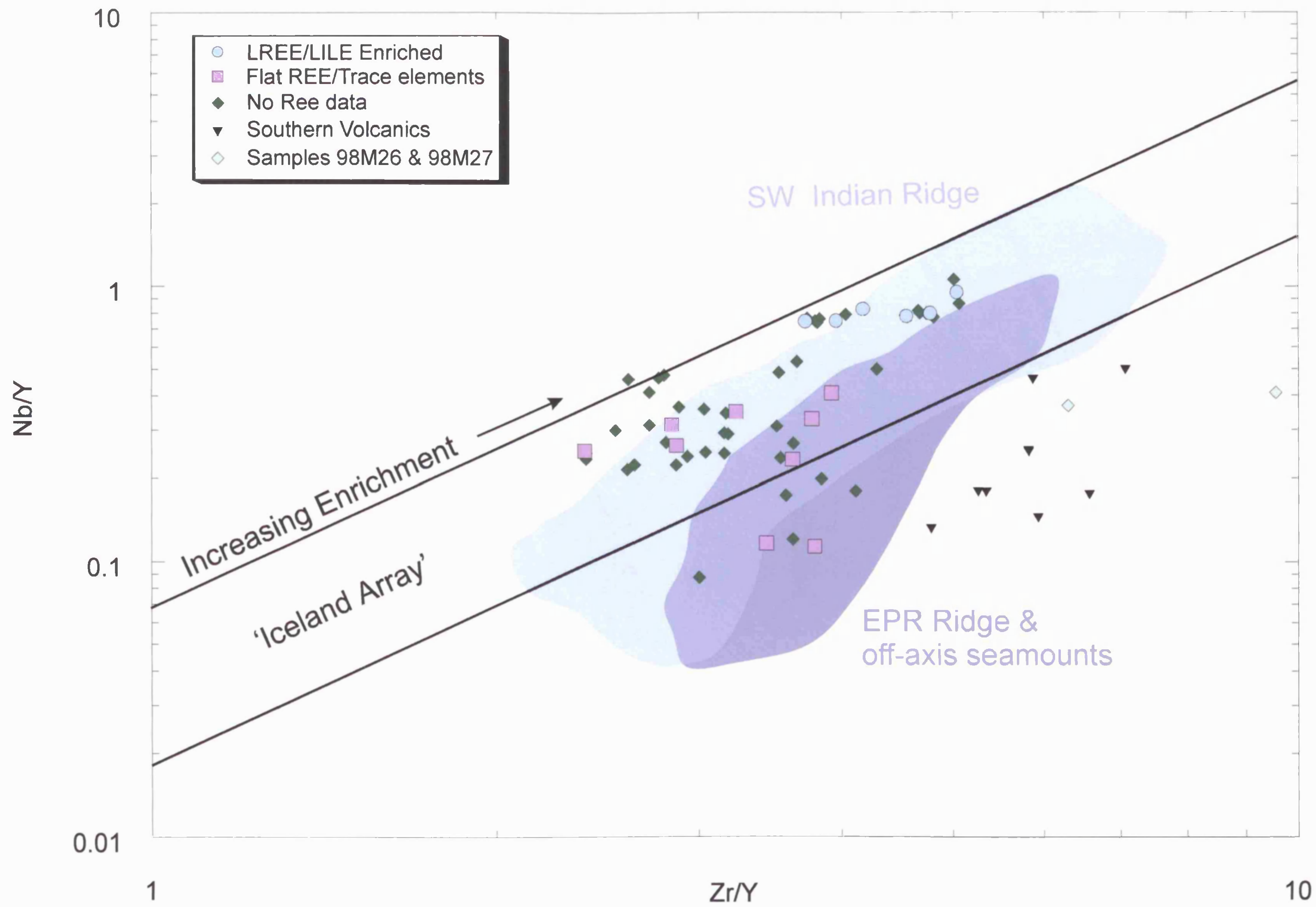

Fig. 3.22: Plot of the variation of Log (Nb/Y) vs. Log (Zr/Y) for the basalts and dolerites of the Bayankhongor ophiolite. Iceland Array after Fitton *et al.* (1997). East Pacific Rise (EPR) ridge and off-axis, non-plume related seamount field is based on data taken from Niu *et al.* (1999), Cousens (1996), and Niu & Batiza (1997). Field of SW Indian ridge is based on data from Mahoney *et al.* (1998).

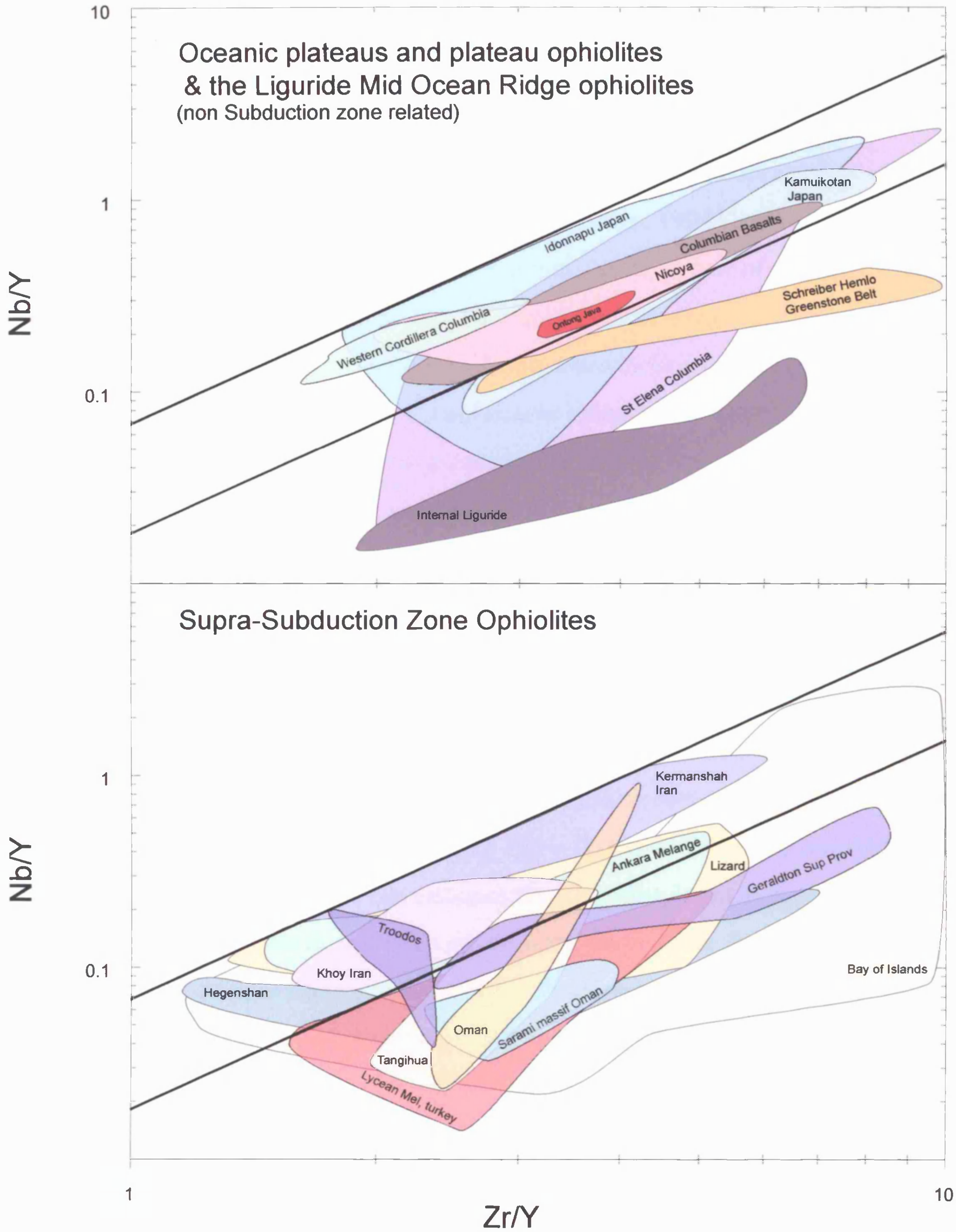

Fig. 3.23: Plot of the variation of Log (Nb/Y) vs. Log (Zr/Y) for basalts from various tectonic settings. Fields are Oceanic plateaus: Ontong Java and Colombian Basalts (Kerr *et al.* 2000); Plateau ophiolites: Nicoya Complex Costa Rica (Sinton *et al.* 1997; Hauff *et al.* 2000), St. Elena Columbia (Hauff *et al.* 2000), Western Cordillera Columbia (Millward *et al.* 1984), Idonnapu Greenstones Japan (Ueda *et al.* 2000), Kamakuikotan Japan (Kimura *et al.* 1994), and Schreiber Hemlo Greenstone Belt Superior Province Canada (Polat & Kerrich 1999); N-MORB ophiolite: Internal Liguride ophiolite Italy (Rampone *et al.* 1998); Supra-Subduction Zone Ophiolites: Troodos (Cameron 1985), Oman (Alabaster *et al.* 1992), Sarami Massif Oman (Einaudi *et al.* 2000), Lycean Mélange Turkey (Collins & Robertson 1998), Ankara Mélange Turkey (Tankut *et al.* 1998), Khoy ophiolite Iran (Hassinpak & Ghazi 2000), Kermanshah ophiolite Iran (Ghazi & Hassinpak 1999), Bay of Islands ophiolite Canada (Jenner *et al.* 1991), Geraldton Greenstone Belt Superior Province Canada (Tomlinson *et al.* 1996), Lizard ophiolite UK (Roberts *et al.* 1993), Hegenshan ophiolite Inner Mongolia (Robinson *et al.* 1999).

field evidence for voluminous magmatism, such as sheet lava flows, that would be expected for melting due to a hot mantle plume. Therefore, it is considered unlikely that the Bayankhongor ophiolite was formed by the interaction of an enriched mantle plume with the depleted upper mantle.

Supra-subduction marginal basin setting

Most of the world's ophiolites including those commonly cited as ocean crust analogues, such as Oman (Searle *et al.* 1999) and Troodos (Robertson *et al.* 1994), are now considered to have formed within a supra-subduction zone environment, either as part of a back-arc basin or due to spreading of MORB oceanic crust trapped within the fore-arc after the initiation of an intra-oceanic subduction zone (Shervais 2001). A supra-subduction setting provides the highest preservation potential for the oceanic crust because being on the upper plate of the subduction zone, it is more likely to be thrust onto a continental passive margin when it arrives at the subduction zone than the oceanic crust from the subducting plate (Casey & Dewey, 1984; Cloos 1993; Robertson & Xenophontos 1994; Searle 1999; Shervais 2001). Supra-subduction ophiolites and modern marginal basin crust have some general characteristics that allow them to be distinguished from Atlantic- or Pacific-type crust (Saunders and Tarney 1984; Pearce *et al.* 1993; Shervais 2001). Because the spreading centre at which the marginal basin crust is being accreted is located above the subduction zone, it tends to inherit a 'subduction signature' in the same way as island arcs (i.e. calc-alkaline compositions, LILE enrichments and depletion of HFSE; Saunders and Tarney 1984; Pearce *et al.* 1993; Shervais 2001). In newly initiated subduction zones, hot asthenosphere flowing into the gap created by the sinking plate margin results in rapid decompression melting with fluid enhanced lowering of the solidus that leads to extensive melting of the shallow asthenospheric wedge, creating refractory melts such as boninites and high-Mg andesites (Casey & Dewey 1984; Stern and Bloomer 1992), which are found in the fore-arc region of the Isu-Bonin arc (Casey & Dewey 1984; Stern and Bloomer 1992) and ophiolites such as Troodos (Casey & Dewey 1984; Robertson and Xenophontos 1994).

The Bayankhongor ophiolite rocks do not have a chemical 'subduction signature' (Figs. 3.7a & 3.7b) nor do they contain boninites or high Mg-andesites, but this does not preclude their formation in a supra-subduction environment because not all marginal basin basalts have a 'subduction signature'. Many modern back arc basins such as the Lau Basin (Kamenetsky *et al.* 1997; Ewart *et al.* 1998), North Fiji Basin (Lagabrielle *et al.* 1997), and East Scotia Ridge (Leat *et al.* 2000) produce basalts which are essentially indistinguishable from normal MORB. In addition the Lau and East Scotia ridge basins also produce E-MORB and T-MORB, but it is not clear whether these are related to mantle plumes located nearby (Ewart *et* *al.* 1998; Leat *et al.* 2000). However, if these basins were obducted onto a passive margin it would be possible to identify them as supra-subduction if the sedimentary cover were preserved as most marginal basins will contain volcanogenic sediments derived from the accompanying arc (Shervais 2001). The only sediments in direct contact with the Bayankhongor ophiolite pillow basalts, are a small 1 m thick bed of chert (Chapter 2), which does not provide much information on the tectonic environment as cherts are deposited in both marginal basins and larger Atlantic-type basins. However, the Delb Khairkhan mélange also contains cherts similar to those in contact with the ophiolite, as well as metaliferous sediments that may have formed the cover for the oceanic crust (Chapter 2). Samples 98M26 and 98M27 were collected from the Delb Khairkhan mélange and do have island-arc like chemistry (Figs. 3.11, 3.18, 3.19). If the Delb Khairkhan mélange is indeed related to the cover of the ophiolite then the occurrence of island arc related basalts within this cover sequence might suggest that the ophiolite was formed as part of a supra-subduction zone marginal basin. The Agardagh Tes-Chem ophiolite located in Tuva Southern Siberia (Fig. 3.1), is the same age as the Bayankhongor ophiolite and has a similar range of initial $\varepsilon_{Nd(570)}$ = -0.2 to +8.4, with most of the basalts concentrated around $\varepsilon_{Nd(570)}$ = +5.5 to +7.7, but the Agardagh Tes-Chem rocks contain basalts with a 'subduction signature' formed within the ophiolite (Pfänder *et al.* submitted). Based on geochemical and isotopic modelling Pfänder *et al.* (submitted) suggest that the ophiolite was produced in a back arc setting and that the range in initial ε_{Nd} observed, can be explained by assimilation of subducted sediments. This model could be applied to explain the range of compositions within the Bayankhongor basalts, but mixing of sediment in the melt would almost certainly result in the creation of negative Nb and Ti anomalies which are not observed for the ophiolitic rocks.

Normal oceanic basin with heterogeneous upper mantle

Recent advances in ocean drilling technology and direct sampling by submersible have allowed higher resolution sampling of the present day ocean floors and the resultant determination of smaller scale chemical variations (Perfit & Chadwick 1998). These high resolution studies have revealed that basalts accreted to the oceanic crust along mid-ocean ridges contain marked chemical variations that question the validity of previous estimates of average N-MORB over a variety of scales (Reynolds *et al.* 1992; Perfit *et al.* 1994; Shen and Forsyth 1995; Perfit & Chadwick 1998; Dosso *et al.* 1999; Lundstrom *et al.* 2000). Studies of along-axis variation within the East Pacific Rise (EPR; e.g. Reynolds *et al.* 1992) and Mid Atlantic Ridge (MAR; e.g. Dosso *et al.* 1999, Hannigan *et al.* 2001, and Niu *et al.* 2001) have shown that basalts with depleted mantle N-MORB signatures are dominant, but that at many places along the length of the ridge more evolved T-MORB are produced. These studies have also shown that the more evolved melts seem to be concentrated along the axis of the ridge which has been suggested to relate to occasional focussed mantle upwelling which samples deeper more enriched mantle (Rubin *et al.* 2001, Niu *et al.* 2001). However, along-axis variations such as those documented for the EPR and MAR would only account for the flat REE signatures observed in the Bayankhongor basalts and do not provide a mechanism for producing the more evolved E-MORB basalts.

Extremely slow spreading ridges such as the SW Indian ridge produce diverse magma compositions and commonly produce enriched E-MORB magmas, which is suggested to relate to the smaller degree of partial melt produced by slow spreading ridges resulting in extreme fractionation of trace elements and REE (le Roex *et al.* 1992, White 2001). The range of compositions produced along the SW and SE Indian ridges are similar to those of the Bayankhongor ophiolite (Figs. 3.7a, 3.7b, 3.8a, 3.8b). However, the Indian Ocean ridge is further complicated by the unique mantle compositions within this basin compared to the Atlantic or Pacific (Mahoney *et al.* 1998).

The greatest degree of basalt heterogeneity, without the inclusion of an enriched mantle plume, is shown by the cross-axis variation of the EPR (Reynolds *et al.* 1992; Perfit *et al.* 1994; Niu & Batiza 1997; Perfit & Chadwick 1998). High resolution submersible, rock core and dredging studies of transects accross the axis of the EPR, have shown that whilst N-MORB basalts are dominantly produced at the axial ridge, more evolved E-MORB are exclusively produced by off-axis pillow ridge flows (Perfit *et al.* 1994; Perfit *et al.* 1998) and small off-axis non-plume related seamounts (Fig. 3.23; Batiza & Vanko 1984; Davis & Karsten 1986; Cousens 1996; Niu & Batiza 1997; Reynolds & Langmuir 2000). These studies also show that not only do the trace element and REE concentrations of the basalts vary, but that their isotopic signatures are different also (Cousens 1996; Perfit & Chadwick 1998). The scale of the variations observed has led many authors to suggest that the only way to account for the compositional differences between on axis and off-axis basalts in the absence of a plume, is to invoke a heterogeneous mantle source consisting of a dominant depleted mantle surrounding smaller blebs or streaks of enriched mantle (Reynolds *et al.* 1992; Perfit *et al.* 1994; Cousens 1996; Niu & Batiza 1997; Perfit & Chadwick 1998). The scale of the heterogeneities is not yet well constrained for the EPR, but similar variation over small areas in the basalts of Maquarie Island, and consideration of re-equilibration rates of mantle, led Kamenetsky *et al.* (2000) to suggest that mantle heterogeneities must be very small.

A model, based on those of Perfit *et al.* (1994), Cousens (1996), and Niu *et al.* (1999) to account for the production of off-axis E-MORB and on axis N-MORB is shown in Figure

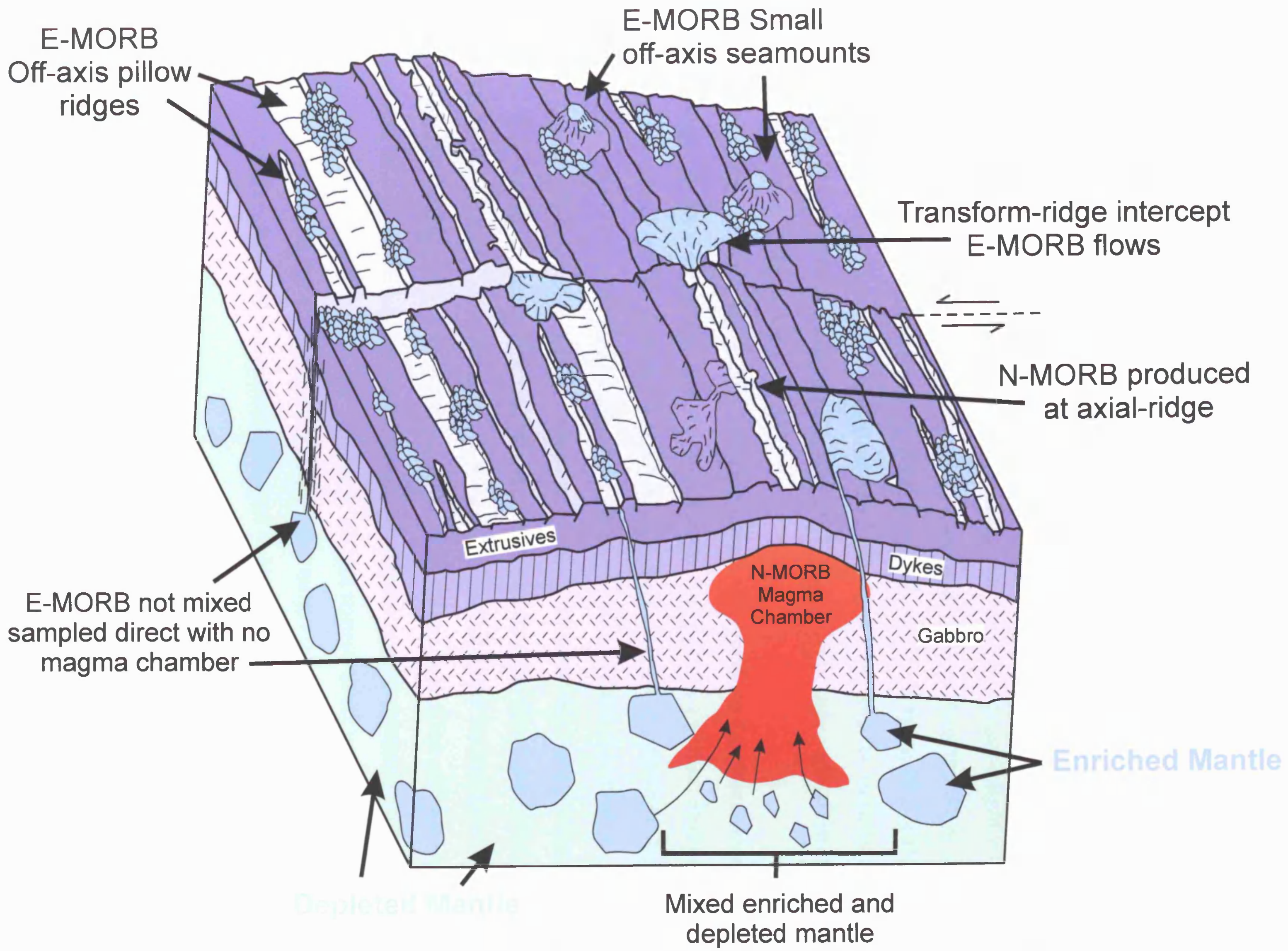

Fig. 3.24: Cartoon model depicting the possible sites of N-MORB and E-MORB basalt eruptions for the Bayankhongor ophiolite based on models for the East Pacific Rise (Perfit *et al.* 1994; Cousens 1996; and Niu *et al.* 1999).

3.24. The implications of the model are that magmas produced at the ridge axis are a mixture of dominantly depleted mantle and enriched mantle that become mixed and homogenised in the magma chamber below the ridge axis before eruption (Perfit *et al.* 1994; Cousens 1996; Niu & Batiza 1997). The amount of mixing does not always result in complete homogenisation and as a result transitional T-MORB basalts are produced that have flatter REE patterns (Perfit *et al.* 1994; Niu & Batiza 1997) and slightly more enriched Nd isotope signatures (Cousens 1996). Off-axis eruptions are smaller degree partial melts and tend to preferentially sample the less refractory enriched mantle (Perfit *et al.* 1994). Also there is no off-axis magma chamber and instead the enriched E-MORB melts pass straight through the crust and are erupted as pillow ridges or off-axis seamounts without assimilation or homogenisation with the surrounding N-MORB crust (Perfit *et al.* 1994; Niu & Batiza 1997). An additional mechanism for producing the E-MORB eruptions from the same type of mantle is from diffuse locally concentrated extension at the transition between transform faults and ridge systems (Fig. 3.24; Allen *et al.* 1993).

It appears that this model provides a mechanism that could produce the observed geochemical and isotopic variation of the Bayankhongor ophiolite rocks within a normal mid-oceanic setting. It does not require complex arguments over the preservation of MORB type crust above a subduction zone without producing a geochemical 'subduction signature', and fits the field evidence of the extrusive section containing only pillow basalts and no voluminous sheet flows. However, it cannot explain the occurrence of basalts with island-arc like chemistry within the Delb Khairkhan mélange, but this is not a limiting factor because the original relationship of these rocks to the ophiolite is not well constrained. One of the major drawbacks of a model involving production of the Bayankhongor ophiolite rocks within a normal ocean basin, is that it is very difficult to obduct normal oceanic crust (Cloos 1993). Nevertheless this it is the simplest and arguably best model to explain the geochemical and isotopic variation observed in the Bayankhongor ophiolitic rocks.

Tectonic environment of the Southern Volcanics

The relationship of the Southern Volcanic rocks to the ophiolite is poorly constrained by current field data. All that is known is that the volcanic rocks are confined to a single thrust sliver located to the south of the Delb Khairkhan Melange (Fig. 3.2), that they are nearly undeformed and that they may be considerably younger than the ophiolite rocks (*c.* 474 Ma based on zircon dating of cross cutting rhyolite dykes Chapter 4), which is consistent with the interpreted Ordovician age of poorly preserved fossils from overlying conformable sediments (Dergunov *et al.* 1997). If the Southern Volcanics really are Ordovician in age then this causes problems for their interpretation as part of an island arc complex related to subduction of the Bayankhongor ocean, because crustal melt granites that intrude the Bayankhongor ophiolite, Delb Khairkhan mélange, and Burd Gol mélange suggest that the ocean was closed by 540 Ma (Chapter 4). However, it is unclear whether the granites are definitely related to collisional magmatism and it is therefore possible, but considered unlikely, that subduction continued after 540 Ma (Chapter 4).

Another possibility is that the Southern Volcanics are not island arc derived in the *sensu stricto* sense, but that they are related to post-collision magmatism caused by slab break-off after collision of the Hangai and Baidrag continents and obduction of the ophiolite. Slab break-off melting was proposed by Davies & Von Blanckenburg (1992) to explain the occurrence of alkaline and calc-alkaline magmatism within contractional syn-collisional settings. In the slab break-off model, the subducted oceanic slab detaches under its own weight from the partially subducted continental crust of the lower plate. Hot asthenosphere then flows into the space left after removal of the subducted slab and this combined with the removal of the negatively buoyant slab results in isostatic rebound and extension in the upper plate. The combination of hot asthenosphere and extensional faulting produces melting of the lithospheric mantle, which has the composition of the supra-subduction mantle wedge resulting in volcanic rocks with an essentially arc-like chemistry (Davies & von Blanckenburg 1992; von Blanckenburg & Davies 1995; Nemcok *et al.* 1998). The slab break-off mechanism has been suggested to account for post-collisional arc-like magmatism in the Alps (Davies & von Blanckenburg 1992; von Blanckenburg & Davies 1995) and also the Carpathian-Pannonian region (Nemcok *et al.* 1998). This model is consistent with the current interpretation that the Southern Volcanics post-date obduction of the Bayankhongor ophiolite at 540 Ma. However, there is at present no evidence for accompanying extensional faulting in the region as the structure is dominated by thrust faults, but with more detailed mapping of the Southern Volcanics and Burd Gol mélange, extensional faults may be revealed.

Whether the Southern Volcanics represent part of a true island arc complex, or were derived by post-collisional slab break-off magmatism cannot be resolved by the existing data and requires more extensive sampling and detailed structural mapping of the tectonic relationship of the volcanics to the rest of the Bayankhongor ophiolite zone.

Summary

The new geochemical and Nd isotope data for the Bayankhongor ophiolitic rocks allow two compositional groups to be distinguished. Group 1 are enriched in LREE/LILE and have initial $\varepsilon_{Nd(569)} = +2.4$ to $+6.2$. Primitive mantle normalised trace element patterns and chondrite normalised REE patterns of the enriched group resemble those of OIB and off-axis

E-MORB EPR basalts. Group 2 have flat REE and trace element patterns and initial $\varepsilon_{Nd(569)}$ = +7.0 to +8.9 which is close to that of depleted mantle at 569 Ma. Primitive mantle normalised trace element patterns and chondrite normalised REE patterns of the group 2 basalts resemble those of N-MORB to T-MORB erupted on axis at the EPR. Gabbro and pyroxenite samples can also be divided into these two groups based on their ND isotopic compositions, but they do not show significant trace element or REE variation. A tectonic model of mid-ocean ridge (group 2) and off-axis (group 1) melting above a heterogeneous mantle, similar to that proposed by Perfit *et al.* (1994) for the EPR, is the simplest mechanism to produce the observed variations (Fig. 3.24).

The Southern Volcanics that form a thrust sliver to the south of the ophiolite have supra-subduction arc-like chemistry and their tectonic relationship to the ophiolite remains unclear.

Submitted for publication to *Chemical Geology*, 1st July 2001.

Co-Authors: Jörg Pfänder and Tim Brewer

Chapter 4:

Geochronology of the Bayankhongor Ophiolite Zone, Central Mongolia: implications for timing of accretion and collisional deformation in the Central Asian Orogenic Belt.

Introduction

The Central Asian Orogenic Belt (CAOB) is a complex collage of island-arcs, continental blocks and fragments of oceanic crust that amalgamated during the Palaeozoic to Mesozoic. Recent studies provide growing evidence that continental growth occurred through a process of subduction-accretion with punctuated collisional events resulting in the formation of ophiolitic sutures between accreted blocks (Coleman, 1989; Hsü et al., 1991; Şengör et al., 1993; Mossakovsky et al., 1994; Buchan et al., 2001). However despite an improved understanding of the crustal growth mechanisms, a paucity of reliable geochronological data has hindered correlation of sutures and collisional deformation within the orogen, or has led to questionable models based solely on lithological similarity. One such example is the grouping of high-grade gneiss terranes in western Mongolia and Tuva into a singular Archaean to Palaeoproterozoic continental block named the Tuva-Mongolian Massif (e.g. Dergunov et al., 1997; Mossakovsky et al., 1994). However, Kozakov et al. (1999) showed that granulite-facies gneisses in Tuva, previously assumed to represent part of the Tuva-Mongolian Massif, are early Cambrian in age (536 ± 6 Ma, U-Pb single zircon). Miscorrelation has led to confusing regional relationships, and misunderstanding of the mechanisms of continental growth (see Lamb and Badarch, 1997 and Buchan et al., 2001 for detailed discussion).

Mongolia occupies a central position within the Central Asian collage and is therefore, pivotally located for understanding crustal growth in the region. This paper presents new zircon geochronological data from granites and rhyolite dykes that intrude the Bayankhongor ophiolite zone, which is the largest ophiolitic suture in Mongolia, and possibly all of Central Asia (Fig. 4.1, Buchan et al., 2001). The new data are combined with previously published K-Ar and Ar-Ar data from metamorphic micas associated with faults within the ophiolite zone (Teraoka et al., 1996; Kurimoto et al., 1998; Takahashi et al., 1998; Delor et al., 2000; Höck *et al.*, 2000). This combined data set provides important constraints on the timing of obduction of the

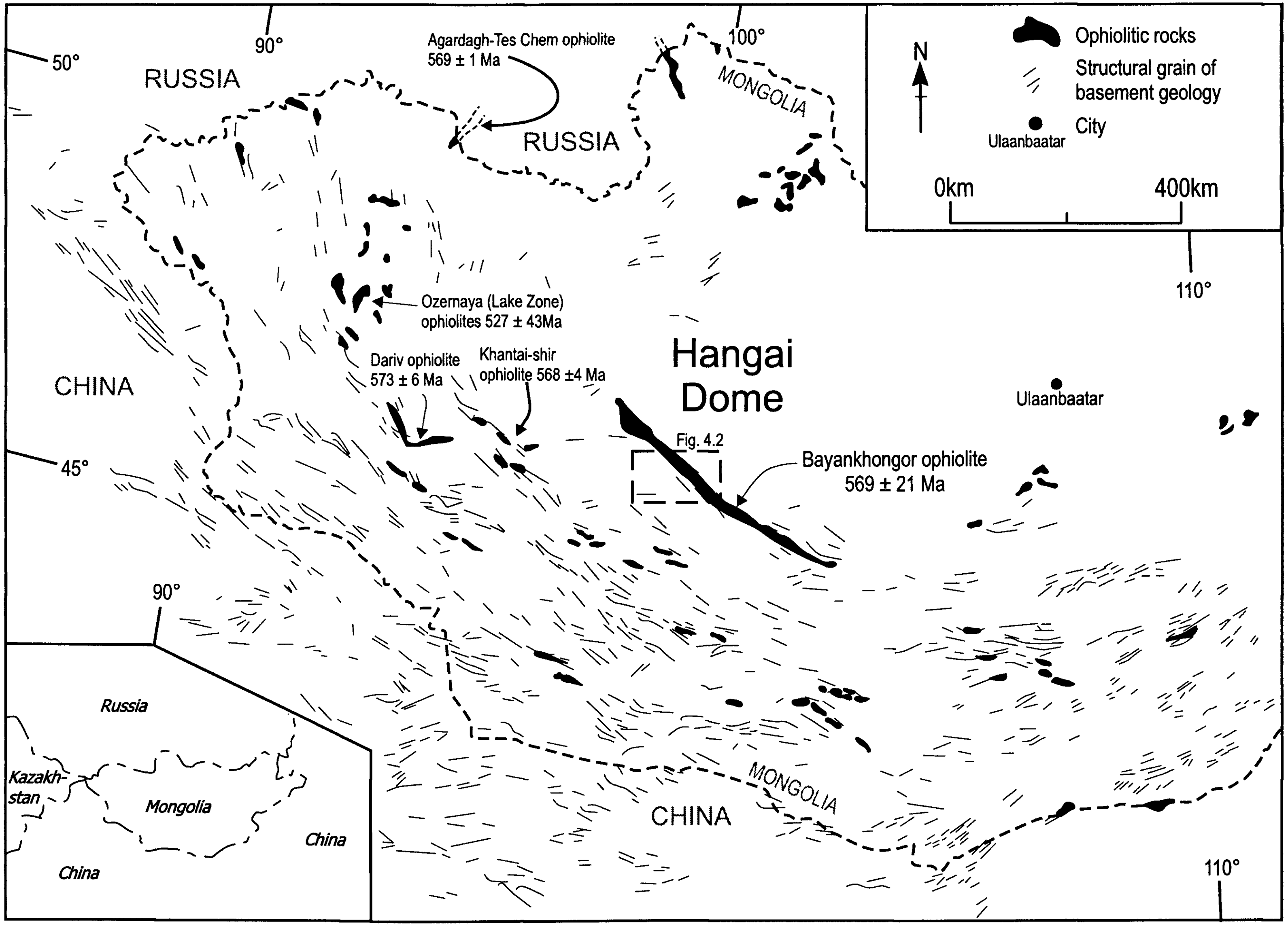

Fig. 4.1: Ophiolite occurrences in Mongolia, the Bayankhongor ophiolite is the largest. Isotopic age data for the highlighted ophiolites demonstrates marked correlation of ophiolites created at around 570 Ma. The trace of basement structural grain indicates that these ophiolites occur along a gently curving semi-continuous belt. Sources of age data: Bayankhongor (Kepezhinskas et al. 1991), Khantaishir and Dariv (Salnikova *pers comm.*), Ozernaya (Kovalenko et al. 1996a) and Agardagh Tes-Chem (Pfänder et al. 1999).

Bayankhongor ophiolite and subsequent deformation. In addition, it is demonstrated that the deformation events associated with creation of the Bayankhongor granites can be traced on a regional scale north-westward along-strike to Tuva, southern Siberia. The correlation of these deformation events suggests that they represent a major magmatic episode in the history of the CAOB.

Geological Setting

The Bayankhongor ophiolite zone (Fig. 4.1) is situated on the southern side of the Hangai dome that formed during regional Cenozoic uplift (Windley and Allen, 1993; Barry and Kent, 1998; Cunningham, 1998, Cunningham, 2001). The ophiolite forms a NW-SE striking sub-linear zone, approximately 300 km long and up to 20 km wide (Figs. 4.1, 4.2). Previous mapping enables a four-fold tectonic subdivision of the region from south to north: the Baidrag block, Burd Gol mélange, Bayankhongor zone and Dzag zone (Fig. 4.2; Teraoka et al., 1996; Tomurtogoo et al., 1998; Buchan et al., 2001).

The Archaean to Palaeoproterozoic is composed of tonalitic gneiss, granulite and amphibolite, with minor marble and quartzite. A tonalitic gneiss from this blocks was dated at 2650 ± 30 Ma (U-Pb zircon, Table 4.1; Mitrofanov et al., 1985), and the block is interpreted as a microcontinent (Mitrofanov et al., 1985; Kozakov, 1986; Kozakov, 1997).

The Burd Gol mélange (Fig. 4.2) consists of lenses of sedimentary and igneous rocks enclosed in a matrix of pelite and graphite schists, which are cut by abundant quartz veins. From palaeontological dating of stromatolites in limestone lenses, Mitrofanov et al. (1981) suggested that the Burd Gol mélange is Neoproterozoic in age. Within the mélange, the metamorphic grade increases towards the north (Buchan et al., 2001). Metamorphic white-micas within the mélange have ages ranging from 699 ± 35 Ma to 533 ± 3 Ma (Table 4.1; Teraoka et al., 1996; Höck et al., 2000).

North of the Burd Gol mélange, there is a small area of interbedded marine mudstone and limestone which contain Carboniferous fossils (Fig. 4.2; Dergunov et al., 1997). Between the Carboniferous sedimentary rocks and the Bayankhongor ophiolite zone, there is a thrust-sliver of volcanic rocks (Southern Volcanics in Fig. 4.2) that Buchan (unpubl. data) have shown to have island arc-like geochemical characteristics. The Southern Volcanics have previously been assigned to the Ordovician (Dergunov et al., 1997) or Devonian periods (Tungalag, 1996), based on palaeontological evidence and lithological correlation with similar units elsewhere. Zircons from rhyolite dykes that cross-cut the Southern Volcanics have been dated as part of this study.

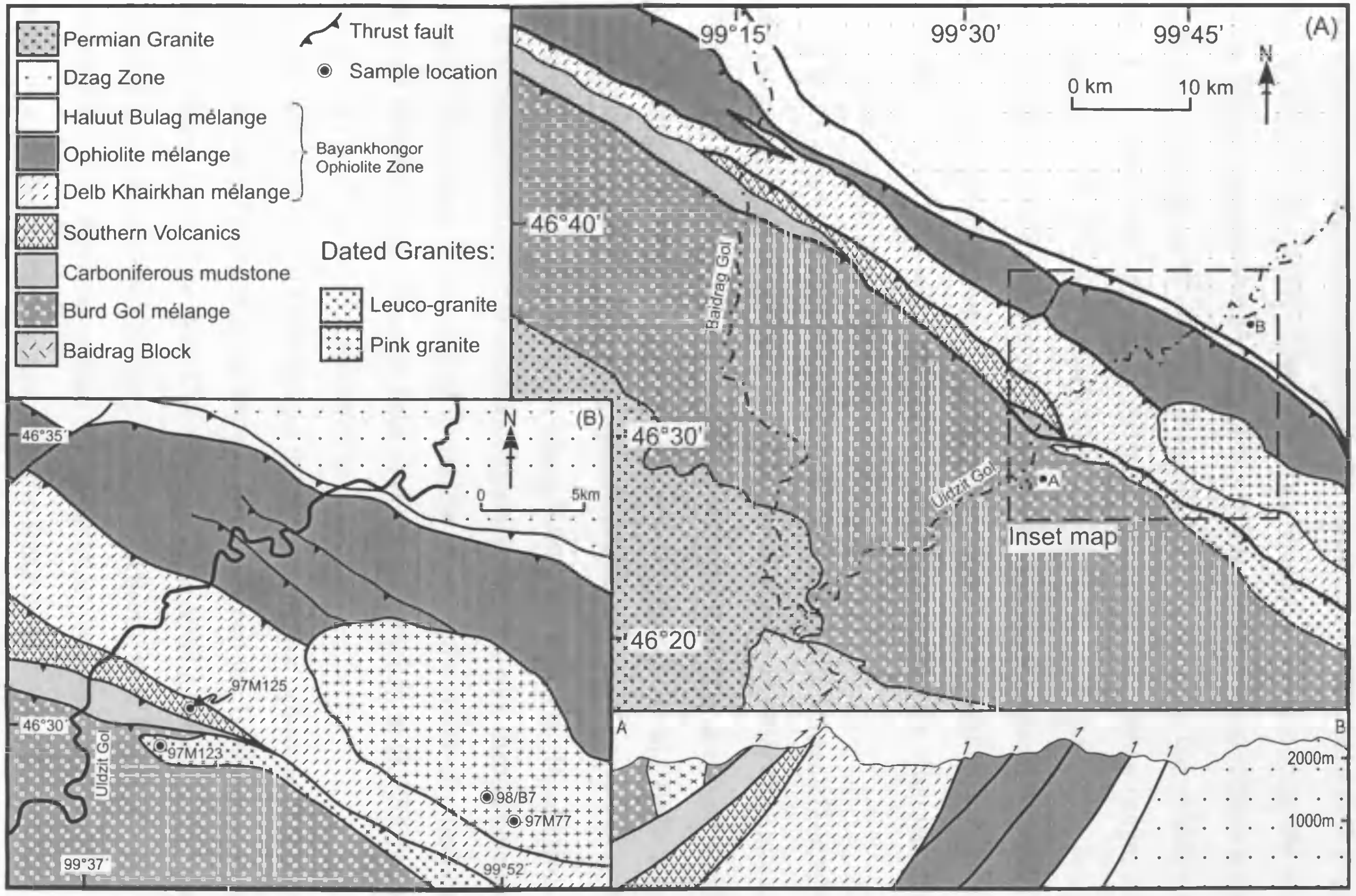

Fig. 4.2: Regional geology of the Bayankhongor area. Inset map shows detail of study area and sample locations. Location of Figure shown in Figure 4.1.

The Bayankhongor zone is divided into three sub-units: the Delb Khairkhan mélange, ophiolite mélange, and the Haluut Bulag mélange (Fig. 4.2, Buchan et al., 2001). The Delb Khairkhan mélange lies to the south of the ophiolite and contains sedimentary and volcanic rocks of Meso-Neo Proterozoic to Ordovician age enclosed in a matrix of pelitic schists (Ryantsev, 1994; Dergunov et al., 1997). The ophiolite mélange contains a complete ophiolite stratigraphy (Moores, 1982), dismembered into blocks enclosed within a serpentinite matrix. Gabbros within the ophiolite mélange have been dated at 569 ± 21 Ma (Sm-Nd cpx-whole rock isochron on gabbro; Kepezhinskas et al., 1991). Despite a relatively large error range, this age compares well with more precise U-Pb ages for ophiolites along strike to the west (Fig. 4.1). Metamorphic amphiboles that form lineations within pillow basalts near Bayankhongor City have an age of 484.5 ± 5.9 Ma (Ar-Ar, Table 4.1.; Delor et al., 2000). The predominantly sedimentary Haluut Bulag mélange, contains lenses of bedded limestone, sandstone, siltstone, and locally vesicular basalt, enclosed in a matrix of pelitic schist.

The Dzag zone (Fig. 4.2) consists of asymmetrically folded chlorite-mica schists that contain relict sedimentary features that suggest they are turbidites (Buchan et al., 2001). K-Ar ages (Table 4.1) for white-micas associated with the thrust separating the ophiolite zone and Dzag zone range from 395 ± 20 Ma to 454 ± 9 Ma (Teraoka et al., 1996; Kurimoto et al., 1998).

The structure of the Bayankhongor area is dominated by NW-SE striking, NE directed thrusts, which have juxtaposed the different litho-tectonic units. In addition, the litho-tectonic units have been internally dismembered by sinistral strike-slip displacements, which have contributed to mélange formation. It is unclear whether the strike-slip deformation was a separate event from thrusting, but based on field observations Buchan et al. (2001) suggest that the two were coeval in a NE directed transpressive regime.

Buchan et al. (2001) interpreted the Bayankhongor ophiolite as a suture marking the position of an early Palaeozoic subduction zone between the Baidrag block to the south, and the Dzag zone to the north. The Burd Gol mélange represents an accretionary wedge built up against the Baidrag continental block to the south. Subduction was to the southwest, based on the dominant polarity of thrusting within the Bayankhongor ophiolite zone. The ophiolite was obducted in a northeasterly direction over the Dzag zone that represents part of a passive margin to a continent located beneath the sedimentary cover of the Hangai region.

Several large granite bodies intrude the rocks of the Bayankhongor zone (Fig. 4.2; Takahashi & Oyungerel, 1998; Takahashi et al. 1998a); many cut major faults, but are themselves undeformed and so provide useful time constraints on faulting. Takahashi et al.

Table 4.1. *Summary of isotopic age determinations of lithotectonic units in the Bayankhongor area from past studies.*

Lithotectonic unit	Age	Isotopic method	Mineral analysed	Age interpretation	Location	Source
Dzag	453.9 ± 9.1 Ma	K-Ar	white mica	Deformation	N46° 45.93' E99° 26.98'	Kurimoto *et al.* 1998
Dzag	447.4 ± 9.0 Ma	K-Ar	white mica	Deformation	N46° 19.88' E100° 14.50'	Kurimoto *et al.* 1998
Dzag	395.0 ± 20.0 Ma	K-Ar	muscovite	Deformation	N46° 28.67' E100° 11.91'	Teraoka *et al.* 1996
Dzag	440.0 ± 22.0 Ma	K-Ar	muscovite	Deformation	N46° 32.83' E99° 56.65'	Teraoka *et al.* 1996
Bayankhongor Ophiolite	569.0 ± 21.0 Ma	Sm-Nd	plag, cpx, amph, whole rock isochron.	Crystallisation	Unknown	Kepezhinskas *et al.* 1991
Bayankhongor Ophiolite	484.5 ± 5.9 Ma	Ar-Ar	Amphibole	Deformation	SE Bayankhongor City	Delor *et al.* 2000
Burd Gol Melange	699.0 ± 35.0 Ma	K-Ar	muscovite	Deformation	N46° 14.84' E99° 43.26'	Teraoka *et al.* 1996
Burd Gol Melange	533.0 ± 3.0 Ma	Ar-Ar	biotite	Deformation	Mount Ushgoeg	Höck *et al.* 2000
Baidrag Block	2650 ± 30 Ma	U-Pb	zircon	Deformation	N46° 15.823' E99° 21.335'	Mitrofanov *et al.* 1985
Palaeozoic granites:						
Khangay	249 ± 12 Ma	K-Ar	Biotite	Crystallisation	N47° 01.02' E98° 33.89'	Oyungerel & Takahashi 1999
Daltyn-am	247 ± 10 Ma	Rb-Sr	Whole Rock	Crystallisation	N46° 28.75' E100° 02.35'	Oyungerel & Takahashi 1999
Tsakhyr uul	287 ± 8 Ma	Rb-Sr	Whole Rock	Crystallisation	N46° 28.75' E100° 02.35'	Arakawa *et al.* 1998
Tsakhyr uul	469 ± 9 Ma	K-Ar	Biotite	Crystallisation	N46° 23.6' E99° 49.7'	Oyungerel & Takahashi 1999
Tsakhyr uul	408 ± 20 Ma	K-Ar	Biotite	Crystallisation	N46° 23.6' E99° 49.7'	Zabotkun *et al.* 1988
Tsakhyr uul	451 ± 20 Ma	K-Ar	Biotite	Crystallisation	N46° 23.6' E99° 49.7'	Zabotkun *et al.* 1988
Tsakhyr uul	519 Ma	K-Ar	Biotite	Crystallisation	N46° 23.6' E99° 49.7'	Andreas 1970
Tsakhyr uul	551 Ma	K-Ar	Biotite	Crystallisation	N46° 23.6' E99° 49.7'	Andreas 1970

(1998a; 1998b; 1998c) and Oyungerel (1998) documented the regional petrology, metallogeny and magnetic susceptibility of many of these granites. They suggested that dominantly magnetite-bearing granites occur south of the Dzag zone, whereas dominantly ilmenite-bearing granites occur in the Dzag zone and to the north. Furthermore, they pointed out that this zonation relates to mineralisation, the magnetite-bearing granites being associated with Au-Cu mineralisation, and the ilmenite-bearing with Sn-W deposits (Oyungerel, 1998). However, they did not speculate on the relation of the zonation to either source chemistry or tectonic environment of emplacement. Takahashi et al. (1998c) suggested that the zonation also relates to the time of granite emplacement, the ilmenite series being Precambrian-early Palaeozoic whereas, the magnetite series are mostly late Palaeozoic. This interpretation is problematic because most of the dating is based on K-Ar (Oyungerel & Takahashi, 1999) or Rb-Sr ages (Arakawa et al., 1998; Takahashi et al., 1998a; Oyungerel & Takahashi, 1999), both of which are easily disturbed during deformation. It is therefore likely that many of these ages are younger than the true crystallisation ages of the granites.

Analytical techniques

Major and trace element geochemistry

Major and trace elements (Table 4.2) were analysed by XRF at the University of Leicester, using conventional techniques described by Tarney and Marsh (1991). Major elements were measured on fused glass discs using a lithium tetraborate-metaborate flux; trace elements were measured on pressed powder pellets using a Moviol binding agent. Only major element totals between 98.5-101.5% were accepted. For major elements the typical lower limit of detection (LLD) is 0.01% and precision is better than 0.5% at 100 times LLD. XRF trace element reproducibility is within 5% for international reference materials.

Samples used for REE analysis were digested using microwave digestion in a combined solution of HF-HNO_3. The REE were separated from the bulk sample using Dowex AG 50W-8X cation-exchange resin. After separation, REE concentrations (Table 4.2) were determined using an ICP-Optical Emission Spectrometer at the University of Leicester, following the methods described by Harvey et al. (1996). The analytical precision is of the ICP-OES data is ± 5 %.

Nd isotope analysis

Nd isotopic compositions (Table 4.3) were determined using a Finnigan MAT 261 multicollector thermal ion mass spectrometer in static mode at the Max-Planck-Institut für

Chemie in Mainz, Germany. Nd isotopic ratios and Nd, Sm concentrations were analysed by isotope dilution using a mixed ^{150}Nd-^{149}Sm spike. The spike was added prior to sample digestion in HF-HNO_3 within closed Teflon beakers for >48 hours at 200 °C. The REE fraction was separated from the bulk sample using Biorad AG 50W-X12 cation-exchange resin. Sm and Nd were separated from the other rare earth elements using HDEHP-coated Teflon powder. Total procedural blanks were <30 pg for Nd. Repeated measurements of the La Jolla standard gave $^{143}Nd/^{144}Nd = 0.511837 \pm 0.000036$, $^{145}Nd/^{144}Nd = 0.348405 \pm 0.000022$ and $^{150}Nd/^{144}Nd = 0.236493 \pm 0.000081$ (2σ, n = 38; see Table B5).

Single zircon evaporation technique

Samples were crushed and ground using a jaw crusher and steel disc mill. The ground material was fed over a Rodgers table and heavy minerals were separated from the concentrate using heavy liquids. The resulting heavy mineral concentrate was then fed through a Franz magnetic separator and single zircons were hand picked from the non-magnetic fraction.

The evaporation technique, established by Kober (1986; 1987), involves repeated evaporation and deposition of Pb isotopes from chemically untreated zircons using a double Re filament arrangement. The laboratory procedures used and comparisons with conventional zircon dating are published in detail elsewhere (Kröner and Todt, 1988; Kröner et al., 1991; Kröner and Hegner, 1998). Isotopic measurements were carried out on a Finnigan MAT 261 mass spectrometer at the Max-Planck-Institut für Chemie in Mainz. No correction for mass fractionation was carried out as the effect has been shown to be negligible (Kröner et al., 1999). Measurement of a chip of Curtin University SHRIMP II standard CZ3 yielded a $^{207}Pb/^{206}Pb$ age of 564.8 ± 1.4 Ma, identical to the adopted age of 564 Ma for this standard (Pidgeon et al., 1994).

Internal reproducibility of the evaporation data has been estimated by comparison of conventional U-Pb ages with evaporation ages for fragments of large grains from the Phalaborwa Complex, South Africa. These zircons, used as a laboratory standard, are euhedral, colourless to slightly pink and completely homogeneous when examined under cathodoluminescence. Conventional U-Pb analyses of six separate grain fragments from this sample yielded a $^{207}Pb/^{206}Pb$ age of 2052.2 ± 0.8 Ma (2σ)(W. Todt, unpublished data), whereas the mean $^{207}Pb/^{206}Pb$ ratio for 18 grains, evaporated individually over a period of 12 months, is 0.126634 ± 0.000026 (2σ error of the population), corresponding to an age of 2051.8 ± 0.4 Ma, identical to the U-Pb age.

Table 4.2 *Whole rock major and trace element analyses for samples dated in this study.*

Sample	97M77	97M123	97M125
Lithology	Granite	Granite	Rhyolite Dyke
SiO_2	66.49	72.46	70.71
TiO_2	0.51	0.30	0.29
Al_2O_3	15.86	14.69	15.30
Fe_2O_3 †	3.32	1.97	2.56
MnO	0.07	0.04	0.03
MgO	0.77	0.41	0.12
CaO	1.54	1.73	1.78
Na_2O	4.57	4.39	6.32
K_2O	4.90	4.09	1.51
P_2O_5	0.18	0.12	0.08
LOI	1.27	0.52	2.28
Total	99.46	100.72	100.98
A.S.I	1.02	0.99	1.00
$Temp_{Zrsat}$ ‡	814	753	752
Sc	3.7	5.2	3.8
V	35.5	23.2	27.2
Cs	4.2	2.9	2.9
Cu	9.7	1.2	1.0
Mo	1.4	1.6	1.6
Sn	3.0	2.4	2.6
Cr	<1	<1	1.5
Co	8.9	5.7	6.4
Ni	2.4	5.9	2.3
Zn	47.5	40.2	38.8
Ga	19.4	19.3	17.2
Rb	128.3	102.6	31.5
Sr	577.1	585.5	295.5
Y	14.5	10.8	11.7
Zr	254.0	116.6	117.6
Nb	16.9	8.1	3.5
Ba	1403.1	534.4	168.5
Pb	22.2	21.7	4.7
Th	13.5	7.9	4.8
U	2.4	1.7	0.9
La	53.44	17.29	7.86
Ce	103.00	36.03	18.66
Nd	25.63	13.96	10.70
Sm	6.08	3.25	2.47
Eu	1.75	0.84	0.75
Gd	5.25	2.95	2.66
Dy	3.59	2.14	2.13
Er	1.93	1.22	1.14
Yb	1.18	0.96	0.87
Lu	0.24	0.14	0.18
10000*Ga/Al	2.31	2.48	2.12

Major elements in wt. %, trace elements in ppm.
LOI: Loss on ignition determined at 1050 °C.
† Total iron as Fe_2O_3
‡ Zircon saturation temperature (Watson & Harrison 1983).
A.S.I. Aluminium Saturation Index (Zen 1986)

Table 4.3. *Sm-Nd isotopic data for dated samples.*

Sample	Lithology	Sm (ppm)	Nd (ppm)	$^{147}Sm/^{144}Nd$	$^{143}Nd/^{144}Nd$ (Measured)	$^{143}Nd/^{144}Nd$ (Initial)	T_{DM}^{a} (in Ma)	T_{DM}^{b} (in Ma)	ε_{Nd} (initial)
97M77	Granite	6.08	25.63	0.0867	0.512089 ± 14	0.511783	1270	1350	-3.1
97M123	Granite	3.25	13.96	0.0965	0.512083 ± 19	0.511742	1384	1417	-3.9
97M125	Rhyolite	2.47	10.70	0.1285	0.512622 ± 15	0.512223	943	738	+3.8

Uncertainties for the $^{143}Nd/^{144}Nd$ ratios are 2σ (mean) errors in the last two digits.

ε_{Nd} values are calculated for crystallisation ages given in table 4 relative to CHUR with present day values of $^{143}Nd/^{144}Nd = 0.512638$ and $^{147}Sm/^{144}Nd = 0.1966$ (Jacobsen & Wasserberurg 1980). Error is ± 0.4 calculated from external reproducibility.

a Single-stage Nd Model ages are calculated with a depleted-mantle reservoir and present-day values of $^{143}Nd/^{144}Nd = 0.513151$ and $^{147}Sm/^{144}Nd = 0.214$ (Goldstein *et al.* 1984)

b Two-stage model age following method of DePaolo *et al.* (1991) assumes average upper crustal evolution (1st stage) of source until time of crystallisation of granite. Thereafter evolution is calculated using measured values (2nd stage).

Table 4.4. *$^{207}Pb/^{206}Pb$ isotopic age data from zircon evaporation (see Fig. 4.2 for sample location; ages in **bold type** are interpreted crystallisation ages of the sample).*

Sample No.	Location	Zircon colour and morphology	Measurement no.	Number of Grains	Mass scans*	Evaporation temp. (°C)	Mean $^{207}Pb/^{206}Pb$ ratio† and 2 σ (mean) error	$^{207}Pb/^{206}Pb$ age an 2 σ (mean) error
97M77 (a)	N46° 26.360' E99° 52.044'	Prismatic, clear to light pink, idiomorphic	Single	3	136	1601	**0.058405 ± 315**	**545 ± 2 Ma**
97M77 (b)		Short-prismatic, clear to yellow, idiomorphic, rounded ends	1	3	79	1598	0.060377 ± 317	617 ± 11 Ma
			2	4	39	1598	0.060122 ± 238	608 ± 9 Ma
			3	2	37	1595	0.060283 ± 125	614 ± 5 Ma
			1-3		155		0.060290 ± 175	614 ± 6 Ma
97M77 (c)		Long-slightly rounded ends, pink, idiomorphic	Single	3	80	1598	0.068214 ± 87	875 ± 3 Ma
97M123	N46° 30.022' E99° 38.251'	Long-prismatic, needle-like, clear, idiomorphic	1	4	67	1595	0.058240 ± 206	539 ± 8 Ma
			2	7	37	1570	0.058194 ± 211	541 ± 8 Ma
			3	5	18	1598	0.058114 ± 266	534 ± 10 Ma
			1-3		122		**0.058238 ± 136**	**539 ± 5 Ma**
97M125 (a)	N46° 31.307' E99° 39.346'	Short prismatic, clear to pink, idiomorphic	Single	4	65	1603	**0.056551 ± 213**	**474 ± 8 Ma**
97M125 (b)		Pink to Brown, idiomorphic	Single	2	121	1550	0.097548 ± 122	1578 ± 2 Ma
M98/B7	N46° 26.538' E99° 51.229'	Clear to yellow-brown, long-prismatic, idiomorphic to slightly rounded	1	Single	88	1599	0.058238 ± 38	534 ± 1 Ma
			2	Single	77	1598	0.058229 ± 43	538 ± 2 Ma
			3	Single	88	1595	0.058226 ± 41	538 ± 2 Ma
			4	Single	88	1597	0.058272 ± 37	540 ± 1 Ma
			1-4		341		**0.058242 ± 20**	**539 ± 1 Ma**

*Number of $^{207}Pb/^{206}Pb$ ratios evaluated for age assessment.

†Observed mean ratio corrected for non-radiogenic Pb where necessary. Errors based on uncertainties in counting statistics.

Table 4.4 lists the calculated $^{207}Pb/^{206}Pb$ ratios and errors which are the weighted means of all measurements. The $^{207}Pb/^{206}Pb$ spectra are shown in histograms (Figs. 4.6-4.9) to permit visual assessment of the data distribution from which the ages are derived. Since the evaporation technique only provides Pb isotope ratios, there is no *a priori* way to determine whether a measured $^{207}Pb/^{206}Pb$ ratio represents a concordant age. Thus, in principal, all $^{207}Pb/^{206}Pb$ ages determined by this method are necessarily minimum ages. However, a number of studies have shown that there is a strong likelihood that these data represent crystallisation ages when: a) the $^{207}Pb/^{206}Pb$ ratio does not change appreciably with increasing temperature of evaporation; and/or b) repeated analysis of grains from the same sample at high evaporation temperatures yields the same isotopic ratios within error.

The rationale behind this is that it is highly unlikely that each grain in a zircon population has lost exactly the same amount of Pb, and therefore that grains with Pb loss would yield highly variable $^{207}Pb/^{206}Pb$ ratios and ages. Comparative studies using single zircon evaporation, conventional U-Pb dating and ion-microprobe analysis have shown that this is correct (e.g. Kröner et al., 1991; Cocherie et al., 1992; Jaeckel et al., 1997; Karabinos, 1997).

Petrography, geochemistry and zircon geochronology

Sample 97M123- Leucogranite

Sample 97M123 was taken from a leucocratic granite pluton, which intrudes the Burd Gol mélange approximately 1 km east of Uldzit Gol (Fig. 4.2), and forms part of the Tsakhir Uul granite complex (Oyungerel & Takahashi, 1998). The granite appears to have been emplaced along a thrust fault that separates the Burd Gol mélange from Carboniferous rocks to the north. A weak foliation is developed on the northern margin of the granite along the thrust fault, but is only found over a width of a few metres.

Petrography

97M123 is a medium to course-grained biotite-bearing leucogranite. Large (5 mm) phenocrysts of zoned plagioclase, microperthite and quartz are enclosed in an interlocking matrix of finer-grained plagioclase, orthoclase, rare microcline and quartz. The plagioclase phenocrysts have been slightly resorbed around their edges suggesting a possible xenocrystic origin. Rare graphic intergrowths of quartz and potassium feldspar occur in the matrix. Biotite forms anhedral, randomly orientated laths around 2-3 mm in length; muscovite is rare. Zircon and apatite are the main accessory phases and opaques are minor. The bulk of the rock is very fresh, but some of the larger plagioclase phenocrysts have altered cores in which sericite and epidote have replaced plagioclase.

Geochemistry

Sample 97M123 has the highest SiO_2 (72.46 wt.%) concentration of the dated samples, but has similar Na_2O (4.39 wt.%) and K_2O (4.09 wt.%) concentrations to the pink granite sample 97M77 and a CaO (1.73 wt.%) concentration close to that of the rhyolite sample 97M125 (Table 4.2). It has an A.S.I. = 0.99 (Aluminium Saturation Index, Zen 1986; Table 4.2), which indicates that the leucogranite is slightly metaluminous (Fig. 4.3). Primitive mantle normalised trace element patterns (Fig. 4.4) indicate enrichment in LILE (e.g. Rb = 102.6 ppm, Ba = 534.4 ppm) and selective enrichment of HFSE such as Th (7.9 ppm) and Zr (116.6 ppm), but depletion of others indicated by negative Nb (Nb/La_{PRIMA}= 0.47) and Ti (Ti/Zr_{PRIMA}= 0.14) anomalies. Chondrite normalised REE patterns (Fig. 4.5) indicate enrichment of LREE relative to HREE (La/Yb_{chnd} = 12.9). These trace and rare-earth element characteristics are typical of average upper continental crust patterns suggested by Taylor and McLennan (1981). Measured Nd isotopic compositions give a calculated initial ε_{Nd} = -3.9, and two-stage depleted mantle model age of 1495 Ma (DePaolo, 1991; Table 4.3).

Geochronology

All zircons from sample 97M123 are transparent, euhedral, prismatic, needle-like crystals that have magmatic morphologies (Fig. 4.6). Because the zircons are small, approximately 50 to 120 μm in length, several grains were analysed together (Table 4.4). The measurements were repeated three times with a different number of zircons each time in order to check that the number of grains did not affect the measured ratios (Fig. 4.6, Table 4.4). Three repeat measurements yielded consistent $^{207}Pb/^{206}Pb$ ratios with a mean of $^{207}Pb/^{206}Pb$ = 0.058238 ± 136, corresponding to an age of 539 ± 5 Ma (Fig. 4.6, Table 4.4). This age is interpreted to reflect the time of crystallisation of the leucogranite.

Sample 97M77 & M98/B7- Granite

Samples 97M77 and M98/B7 were collected from different locations within the same, previously unmapped, granite intrusion approximately 15 km southeast of Uldzit Gol (Fig. 4.2). This undeformed granite has intruded the Delb Khairkhan mélange and the ophiolite mélange, and cuts the thrust fault separating them, as well as other internal faults within the mélanges (Fig. 4.2).

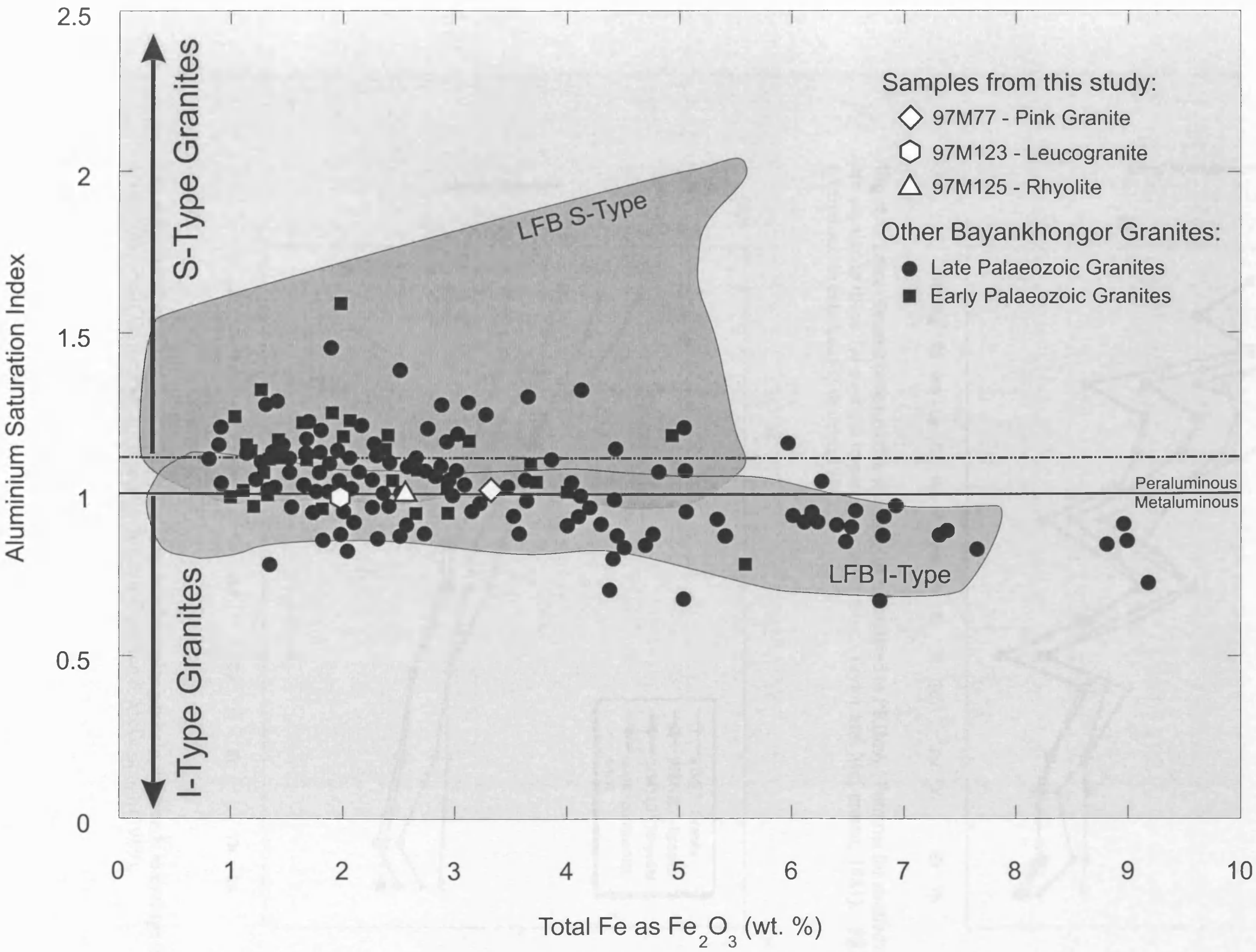

Fig. 4.3: Aluminium Saturation Index vs. total FeO demonstrating the dominantly transitional nature between S-type and I-type granites in the Bayankhongor area. S- and I-type fields after Blevin and Chappell (1995), additional Palaeozoic granite data from Takahashi et al. (1999).

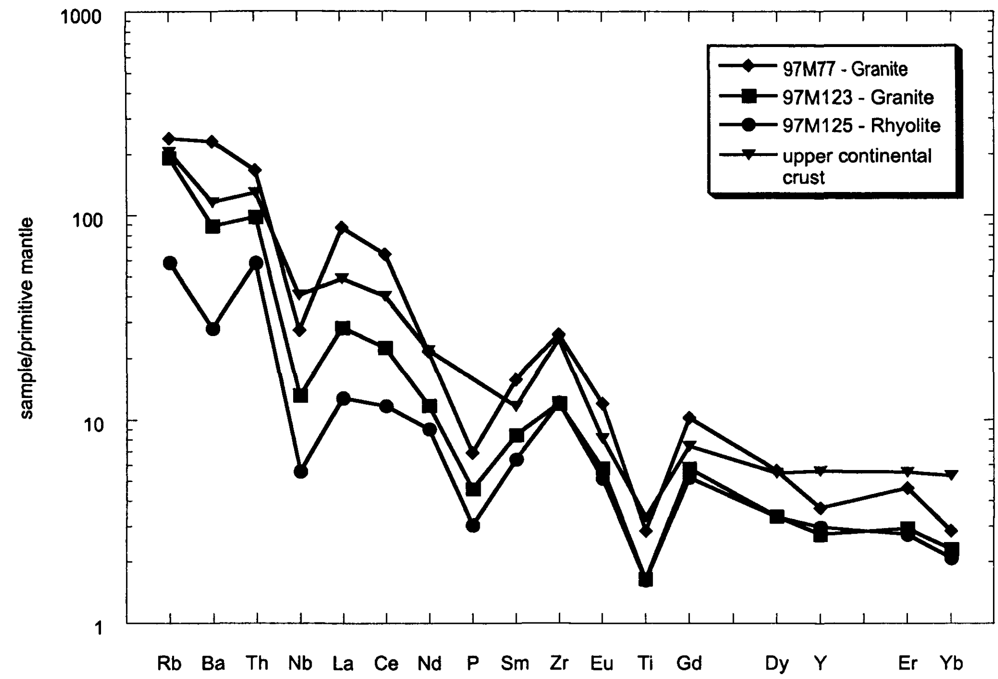

Fig. 4.4: Trace element patterns of dated samples normalised to PRIMA. Patterns for studied rocks are similar to those for average upper continental crust (Taylor and McLennan, 1981). PRIMA normalisation data from Hofmann (1988).

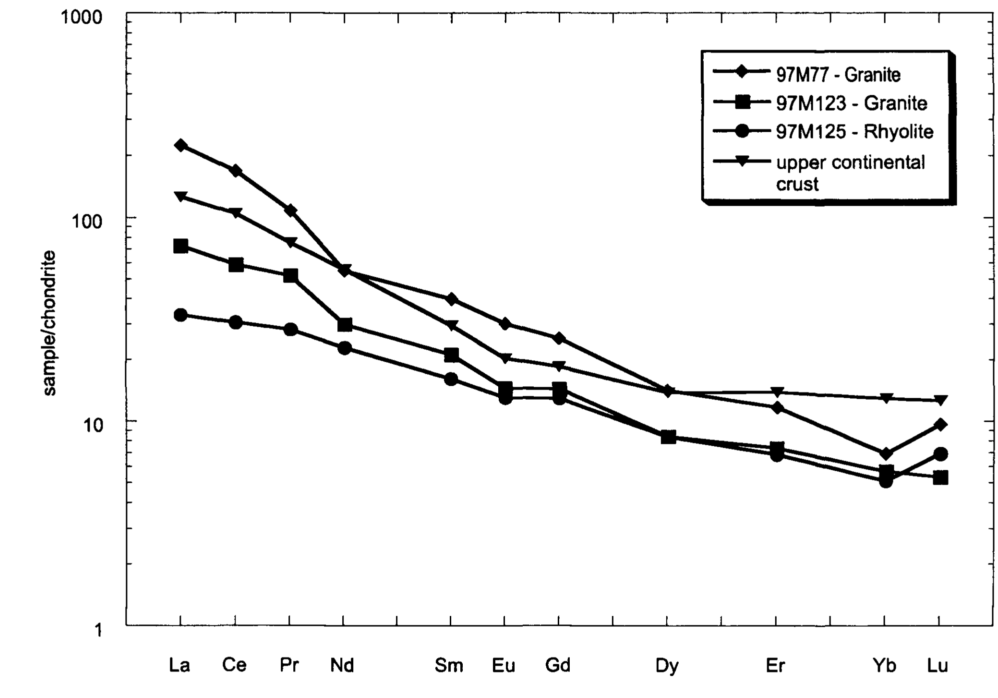

Fig. 4.5: Chondrite normalised REE patterns for dated samples have similar trends to average upper continental crust (Taylor, 1981). Normalisation data from Sun & McDonough (1989).

Petrography

Both samples are medium-grained ($\leq$ 5 mm) biotite-bearing pink granites. The grain size in the pluton varies with some very coarse-grained areas containing feldspar crystals up to 6-10 cm in length. The samples are roughly equigranular with quartz, plagioclase, microcline, microperthite, and orthoclase forming a matrix of intergrown crystals with consertal texture. Local graphic intergrowths of quartz and potassium feldspar are also present. Biotite forms 2-5 mm laths which are almost totally altered to chlorite. Plagioclase and some potassium feldspars are also heavily altered to sericite and clay minerals. Iron oxide-rich veins cut the samples, but they are only a few millimetres wide. Sphene and zircon are the dominant accessory phases, and apatite and opaques are minor.

Geochemistry

Because samples 97M77 and M98/B7 were taken from the same granite, only sample 97M77 was chemically analysed. Sample 97M77 has the lowest SiO_2 (66.5 wt.%) and CaO (1.54 wt.%) compositions of the dated samples, but has similar Na_2O (4.57 wt.%) and K_2O (4.9 wt.%) concentrations to the leucogranite sample 97M123 (Table 4.2). Its A.S.I. = 1.02 (Table 4.2) is the highest of the analysed samples and suggests that it is slightly peraluminous (Fig. 4.3). Primitive mantle normalised trace-element patterns (Fig. 4.4) indicate enrichment in LILE (e.g. Rb = 128.3 ppm and Ba = 1403.1 ppm) and selective enrichment of HFSE such as Th (13.5 ppm) and Zr (254.0 ppm), but depletion in Nb and Ti, indicated by marked negative anomalies in Figure 4.4 (Nb/La_{PRIMA}= 0.32, Ti/Zr_{PRIMA}= 0.11) as was the case for the leucogranite. Chondrite normalised REE patterns (Fig. 4.5) show enrichment of LREE relative to HREE (La/Yb_{chnd} = 32.5). Sample 97M77 has similar Nd isotopic characteristics to 97M123 with an initial ε_{Nd} = -3.1 and a two-stage depleted mantle model age of 1545 Ma (DePaolo, 1991; Table 4.3).

Geochronology

Sample M98/B7: zircons from M98/B7 are prismatic, clear to yellow-brown and idiomorphic to slightly rounded. The grains are relatively large, approximately 150-200 μm in length, compared with other populations and thus were analysed as single grains. The experiments were repeated four times with separate single grains to confirm the calculated age. The $^{207}Pb/^{206}Pb$ ratios from each run were with a mean value of $^{207}Pb/^{206}Pb$ = 0.058242 $\pm$ 20 (Table 4.4) corresponding to an age of 539 $\pm$ 1 Ma (Fig. 4.7). This age most likely represents the time of crystallisation of the granite.

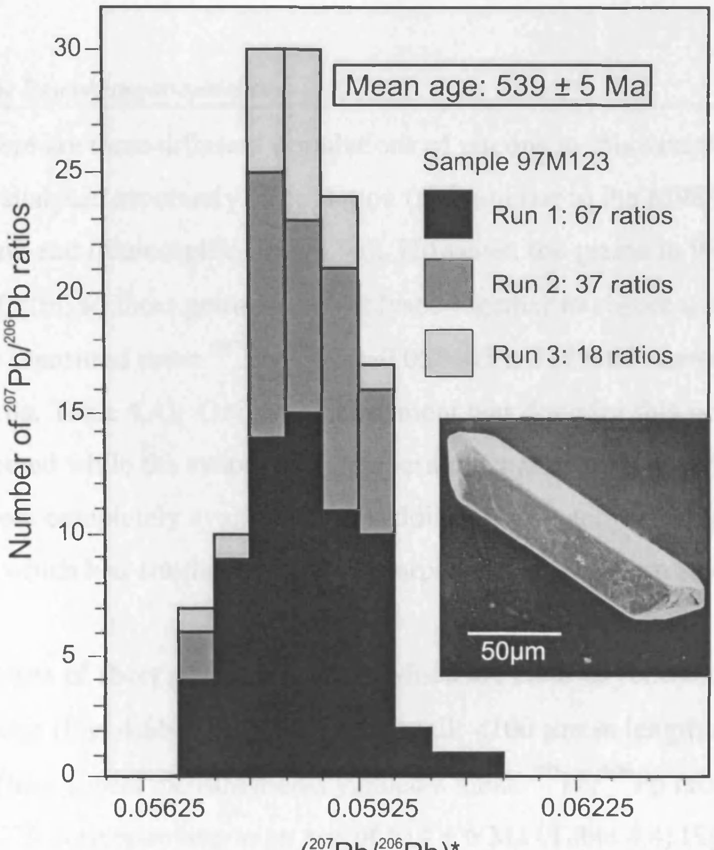

Fig. 4.6: Histogram of measured $^{207}Pb/^{206}Pb$ ratios for sample 97M123.

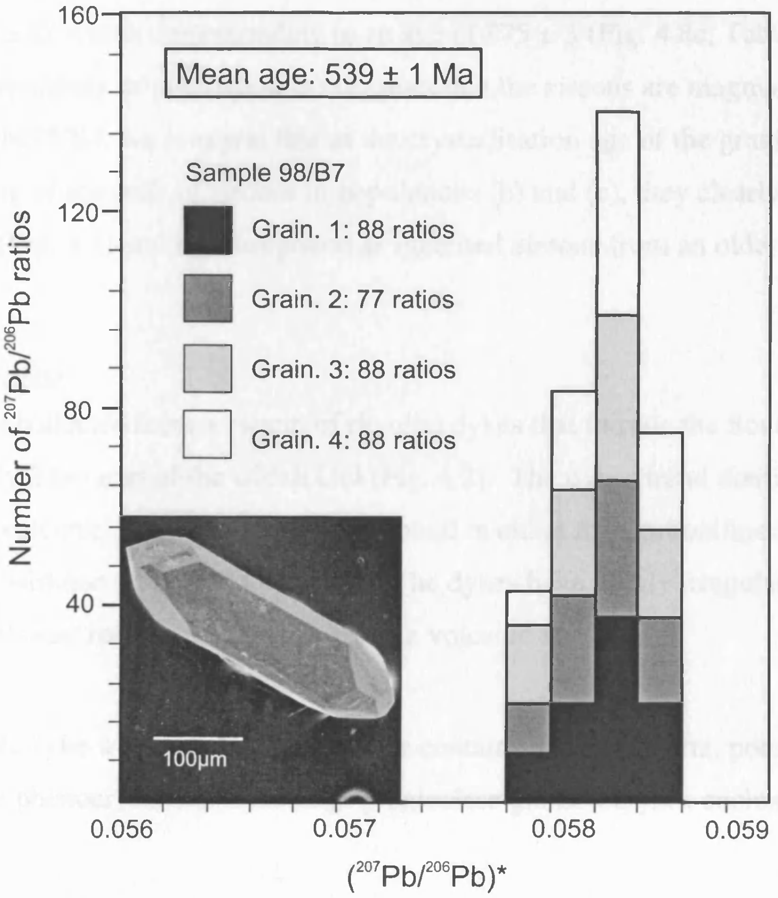

Fig. 4.7: Histogram of measured $^{207}Pb/^{206}Pb$ ratios for sample M98/B7.

Sample 97M77: there are three different populations of zircons in this sample(97M77 a-c, Table 4.4) that were each analysed separately. Population (a) is similar to the M98/B7 zircons: prismatic, clear to light pink and idiomorphic (Fig. 4.8a). However, the grains in 97M77 are smaller, (approximately 60 μm) so three grains were analysed together to ensure a strong signal during measurement. The measured mean $^{207}Pb/^{206}Pb = 0.058405 \pm 315$ ratio corresponds to an age of 545 ± 2 Ma (Fig. 4.8a, Table 4.4). Only one experiment was done for this population, and 136 mass scans were collected while the evaporation temperature was as high as 1601°C, ensuring that the grains were completely evaporated. In addition, the determined age compares well with that of M98/B7 which had similar population morphology and is from the same granite pluton.

Population (b) consists of short prismatic zircons which are clear to yellow and have slightly rounded terminations (Fig. 4.8b). The grains are small, <100 μm in length and so several were analysed together. Three repeat measurements yielded a mean $^{207}Pb/^{206}Pb$ ratios between of $^{207}Pb/^{206}Pb = 0.060290 \pm 175$ corresponding to an age of 614 ± 6 Ma (Table 4.4; Fig. 4.8b).

Population (c) contains long, thin, pink, prismatic grains with rounded ends (Fig. 4.8c). They are about 80 μm in length and so several grains were therefore analysed together (Table 4.4). A single experiment for this population with 80 isotopic ratios produced a mean ratio of $^{207}Pb/^{206}Pb = 0.068214 \pm 87$ which corresponding to an age of 875 ± 3 (Fig. 4.8c; Table 4.4).

Because the morphology of population (a) suggests that the zircons are magmatic and the age is similar to that of M98/B7, we interpret this as the crystallisation age of the granite. Despite slightly rounding of the ends of zircons in populations (b) and (c), they clearly have magmatic morphology (Fig. 4.8) and are interpreted as inherited zircons from an older source rock.

Sample 97M125- Rhyolite

This sample was collected from a swarm of rhyolite dykes that intrude the Southern Volcanics approximately 2 km east of the Uldzit Gol (Fig. 4.2). The dykes trend dominantly NE and are confined to the volcanic unit because none are found in either the Carboniferous rocks to the south or the Delb Khairkhan mélange to the north. The dykes have highly irregular contacts with the surrounding volcanic rocks and in places contain volcanic xenoliths.

Petrography

A single 3m wide dyke was sampled. The sample contains 3-5 mm quartz, potassium feldspar and plagioclase phenocrysts and some large plagioclase glomerocrysts, enclosed in a

Special Note

Page 113 missing from the original

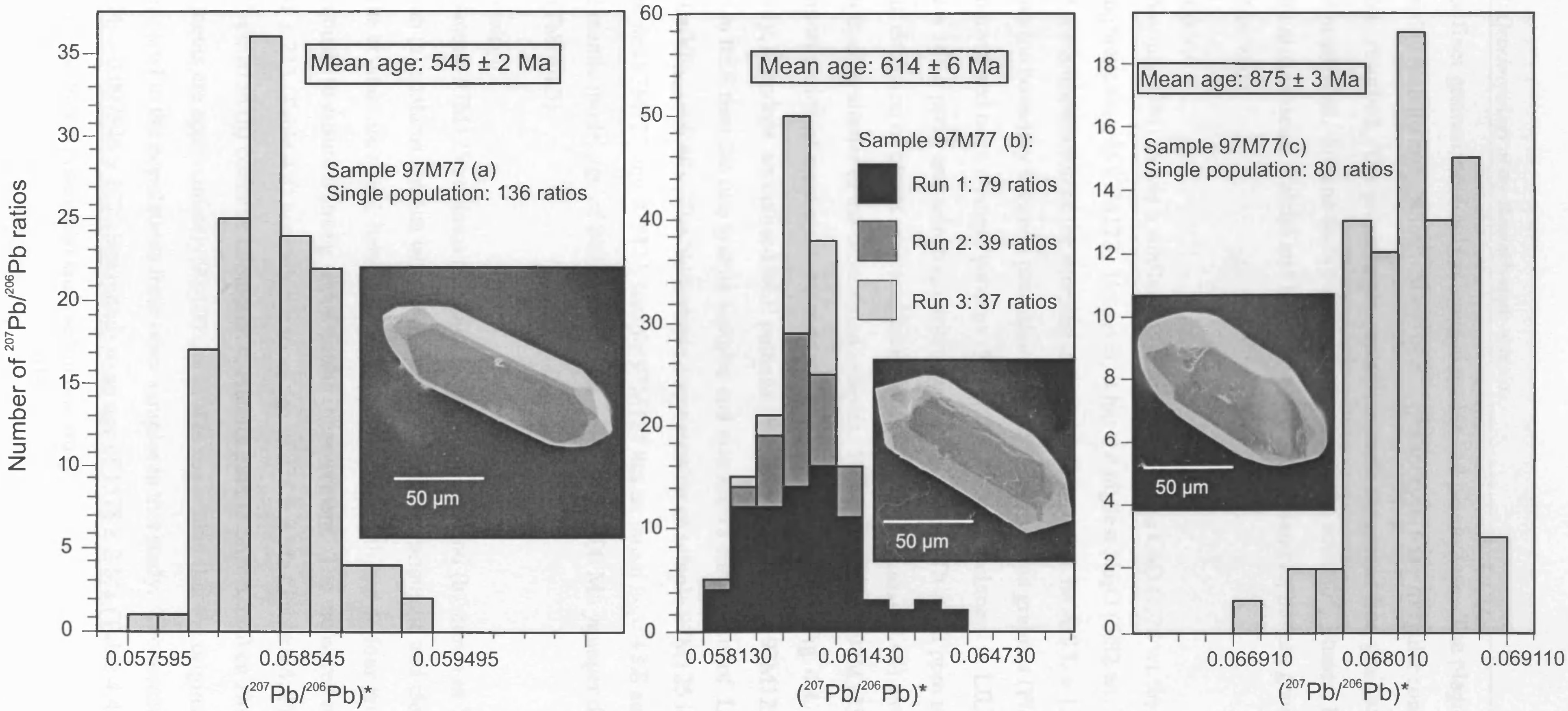

Fig. 4.8: Histograms of measured $^{207}Pb/^{206}Pb$ ratios for three morphologically distinct zircon populations in sample 97M77. See table 4.4 for morphological description.

matrix of finer grained, randomly orientated quartz and plagioclase. The plagioclase phenocrysts are altered to sericite and epidote. Some quartz phenocrysts have irregular rounded margins and are slightly resorbed. The groundmass contains a small amount of fine-grained (<1 mm) anhedral muscovite. Sphene and opaques are the dominant accessory phases, but apatite and zircon are also present. Calcite and hematite veins cut the sample, but are generally only a few millimetres wide.

Geochemistry

Sample 97M125 has a similar SiO_2 (70.71 wt.%) and CaO (1.78 wt.%) concentration to the leucogranite sample 97M123. However, it has the highest Na_2O (6.32 wt. %) and lowest K_2O (1.51 wt.%) concentration of the samples analysed in this study. Its A.S.I. = 1.00 (Table 4.2) lies exactly on the boundary between peraluminous and metaluminous granites (Fig. 4.3). Primitive mantle normalised trace element patterns (Fig. 4.4) indicate enrichment in LILE (e.g. Rb = 31.4 ppm, Ba = 168.5 ppm) and selective enrichment of HFSE (e.g. Th = 4.8 ppm and Zr = 117.6 ppm), but depletion of others indicated by negative Nb (Nb/La_{PRIMA}= 0.44) and Ti (Ti/Zr_{PRIMA}= 0.13) anomalies, similar to the other dated samples. However, sample 97M125 has a generally lower concentration of trace elements than either 97M123 or 97M77 (Fig. 4.4, Table 4.2). Conversely, chondrite normalised REE patterns (Fig. 4.5) indicate that 97M125 is generally more enriched in REE than the two granite samples and also shows enrichment of LREE relative to HREE (La/Yb_{chnd} = 6.48). The Nd isotopic concentration of sample 97M125 is very different from samples 97M123 and 97M77, sample 97M125 has an initial ε_{Nd}= +3.8 and a two-stage depleted mantle model age of 885 Ma, which is around 750-800 Ma younger than 97M123 and 97M77 (Table 4.3).

Geochronology

Sample 97M125 contains two zircon populations (a) and (b) shown in Table 4.4. Population (a) contains zircons which are short, idiomorphic, prismatic and clear to pink (Fig. 4.9a). The crystals are small, between 50 and 100 μm in length and so four grains were analysed simultaneously to ensure a strong signal during measurement. The measured mean $^{207}Pb/^{206}Pb$ = 0.056551 ± 213 (Table 4.4) corresponds to an age of 474 ± 8 Ma (Table 4.4; Fig. 4.9a).

Population (b) contains idiomorphic, slightly pink to brown, broken zircons (Fig. 4.9b). The fragments are approximately 80-100 μm in size suggesting that the original zircons were large compared to the populations from other samples in this study. The measured mean $^{207}Pb/^{206}Pb$ = 0.097548 ± 122 corresponds to an age of 1578 ± 2 Ma (Table 4.4; Fig. 4.9b), making this the oldest population analysed in this study.

The zircon morphology suggests population (a) is of magmatic origin and the age of 474 Ma is interpreted to reflect the time of crystallisation of the rhyolite dykes. The large broken zircons of population (b) do not appear to have been abraded in any way as the terminations of the fragments are not noticeably rounded and therefore, it appears that these are also magmatic. The older age of population (b) means that it must be interpreted as an inherited population from the melt source(s).

Discussion

Interpretations of the structural and lithological characteristics of the Bayankhongor Zone suggest that the major lithotectonic units were amalgamated by a mechanism of subduction-accretion (Buchan et al., 2001). The analysed granites and rhyolite dykes intrude the accreted blocks and so provide important constraints on the relative timing of accretion and the duration of subduction and collision. The new data indicate that there were at least two Palaeozoic granite-forming events at *c.* 540 Ma and *c.* 474 Ma. An important consideration is whether the granite magmas were produced during collisional accretionary processes, or by subduction prior to accretion.

Magma sources and tectonic setting:

The limited chemical data base of just three samples in this study, makes it difficult to draw firm conclusions on the nature of magma source components and the emplacement environment. However, by combining these data with those from previous studies of granites in the Bayankhongor area (e.g. Takahashi et al., 1999), and of the rocks that the granites and rhyolite dykes intruded (e.g. Buchan et al., 2001), we can establish some important constraints.

Central Asia contains many large A-type granite plutons that were intruded during the Palaeozoic, predominantly in the Permian (Jahn et al., 2000). It is therefore important to determine whether the granites analysed in this study reflect A-type magmatism, which would define a specific tectonic environment for their emplacement. Whalen et al. (1987) defined a chemical discrimination to separate A-type granites from the I- and S-type granites of Chappel and White (1974), based on the ratio of Ga/Al in the granite which can be plotted against several trace and major elements that tend to be concentrated in A-type granites. One commonly used is Ga/Al versus Y in which an A-type granite is determined to have a 10000Ga/Al ratio > 2.6 and a concentration of Y > 80 ppm. Any granite with a value below this is deemed either an I- or S-type. The granites in this study have 10000Ga/Al = 2.1-2.4 and Y concentrations between 10.8 and 14.5 ppm (Table 4.2) which suggests that they are not A-type granites.

Chappell and White (1992) define S-type granites as only peraluminous (A.S.I. > 1.1, Fig. 4.3), due to concentration of Al in clay minerals during chemical weathering of sedimentary source rocks, and I-type as generally metaluminous to mildly peraluminous (A.S.I. <1.0, Fig. 4.3) because their igneous source rocks have not inherited the same weathering products. All three dated rocks in this study have major element characteristics that indicate they are compositionally transitional between metaluminous and peraluminous granites (i.e. A.S.I. between 0.99 and 1.02; Fig. 4.3) and are therefore transitional between I-type and S-type granites. Our data combined with that of Takahashi et al. (1999; Fig. 4.3) indicate that these compositional characteristic are shared by the majority of Palaeozoic granites found in the Bayankhongor area. This is not surprising because the greater part of the Bayankhongor area is composed of mélanges containing both igneous (dominantly mafic) and sedimentary lithologies (Buchan et al., 2001; Buchan, unpubl. data). Therefore, even if the magma source in the deep crust was relatively homogeneous, the rising magma could acquire transitional characteristics by assimilating some of the wall rocks into the magma. As different magma bodies would have passed through mélanges with varying proportions of igneous and sedimentary material, they could correspondingly assimilate different quantities of each and become more peraluminous or metaluminous. This is probably the most likely explanation for the spread of data in Fig. 4.3.

Despite the apparent similarities in source chemistry of Bayankhongor granites, the Sm-Nd isotopic characteristics of the studied samples reveal some marked differences. Granite samples 97M123 and 97M77 have enriched (low Sm/Nd) source characteristics indicated by an initial $\varepsilon_{Nd\,(540)} \approx -3$ (Table 4.3), whereas the rhyolite sample 97M125 has an initial $\varepsilon_{Nd\,(474)} = +3.8$ (Table 4.3) indicating a moderately depleted source. Recalculating ε_{Nd} of the granite samples to the crystallisation age of the rhyolite dyke at 474 Ma gives $\varepsilon_{Nd\,(474)} = -4.8$ for the leucogranite (97M123) and $\varepsilon_{Nd\,(474)} = -4.1$ (97M77) indicating that the granites and rhyolite dykes must have different source components, or at least a different mixture of components.

There are three scenarios that could account for these differences in source characteristics. The first and perhaps the more obvious is that the rhyolite dykes were emplaced 70 Ma after the granites and therefore, different sources may have been available at the different times as the accretionary complex developed. A problem with this interpretation is that the two granites, which lie to the north and south of the rhyolite dykes, appear to share the same magma source in terms of both major/trace element and isotopic characteristics. Thus it seems likely that this source would have been available across the entire area between the granites at 544 Ma but not necessarily at 474 Ma. However, this conclusion relies on the assumption that the granites were emplaced vertically whereas studies of Himalayan S-type leucogranites have shown that many granites are emplaced laterally as sills (e.g. Searle et al., 1999). However, the emplacement mechanism of the two granites may not be important, as consideration of the field relations of the Southern Volcanic rocks shows that they are completely fault bounded except where they come into contact with the younger Carboniferous sedimentary rocks (Fig. 4.2). This suggests that the Southern Volcanics may have been juxtaposed with the rest of the Bayankhongor units after the rhyolite dykes were emplaced. Indeed the rhyolites may have been an integral part of the volcanism. Late juxtaposition would also account for the fact that the volcanic rocks are less intensely deformed than surrounding units (Buchan et al., 2001).

Both of the above suggestions are complicated by spatial relationships and timing of deformation, but are possible due to the tectonic complexity of subduction-accretion environments. However, the final scenario does not require large movements of the volcanic rocks in order to account for differences in source chemistry. The multiple zircon populations of 97M77 and 97M125 (Table 4.4) indicate that older rocks were at least partially assimilated into the magma. Therefore, just as the mixed lithologies in the mélanges could be responsible for the similarities in major element chemistry, it could also account for the differences in isotopic chemistry. If it is assumed that the major thrust units in the Bayankhongor zone are continuous to depth, then it is probable that the two granites have sampled most of the same lithologies and therefore have comparable chemical and isotopic characteristics. However, the rhyolite dykes were intruded solely into the Southern Volcanic rocks, fragments of which are found as partially resorbed xenoliths within the dykes. Therefore, the volcanic rocks may be responsible for the difference in isotope chemistry. Also, the fact that there are only dykes and no larger intrusive bodies of this age, may suggest that this was a relatively small partial melt fraction that would be more easily susceptible to changes in isotopic composition due to mixing. However, this could also reflect a problem of sampling over a small area. The inherited zircon population in the rhyolite (97M125) is an important factor in the mixing scenario because its age of 1578 ± 2 Ma (Table 4.4) is comparable to the Nd model age of the granite samples (1417 Ma, Table 4.3), taking into account mixing of younger rocks with the granite magma, suggesting that the same source may have contributed in part to the rhyolite magma. At present it is difficult to resolve these questions because the tectonic relationship of the Southern Volcanics to the rest of the Bayankhongor units is not completely understood; i.e. it is unclear whether the volcanics were built on top of the Burd Gol accretionary complex (Fig. 4.2) during subduction of the

Bayankhongor ophiolite crust, or whether they represent part of a separate island arc that was later accreted (C. Buchan unpubl. data).

However, the following constraints on the possible sources of the granites and rhyolite dykes can be suggested. Both granite samples (97M77 and 97M123) crystallised from a melt extracted from an enriched source which has a minimum crustal-residence age (O'Nions et al., 1983) of between 1350 Ma and 1417 Ma based on two-stage Nd model ages (Table 4.3). It is likely that the actual time of crust-mantle differentiation of the granite magma source was significantly older and more enriched than the granite magma (i.e. had a more negative ε_{Nd} value), because the chemical and isotopic characteristics of the magma were modified by assimilation of younger crust as indicated by the inherited zircon populations of 97M77 and the general transitional character between I-type and S-type granite (Arndt & Goldstein, 1987).

Therefore, the most likely sources would be either sediments produced by erosion of old continental crust or the continental crust itself. Buchan et al. (2001) suggest that the Bayankhongor ophiolite was obducted onto the Dzag Zone (Fig. 4.2), which represents the passive margin of a continent that lies beneath the Hangai region (Fig. 4.1). The ophiolite was later deformed during the collision and suturing of the Baidrag block and the Hangai continent. Granite occurrences are common in collisional settings where sediments or quartz-feldspathic continental basement is melted due to increased pressure and temperature on burial by thrust stacking. Therefore, the Hangai continent and original passive margin sedimentary cover are strong candidates for the granite source. Unfortunately, the proposed Hangai continent is not exposed in the study area and so there are no data on its chemical and isotopic characteristics. Nevertheless, a comprehensive study of depleted mantle model ages from granites in the Hangai region by Kovalenko et al. (1996b) identified several bodies with model ages in the range 1200-1600 Ma similar to those determined for the two granites of this study. Because of the depleted magma signature ($\varepsilon_{Nd} = +3.8$) of the rhyolites and much younger depleted mantle model age (943 Ma single-stage, 738 Ma two-stage), it is unlikely that the main magma source of the rhyolite was the same continental material. In order to achieve these characteristics from a bulk melt that was initially enriched, assimilation of large amounts of depleted oceanic and/or island arc volcanic rocks would be required because these contain much lower concentrations of Nd than the continental basement rocks and so would have little effect on the overall magma concentrations. Conversely a small amount of an enriched melt mixed with an initially depleted melt could easily cause the resultant magma to have more enriched characteristics. Therefore, it is more likely that the initial rhyolite magma was more depleted (for example a depleted mantle melt at 474 Ma would be expected to have an initial $\varepsilon_{Nd\,(474)} \approx +8.9$) and that a small amount of continental basement or sediment was mixed with the magma resulting in a lower ε_{Nd} value and older model age. This would also be consistent with the inherited zircon population found in the rhyolite with an age of 1577 Ma which requires an older crust component.

Field evidence of a contractional or transpressional regime throughout the Palaeozoic (Buchan et al., 2001), combined with the chemical and isotopic characteristics of the granite samples 97M77 and 97M123 strongly supports a collisional setting for granite generation. The zircon saturation temperatures determined for the samples are between 750 to 800 °C (Table 4.2) which is within the range that Thompson (1999) suggests is obtainable during collisional burial resulting in high degrees of melting. Therefore, it seems most likely that the granites were emplaced during collision of the Bayankhongor ophiolite and Burd Gol mélange with the Dzag zone and Hangai continent, and that the rocks of the Hangai continental crust and/or the Dzag passive margin were the main magma source. The rhyolite dykes, may also have been produced during this collision or may be arc related and later juxtaposed by faulting.

Emplacement timing and the tectonic history of the Bayankhongor Ophiolite Zone:

Having considered the possible magma source components of the granites and rhyolite dykes and established that they were likely produced during terrane collision, it is now possible to examine the constraints that our ages provide for the timing and duration of deformation within the Bayankhongor accretionary system. The pink granite (97M77) and leucogranite (97M123) provide constraints on the deformation in the Bayankhongor ophiolite zone and the Burd Gol mélange. The pink granite (97M77 & M98/B7) cross-cuts the thrust fault that juxtaposes the ophiolitic rocks with the Delb Khairkhan mélange, as well as several smaller internal faults within the ophiolite mélange (Fig. 4.2). The pink granite itself is not deformed which suggests that none of these faults moved significantly after intrusion. This provides constraints on the timing of obduction of the ophiolite rocks, as they must have been in place before intrusion of the pink granite at 544 Ma. In addition, the whole ophiolite zone including the Delb Khairkhan mélange must have collided or been accreted to the Burd Gol accretionary complex by 539 Ma, because the leucogranite has the same crystallisation age and so it can be assumed that it was produced by the same or coeval event. If the Hangai continent was the source for the granite magmas, then this must also have at least begun colliding with the ophiolite and accretionary complex by 540 Ma. The ophiolite is interpreted to have formed at 569 ± 21 Ma (Kepizhinskas et al., 1991; Table 4.1), which only gives 30 My between formation and closure of the ocean. Höck et al. (2000) published an Ar-Ar plateau age of 533 ± 3 Ma for biotite from a garnet-kyanite gneiss which forms part of the Burd Gol mélange south of Mount Ushgoeg (Figs. 4.10 & 4.11, Table 4.2), which is comparable to the granite ages of this study. Because the Ar-Ar ages record the cooling phase of deformation, the data suggest that parts of the Burd Gol mélange experienced reasonably high-grade metamorphism associated with a regional deformation event at approximately the same time as the granites were produced, which is consistent with a collisional interpretation. Foliation of the leucogranite (97M123) along the thrust faults forming its northern margin (Fig. 4.2) suggests that it was either emplaced syn-tectonically and as a result was foliated, or deformed later by post-intrusion movement. Also, K-Ar ages of cleavage forming white mica in the Dzag Zone (Kurimoto et al., 1999; Fig. 4.2, Table 4.1) near to its thrust contact with the ophiolite zone (Fig. 4.11), indicate that these micas cooled below their closure temperature around 450 Ma (Table 4.2). This suggests that deformation and associated metamorphism continued within the thrust zone between the Dzag and ophiolite zones. In addition, recent Ar-Ar data indicate that amphiboles developed on cleavage planes, associated with thrust deformation in pillow basalts of the Bayankhongor ophiolite formed around 485 ± 6 Ma, suggesting that parts of the ophiolite were still undergoing deformation at this time (Delor et al., 2000; Figs. 4.10 & 4.11). In this case, the rhyolite dykes may have intruded during the final stages of the collisional process before regional cooling began or alternatively, the rhyolite dykes could represent a second magmatic event between 480 and 470 Ma.

In summary, the combined isotope-geochronological data for the Bayankhongor area suggests that the Bayankhongor ophiolite was formed at 569 Ma. After a period of subduction-accretion lasting around 30 Ma the ophiolite was accreted to the Burd Gol accretionary complex and subsequently obducted onto the Dzag passive margin during collision with the Hangai continent between 540 Ma and 450 Ma (Fig. 4.10).

Regional constraints on deformation in the Central Asian Orogenic Belt

Geochronological data from ophiolites in western Mongolia and Tuva (southern Siberia), suggest that ophiolite rocks that cover a large area of what is now the CAOB may have been formed in one or more ocean basins at *c.* 570 Ma. Figures 4.10 and 4.11 show the remarkable correlation for the ages of the Bayankhongor (569 ± 21 Ma; Kepezhinskas et al., 1991), Khantaishir (568 ± 4 Ma; E.B. Salnikova *pers comm.*), Dariv (573 ± 6 Ma; Salnikova *pers comm.*), Ozernaya (527 ± 43 Ma; Kovalenko et al., 1996a) and Agardagh Tes-Chem (569 ± 1 Ma; Pfänder et al., 1999). These preserved remnants of oceanic crust occur along a gently curving semi-continuous belt of oceanic crust all of which, with the possible exception of the Ozernaya ophiolites, was produced around 570 Ma (Fig. 4.1). Kozakov et al. (1999) and

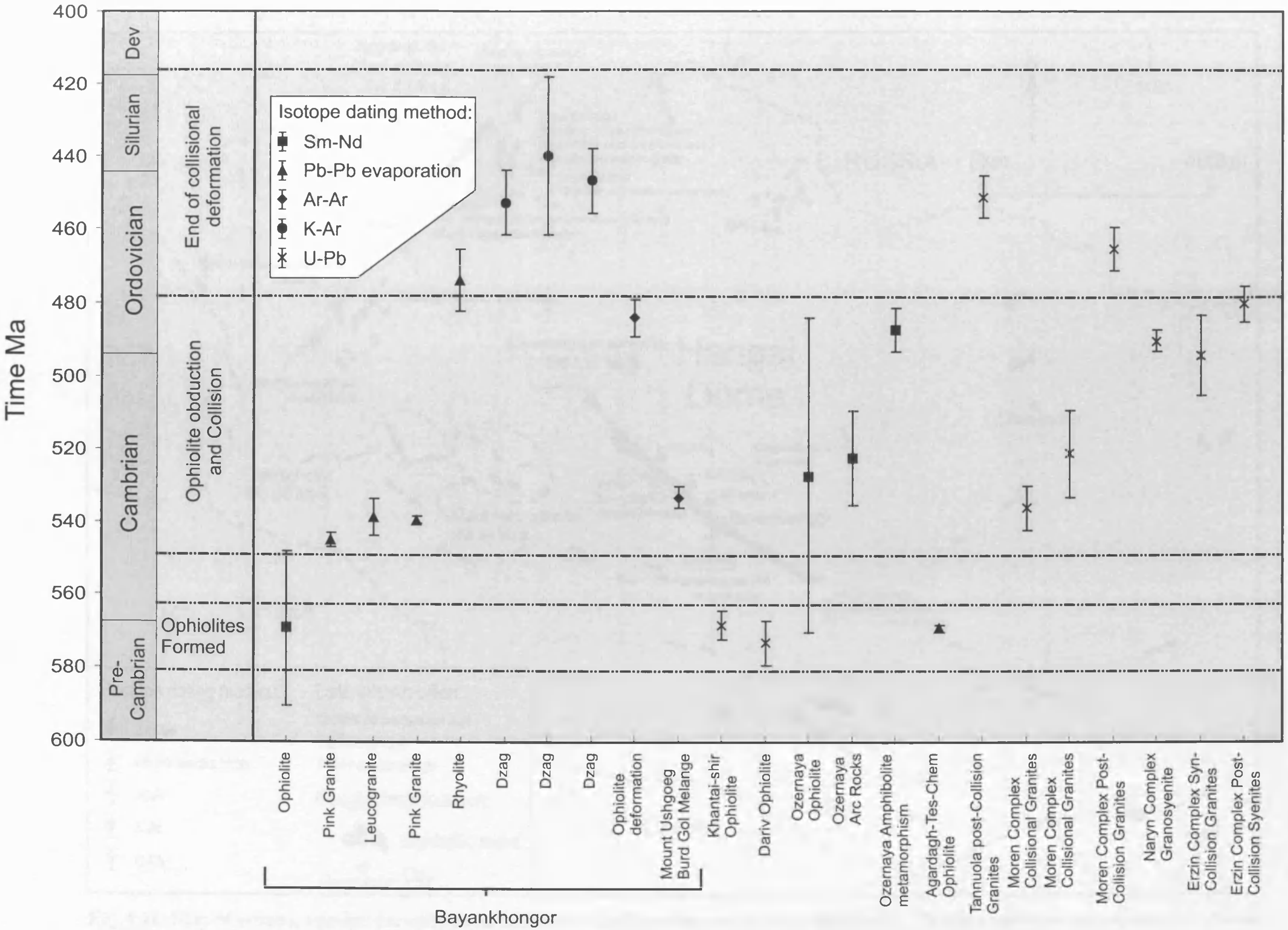

Fig. 4.10: Compilation of isotopic age data associated with Palaeozoic ophiolite belts in Western Mongolia and Southern Tuva. Isotopic ages for ophiolites group around 569 Ma and ages associated with collisional deformation suggest events at *c.* 540 Ma and *c.* 450 Ma providing evidence of an arcuate belt from Bayankhongor to Agardagh Tes-Chem, which shares a common deformation history. The difference in age and large error of the Ozernaya ophiolites could be associated with the effects of amphibolite metamorphism in this area. See Table 4.1 and Fig. 4.11 caption for data sources.

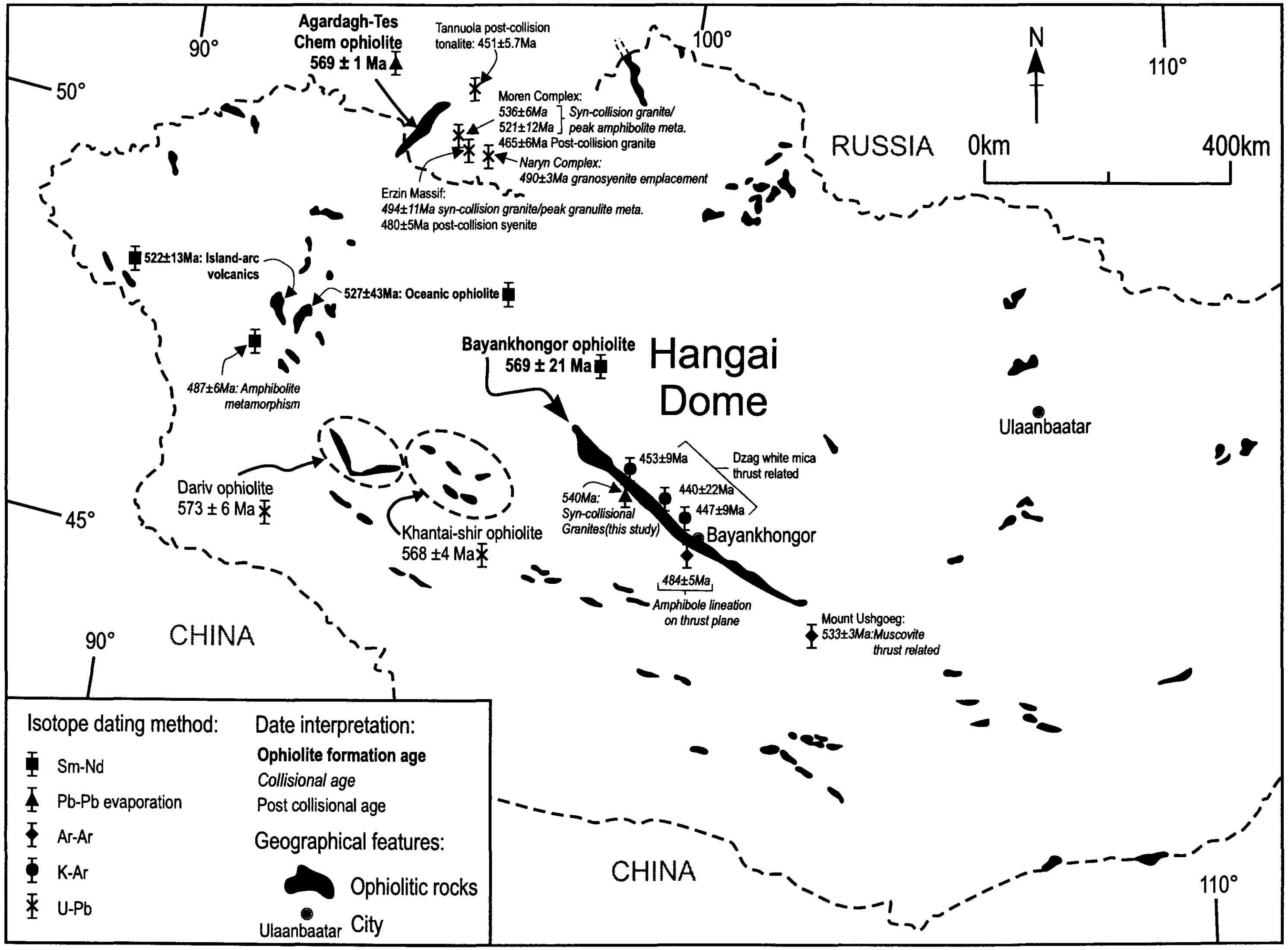

Fig. 4.11: Map of isotopic age data for ophiolites, collision related granites and metamorphic rocks. The data demonstrate a strong correlation for the history of ophiolites in western Mongolian and southern Tuva. See Table 4.1 for Bayankhongor data sources. Other data sources: Tannuola (U-Pb zircon, Kozakov et al. 1999a), Moren, Erzin, and Naryn complexes (U-Pb zircon, Kozakov et al. 1999b; Salnikova et al. 2001), Ozernaya (Sm-Nd whole rock and amphibole mineral isochron, Kovalenko et al. 1996) and Agardagh Tes-Chem (Pfänder et al. 1999).

Salnikova et al. (2001) carried out a detailed geochronological study of the geologically complex region to the east of the Agardagh Tes-Chem ophiolite (Fig. 4.10), which has previously been assumed to form part of a Precambrian microcontinent known as the Tuva-Mongolian Massif. They found that the Erzin Massif, Moren and Naryn complexes that make up this area were not metamorphosed in the Precambrian, as previously suggested by Mossakovsky et al. (1995, among others), but instead the earliest metamorphism in the Moren Massif took place around 536 ± 6 Ma. From their analyses, they produced a detailed geochronological model for accretion and collision involving initial amalgamation of the three complexes between approximately 536 Ma and 490 Ma followed by a prolonged period of deformation which ended with the intrusion of several post-collision granites and syenites at around 480 Ma to 450 Ma (Figs. 4.10 and 4.11). The time scale proposed by these authors is similar to that suggested here for the Bayankhongor area, with collision and ophiolite obduction at approximately 540 Ma and cessation of major regional deformation at around 450 Ma (Fig. 4.10). In addition, Kovalenko et al. (1996) proposed that the Ozernaya island arcs and ophiolites (Fig. 4.11) were obducted and accreted at around 490 Ma based on a Sm-Nd age of 487 ± 6 Ma for amphibolite metamorphism in the area (Figs. 4.10 and 4.11). These combined data sets for the western Mongolian and south west Tuva ophiolites, provide strong evidence for a regional correlation of a collisional suture and associated regional metamorphism and contractional/transpressional deformation. In addition, they help to define the possible margins of the Hangai cratonic nucleus suggested by Cunningham (2001) to be a major control on the localisation of Cenozoic uplift and active growth of the Mongolian Altai mountain range, which lies to the west and southwest of the Hangai block. At present, detailed models for the genesis of the ophiolites is only available for the Bayankhongor ophiolite (Buchan et al. 2001, C. Buchan unpubl. data) and Agardagh Tes-Chem ophiolite (Pfänder et al., submitted to Contrib. Min. Pet., 2001), making it difficult to produce a comprehensive reconstruction of the genetic relationships of these ophiolites in a singular ocean basin, or multiple coevally closing ocean basins. However, the data presented here indicate that a large part of the CAOB was formed at similar times and may also have been part of the same oceanic system prior to 540 Ma.

Submitted for publication to *Earth and Planetary Science Letters*, 8th June 2001.

Co-Authors: Jörg Pfänder, Alfred Kröner, Tim Brewer, Onongin Tomurtogoo, Dondov Tomurhuu, Dickson Cunningham, and Brian Windley.

Chapter 5:

Evolution of the Bayankhongor Ophiolite, discussion of subduction zone architecture and obduction mechanisms.

Introduction

The previous chapters have presented a wealth of new data that provide constraints on the structural and lithological relationship of the major lithotectonic units of the Bayankhongor Ophiolite zone, the tectonic setting in which the ophiolite and Southern Volcanics were formed, and the timing of accretion, collision, and obduction of the ophiolite and its neighbouring units. In addition, it was shown that the Bayankhongor Ophiolite may share a common subduction-accretion history with several other ophiolites in western Mongolia and southern Tuva, that all formed at *c.* 570 Ma and were obducted during collisional events at *c.* 540 Ma (Figs. 5.1, see discussion, Chapter 4).

In this section, the conclusions highlighted in the previous chapters are summarised and their implications for the architecture of the Bayankhongor subduction-accretion system are discussed. Tectonic models for the obduction of the ophiolite onto the passive margin of the Hangai continent are presented.

Constraints on subduction zone architecture

Figure 5.2a shows a representative cross-section demonstrating the field relations of the five major lithotectonic units of the Bayankhongor region: the Baidrag block, Burd Gol mélange, Bayankhongor Ophiolite zone, Dzag zone, and Hangai block. The structural and lithological characteristics of these units suggest that the Bayankhongor Ophiolite is a suture marking the position of an early Palaeozoic subduction zone between the Baidrag block to the south, and the Dzag zone to the north. The Burd Gol mélange represents an accretionary wedge built up against the Baidrag continental block. Subduction was to the southwest, based on the dominant polarity of thrusting within the Bayankhongor Ophiolite zone. The ophiolite was obducted in a north-easterly direction over the Dzag zone that represents part of a passive margin to the Hangai continental block located beneath the sedimentary cover of the Hangai region (Fig. 5.1; see discussion, Chapter 4). This interpretation defines the genetic nature of each of the units (e.g. Burd Gol mélange as an accretionary complex), but it places few constraints on their pre-obduction geometry.

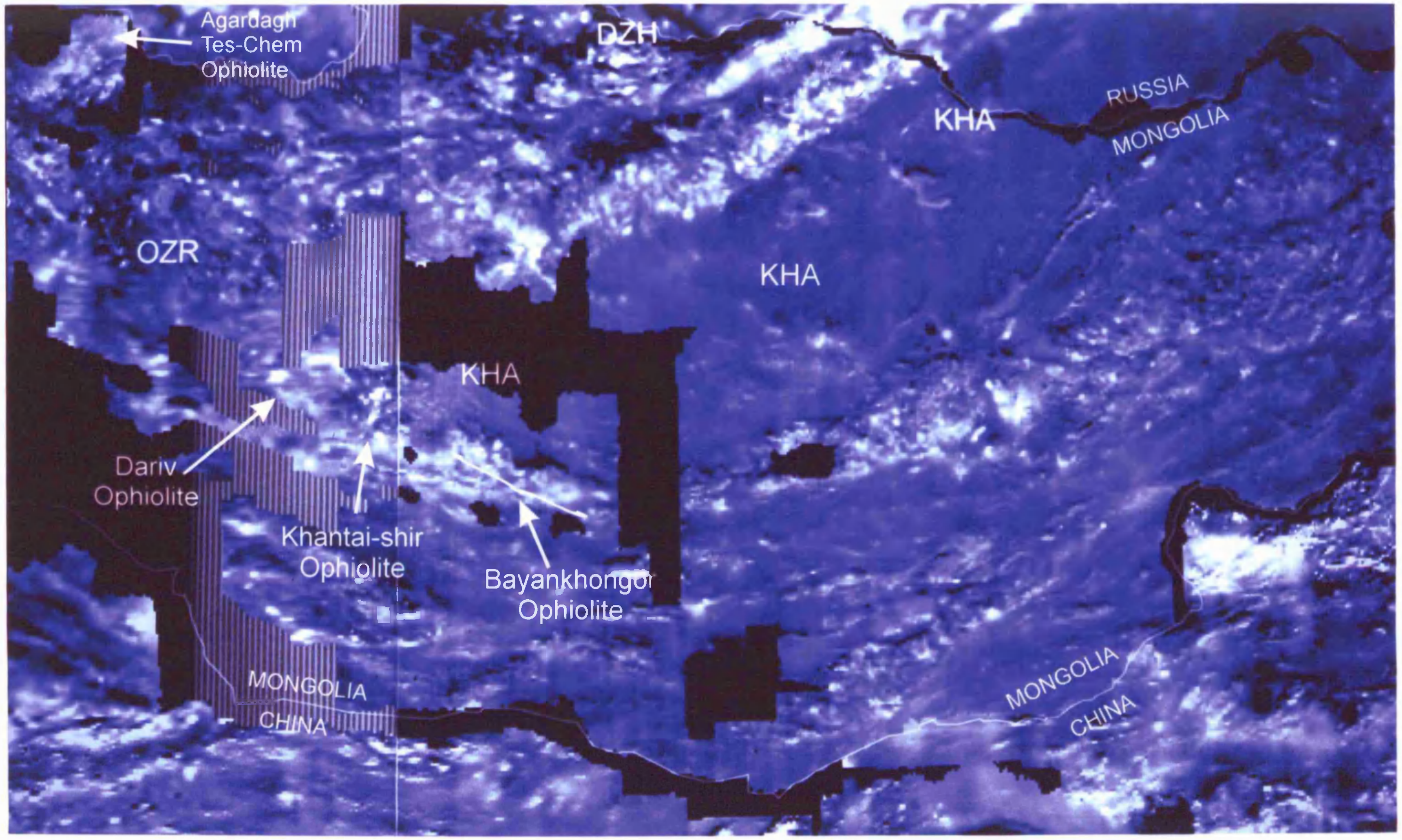

Fig. 5.1: Aeromagnetic map of central and western Mongolia (Mongolian Academy of Sciences unpublished data). Areas of highest magnetism shown in white and lowest magnetism in dark blue. Black or striped areas have no data. The magnetic data define the margins of the unexposed Hangai continental block (see discussion Chapter 4) denoted by the symbol KHA, as an area with relatively low magnetism surrounded by more magnetic bodies, which correspond largely to ophiolite belts. The positions of the Bayankhogor, Khantai-shir, Dariv,Ozernaya (OZR), Aghardagh Tes-Chem, and Dzhida (DZH) ophiolite belts are marked.

The Bayankhongor Ophiolite lies structurally below the Burd Gol accretionary complex (Fig. 5.2a). Therefore, by simple restoration of the thrust units (Fig. 5.2b), this relationship implies that the Bayankhongor oceanic crust was originally located outboard of the Burd Gol accretionary complex and thus may have formed part of the subducting oceanic slab (Fig. 5.2b). Placing the Bayankhongor Ophiolite as part of the lower plate in the subduction system is consistent with the MORB geochemistry of the ophiolitic rocks, and lack of an island arc-like 'subduction-signature' that is normally associated with ophiolites produced in a supra-subduction setting such as the Californian Coast Range (Shervais 2001), and Oman ophiolites (Searle 1999). However, many supra-subduction zone ophiolites have a mixed genetic history where parts of the ophiolite have N-MORB chemistry whilst other sections have island arc-like chemistry (Searle 1999; Shervais 2001). Such mixed chemistry is interpreted to result from formation of N-MORB oceanic crust in a 'normal' oceanic basin, followed by initiation of an intra-oceanic subduction zone which traps a piece of oceanic crust in the hanging wall of the subduction zone (Casey & Dewey 1984; Robertson & Xenophontos 1993; Searle 1999; Shervais 2001). Rapid trench roll-back caused by the sinking slab, causes the supra-subduction oceanic crust to extend rapidly resulting in decompression melting of the subduction zone mantle, producing oceanic crust with island arc-like chemistry (Wood 1980; Pearce 1982; Stern & Bloomer 1992; Shervais 2001). The Delb Khairkhan mélange (Fig. 5.2a) contains basalts that have island arc-like geochemistry and also deep ocean cherts and metaliferous sediments thought to be derived from the ophiolite cover sediments. If the Delb Khairkhan mélange does represent ocean floor sediments, then it is possible that unexposed parts of the Bayankhongor oceanic crust were created in a supra-subduction zone setting after oceanic crust was trapped in the hanging wall on initiation of a subduction zone.

It is clear from the constraints provided by field and geochemical data, that the architecture of the Bayankhongor subduction-accretion system may have been very complex. Any models for the tectonic evolution of the area must be constrained by the present geometry of the major units (Fig. 5.2a), but must also account for the MORB-like chemistry of the ophiolitic rocks, and the supra-subduction zone nature of the Delb Khairkhan mélange basalts. In the following section, three tectonic models are discussed which involve mechanisms for formation and closure of the Bayankhongor oceanic basin, which can account for all of the constraints highlighted.

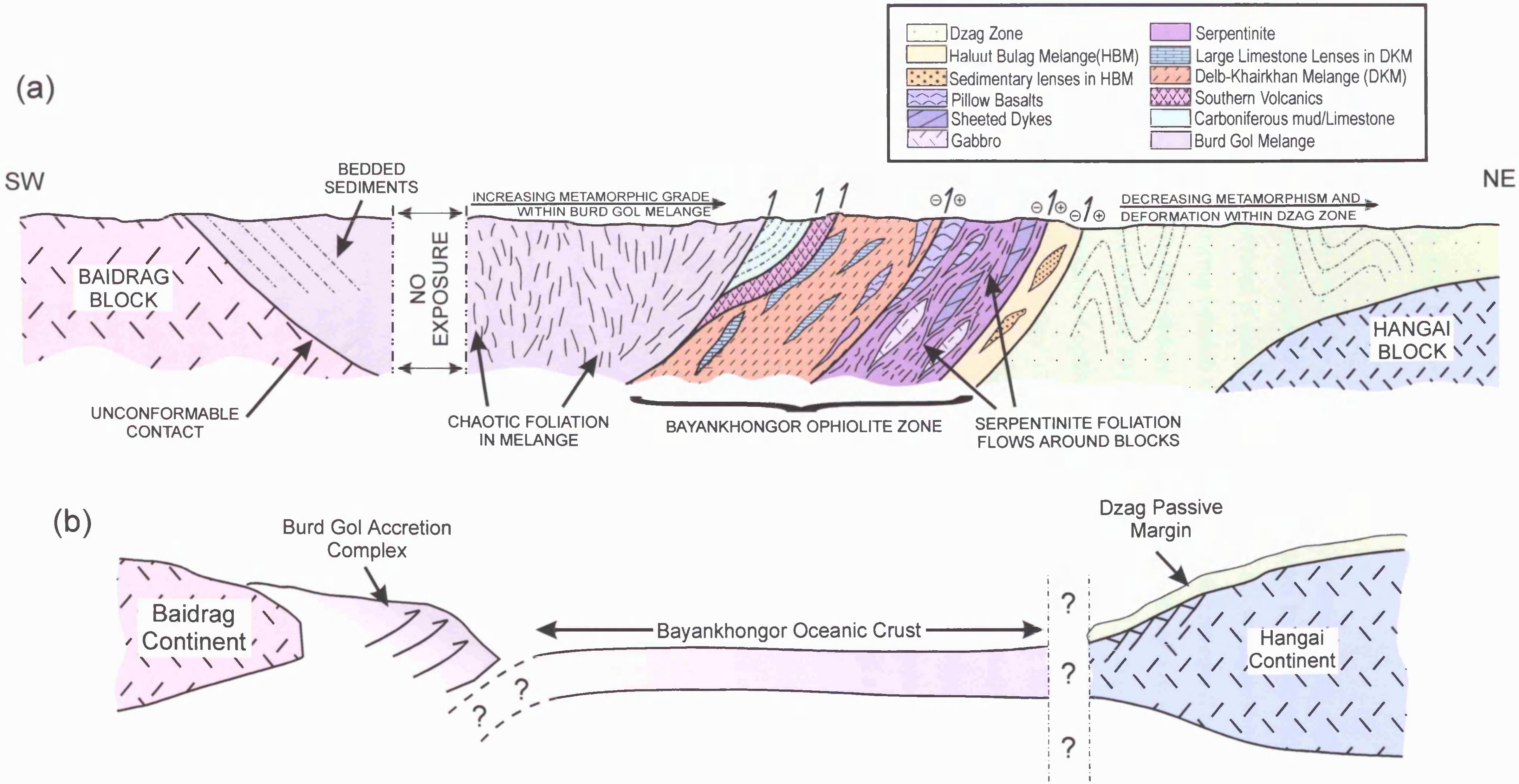

Fig. 5.2: (a) Representative cross-section through the Bayankhongor area showing general field relations of major lithotectonic units. Trace of principal fabrics are also shown. (b) Schematic restoration (not to scale) of thrust units depicting their possible pre-collision relationship based on structural and lithological characteristics of the major lithotectonic units (see Chapter 2 for discussion). It is unclear whether the Bayankhongor oceanic crust was attached to the Hangai continental block.

Tectonic models for the evolution of the Bayankhongor Ophiolite

Obduction of the Bayankhongor Ophiolite from the subducting slab

Based on the present geometry of lithotectonic units in the Bayankhongor area, the most obvious tectonic model is one involving derivation of the Bayankhongor Ophiolite from the oceanic plate subducting beneath the Baidrag continental margin (Fig. 5.2b). Transferring dense oceanic crust from the subducting plate onto the margin of a relatively buoyant continent is problematic (Moores 1982; Casey & Dewey 1984; Cloos 1993; Shervais 2001). However, many early models of ophiolite obduction considered that it would be possible to do so by means of 'flake tectonics' (Temple & Zimmerman 1969; Moores 1970; Oxburgh 1972; Ben-Avraham *et al.* 1982). The 'flake tectonics' models involve obduction of a sliver of oceanic crust onto the overriding continental margin after it is separated from the subducting plate either by occasional splitting of the plate as it bends at the subduction zone (Oxburgh 1972), or by collision of a non-subductable body such as a continental fragment or seamount with the subduction zone (Temple & Zimmerman 1969; Moores 1970; Oxburgh 1972; Ben-Avraham *et al.* 1982). Moores (1982) and Casey & Dewey (1994) considered that these models for obduction are unlikely due to the great strength of oceanic crust which means that it is unlikely that it would easily break whilst subducting or even after collision of an unsubductable body. In addition, Cloos (1993) demonstrated by mathematic modelling of subduction systems, that nearly all oceanic crust located on the subducting plate would be consumed at a subduction zone because of the greater density and relative strength of the subducting oceanic crust compared to the overriding continental margin. Cloos (1993) also suggested that even large relatively buoyant bodies such as seamounts would also be subducted fully intact, which is consistent with recent seismic reflection and bathymetric studies of the Middle America convergent margin, which have shown that seamounts and aseismic ridges are currently being subducted completely intact below the Osa Peninsula (Ranero & von Huene 2000). Moreover, it has been shown that the subduction of topographic highs such as seamounts results in erosion rather than growth of the overriding accretionary wedge (Fig. 5.3) as material is torn from the wedge by the seamount and carried deep into the subduction zone (Okamura 1990; Meschede *et al.* 1999; Ranero & von Huene 2000). Borehole studies of the Eratosthenes seamount, which is being subducted beneath the Troodos ophiolite and is partly responsible for its uplift, have interpreted the seamount as a fragment of the passive continental margin of North Africa and predicted that in time it will also be consumed (Robertson *et al.* 1996). Larger, buoyant bodies such as island-arcs are also

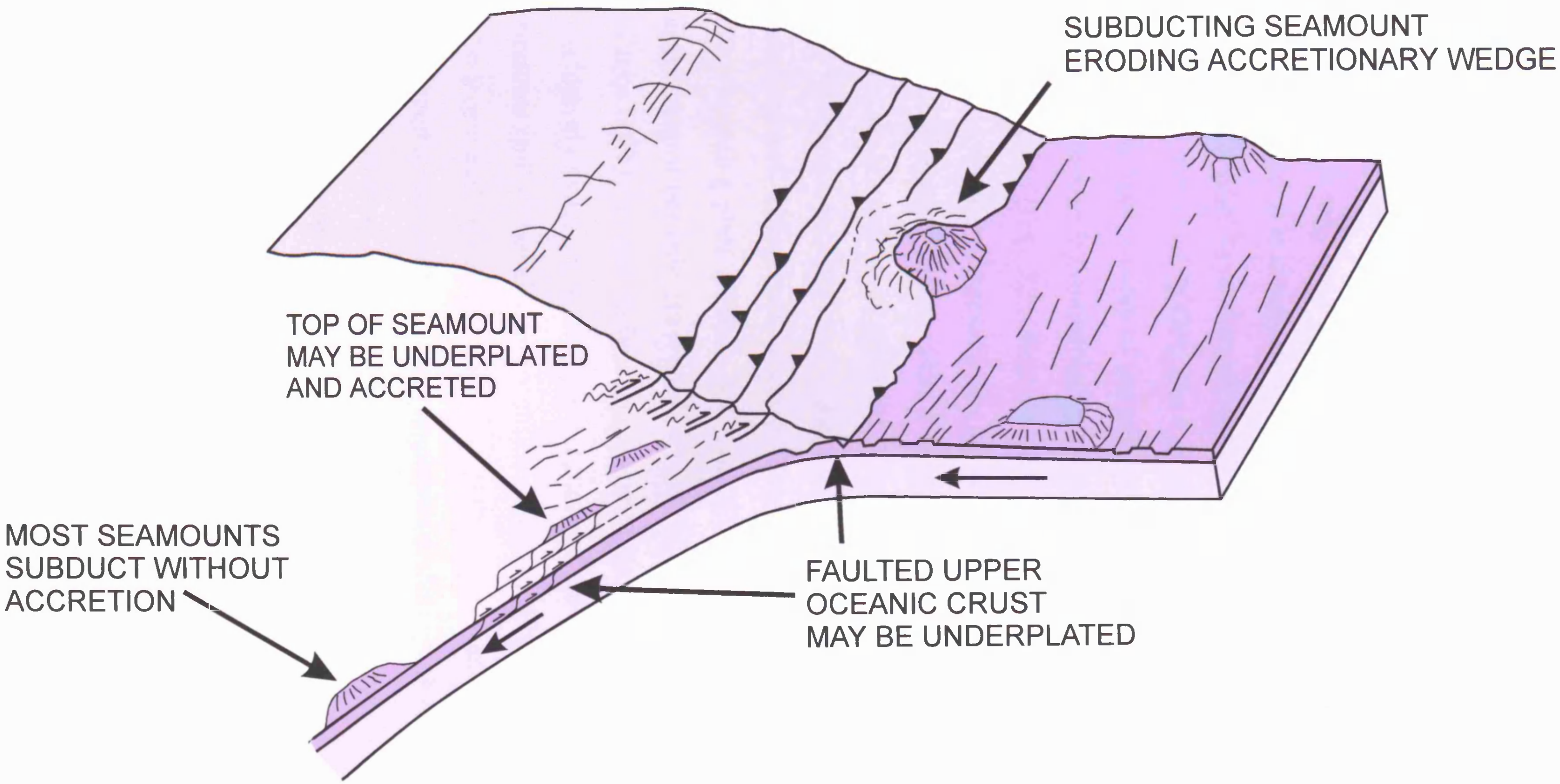

Fig. 5.3: Model for underplating of oceanic crust and seamounts from the subducting oceanic plate to the overriding accretionary wedge after Barr *et al.* (1999). Note that most seamounts are subducted completely intact and may in fact cause subduction-erosion of the accretionary complex as material is scraped from the upper plate (Cloos 1993, Ranero & von Huene 2000).

currently being consumed at subduction zones such as the Halmahera Arc in Indonesia, from which it is predicted there will be no trace that the arc ever existed (Hall & Wilson 2000). These studies demonstrate that the predictions made by Cloos (1993) appear to be correct for modern tectonic settings and thus suggest that it is unlikely that 'flake tectonics' are responsible for ophiolite obduction. Therefore, it is also unlikely that the Bayankhongor Ophiolite could have been derived from a subducting plate in this way.

Whilst it may not be possible to obduct a large slab of oceanic crust from the subducting plate, it is considered possible to accrete small sections to the overriding accretionary wedge by underplating processes (Barr *et al.* 1999; Ellis *et al.* 1999; Hashimoto *et al.* 1999; Ueda *et al.* 2000). The Cretaceous accretionary complexes along the margin of Japan contain many slivers of oceanic pillow basalts that have been incorporated within the accretionary wedge by underplating of oceanic crust to the base of the wedge from the subducting plate (Fig. 5.3; Okamura 1990; Hashimoto & Kimura 1999; Ueda *et al.* 2000). Şengör *et al.* (1993) suggested that all of the ophiolites in Central Asia represent off-scraped fragments of oceanic crust within a large accretionary wedge similar to those in Japan and therefore, do not represent ophiolitic sutures marking the position of former oceans.

The mechanism of underplating of subducted sediment to the accretionary wedge is reasonably well understood, because the sediment is relatively buoyant and so tends to stick to the overriding plate (Shreve & Cloos 1986; Moore & Byrne 1987). However, models of underplating of oceanic crust are less clear because of the same buoyancy problems outlined by Cloos (1993) for the obduction of large slabs. What is known is that the underplated crust is exclusively made up of the upper sections of the oceanic crust or uppermost levels of seamounts (pillow basalts and occasionally dykes, Fig. 5.3), and almost never contains gabbros or mantle material (Barr *et al.* 1999; Ueda *et al.* 2000). Also the basalts tend to have experienced metamorphism from amphibolite, through blueschist to eclogite facies (Barr *et al.* 1999, Ueda *et al.* 2000). Models for the underplating process involve the initiation of deep level duplex systems in the upper oceanic crust resulting in the transfer of fragments from the footwall to the hanging wall of the subduction zone (Fig. 5.3; Barr *et al.* 1999; Ueda *et al.* 2000). A corollary of these models is that the oceanic fragments are small on the scale of tens of kilometres, and that they become mixed with the accreted sediments rather than form continuous belts (Okamura 1990; Barr *et al.* 1999; Ueda *et al.* 2000). Therefore, it seems unlikely that the Bayankhongor Ophiolite could have formed by underplating because it contains a full ophiolite stratigraphy, including pyroxenites that may form part of the residual mantle section, and has a continuous strike length of at least 300 km. Thus, in addition to the evidence that the Bayankhongor Ophiolite marks the collisional suture between two continental fragments, it appears that the interpretation of Şengör *et al.* (1993) that Central Asian ophiolites represent off-scraped fragments of oceanic crust within an accretionary wedge is not correct, at least in the case of the Bayankhongor Ophiolite.

Supra-subduction zone entrapment models

The model of supra-subduction zone ophiolite formation is widely accepted as the mechanism that provides the highest potential for obduction of oceanic crust onto a continental margin to form an ophiolite, primarily because it eliminates the problem of the negative buoyancy of the oceanic crust (Searle 1999; Shervais 2001). Shervais (2001) reviewed this concept and demonstrated that the majority of the worlds ophiolites can be interpreted as having either formed completely within a supra-subduction setting, or were trapped within the hanging wall on initiation of an intra-oceanic subduction zone. In fact even the Italian Liguride ophiolites, that Shervais (2001) cited as possibly the only 'normal' ocean ophiolites, have recently been suggested to have been obducted from a supra-subduction setting (Hoogerduijn Strating 1991). Whilst the Bayankhongor ophiolitic rocks lack the geochemical 'subduction-signature' (enrichment of LILE and depletion of the HFSE: Ti, Nb, Ta, Hf) that most clearly identifies supra-subduction ophiolites, the occurrence of island arc-like rocks with ocean floor sediments in the Delb Khairkhan mélange, suggests that the ophiolite may be an example of oceanic crust that was trapped in the hanging wall of the subduction zone. Using the defined constraints for subduction zone architecture of the Bayankhongor accretionary system, there are two possible tectonic models that involve obduction of the Bayankhongor Ophiolite from a supra-subduction zone setting, and these will now be discussed.

The Burd Gol mélange: accretionary complex, or fore-arc basin?

The most common model for creation of a supra-subduction zone ophiolite is by entrapment of a piece of oceanic crust outboard of a continental block (Fig. 5.4) after initiation of an intra-oceanic subduction zone along a transform fault (Casey & Dewey 1984; Searle 1999; Shervais 2001). Subduction related magmatism produces arc volcanoes either on the trapped oceanic crust itself or on the margin of the continent, and the trapped supra-subduction oceanic crust eventually becomes the floor to a fore-arc basin (Stern & Bloomer 1992; Saleeby 1992; Godfrey & Klemperer 1998; Shervais 2001). One of the best examples of this model is that for the Coast Range ophiolite which forms the basement to the Great Valley fore-arc basin in California (Saleeby 1992; Godfrey & Klemperer 1998). The geometry of the Coast Range system is such that it clearly demonstrates the supra-subduction nature of the Coast Range ophiolite from field relations alone because the Franciscan accretionary complex lies beneath the ophiolite and is thought to be derived from accretion of sediments from an oceanic plate subducting beneath the Coast Range ophiolite (Saleeby 1992; Godfrey & Klemperer 1998; Shervais 2001). This model could be applied to the Bayankhongor Ophiolite, but requires the Burd Gol mélange to be reinterpreted as a deformed fore-arc basin rather than an accretionary complex (Fig. 5.4a). If this were the case, then the island arc-like basalts of the Delb Khairkhan mélange could have been derived either by initial spreading of the supra-subduction oceanic crust, or by basalts being shed into the fore-arc basin as olistostromes from an arc located on the Baidrag continental margin (Fig. 5.4). The Haluut Bulag mélange would represent part of an accretionary complex below the ophiolite crust similar to the Franciscan complex, which was either small or was partially under-thrust beneath the ophiolite as it was obducted onto the passive margin of the Hangai continental block. Similar under-thrusting of the accretionary wedge has been proposed for the Hawasina complex beneath the Oman ophiolite (Searle 1999). Deformation of the Burd Gol fore-arc basin on collision of the Baidrag and Hangai continental blocks may have resulted in the mélange that now forms the northern section of the unit, whilst bedded unconformable sediments are preserved in the south (Fig. 5.4). However, the relationship of the southern bedded sediments with the mélange which forms the bulk of the Burd Gol unit, is unclear due to poor exposure (Fig. 5.2). The resultant geometry of lithotectonic units after collision and obduction of the ophiolite is consistent with those observed today (Figs. 5.2 & 5.4) and so the suggested model is reasonable. However, the reinterpretation of the Burd Gol mélange is problematic because it is dominated by deep ocean sediments and graphitic schists, and also contains numerous large quartz veins (2-3 m width) that provide evidence of large-scale fluid infiltration similar to that observed in the Nankai accretion complex (Agar 1990; Maltman *et al.* 1992). In addition, the Great Valley fore-arc basin contains volcanogenic tephra and tuff horizons as would be expected if the basin was in the vicinity of an arc volcano (Saleeby 1992; Godfrey & Klemperer 1998), but these have not been observed in the Burd Gol mélange. Moreover, there is currently little evidence for an arc at all, but this may be due to the lack of detailed studies of the Burd Gol mélange and Baidrag block.

Double subduction zone model

The final model is more complex because it involves two subduction zones (Fig. 5.5), but is really a compromise between the two preceding models. In the double subduction zone model, one plate composed completely of oceanic crust is subducted to the SW beneath the Baidrag continental block (Fig. 5.5a). At the same time, the oceanward end of the subducting plate forms the hanging wall of a second subduction zone along which oceanic crust attached to the Hangai continental block is consumed (Fig. 5.5a). In this case, the future

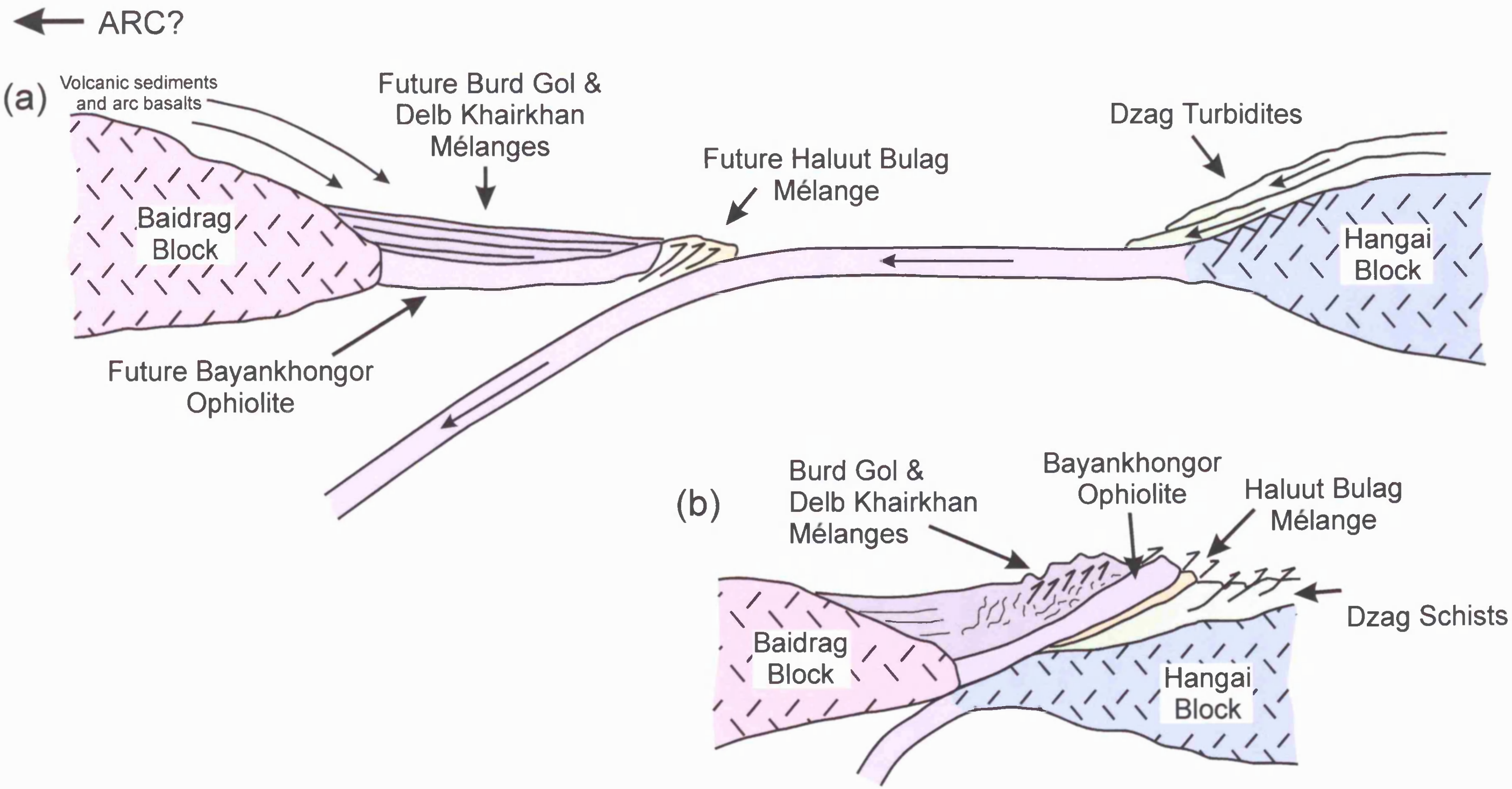

Fig. 5.4: Supra-subduction zone model for the Bayankhogor subduction accretion system. (a) The ophiolite crust is trapped in the hanging wall of the subduction zone. The Burd Gol mélange is reinterpreted to represent a fore-arc basin and the Haluut Bulag mélange represents an accretion complex forming beneath the trapped ophiolite. (b) Geometry of units after collision of the Baidrag and Hangai continental blocks. The Haluut Bulag mélange and the Bayankhongor ophiolite are obducted onto the Dzag passive margin. The Burd Gol fore-arc sediments are deformed and internally thrusted to produce the mélange structure.

Bayankhongor Ophiolite is located at the supra-subduction zone position of the oceanic plate that is being subducted beneath the Baidrag block (Fig. 5.5a), and the Burd Gol mélange is interpreted as an accretionary wedge formed by accretion of material to the margin of the Baidrag block. The basalts of the Delb Khairkhan mélange might either be generated by supra-subduction zone magmatism within the Bayankhongor Ophiolite plate, or by island arc magmatism in an arc volcano located on the margin of the Baidrag block. The Haluut Bulag mélange represents part of an accretionary complex formed structurally below the ophiolite by accretion of material to the upper plate in the second northern subduction zone (Fig. 5.5a). After a period of subduction, the oceanic crust attached to the Hangai continent is completely consumed and the Bayankhongor Ophiolite and Haluut Bulag mélange are obducted onto the Dzag passive margin (Fig. 5.5b). At the same time, subduction of the Bayankhongor Ophiolite plate continues beneath the Baidrag block and as a result the Hangai block and Bayankhongor Ophiolite move together towards the subduction zone (Fig. 5.5b). When the Hangai block reaches the subduction zone at the margin of the Baidrag block, the two continental blocks collide and the Burd Gol and Delb Khairkhan mélanges are thrust on top of the Bayankhongor Ophiolite and Dzag passive margin (Fig. 5.5c). The resultant geometry is the same as the previous model (Fig. 5.5c), but in this case there is no requirement to reinterpret the Burd Gol mélange as a fore-arc basin.

Whilst this is a complex situation, modern examples of double subduction systems do exist and one of the best examples is the Philippine sea plate which is currently being subducted westward along the Philippine, Manila, and Ryukyu trenches, but at the same time forms the upper plate at its eastern margin along the Mariana trench (Lee & Lawver 1995; Hall *et al.* 1995). In addition a very similar double subduction model, was proposed by Corfield *et al.* (1999) and Robertson (2000) to explain the occurrence of accretionary mélanges structurally above and below the Spontang ophiolite in the Indus suture of the Ladakh Himalaya. The double subduction model, despite its complexity, is consistent with the current geometry of lithotectonic units in the Bayankhongor area and accounts for the apparent paradox in geochemical signatures of the ophiolitic rocks and basalts from the Delb Khairkhan mélange. In addition, it removes the problem of obducting oceanic crust from the subducting oceanic plate by placing one end of that plate in a supra-subduction setting itself. Therefore, the double subduction model satisfies all the criteria for a satisfactory tectonic model for the evolution of the Bayankhongor Ophiolite and is interpreted to be the most consistent model for the data presented in this study.

Supra-subduction zone settings and ophiolitic serpentinite mélanges

Many ophiolites are preserved as serpentinite mélanges similar to that of the Bayankhongor Ophiolite and the mechanism for their generation is unclear (Saleeby 1984; Robertson 2000). Saleeby (1984) suggested that the ophiolitic mélanges were formed on the ocean floor along transform faults where hydration of the mantle lithosphere resulted in upwelling of serpentinite along fractures within the transform zone with the result being a mixture of serpentinite and blocks of coherent oceanic crust. Saleeby (1984) further suggested that these transform fault mélanges might be accreted to the toe of an accretionary wedge due to their relative buoyancy compared to the subducting oceanic plate, or that they might be preserved when a new subduction zone formed along a transform fault similar to serpentinites found in dredges along the Marianas trench. It is difficult to imagine that mélanges incorporated into an accretionary wedge could be preserved as a continuous linear belt such as the Bayankhongor Ophiolite, and the serpentinites dredged along the Marianas trench have been shown to be derived from serpentinite diapirs that form seamount like structures in the Marianas fore-arc (Fryer *et al.* 1985; Keen *et al.* 1989). Therefore it is unlikely that serpentinite mélanges created in an ocean basin prior to subduction would be preserved. However, Saleeby (1984) may not have been completely wrong, instead his model might be more consistent with a supra-subduction setting.

Oblique or transpressional subduction is a common feature of modern convergent margins (e.g. the Ryukyu trench, Lallemand *et al.* 1999). In oblique subduction settings, trench-parallel strike-slip faults are common and cause lateral translation of parts of the accretionary complex and the associated fore-arc crust (McCaffrey 1992; Lallemand *et al.* 1999; Mazzotti *et al.* 1999). In a situation where the fore-arc is floored by oceanic crust, the influence of transpressional deformation may either result in the initiation of new strike-slip faults within the oceanic crust, or more likely, reactivation of existing transform faults and fracture zones in the oceanic crust and hence generation of serpentinite mélanges. In addition to such faulting, serpentinite diapirs similar to those in the Marianas fore-arc, could form in response to hydration of mantle peridotites in the fore-arc oceanic crust by fluids released by dehydration of the subducting slab (Fryer *et al.* 1985; Keen *et al.* 1989). Serpentinite diapirism would effectively reduce the strength of the fore-arc crust making it more susceptible to faulting and hence formation of ophiolitic serpentinite melanges. The resulting melanges would be obducted onto a continental passive margin with the rest of the fore-arc crust and be preserved as an ophiolitic mélange.

The Bayankhongor mélange may have formed in this way because sinistral strike slip faulting is documented in the ophiolite mélange and the neighbouring Delb Khairkhan and Haluut Bulag mélanges. Extensive serpentinisation of the mantle peridotite section of the

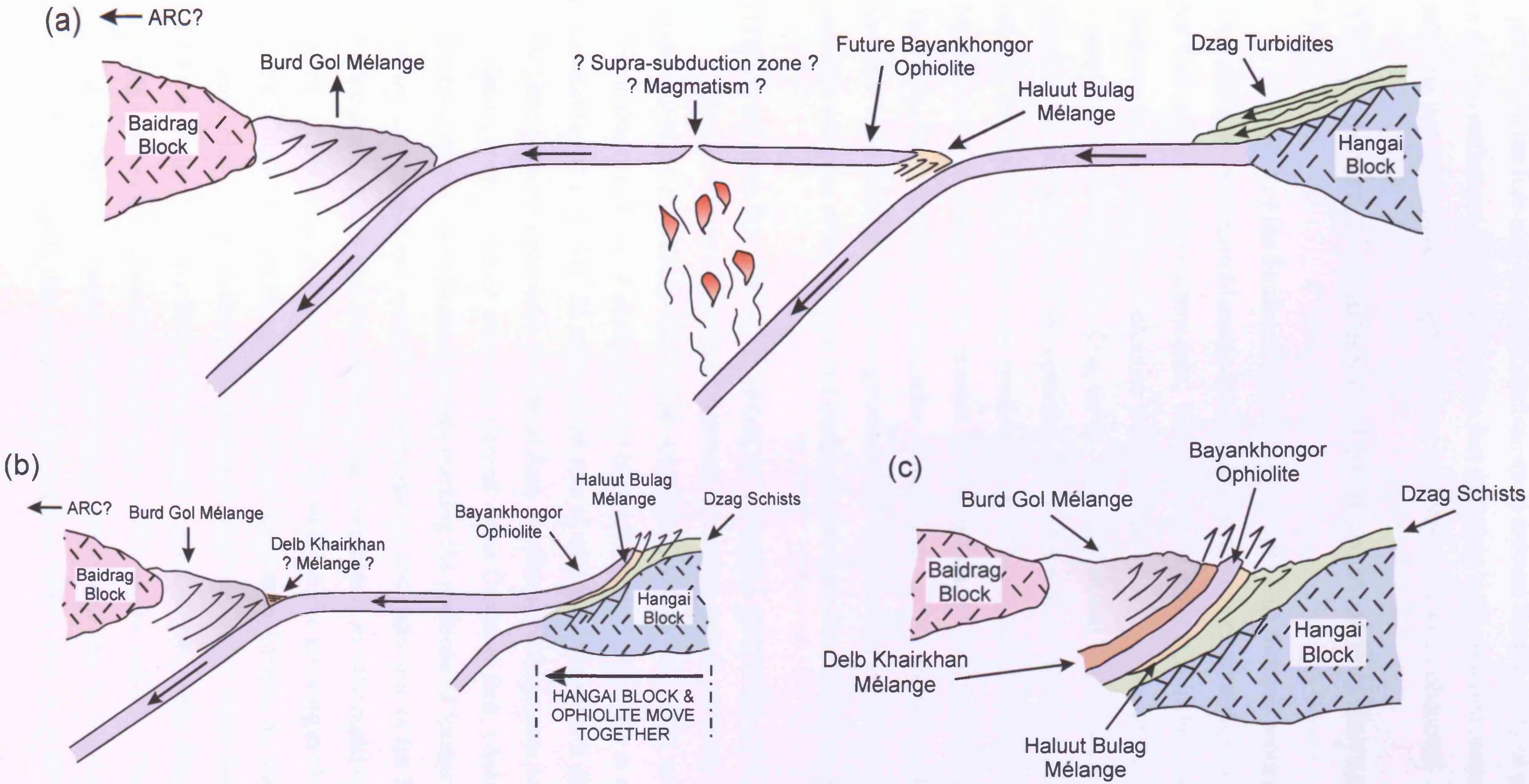

Fig 5.5: Double subduction zone model for the tectonic evolution of the Bayankhongor ophiolite zone. (a) A plate composed entirely of oceanic crust subducts beneath the Baidrag continental block and the Burd Gol mélange is created by accretion of sediments from the subducting slab. The future Bayankhongor ophiolite is located at the oceanward end of the plate which itself lies in the hangin wall of a second subduction zone, where oceanic crust attached to the Hangai continent is being consumed. (b) The Bayankhongor ophiolite is obducted onto the Dzag passive margin after all of the oceanic crust attached to the Hangai continent is consumed. The Hangai continental block then mves together with the subducting oceanic plate towards the margin of the Baidrag block. (c) The Hangai and Baidrag blocks collide and the Burd Gol and Delb Khairkhan mélanges are thrust over the ophiolite and passive margin.

ophiolite in the fore-arc, is a good mechanism to account for the rarity of preserved peridotites in the Bayankhongor Ophiolite, and the fact that there is no apparent metamorphic sole suggests that the base of the ophiolite was relatively cold when obducted.

The Southern Volcanics and evolution of the Bayankhongor Ophiolite

Inclusion of the Southern Volcanics in evolutionary tectonic models for the Bayankhongor area is problematic because their structural relationship with the other units is not well constrained by current data. However, there is strong geochemical and isotopic evidence that the Southern Volcanics were formed in conjunction with the rhyolite dykes that crosscut them (see discussion, Chapter 4). This implies that the volcanic rocks were generated after obduction of the ophiolite and collision of the Baidrag and Hangai continents, because the rhyolites dykes were created at *c.* 474 Ma whereas the ophiolite was emplaced *c.* 540 Ma based on the age of the granites that intrude the ophiolite and Burd Gol mélange. Therefore, the best model for derivation of the island arc-like chemistry of the Southern Volcanic rocks remains that of magmatism after delamination of the remains of a subducted slab after collision of the Hangai and Baidrag continents (See discussion, Chapter 4).

Implications for the Palaeozoic crustal growth of Central Asia

The mechanism of continental growth of Central Asia is currently debated between models invoking continuous subduction-accretion (Şengör *et al.* 1993), or punctuated accretion due to closure of multiple ocean basins (Coleman 1989; Hsü *et al* 1991; Mossakovsky *et al.* 1994). In terms of the role of ophiolites the models differ in that the former interprets the ophiolites of Central Asia as offscraped fragments within a massive accretionary complex which forms the Central Asian Orogenic Belt, whereas the latter interprets ophiolites as collisional sutures marking the positions of former oceanic basins. The discussion of tectonic models for the evolution and obduction of the Bayankhongor Ophiolite demonstrates that it is unlikely that it represents an offscraped fragment incorporated into an accretionary complex. In addition, the growing evidence for a continental block beneath Hangai (Fig. 5.1; see discussion, Chapter 4), and the Baidrag continental block suggests that discrete ocean basins may have existed during the history of the Central Asian Orogenic Belt and as a result, continual subduction along one major subduction zone as suggested by Şengör *et al.* (1993) seems unlikely. The data presented in this study are more consistent with a crustal growth mechanism for the Central Asian Orogenic Belt similar to that suggested by Coleman (1989), Hsü *et al* (1991), and

Mossakovsky *et al.* (1994) which involved subduction-accretion with punctuated collisions due to closure of multiple oceanic basins.

Scope for future research

Whilst it is not possible to present a unique tectonic model for the evolution of the Bayankhongor Ophiolite at this stage, the new data provide a significant step forwards in understanding the geology of the ophiolite zone, and a firm basis from which future studies can build. Particular problems that have become apparent from this study are as follows:

1. The lack of evidence for the existence of a magmatic arc despite the discovery of basalts with island arc-like chemistry in the Delb Khairkhan mélange.
2. Whether the Burd Gol mélange definitely represents an accretionary complex as suggested by this study, or could be a deformed fore-arc basin.
3. Confirmation of the relationship of the Burd Gol mélange with the Baidrag continental block.
4. The mechanism for post-collisional generation of the Southern Volcanic rocks.
5. More definitive evidence for, or against the interpretation that the Bayankhongor Ophiolite was obducted from a supra-subduction zone setting.
6. Structural evolution of the Dzag belt and Hangai margin.
7. Along strike continuity of the suture all the way to Tuva and also to the east.

Problems 1-3, may be solved by more detailed geological mapping of the Burd Gol mélange and Baidrag block as the present study only examined these units during reconnaissance studies and previously published maps contain no detailed structural or lithological data. The mechanism by which the Southern Volcanic rocks were produced requires more detailed structural mapping in order to better constrain their relationship with the Bayankhongor Ophiolite zone and Burd Gol mélange, but would also benefit from detailed geochemical and isotopic studies in order to build on the initial data presented in this study. Whether the Bayankhongor Ophiolite was ever in a supra-subduction setting would be most effectively answered by sedimentilogical studies of the sediments contained within the Delb Khairkhan mélange in order to test whether there are any volcanogenic sediments, and whether the metaliferous sediments and cherts from the mélange were derived from the ophiolite cover. However, the most pressing and perhaps most exciting problem for future workers is the relationship of ophiolites in Western Mongolia and southern Tuva that all appear to have formed *c.* 570 Ma and been obducted *c.* 540 Ma. This question will only be answered by comprehensive studies of the tectonic evolution of the other ophiolites in order to compare their generation with that suggested here for the Bayankhongor Ophiolite. But whatever the outcome of such studies, it is clear that ophiolites played an important role in the Palaeozoic crustal growth of Mongolia, and are critical to understanding mechanisms of crustal growth in Central Asia.

Appendix A

Additional photographic plates illustrating characteristic lithologies and features of the major lithotectonic units described in Chapter 2

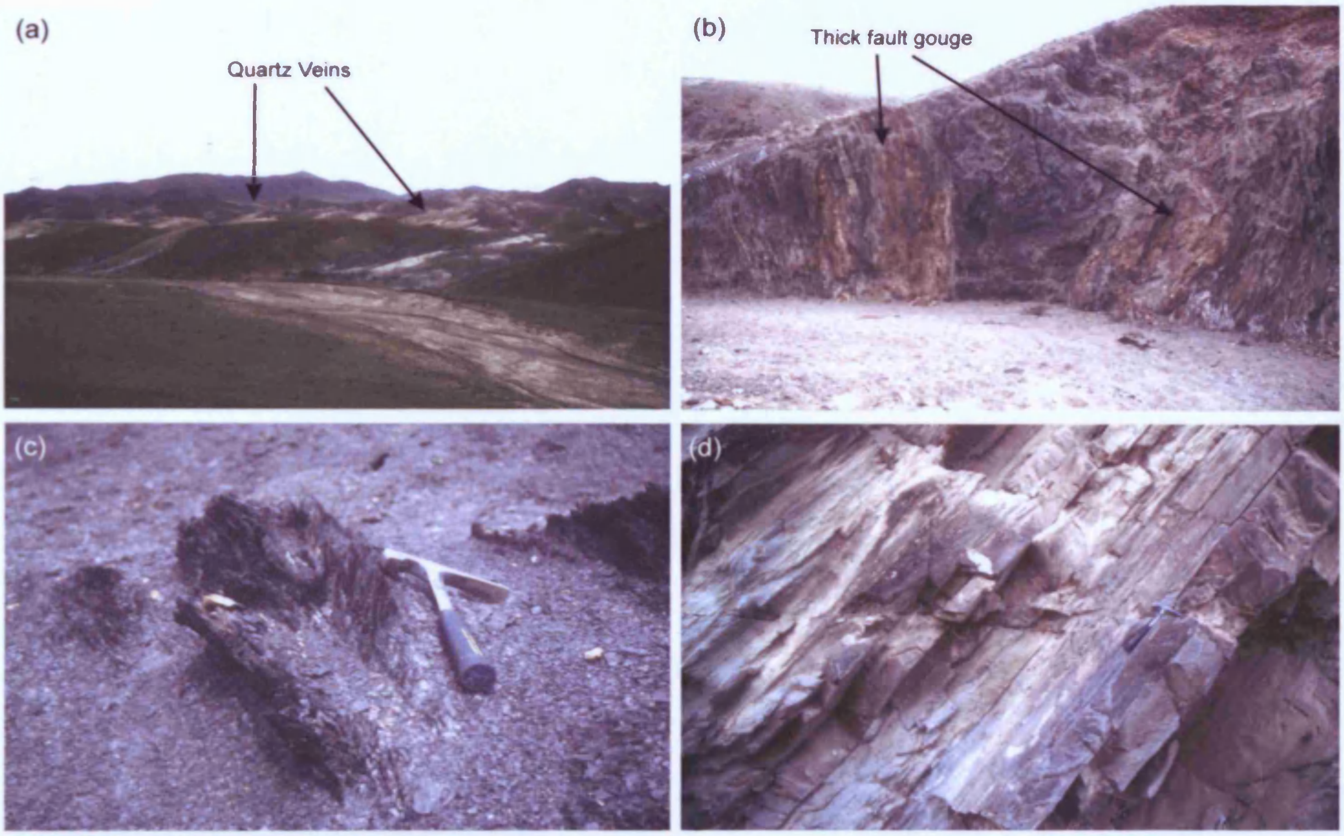

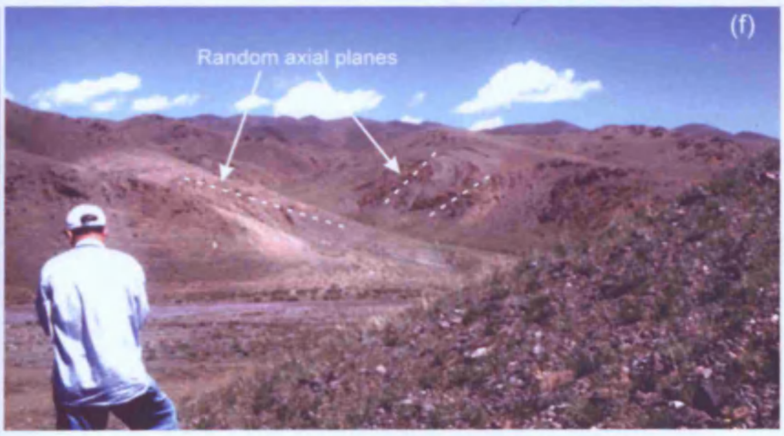

Plate A1: Representative features of the Burd Gol mélange. (a) Large quartz veins (2-3 m wide) cross-cutting black-graphite schist mélange matrix. (b) Steep foliation within brittle fault zone with wide (3-4 m) yellow fault gouge zones. (c) Close up of graphite schist outcrop. Graphite schists are very soft and fissile and therefore, are eroded easily into low rounded hills (see a). (d) Well preserved turbidites within mélange block. (E) Close up of well preserved calc-turbidites from Fig. 2.6g. (f) Blocks of folded siltstone within pelitic matrix. Displacements between individual blocks have resulted in a mismatch of the orientation of axial planes of folds.

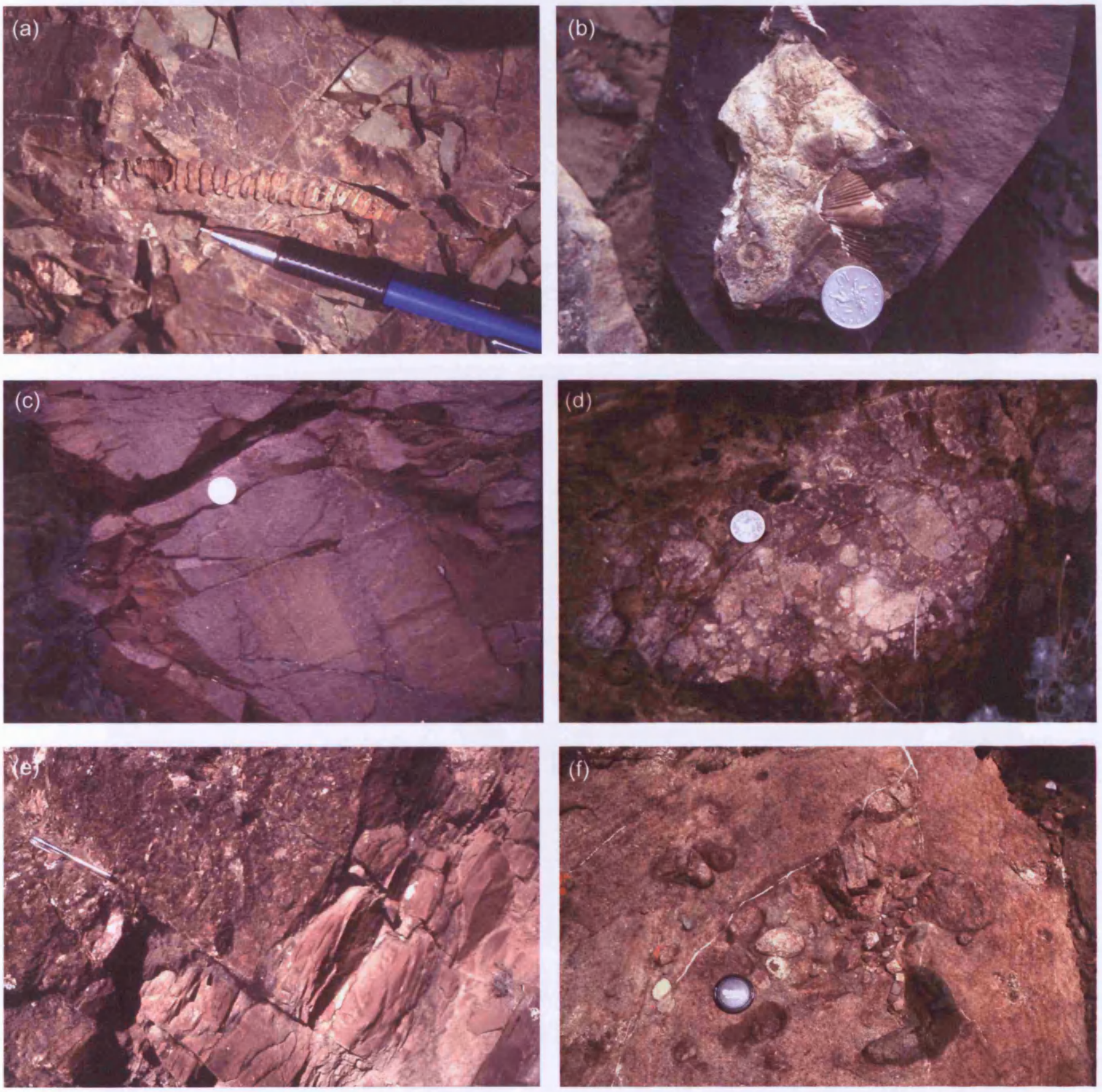

Plate A2: Representative lithologies from the Carboniferous sediments and Southern Volcanics. (a) Section through a Carboniferous crinoid within green marine mudstone. (b) Carboniferous brachiopods, crinoids, and shell fragments within green marine mudstone. (c) Dacite flow, red colouration is due to iron alteration. (d) Volcanic breccia. (e) & (f) Volcanogenic sandstone and conglomerate.

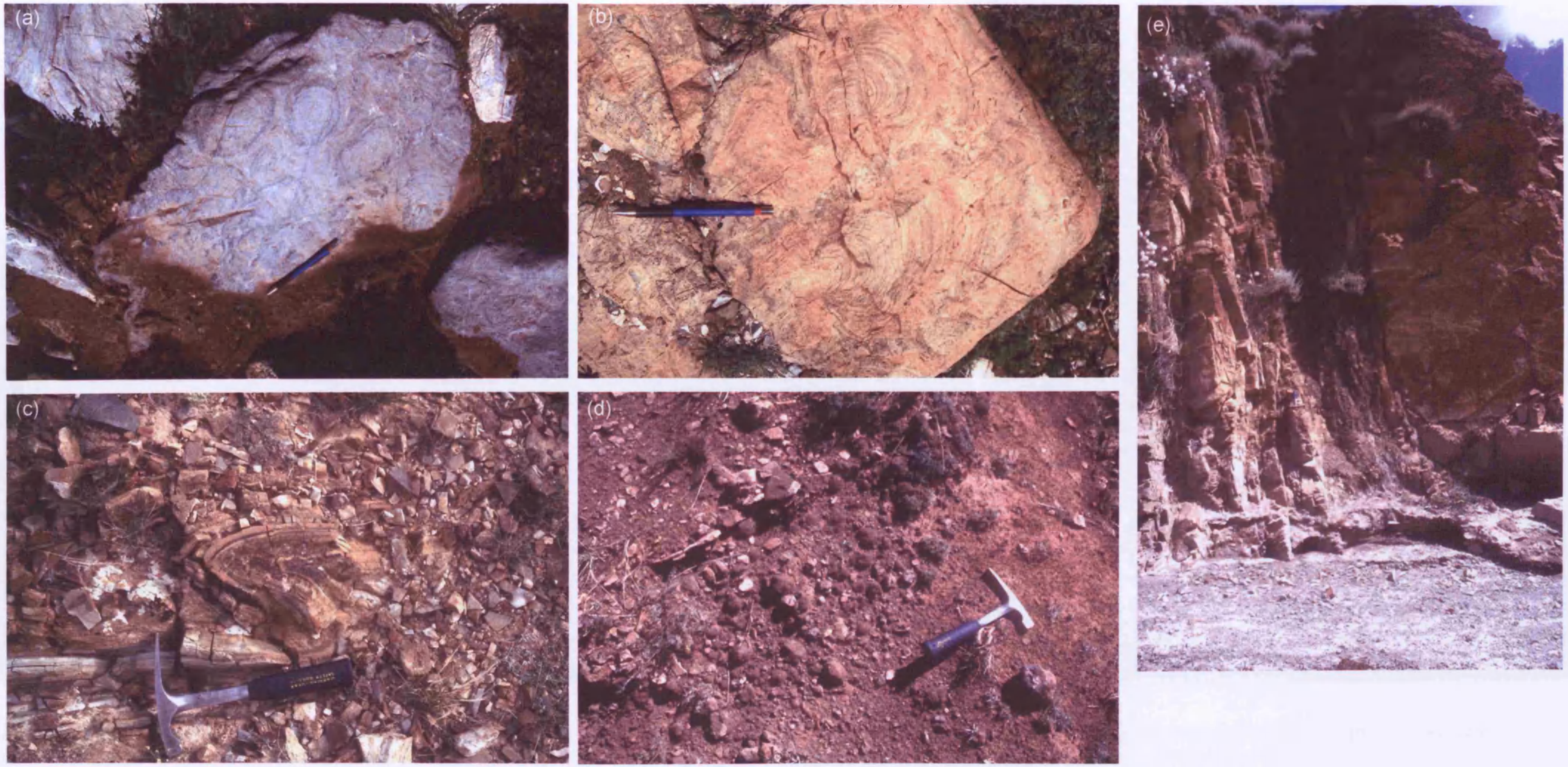

Plate A3: Representative lithologies and features from the Delb Khairkhan mélange. (a) & (b) Stromatolitic limestone which forms prominent ridge in study area (see Figs. 2.3-2.5). (C) Folded mudstones, asymmetry of fold indicates sinistral sense of shear. Looking NE horizontal surface. (d) Iron nodules within iron rich sedmient, probably derived from ocean floor black-smoker-type mineralisation. (e) Near vertical fabric within fault zone in Delb Khairkhan mélange pelitic matrix. Dark zone in centre of field of view contains fault gouge..

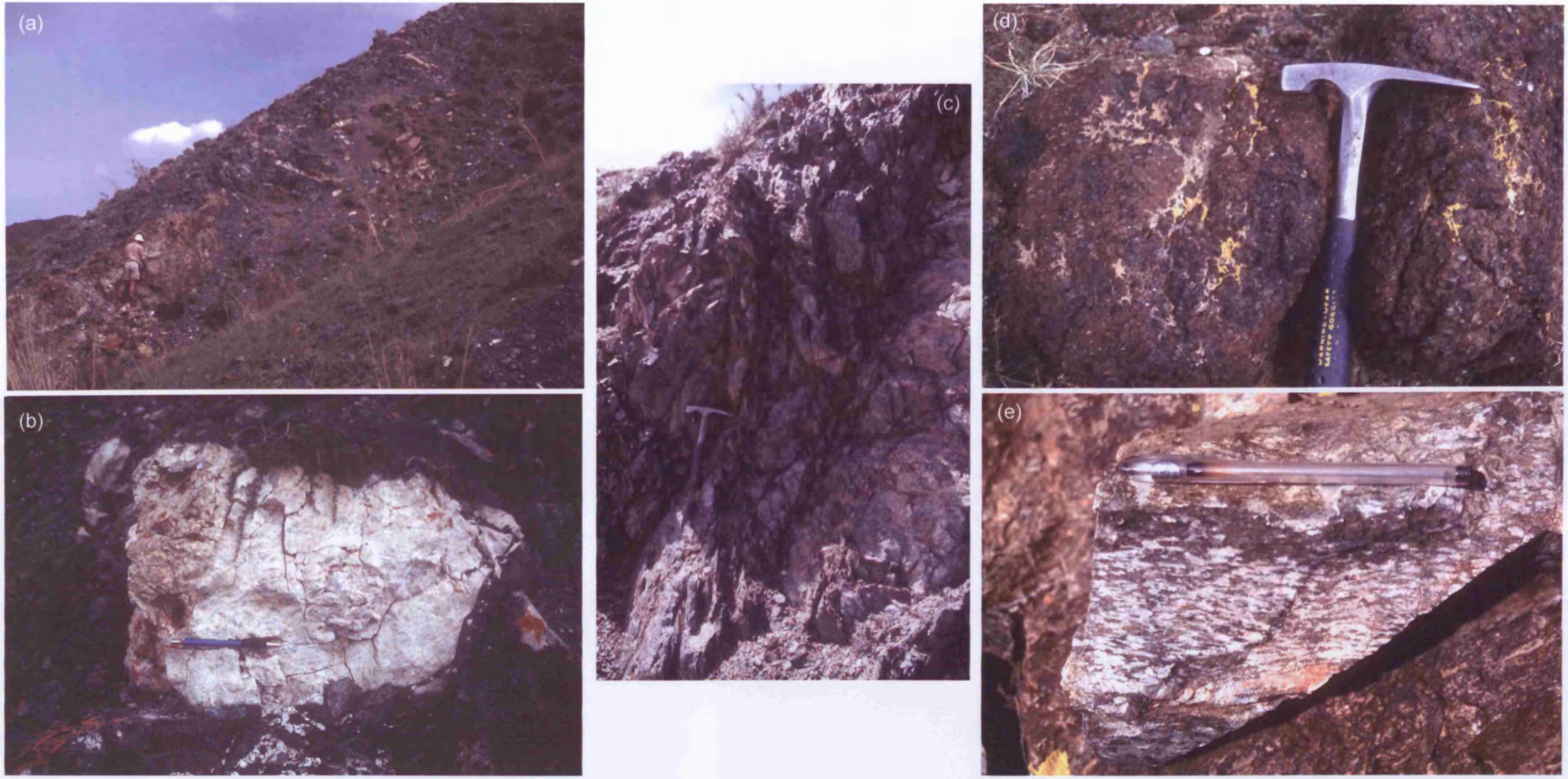

Plate A4: The serpentinite matrix of the ophiolite mélange and the cumulate section of the ophiolite. (a) Typical outcrop of serpentinite crosscut by rhodimgitised gabbro and doleritw dykes. Person in bottom left of view is examining a large ophicalcite block. (b) Close up of rhodingitised gabbro. (c) Close up of flaky serpentinite shear fabric. (d) Close up of fresh pyroxenite. (e) Foliated gabbro. Some of the foliation appears deformed either by flow of liquid or by post-crystallisation ductile shearing.

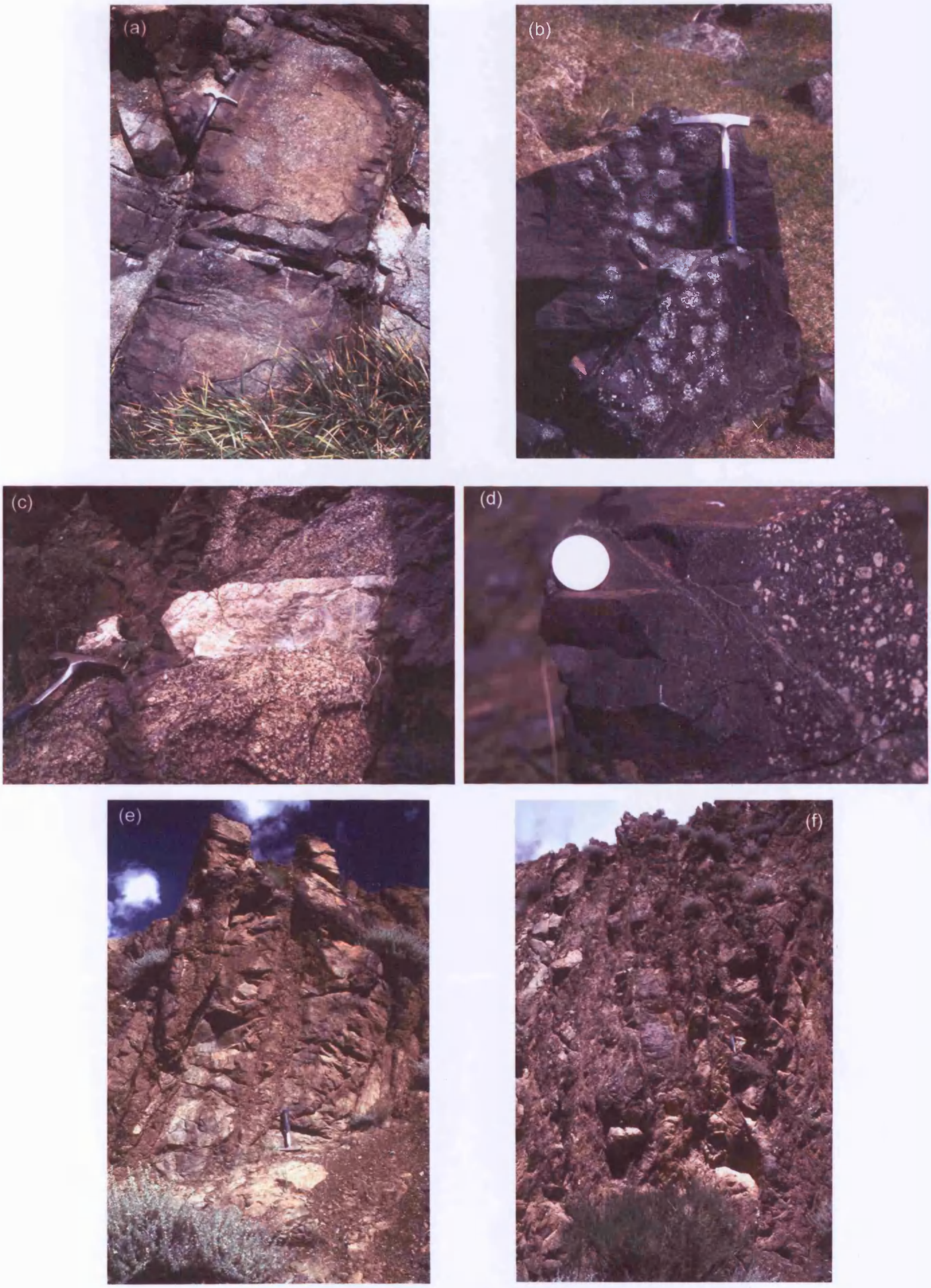

Plate A5: Sheeted dyke complex. (a) Close up of porphyritic sheeted dyke. (b) Aphyric dyke containing resorbed plagiophyric xenoliths. (c) Gabbro screen between dykes with plagiogranite dyke. (d) Porphyritic dyke with clinopyroxene phenocrysts. (e) & (f) Sheared dykes within sheeted dyke complex, shear-sense indicators often indicate normal faulting suggesting that these may be associated with ocean floor extension.

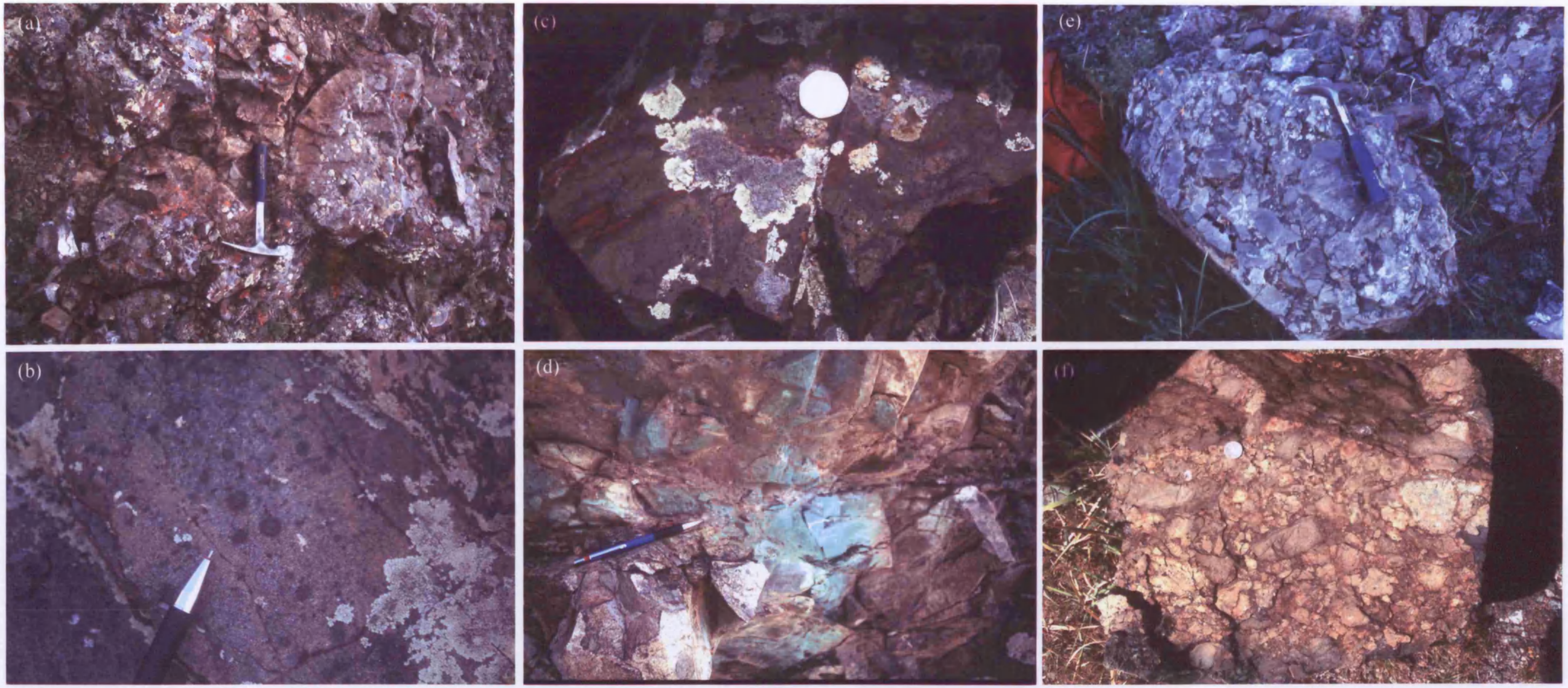

Plate A6: Pillow Basalts. (a) Close up of typical porphyritic pillow outcrop, plagioclase phenocrysts are visible in the pillow to the right of the view. (b) Vesicular pillow basalt. (c) Pillow with crosscutting jasper veins. (d) Malachite mineralisation on fault surface associated with reticulate vein networks. (e) & (f) Pillow breccia, brown colouration in (f) is caused by surface weathering

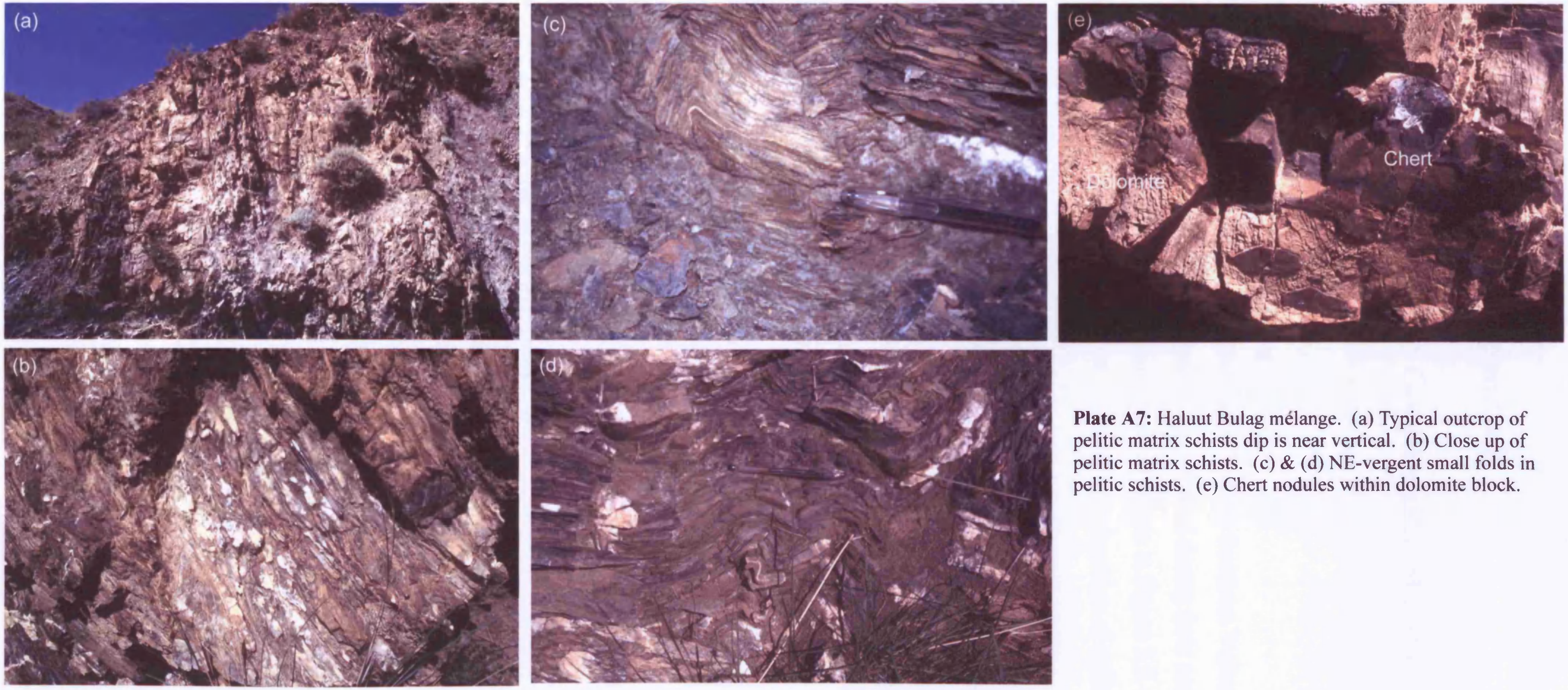

Plate A7: Haluut Bulag mélange. (a) Typical outcrop of pelitic matrix schists dip is near vertical. (b) Close up of pelitic matrix schists. (c) & (d) NE-vergent small folds in pelitic schists. (e) Chert nodules within dolomite block.

Appendix B

Analytical Procedures and Geochemical Standards Data

Sampling procedure and processing

Samples were chosen from the ophiolitic rocks and the Southern Volcanics in order to cover the whole compositional and lithological range observed during field mapping. Samples were collected from each of three transect areas shown in Figure 3.2. In addition, ophiolitic samples were collected during reconnaissance investigations of ophiolite exposures along-strike as far as Bayankhongor City (Fig. 3.1). For information on the Lat./Long. co-ordinates of each sample locality and the data available for individual samples refer to Appendix C. Outcrops affected by vein networks or highly altered regions were avoided. To ensure the freshest possible samples were analysed, weathered and altered surfaces of samples were carefully removed by hand before rocks were crushed using a fly-press (to allow further elimination of altered sections within samples) and powdered using an agate Tema® Mill (Grinding time approximately 15 minutes per sample).

Major and trace element analysis

Major and trace elements (Tables 3.1 & 3.2) were analysed by XRF at the University of Leicester. Major elements were determined using fused glass beads made from 'ignited' sample powders. The sample powders are ignited in order to determine loss of mass on ignition (LOI), which provides an estimate of volatile content of the samples. LOI determination was carried out using the following procedures: small aliquots (~ 5 g) of sample powder were dried over night in an oven at approx. 120 °C, a known amount of sample was then weighed into a ceramic crucible (also of known weight) and placed into a muffle furnace at 950 °C for 1½ hours (the furnace door was opened during this period to prevent the build up of gases that could prevent full volatile loss), the samples were then cooled in a dessicator and re-weighed to determine the percentage of weight loss on ignition;

$$\mathrm{LOI} = 100 \times \left[\frac{(\text{crucible} + \text{sample})_{\text{before}} - (\text{crucible} + \text{sample})_{\text{after}}}{(\text{crucible} + \text{sample})_{\text{before}} - \text{crucible}} \right].$$

To make glass fusion beads, 0.8000g of ignited sample powder was thoroughly mixed with 4.0000g of tetraborate-metaborate flux (corrected for LOI of flux determined daily) in a platinum crucible. The sample/flux mixture was then heated to approximately 1200 °C for 15 minutes using a burner, and the crucible was periodically shaken in order to ensure total homogenisation and melting took place. The molten mixture was then cast into a glass bead using a platinum casting plate heated to approximately 1100 °C, and then cooled using air jets before being ejected into a ceramic dish and left to cool further to room temperature.

Trace elements were determined using pressed powder pellets made by mixing ~ 7g of dry sample powder (not ignited) with 8 – 15 drops of Moviol 88 binding agent. The mixture was placed into an electrical hydraulic piston press and a force of 10 tons was applied. The pressed pellets were then removed and dried at room temperature overnight.

XRF machine conditions

Samples were analysed for major and selected trace elements (see Tables 3.1a-c, 3.2, and 4.2) in the University of Leicester Geology Department on either a Philips PW1400 or an ARL 8420+ wavelength-dispersive XRF spectrometer. The X-ray source was a 3 kW Rh tube. Details of the programme parameters used for trace element measurement are listed in Table B1, and for major elements in Table B2. Only major element totals between 98.5-101.5% were accepted. For major elements the typical lower limit of detection (LLD) is 0.01% and precision is better than 0.5% at 100 times LLD. XRF major and trace element reproducibility for international reference materials is shown in Table B3 and is on average within 5%.

REE measurement

Analysis of REE was carried out on a selection of samples using inductively coupled plasma optical emission spectrometry (ICP-OES) at the University of Leicester Geology Department.

Sample preparation

Samples preparation was carried out using microwave digestion for most samples or by fusion digestion if the samples contained relatively high concentrations of refractory accessory minerals such as zircons (e.g. in the granite samples used for geochronology), in order to ensure samples are completely dissolved.

Microwave digestion

0.3g aliquots of sample powder, are weighed into clean CEM digestion vessels and moistened with a few drops of de-ionised water. 10 ml of 48% HF and 4 ml 16M HNO3 is then added. Rupture membranes are installed in the vent fittings, which are then screwed on to the vessel caps. For each batch of samples, one vessel should have a cap which is attached to the pressure sensing line, to monitor the pressure inside the vessels. Eight samples at a time are placed in a carousel within the CEM MDS-2000 microwave sample preparation system. The fan speed set is to 60% and the pressure inside the vessels ramped to 80 psi over a 20 min period with the microwave power at 100%. Once the pressure has reached 80 psi it is held at that level for a further 60 min, with the power again at 100%. The samples are then allowed to cool before removal from the microwave cavity. Remaining vapours are vented by hand in a fume cupboard, and the resultant solutions transferred to 50 ml PTFE beakers. The PTFE beakers are then placed on a hot plate at c. 200 °C and the samples evaporated to incipient dryness. A further 4 ml of 16M HNO3 is added to each sample, to ensure the complete removal of excess fluoride ions, and the solutions evaporated to complete dryness. The remaining precipitate is then dissolved in 1.7M HCl with gentle heating until a clear solution is obtained. The samples are now ready for the separation stage.

Fusion Digestion

Aliquots of 0.2 g of sample powder are weighed into clean platinum crucibles, followed by 0.3g of lithium metaborate flux. The crucibles are placed on to a Spartan gas burner and fused at a temperature of c. 1200 °C for 15 minutes, until the liquid is satisfactorily homogenised. The hot melts are quenched, by immersing the bottom of the crucibles into a beaker of cold water, and the cool glasses transferred to clean, 50 ml PTFE beakers. 15 ml of 48% HF and 4 ml of 16M HNO_3 is then added to the beakers, which are placed on a hot plate at c. 200 °C, removing B by volatilisation. The solutions are evaporated to incipient dryness. A further 4 ml of 16M HNO_3 is then added to each beaker and the samples evaporated on the hot plate to complete dryness. The resultant precipitate is dissolved in 30 ml of 1.7M HCl with gentle heating until a clear solution is observed. The samples are now ready for the separation stage.

REE separation

Quartz glass columns of 180 mm length and 8 mm internal diameter are used. The columns have a 100 ml reservoir at the top and a plug of quartz glass wool, to act as a sinter, at the bottom. 5g of resin (Dowex AG 50W-8X, 200-400 mesh) is loaded on to the columns in 1.7M HCl and settled at a height of 130 mm. The resin is washed with 50 ml of 6M HCl, followed by 50 ml of de-ionised water and the pH adjusted to match that of the sample solutions with 50 ml of 1.7M HCl. The samples are loaded on to the columns in 30 ml of 1.7M HCl. All the major constituents, including Ca and Fe which are potential spectral interference in the ICP-OES, and most of the trace elements in the solution are then eluted, by washing the resin with a further 100 ml of 1.7M HCl. This fraction is discarded. The REE, which are quantitatively held on the resin, are then eluted by washing with 80 ml of 6M HCl. This fraction is collected in 100 ml Pyrex beakers and evaporated to dryness on a sand bath at c. 110 °C. The samples are converted to nitrates by the addition of 4 ml of 16M HNO_3 and then re-dissolved in 3 ml of 5% HNO_3 and stored in polypropylene tubes prior to analysis. After use, the columns are cleaned in the same way as before their first use and can then be re-used for the next batch of samples.

ICP-OES analysis

Analysis was carried out at the University of Leicester using a Philips PV 8060 ICP-OES and simultaneous spectrometer. The sample solution is carried in an aerosol in argon to the centre of the plasma flame where it reaches a temperature of about 8000 K. At this extreme temperature atomisation of the analyte solution occurs. The basis for all emission spectrometry is that atoms or ions in an energised state will spontaneously revert to a lower energy state and emit a photon of light energy, at a characteristic wavelength, as they do. For quantitative analysis it is assumed that the intensity of light emitted is proportional to the concentration of the element in solution. The light emitted by the atoms of the elements in the ICP is focused into a spectrometer where a diffraction grating resolves the light into its component wavelengths. The intensity of light emitted at each given wavelength is then converted to an electrical signal by photomultiplier tubes located at specific wavelengths for each element line. Using calibration lines which relate elemental concentration with intensity of light emitted, the electrical signal is converted into a concentration measurement. The results of ICP-OES analysis are listed in several tables throughout the text, refer to Appendix C for specific sample details. Table B4 contains details of detection limits for the REE, values determined for the international reference standard JB-1A, and an estimate of the confidence of reproducibility of analysis.

Nd Isotope analysis

Nd isotopic compositions were determined using a Finnigan MAT 261 multicollector thermal ion mass spectrometer in static mode at the Max-Planck-Institut für Chemie in Mainz, Germany. Nd isotopic ratios and Nd, Sm concentrations were analysed by isotope dilution using a mixed ^{150}Nd-^{149}Sm spike. The spike was added prior to sample digestion in HF-HNO_3 within closed Teflon beakers for >48 hours at 200 °C. The REE fraction was separated from the bulk sample using Biorad AG 50W-X12 cation-exchange resin. Sm and Nd were separated from the other rare earth elements using HDEHP-coated Teflon powder. Total procedural blanks were <30 pg for Nd. Nd isotopic ratios were normalised to $^{146}Nd/^{144}Nd = 0.7219$. Repeated measurements of the La Jolla standard gave $^{143}Nd/^{144}Nd = 0.511837 \pm 0.000036$, $^{145}Nd/^{144}Nd = 0.348405 \pm 0.000022$ and $^{150}Nd/^{144}Nd = 0.236493 \pm 0.000081$ (2σ, n = 38; see Table B5).

Table B1: XRF programme parameters for trace element measurement during this study.

Channel	Count time (secs)	X-Ray line	No. of cycles
Zr-	40	Zr Kb low angle background	3
Zr	80	Zr Kb peak	3
Zr+	40	Zr Kb high angle background	3
Nb-	40	Nb Ka low angle background	3
Nb	80	Nb Ka peak	3
Nb+	40	Nb Ka high angle background	3
Y-	40	Y Ka low angle background	3
Y	80	Y Ka peak	3
Y+	40	Y Ka high angle background	3
Sr-	20	Sr Ka low angle background	3
Sr	50	Sr Ka peak	3
Sr+	20	Sr Ka high angle background	3
Rb	50	Rb Ka peak	3
Rb+	20	Rb Ka high angle background	3
U-	50	U La low angle background	3
U	100	U La peak	3
U+	50	U La high angle background	3
Pb-	50	Pb Lb low angle background	3
Pb	100	Pb Lb peak	3
Pb+	50	Pb Lb high angle background	3
Th-	50	Th La low angle background	3
Th	100	Th La peak	3
Th+	50	Th La high angle background	3
RC	20	Rh Ka Compton peak	2
Cr-	20	Cr Ka low angle background	3
Cr	50	Cr Ka peak	3
Ba	80	Ba La peak	3
Ba+	40	Ba La high angle background	3
V	50	V Ka peak	3
V-	20	V Ka low angle background	3
Sc	100	Sc Ka peak	3
Sc-	100	Sc Ka low angle background	3
RC	20	Rh Ka Compton peak	2
Ni-	20	Ni Ka low angle background	3
Ni	40	Ni Ka peak	3
S	20	S Ka peak	3
S+	10	S Ka high angle background	3
Ce-	100	Ce Lb low angle background	5
Ce	100	Ce Lb peak	5
Ce+	100	Ce Lb high angle background	5
Nd	100	Nd La peak	5
La-	100	La La low angle background	5
La-	100	La La peak	5
Zn	40	Zn Ka peak	3
Zn+	20	Zn Ka high angle background	3
Ga-	20	Ga Ka low angle background	3
Ga	40	Ga Ka peak	3
Ga+	20	Ga Ka high angle background	3
Ni-	20	Ni Ka low angle background	3
Ni	40	Ni Ka peak	3
S	20	S Ka peak	3
S+	10	S Ka high angle background	3

Table B2: XRF programme parameters for major element measurement during this study.

Element	No. of cycles	Counting time on peak (secs)	Counting time on background (secs)
SiO_2	1	20	12
TiO_2	1	20	20
Al_2O_3	1	40	20
Fe_2O_3	1	10	8
MnO	1	40	20
MgO	1	50	40
CaO	1	10	8
Na_2O	1	50	20
K_20	1	20	20
P_2O_5	1	80	80

Table B3: Measured trace element concentrations (ppm) of XRF standards and in house reference materials measured using long count times.

Measurements made in 1997

	La	Nb	Nd	Pb	Rb	Sc	Sr	Th	U	Y	Zr	Ba	Ce	Co	Cr	Cu	Ga	Ni	S	V	Zn
:BCS313/1	ND	ND	2.6	1.6	ND	ND	2.2	ND	ND	ND	27.6	ND	ND	ND	6	ND	1	Nd	90	7	7
:NIM-G	108.3	55.6	73.9	39.4	315.4	ND	11.5	50.7	16.3	140.9	280.5	99	ND	ND	14	13	27	3	260	6	51
:MRG-1	11.6	20.0	17.6	4.9	7.5	56.0	265.8	1.6	ND	14.7	108.3	57	ND	86	430	133	18	194	1336	526	193
:MA-N	36.1	170.6	0.0	42.3	3778.0	ND	89.6	ND	11.6	ND	29.8	60	ND	ND	ND	140	59	14	483	11	210
:STM-1	135.8	269.1	79.1	18.9	117.0	ND	711.7	31.9	7.9	49.1	1357.2	560	ND	11	ND	10	33	4	157	9	212
:PCC-1	ND	ND	ND	8.4	ND	9.8	1.1	ND	ND	ND	ND	ND	ND	72	2117	12	2	2318	724	27	44
:BHVO-1	16.2	19.3	25.8	3.3	10.0	32.6	390.9	ND	ND	29.1	179.3	128	ND	51	263	141	21	119	245	283	93
:G-2	91.4	12.3	49.9	32.2	167.7	4.0	477.9	26.4	1.7	11.3	319.6	2068	ND	7	7	10	21	3	406	39	77
:GSP-1	127.7	25.9	143.6	64.0	245.3	7.3	235.8	98.5	2.2	30.2	555.5	1247	ND	8	16	38	23	12	1077	50	91
:BIR-1	ND	ND	1.7	5.0	ND	41.5	107.5	ND	ND	13.9	16.5	21	ND	49	308	128	17	158	155	274	63
:BCR-1	25.6	12.6	29.9	13.5	47.2	32.1	331.7	6.0	1.8	38.2	198.2	702	ND	48	ND	32	21	12	972	365	112
:S-ORE	9.9	4.9	12.8	239.2	24.8	20.8	107.5	5.9	ND	16.8	76.8	265	ND	347	543	8115	16	13130	120600	293	279
:JR-1	19.2	16.1	23.8	20.3	251.1	4.7	28.5	27.8	8.3	46.3	101.0	46	ND	ND	ND	ND	17	ND	338	8	32
:JR-2	15.0	18.7	19.8	22.6	299.0	4.5	8.4	31.8	9.9	50.9	95.6	34	ND	ND	5	ND	15	ND	160	6	28
:JGB-1	0.0	2.7	4.2	ND	6.0	37.2	326.1	ND	ND	10.6	31.4	66	ND	63	35	90	19	28	2455	609	103
:JA-1	6.2	1.4	11.5	4.1	10.2	29.2	256.2	ND	ND	31.7	84.3	297	ND	22	0	38	17	4	730	96	79
:JA-2	17.4	10.0	15.1	20.5	70.7	20.5	247.4	5.0	2.5	19.5	120.8	ND	ND	ND	ND	ND	ND	ND	ND	ND	ND
:BOB-1	6.8	4.7	11.6	ND	5.6	35.2	192.2	0.7	ND	27.6	104.7	45	ND	45	220	66	16	104	1406	214	66
:TY-G	33.9	12.7	30.4	1.8	63.7	7.8	66.6	15.2	3.1	48.3	205.9	ND	ND	ND	ND	ND	ND	ND	ND	ND	ND
:AN-G	0.0	1.2	4.5	ND	1.2	20.1	75.4	0.0	ND	6.5	12.2	ND	ND	ND	ND	ND	ND	ND	ND	ND	ND
:JH-1	6.1	4.2	8.8	ND	14.5	75.3	148.1	0.9	ND	14.9	48.4	ND	ND	ND	ND	ND	ND	ND	ND	ND	ND
:JB-2	0.0	0.0	5.2	4.7	6.7	51.9	175.5	ND	ND	25.7	46.9	ND	ND	ND	ND	ND	ND	ND	ND	ND	ND
:JB-3	8.3	2.3	16.9	5.3	14.7	33.9	409.4	0.9	ND	28.4	99.1	ND	ND	ND	ND	ND	ND	ND	ND	ND	ND
:JP-1	ND	ND	ND	ND	ND	7.1	1.3	ND	ND	ND	7.8	18	ND	69	2333	8	ND	2358	1067	29	54
:BE-N	86.6	109.9	67.7	3.8	48.3	28.7	1369.4	10.8	1.6	30.0	274.1	1025	ND	58	316	87	16	267	1348	230	109
:W-1	10.2	7.4	14.6	6.4	21.7	33.9	189.0	2.1	ND	23.8	97.9	144	ND	48	102	112	17	74	954	236	81

ND = Not detected

Table B3: Measured trace element concentrations (ppm) of XRF standards and in house reference materials measured using long count times.

Measurements made in 1998

	La	Nb	Nd	Pb	Rb	Sc	Sr	Th	U	Y	Zr	Ba	Ce	Co	Cr	Cu	Ga	Ni	S	V	Zn
:BCS313/1	2.1	0.8	3.0	0.8	ND	ND	0.5	0.5	ND	ND	28.5	ND	ND	ND	14.1	ND	1.4	2.2	31	7.0	3.4
:NIM-G	109.8	55.8	70.3	39.1	317.5	0.3	9.1	50	15.8	140.2	275.1	101.7	189.5	1.6	20.1	7.4	27.3	4.9	159	3.9	52.5
:MRG-1	7.6	20.2	19.0	4	8	55.7	266.3	ND	0.1	14.5	108.2	58.4	42.5	80.8	517.0	139.5	17.8	197.6	720	559.1	202.5
:MA-N	35.6	170.4	0.0	60	3773.2	ND	88.4	ND	12	ND	31.7	61.6	10.0	0.0	9.7	138.8	61	14.5	523	8.2	239.2
:STM-1	137.1	268.1	80.8	19.8	117.5	0.8	716	32.9	7.9	50.8	1366.5	620.1	255.4	11.5	10.8	5.4	35	2.8	35	5.2	238.4
:PCC-1	0.8	0.3	0.8	7.7	ND	8.4	ND	0.9	0.7	ND	4.4	ND	ND	65.0	2718.4	10.5	1.8	2402.6	570	32.8	45.4
:BHVO-1	14.3	19.1	26.0	3.7	9.7	32.5	394.1	1.2	1.1	28.3	176.3	137.1	44.9	48.7	293.6	139.4	21.3	121.1	143	304.0	105.4
:G-2	88.4	12.3	49.3	31.9	167.7	5.7	474.9	25.2	2.4	11.2	315.2	1889.2	143.0	5.6	5.7	11.3	21.3	1.8	319	36.3	84.6
:GSP-1	128.6	26.5	142.1	63.1	247.7	7.3	235.8	98.4	1.6	29.7	541	1292.3	304.5	9.6	20.6	36.3	22.2	12.6	835	52.5	101.6
:BIR-1	0.2	0.7	2.3	3.1	1.2	41.0	107.7	0.2	0.6	14.5	18.8	15.6	6.6	49.9	394.5	124.6	15.8	168.3	60	307.0	70.4
:BCR-1	28.1	12.1	29.0	13.6	47.5	31.4	331	6.8	2.3	39.7	190.1	745.3	61.1	47.5	0.0	25	21.8	12.4	627	388.4	127.6
:S-ORE	13.4	4.4	13.9	239	26.6	20.9	106	4.1	1.2	17.5	76.9	272.1	98.0	325.6	666.3	7944.2	16.5	13538	120600	310.5	315.2
:JR-1	20.2	15.7	22.6	19.7	249.6	4.4	27.1	27	9.1	45.8	97.7	41.4	31.9	ND	9.3	ND	16.8	1.8	432	10.5	28.9
:JR-2	17.2	19	20.5	21.5	296.2	4.5	6.4	31.8	10.6	50.5	93.2	23.9	27.7	ND	8.6	ND	17.1	1.2	157	7.6	25.6
:JR-3	156.6	574.1	102.7	39.4	464.7	0.2	7.6	113.7	20.3	174.8	1668	62.2	312.7	9.2	9.7	3.6	36.7	3.8	61	5.0	203.4
:JB-2	ND	1	7.0	2.9	6.9	51.4	174.3	ND	0.3	26	50.4	233.9	15.1	49.8	6.5	225	16.9	11.9	32	567.3	106.7
:JB-3	7.9	2.7	17.0	5.6	14.8	35.7	408.3	1.6	ND	28.6	96.1	259.4	28.1	41.4	46.4	194	20	34	44	350.6	94.3
:JP-1	0.8	0.7	ND	ND	ND	8.9	ND	0.1	ND	ND	10.7	8.0	0.1	65.5	2979.7	5.7	2.3	2437.2	151	27.4	44.9
:BOB-1	4.4	4.8	11.9	ND	5.3	34.5	193.1	1.3	0.4	27.9	103.1	49.0	12.2	44.0	273.4	65.6	14.9	108.1	1120	223.3	68.3
:JGB-1	2.2	2.6	5.4	2.2	6.8	38.2	325.6	ND	1.1	11	33.2	74.2	17.9	62.3	40.7	85.7	19.3	23	1946	655.4	113.1
:W-1	9.8	7.1	14.1	6.5	21.6	34.6	186.9	0.9	1.9	23.7	95.4	161.7	27.3	46.8	117.3	112.4	17.8	74.1	735	251.7	86.9
:BE-N	86.9	110	68.5	4.1	48.4	28.1	1369.3	10.4	1.9	30.4	269.2	1009.0	165.4	56.9	383.3	85.3	17.4	280.5	1104	244.7	123.4
:BR	85.2	112.2	67.5	4	48.9	24.1	1386.3	11	1.5	31.6	276.6	1031.6	159.7	56.0	361.5	89.1	16.6	288.3	1739	247.6	161.3

Table B3: Recommended trace elemnet concentrations of XRF standards

	Nb	Zr	Y	Sr	Rb	Th	Ga	Zn	Ni	Cr	V	Ba	La	Ce	Nd
:NIM-G	53	300	143	10	320	51	27	50	8	12	2	120	109	195	72
:MRG-1	20	108	14	266	8.5	0.9	17	191	193	430	526	61	9.8	28	19.2
:MA-N	173	27	1	84	3600	1	59	220	3	3	4.6	42	0.4	1	ND
:STM-1	268	1210	46	700	118	31	36	235	3	4.3	8.7	560	150	259	79
:PCC-1	1	10	0.1	0.4	0.1	0	0.7	42	2380	2730	31	1.2	0.1	0.1	0
:BHVO-1	19	179	27.6	403	11	1.1	21	105	121	289	317	139	15.8	39	25.2
:G-2	12	309	11	478	170	24.7	23	86	5	8.7	36	1882	89	160	55
:GSP-1	27.9	530	26	234	254	106	23	104	8.8	13	53	1310	184	399	196
:BIR-1	2	22	16	108	1	0.9	16	71	166	382	313	7.7	0.9	2.5	2.5
:BCR-1	14	190	38	330	47.2	6	22	129.5	13	16	407	681	24.9	53.7	28.8
:JR-1	15.5	102	46	30	257	26.5	17.6	30	0.7	2.3	ND	40	21	49	25.5
:JR-2	19.2	98.5	51	8	297	32.2	18.2	27.2	0.8	2.6	ND	39	17.5	38	24.8
:JB-2	0.8	52	26	178	6.2	0.3	17	110	14.2	27.4	578	208	2.4	6.5	6.5
:JB-3	2.3	99.4	28	395	13	1.3	20.7	106	38.8	60.4	383	251	9.1	20.5	16.6
:JP-1	1.2	6	1	ND	ND	0.2	0.5	29.5	2460	2970	29	17	0	ND	ND
:BOB-1	4.7	100	26	190	6	1.4	16	63	115	304	234	44	5.6	14.7	10.9
:JGB-1	2.8	13	11	321	4	0.5	18.9	111	25.4	59.3	640	63	4	8	5.7
:W-1	9.9	99	26	186	21.4	2.4	17.4	84	75	119	257	162	11	23.5	14.6
:BE-N	100	265	30	1370	47	11	17	-120	267	360	235	1025	82	152	70
:BR	98	250	30	1320	47	11	19	160	260	380	235	1050	82	151	65

Standards measured with no recommended value quoted are in house reference materials.
ND = Not detected

Table B3: Measured major element concentrations (wt. %) of XRF standards and in house reference materials.

Measurements in 1997

	SiO2	TiO2	Al2O3	Fe2O3	MnO	MgO	CaO	Na2O	K2O	P2O5	Total
:ARSiO2	99.07	ND	0.04	0.01	0.006	0.03	ND	0.57	0.07	0.009	99.79
:BCS372/	20.7	0.17	5.18	3.38	0.06	1.3	66.04	0.3	0.36	0.082	97.58
:BLANK	0.08	ND	ND	0.03	0.007	0.04	ND	0.31	0.092	0.006	0.56
:JGb-1	42.77	1.49	17.37	15.16	0.181	7.46	11.77	1.3	0.285	0.054	97.84
:JP-1	44.11	0.01	0.66	8.66	0.122	45.6	0.5	ND	0.069	0.007	99.7
:JR-1	75.21	0.11	12.37	0.93	0.101	0.06	0.67	4.09	4.409	0.02	97.98
:JR-1	76.44	0.11	12.52	0.93	0.1	0.07	0.67	4	4.25	0.019	99.1
:NIM-G	76.7	0.1	11.85	2.03	0.022	0.02	0.75	3.49	4.923	0.008	99.89
:W-1	52.78	1.04	14.93	11.3	0.166	6.44	10.98	2.21	0.587	0.132	100.57

Measurements in 1998

	SiO2	TiO2	Al2O3	Fe2O3	MnO	MgO	CaO	Na2O	K2O	P2O5	Total
:Alumina	16.82	0.01	83.49	ND	0.013	ND	0.01	ND	0.009	0.007	99.98
:ARSiO2	99.98	0.01	ND	ND	0.01	ND	0.01	0.03	0.004	0.008	100.02
:BCS372/	20.53	0.18	5.34	3.44	0.069	1.54	65.55	0.08	0.629	0.084	97.43
:BLANK	0.02	0.01	0.02	0.01	0.014	0.01	0.01	0.02	0.008	0.006	0.12
:JP-1	44.4	0.02	0.68	8.68	0.127	45.76	0.53	ND	0.006	0.009	99.92
:MRG-1	39.4	3.86	8.58	17.93	0.174	13.73	14.77	0.69	0.192	0.064	99.39
:NIM-G	77.21	0.11	12.25	2.06	0.028	ND	0.77	3.56	5.007	0.007	100.99
:W-1	51.49	1.01	14.96	11.01	0.168	6.67	10.71	2.33	0.631	0.132	99.12

Recommended major element concentrations of XRF standards

	SiO2	TiO2	Al2O3	Fe2O3	MnO	MgO	CaO	Na2O	K2O	P2O5	LOI	Total
:JP-1	42.39	ND	0.62	8.34	0.12	44.72	0.56	0.021	0.003	ND	2.44	99.22
:JR-1	75.41	0.1	12.89	0.96	0.1	0.09	0.63	4.1	4.41	0.02	1.12	99.83
:NIM-G	75.7	0.09	12.08	2.02	0.021	0.06	0.78	3.36	4.99	0.01	0.45	99.56
:W-1	52.46	1.07	15	11.11	0.167	6.62	11	2.16	0.64	0.13	0.52	100.88
:JGb-1	43.44	1.62	17.66	15.16	0.17	7.83	11.98	1.23	0.24	0.05	0.25	99.63

Standards measured with no recommended value quoted are in house reference materials.
ND = Not detected

Table B4: Measured concentrations of REE in ICP-OES standard JB-1a (ppm)

	La	Ce	Pr	Nd	Sm	Eu	Gd	Dy	Er	Yb	Lu
Rec. Values	**38.00**	**67.00**	**7.30**	**26.90**	**5.70**	**1.50**	**4.67**	**3.99**	**2.18**	**2.10**	**0.33**
JB-1a	37.33	64.39	5.23	24.85	4.67	1.61	5.29	4.54	2.68	2.04	0.31
JB-1a	32.87	62.07	7.44	27.92	7.12	1.61	5.19	4.96	3.42	2.04	0.32
JB-1a	36.83	63.36	7.19	26.37	4.93	1.53	4.99	3.97	2.41	1.97	0.29
JB-1a	35.12	64.67	7.40	26.30	5.21	1.51	5.02	3.90	2.18	1.93	0.30
JB-1a	34.09	66.36	7.83	29.11	4.94	1.74	5.06	4.21	2.39	2.05	0.33
JB-1a	37.22	62.08	7.26	26.85	5.72	1.63	5.21	4.22	2.88	2.07	0.33
JB-1a	35.99	63.09	7.56	29.17	5.57	1.56	4.76	3.57	2.18	1.93	0.29
JB-1a	32.27	64.48	8.28	23.85	4.25	1.46	4.92	4.59	2.43	1.91	0.29
JB-1a	35.91	66.50	5.92	22.17	4.96	1.52	4.74	4.02	2.34	2.01	0.31
mean	35.29	64.11	7.12	26.29	5.26	1.57	5.02	4.22	2.55	1.99	0.31
std dev	1.75	1.53	0.90	2.22	0.78	0.08	0.18	0.40	0.37	0.06	0.02
2 SM	1.17	1.02	0.60	1.48	0.52	0.05	0.12	0.26	0.25	0.04	0.01
% reprod.	3.3	1.6	8.4	5.6	9.9	3.4	2.4	6.3	9.8	1.9	3.4
Average reproducibility = 5.1%											

ICP-OES Detection limits (ppm)

	La	Ce	Pr	Nd	Sm	Eu	Gd	Dy	Er	Yb	Lu
	0.8	0.9	0.9	1.0	0.5	0.15	0.8	0.7	0.8	0.14	0.08

Table B5: Measured Values of La Jolla Nd Standard (quoted errors are 2 sigma mean).

All ratios normalised to 146/144 = 0,7219 Recommended value for La Jolla 143/144: 0.511858

Sample	Date	Time	Mass Spec	Nd 143/144	2 SM error	ε_{Nd}	Nd 145/144	2 SM error	150/144	2 SM error
La Jolla	17/11/1998	07:46	MS2	0.511851	8	-15.4	0.348384	3	0.236391	5
La Jolla	15/01/1999	11:35	MS2	0.511855	9	-15.3	0.348406	7	0.236454	4
La Jolla	16/01/1999	00:22	MS2	0.511835	7	-15.7	0.348411	8	0.236493	8
La Jolla	28/01/1999	10:53	MS2	0.511835	4	-15.7	0.348401	2	0.236470	4
La Jolla	28/01/1999	17:39	MS2	0.511827	6	-15.8	0.348401	2	0.236470	4
La Jolla	28/01/1999	23:06	MS2	0.511819	7	-16.0	0.348407	4	0.236480	6
La Jolla	29/01/1999	18:01	MS2	0.511832	8	-15.7	0.348402	4	0.236474	7
La Jolla	28/04/1999	12:29	MS2	0.511816	10	-16.0	0.348406	6	0.236503	6
La Jolla	04/05/1999	19:35	MS2	0.511818	10	-16.0	0.348384	12	0.236501	13
La Jolla	05/05/1999	13:21	MS2	0.511803	9	-16.3	0.348410	9	0.236548	10
La Jolla	28/10/1999	16:36	MS2	0.511850	10	-15.4	0.348401	5	0.236490	7
La Jolla	28/10/1999	17:27	MS2	0.511847	10	-15.4	0.348398	5	0.236478	7
La Jolla	28/10/1999	18:37	MS2	0.511845	4	-15.5	0.348402	3	0.236483	5
La Jolla	28/10/1999	19:47	MS2	0.511835	5	-15.7	0.348403	3	0.236474	6
La Jolla	29/10/1999	13:28	MS2	0.511850	7	-15.4	0.348394	4	0.236462	7
La Jolla	29/08/1999	15:05	MS2	0.511851	8	-15.4	0.348395	5	0.236458	7
La Jolla	02/11/1999	16:24	MS2	0.511832	10	-15.7	0.348408	6	0.236502	9
La Jolla	02/11/1999	18:44	MS2	0.511823	13	-15.9	0.348413	6	0.236525	17
La Jolla	19/11/1999	17:09	MS2	0.511844	10	-15.5	0.348399	12	0.236476	12
La Jolla	26/11/1999	15:40	MS2	0.511827	12	-15.8	0.348396	9	0.236493	8
La Jolla	13/02/2000	10:57	MS2	0.511852	7	-15.3	0.348395	6	0.236494	10
La Jolla	19/02/2000	13:32	MS2	0.511850	6	-15.4	0.348402	6	0.236499	6
La Jolla	03/03/2000	19:10	MS2	0.511840	10	-15.6	0.348398	4	0.236493	6
La Jolla	07/03/2000	11:23	MS2	0.511819	10	-16.0	0.348414	6	0.236544	10
La Jolla	07/03/2000	12:50	MS2	0.511816	7	-16.0	0.348400	3	0.236571	10
La Jolla	07/03/2000	18:58	MS2	0.511806	10	-16.2	0.348400	9	0.236562	10
La Jolla	06/10/2000	20:09	MS2	0.511872	5	-14.9	0.348436	5	0.236484	7
La Jolla	06/10/2000	21:07	MS2	0.511872	13	-14.9	0.348425	5	0.236428	8
La Jolla	07/10/2000	12:38	MS2	0.511865	13	-15.1	0.348432	5	0.236549	9
La Jolla	07/10/2000	20:43	MS2	0.511853	11	-15.3	0.348415	5	0.236534	8
La Jolla	09/12/2000	11:52	MS2	0.511813	10	-16.1	0.348402	10	0.236586	12
La Jolla	09/12/2000	09:38	MS2	0.511810	10	-16.2	0.348410	14	0.236549	17
La Jolla	10/12/2000	20:22	MS2	0.511830	14	-15.8	0.348415	13	0.236515	26
La Jolla	10/12/2000	22:30	MS2	0.511842	7	-15.5	0.348415	13	0.236553	21
La Jolla	01/12/2000	14:50	MS2	0.511830	6	-15.8	0.348394	6	0.236528	13
La Jolla	01/12/2000	15:45	MS2	0.511834	15	-15.7	0.348394	6	0.236528	13
La Jolla	02/12/2000	23:10	MS2	0.511861	14	-15.2	0.348404	8	0.236509	11
La Jolla	02/12/2000	00:15	MS2	0.511853	7	-15.3	0.348405	8	0.236538	10
		Average		**0.511837**			**0.348405**		**0.236493**	
		2 sigma		**0.000036**			**0.000022**		**0.000081**	
		2 sigma mean		**0.000006**			**0.000004**		**0.000013**	
		n =	38							

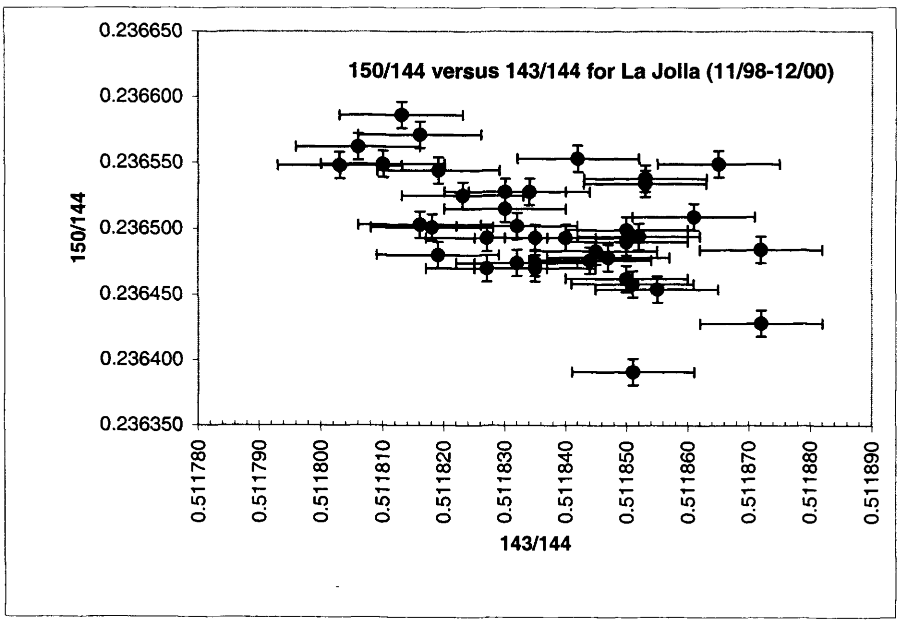

Appendix C

Sample locations and index of associated data

List of Samples and available data.

(Samples submitted to D-Collection are available for viewing from the University of Leicester Geology Department).

Sample	Location	Lithology	Lithotectonic Unit	Purpose	Thin Section	Trace Element Data	Major Element Data	Nd Isotope Ratios	Orientated Sample	Submitted to D-Collection
97M004	N46°12.300' E99°49.500'	Phyllite	Burd Gol Mélange	Kinematics	Yes	Not Measured	Not Measured	Not Measured	Parralel to lineation	No
97M018	N46°16.373' E99°29.018'	Granulite	Baydrag Block	Petrography	Yes	Not Measured	Not Measured	Not Measured	No	No
97M019A	N46°20.030' E99°37.902'	Phyllite	Burd Gol Mélange	Kinematics	Yes	Not Measured	Not Measured	Not Measured	Parralel to lineation	No
97M026	N46°27.679' E99°40.121'	Staurolite Schist	Burd Gol Mélange	Petrography	Yes	Not Measured	Not Measured	Not Measured	No	No
97M027	N46°27.679' E99°40.121'	Sillimanite Schist	Burd Gol Mélange	Petrography	Yes	Not Measured	Not Measured	Not Measured	No	No
97M035	N46°33.614' E99°46.595'	Basalt	Delb Khairkhan Mélange	Petrography	Yes	Not Measured	Not Measured	Not Measured	No	No
97M038	N46°35.867' E99°45.964'	Dol porph	Bayankhongor Ophiolite	Geochemistry	No	Table 3.1c	Table 3.1c	Table 3.3	No	Yes
97M043	N46°35.867' E99°45.964'	Basalt	Bayankhongor Ophiolite	Geochemistry	No	Table 3.1a	Table 3.1a	Not Measured	No	Yes
97M044B	N46°35.727' E99°48.160'	Gabbro	Bayankhongor Ophiolite	Petrography	Yes	Not Measured	Not Measured	Not Measured	No	No
97M045	N46°35.727' E99°48.160'	Gabbro	Bayankhongor Ophiolite	Petrography	Yes	Not Measured	Not Measured	Not Measured	No	No
97M048	N46°35.373' E99°41.010'	Dol porph	Bayankhongor Ophiolite	Geochemistry	Yes	Table 3.1a	Table 3.1a	Not Measured	No	Yes
97M049	N46°35.673' E99°47.133	Muscovite Schist	Dzag Schists	Kinematics	Yes	Not Measured	Not Measured	Not Measured	Parralel to lineation	No
97M050	N46°33.871' E99°47.039'	Gabbro	Bayankhongor Ophiolite	Geochemistry	Yes	Table 3.1b	Table 3.1b	Table 3.3	No	Yes
97M051	N46°34.156' E99°44.911'	Dol aph	Bayankhongor Ophiolite	Geochemistry	No	Table 3.1c	Table 3.1c	Not Measured	No	Yes
97M053B	N46°34.656' E99°45.637'	Gabbro	Bayankhongor Ophiolite	Geochemistry	No	Table 3.1b	Table 3.1b	Not Measured	No	Yes
97M058	N46°35.291' E99°46.944'	Serpentinite	Bayankhongor Ophiolite	Petrography	Yes	Not Measured	Not Measured	Not Measured	No	No
97M067	N46°35.867' E99°45.964'	Dol porph	Bayankhongor Ophiolite	Geochemistry	No	Table 3.1a	Table 3.1a	Table 3.3	No	Yes
97M068B	N46°35.867' E99°45.964'	Dol porph	Bayankhongor Ophiolite	Geochemistry	Yes	Table 3.1c	Table 3.1c	Not Measured	No	Yes
97M070A	N46°35.727' E99°48.160'	Chlorite-Muscovite Schist	Dzag Schists	Kinematics	Yes	Not Measured	Not Measured	Not Measured	Parralel to lineation	No
97M070B	N46°35.727' E99°48.160'	Chlorite-Muscovite Schist	Dzag Schists	Kinematics	Yes	Not Measured	Not Measured	Not Measured	Parralel to lineation	No
97M071A	N46°29.948' E99°56.658'	Basalt	Bayankhongor Ophiolite	Petrography	Yes	Not Measured	Not Measured	Not Measured	No	No
97M074	N46°30.840' E99°56.971'	Basalt	Bayankhongor Ophiolite	Geochemistry	No	Table 3.1a	Table 3.1a	Table 3.3	No	Yes
97M074B	N46°30.840' E99°56.971'	Basalt	Bayankhongor Ophiolite	Geochemistry	No	Table 3.1a	Table 3.1a	Table 3.3	No	Yes
97M075	N46°30.840' E99°56.971'	Basalt	Bayankhongor Ophiolite	Geochemistry	No	Table 3.1c	Table 3.1c	Not Measured	No	Yes
97M076	N46°30.630' E99°56.479'	Dol aph	Bayankhongor Ophiolite	Geochemistry	No	Table 3.1a	Table 3.1a	Table 3.3	No	Yes
97M077	N46° 26.360' E99° 52.044'	Granite	Granite Uldzit Gol Transect	Zircon Dating	Yes	Table 4.2	Table 4.2	Table 4.3	No	Yes
97M078	N46°34.737' E99°43.080'	Dol porph	Bayankhongor Ophiolite	Geochemistry	No	Table 3.1c	Table 3.1c	Not Measured	No	Yes
97M079	N46°34.925' E99°43.002'	Ultramafic	Bayankhongor Ophiolite	Petrography	Yes	Not Measured	Not Measured	Not Measured	No	No
97M083	N46°34.498' E99°42.540'	Interpillow Limestone	Bayankhongor Ophiolite	Petrography	Yes	Not Measured	Not Measured	Not Measured	No	No
97M084	N46°34.498' E99°42.540'	Pillow Breccia	Bayankhongor Ophiolite	Petrography	Yes	Not Measured	Not Measured	Not Measured	No	No
97M085	N46°34.498' E99°42.540'	Pillow Breccia	Bayankhongor Ophiolite	Petrography	Yes	Not Measured	Not Measured	Not Measured	No	No
97M087	N46°34.498' E99°42.540'	Basalt	Bayankhongor Ophiolite	Petrography	Yes	Not Measured	Not Measured	Not Measured	No	No
97M089	N46°33.671' E99°42.302'	Milonitised carbonate schist	Delb Khairkhan Mélange	Kinematics	Yes	Not Measured	Not Measured	Not Measured	Parralel to lineation	No
97M093	N46°33.626' E99°40.662'	Black Schist	Delb Khairkhan Mélange	Petrography	Yes	Not Measured	Not Measured	Not Measured	No	No
97M101	N46°33.008' E99°40.262'	Dacite	Southern Volcanics	Geochemistry	No	Table 3.2	Table 3.2	Not Measured	No	Yes
97M104	N46°32.765' E99°39.827'	Mudstone	Delb Khairkhan Mélange	Petrography	Yes	Not Measured	Not Measured	Not Measured	No	No
97M107	N46°32.706' E99°39.410'	Limestone	Delb Khairkhan Mélange	Petrography	Yes	Not Measured	Not Measured	Not Measured	No	No
97M109	N46°33.604' E99°43.684	Basalt	Bayankhongor Ophiolite	Geochemistry	No	Table 3.1a	Table 3.1a	Table 3.3	No	Yes
97M110	N46°33.604' E99°43.684'	Basalt	Bayankhongor Ophiolite	Geochemistry	No	Table 3.1c	Table 3.1c	Not Measured	No	Yes
97M110C	N46°33.604' E99°43.684'	Basalt	Bayankhongor Ophiolite	Geochemistry	No	Table 3.1a	Table 3.1a	Table 3.3	No	Yes
97M112A	N46°33.604' E99°43.684'	Dol aph	Bayankhongor Ophiolite	Geochemistry	No	Table 3.1c	Table 3.1c	Not Measured	No	Yes
97M112B	N46°33.604' E99°43.684'	Dol aph	Bayankhongor Ophiolite	Geochemistry	No	Table 3.1c	Table 3.1c	Not Measured	No	Yes
97M113	N46°34.000' E99°43.354'	Dol aph	Bayankhongor Ophiolite	Geochemistry	No	Table 3.1c	Table 3.1c	Not Measured	No	Yes
97M114	N46°34.505' E99°43.246'	Dol aph	Bayankhongor Ophiolite	Geochemistry	Yes	Table 3.1c	Table 3.1c	Not Measured	No	Yes
97M115	N46°34.505' E99°43.204'	Dol porph	Bayankhongor Ophiolite	Geochemistry	Yes	Table 3.1c	Table 3.1c	Not Measured	No	Yes
97M115B	N46°34.505' E99°43.204'	Basalt	Bayankhongor Ophiolite	Geochemistry	Yes	Table 3.1a	Table 3.1a	Not Measured	No	Yes
97M116	N46°34.266' E99°43.256'	Dolerite	Bayankhongor Ophiolite	Petrography	Yes	Not Measured	Not Measured	Not Measured	No	No
97M119	N46°31.738' E99°37.789'	Volcanic breccia	Southern Volcanics	Geochemistry	Yes	Table 3.2	Table 3.2	Not Measured	No	Yes
97M123	N46° 30.022' E99° 38.251'	Granite	Granite Uldzit Gol Transect	Zircon Dating	Yes	Table 4.2	Table 4.2	Table 4.3	No	Yes
97M125	N46° 31.307' E99° 39.346'	Rhyolite Dyke	Granite Uldzit Gol Transect	Zircon Dating	Yes	Table 4.2	Table 4.2	Table 4.3	No	Yes
97M126A	N46°31.583' E99°38.739'	Dacite	Southern Volcanics	Geochemistry	Yes	Table 3.2	Table 3.2	Not Measured	No	Yes
97M126B	N46°31.538' E99°38.739'	Dacite	Southern Volcanics	Geochemistry	Yes	Table 3.2	Table 3.2	Not Measured	No	Yes
97M129	N46°31.583' E99°38.739'	Basalt	Bayankhongor Ophiolite	Geochemistry	No	Table 3.2	Table 3.2	Not Measured	No	Yes
98M009	N46°42.904' E99°16.143'	Dacite	Southern Volcanics	Geochemistry	No	Table 3.2	Table 3.2	Not Measured	No	Yes
98M010	N46°46.080' E99°19.052'	Carbonaceous Schist	Haluut Bulag Mélange	Kinematics	Yes	Not Measured	Not Measured	Not Measured	Parralel to lineation	No
98M011	N46°51.418' E99°10.720'	Basalt	Haluut Bulag Mélange	Geochemistry	No	Table 3.1c	Table 3.1c	Not Measured	No	Yes
98M013	N46°49.688' E99°16.989'	Chlorite-Muscovite Schist	Dzag Schists	Kinematics	Yes	Not Measured	Not Measured	Not Measured	Parralel to lineation	No
98M014	N46°49.688' E99°16.989'	Chlorite-Muscovite Schist	Dzag Schists	Kinematics	Yes	Not Measured	Not Measured	Not Measured	Parralel to lineation	No

Sample	Location	Lithology	Lithotectonic Unit	Purpose	Thin Section	Trace Element Data	Major Element Data	Nd Isotope Ratios	Orientated Sample	Submitted to D-Collection
98M016	N46°45.640' E99°17.521	Phyllite	Haluut Bulag Mélange	Kinematics	Yes	Not Measured	Not Measured	Not Measured	Parralel to lineation	No
98M018	N46°45.755' E99°17.296'	Basalt	Bayankhongor Ophiolite	Geochemistry	Yes	Table 3.1c	Table 3.1c	Not Measured	No	Yes
98M019	N46°45.755' E99°17.296'	Basalt	Bayankhongor Ophiolite	Geochemistry	No	Table 3.1c	Table 3.1c	Not Measured	No	Yes
98M020	N46°45.814' E99°17.211'	Basalt	Bayankhongor Ophiolite	Geochemistry	Yes	Table 3.1a	Table 3.1a	Table 3.3	No	Yes
98M021	N46°45.968' E99°16.052'	Dolerite	Bayankhongor Ophiolite	Petrography	Yes	Not Measured	Not Measured	Not Measured	No	No
98M022A	N46°45.314' E99°15.389'	Gabbro	Bayankhongor Ophiolite	Petrography	Yes	Not Measured	Not Measured	Not Measured	No	No
98M022B	N46°45.314' E99°15.389'	Gabbro	Bayankhongor Ophiolite	Geochemistry	No	Table 3.1b	Table 3.1b	Not Measured	No	Yes
98M026	N46°44.261' E99°17.932'	Basalt	Bayankhongor Ophiolite	Geochemistry	Yes	Table 3.2	Table 3.2	Table 3.3	No	Yes
98M027	N46°44.261' E99°17.932'	Basalt	Bayankhongor Ophiolite	Geochemistry	Yes	Table 3.2	Table 3.2	Table 3.3	No	Yes
98M028	N46°43.684' E99°18.189'	Basalt	Bayankhongor Ophiolite	Geochemistry	Yes	Table 3.1a	Table 3.1a	Table 3.3	No	Yes
98M029A	N46°43.689' E99°18.189'	Dolerite	Bayankhongor Ophiolite	Petrography	Yes	Not Measured	Not Measured	Not Measured	No	No
98M030	N46°43.684' E99°18.189'	Basalt	Bayankhongor Ophiolite	Geochemistry	Yes	Table 3.1a	Table 3.1a	Not Measured	No	Yes
98M031	N46°43.684' E99°18.189'	Basalt	Bayankhongor Ophiolite	Kinematics	Yes	Not Measured	Not Measured	Not Measured	Parralel to lineation	No
98M033	N46°45.699' E99°18.796'	Basalt	Bayankhongor Ophiolite	Kinematics	Yes	Not Measured	Not Measured	Not Measured	Parralel to lineation	No
98M034	N46°45.699' E99°18.796'	Basalt	Bayankhongor Ophiolite	Geochemistry	Yes	Table 3.1c	Table 3.1c	Not Measured	No	Yes
98M035	N46°43.526' E99°18.031'	Basalt	Bayankhongor Ophiolite	Geochemistry	Yes	Table 3.1c	Table 3.1c	Not Measured	No	Yes
98M036	N46°43.526' E99°18.031'	Basalt	Bayankhongor Ophiolite	Geochemistry	Yes	Table 3.1c	Table 3.1c	Not Measured	No	Yes
98M037	N46°43.378' E99°17.987'	Basalt	Bayankhongor Ophiolite	Geochemistry	Yes	Table 3.1c	Table 3.1c	Not Measured	No	Yes
98M038	N46°43.378' E99°17.987'	Basalt	Bayankhongor Ophiolite	Geochemistry	Yes	Table 3.1a	Table 3.1a	Table 3.2	No	Yes
98M040	N46°43.378' E99°17.987'	Basalt	Bayankhongor Ophiolite	Geochemistry	Yes	Table 3.1a	Table 3.1a	Table 3.3	No	Yes
98M041	N46°43.378' E99°17.987'	Basalt	Bayankhongor Ophiolite	Geochemistry	Yes	Table 3.1a	Table 3.1a	Not Measured	No	Yes
98M042	N46°43.378' E99°17.987'	Basalt	Bayankhongor Ophiolite	Geochemistry	Yes	Table 3.1c	Table 3.1c	Not Measured	No	Yes
98M043	N46°43.378' E99°17.987'	Basalt	Bayankhongor Ophiolite	Geochemistry	Yes	Table 3.1c	Table 3.1c	Not Measured	No	Yes
98M045	N46°45.755' E99°17.296'	Dacite	Southern Volcanics	Geochemistry	Yes	Table 3.2	Table 3.2	Not Measured	No	Yes
98M046	N46°42.798' E99°16.971'	Dacite	Southern Volcanics	Geochemistry	Yes	Table 3.2	Table 3.2	Not Measured	No	Yes
98M049	N46°43.046' E99°17.430'	Rhyolite	Delb Khairkhan Mélange	Petrography	Yes	Not Measured	Not Measured	Not Measured	No	No
98M050	N46°43.046' E99°17.430'	Basalt	Delb Khairkhan Mélange	Petrography	Yes	Not Measured	Not Measured	Not Measured	No	No
98M051	N46°43.055' E99°17.312'	Gabbro	Bayankhongor Ophiolite	Geochemistry	Yes	Table 3.1b	Table 3.1b	Table 3.3	No	Yes
98M053	N46°43.245' E99°17.164'	Plagiogranite	Bayankhongor Ophiolite	Zircon Dating	Yes	Not Measured	Not Measured	Not Measured	No	No
98M054	N46°42.828' E99°16.664'	Basalt	Bayankhongor Ophiolite	Geochemistry	Yes	Table 3.1c	Table 3.1c	Not Measured	No	Yes
98M055	N46°42.798' E99°16.971	Dacite	Southern Volcanics	Geochemistry	Yes	Table 3.2	Table 3.2	Not Measured	No	Yes
98M056	N46°43.086' E99°16.937'	Dacite	Southern Volcanics	Geochemistry	Yes	Table 3.2	Table 3.2	Not Measured	No	Yes
98M057	N46°43.086' E99°16.937'	Sheared Basalt	Delb Khairkhan Mélange	Kinematics	Yes	Not Measured	Not Measured	Not Measured	Parralel to lineation	No
98M058	N46°43.086' E99°16.937'	Gabbro	Bayankhongor Ophiolite	Geochemistry	No	Table 3.1b	Table 3.1b	Not Measured	No	Yes
98M060	N46°42.904' E99°16.143'	Dacite	Southern Volcanics	Geochemistry	Yes	Table 3.2	Table 3.2	Not Measured	No	Yes
98M062	N46°42.904' E99°16.143'	Dacite	Southern Volcanics	Geochemistry	Yes	Table 3.2	Table 3.2	Not Measured	No	Yes
98M072	N46°42.236' E99°16.357'	Andesite	Southern Volcanics	Geochemistry	Yes	Table 3.2	Table 3.2	Not Measured	No	Yes
98M073	N46°42.236' E99°16.357'	Andesite	Southern Volcanics	Geochemistry	Yes	Table 3.2	Table 3.2	Not Measured	No	Yes
98M074	N46°42.603' E99°15.047'	Andesite	Southern Volcanics	Geochemistry	Yes	Table 3.2	Table 3.2	Not Measured	No	Yes
98M079	N46°45.684' E99°13.143'	pyroxenite	Bayankhongor Ophiolite	Geochemistry	No	Table 3.1b	Table 3.1b	Table 3.3	No	Yes
98M080	N46°45.684' E99°13.143'	Gabbro	Bayankhongor Ophiolite	Geochemistry	No	Table 3.1b	Table 3.1b	Not Measured	No	Yes
98M080	N46°45.733' E99°12.984'	Gabbro	Bayankhongor Ophiolite	Petrography	Yes	Not Measured	Not Measured	Not Measured	No	No
98M088A	N46°12.788' E100°26.680'	Basalt	Bayankhongor Ophiolite	Geochemistry	Yes	Table 3.1c	Table 3.1c	Not Measured	No	Yes
98M088B	N46 12.788' E100° 26.680'	Basalt	Bayankhongor Ophiolite	Geochemistry	Yes	Table 3.1c	Table 3.1c	Not Measured	No	Yes
98M088C	N46°12.788' E100°26.680'	Basalt	Bayankhongor Ophiolite	Geochemistry	Yes	Table 3.1a	Table 3.1a	Table 3.3	No	Yes
98M089A	N46°12.788' E100°26.680'	Basalt	Bayankhongor Ophiolite	Geochemistry	Yes	Table 3.1c	Table 3.1c	Not Measured	No	Yes
98M089B	N46°12.788' E100°26.680	Basalt	Bayankhongor Ophiolite	Geochemistry	Yes	Table 3.1a	Table 3.1a	Not Measured	No	Yes
98M095B	N46°38.579' E99°36.680'	Mica Schist	Delb Khairkhan Mélange	Kinematics	Yes	Not Measured	Not Measured	Not Measured	Parralel to lineation	No
98M096	N46°38.464' E99°36.093'	Pyroxenite	Bayankhongor Ophiolite	Geochemistry	No	Table 3.1b	Table 3.1b	Not Measured	No	Yes
98M097	N46°38.464' E99°36.093'	Gabbro	Bayankhongor Ophiolite	Geochemistry	Yes	Table 3.1b	Table 3.1b	Table 3.3	No	Yes
98M098	N46°38.309' E99°34.874'	Dolerite	Bayankhongor Ophiolite	Geochemistry	No	Table 3.1c	Table 3.1c	Not Measured	No	Yes
98M099B	N46°37.197' E99°35.522'	Basaltic Schist	Haluut Bulag Mélange	Kinematics	Yes	Not Measured	Not Measured	Not Measured	Parralel to lineation	No
98M101A	N46°36.700' E99°35.304'	Mica Schist	Haluut Bulag Mélange	Kinematics	Yes	Not Measured	Not Measured	Not Measured	Parralel to lineation	No
98M101B	N46°36.700' E99°35.304'	Mica Schist	Haluut Bulag Mélange	Kinematics	Yes	Not Measured	Not Measured	Not Measured	Parralel to lineation	No
98M101C	N46°36.700' E99°35.304'	Mica Schist	Haluut Bulag Mélange	Kinematics	Yes	Not Measured	Not Measured	Not Measured	Parralel to lineation	No
98M103	N46°42.671' E99°14.736'	Dacite	Southern Volcanics	Geochemistry	Yes	Table 3.2	Table 3.2	Not Measured	No	Yes
98M104	N46°34.963' E99°31.151'	Dacite	Southern Volcanics	Geochemistry	Yes	Table 3.2	Table 3.2	Not Measured	No	Yes
98M105	N46°35.167' E99°32.325'	Andesite	Southern Volcanics	Geochemistry	Yes	Table 3.2	Table 3.2	Not Measured	No	Yes
98M108A	N46°37.308' E99°41.081'	Basalt	Bayankhongor Ophiolite	Geochemistry	Yes	Table 3.1c	Table 3.1c	Not Measured	No	Yes
98M108B	N46°37.308' E99°41.081'	Basalt	Bayankhongor Ophiolite	Geochemistry	Yes	Table 3.1c	Table 3.1c	Not Measured	No	Yes

Sample	Location	Lithology	Lithotectonic Unit	Purpose	Thin Section	Trace Element Data	Major Element Data	Nd Isotope Ratios	Orientated Sample	Submitted to D-Collection
98M109A	N46°37.308' E99°41.081'	Basalt	Bayankhongor Ophiolite	Geochemistry	No	Table 3.1c	Table 3.1c	Not Measured	No	Yes
98M109B	N46°37.308' E99°41.081'	Basalt	Bayankhongor Ophiolite	Geochemistry	No	Table 3.1a	Table 3.1a	Table 3.3	No	Yes
98M111A	N46°36.537' E99°41.223'	Basalt	Bayankhongor Ophiolite	Geochemistry	No	Table 3.1c	Table 3.1c	Not Measured	No	Yes
98M111B	N46°36.537' E99°41.223'	Basalt	Bayankhongor Ophiolite	Geochemistry	No	Table 3.1c	Table 3.1c	Not Measured	No	Yes
98M111C	N46°36.537' E99°41.223'	Basalt	Bayankhongor Ophiolite	Geochemistry	No	Table 3.1c	Table 3.1c	Not Measured	No	Yes
98M112	N46°36.537' E99°41.223'	Basalt	Bayankhongor Ophiolite	Geochemistry	No	Table 3.1c	Table 3.1c	Not Measured	No	Yes
98M114A	N46°36.537' E99°41.223'	Dolerite	Bayankhongor Ophiolite	Geochemistry	No	Table 3.1c	Table 3.1c	Not Measured	No	Yes
98M114B	N46°36.537' E99°41.223'	Dolerite	Bayankhongor Ophiolite	Geochemistry	No	Table 3.1a	Table 3.1a	Table 3.3	No	Yes
98M115A	N46°37.131' E99°34.309'	Basaltic Schist	Bayankhongor Ophiolite	Kinematics	Yes	Not Measured	Not Measured	Not Measured	Parralel to lineation	No
98M115B	N46°37.131' E99°34.309'	Basaltic Schist	Bayankhongor Ophiolite	Kinematics	Yes	Not Measured	Not Measured	Not Measured	Parralel to lineation	No
98M118A	N46°35.568' E99°37.374'	Mica Schist	Delb Khairkhan Mélange	Kinematics	Yes	Not Measured	Not Measured	Not Measured	Parralel to lineation	No
98M121A	N46°29.779' E99°56.232'	Dolerite	Bayankhongor Ophiolite	Geochemistry	Yes	Table 3.1c	Table 3.1c	Not Measured	No	Yes
98M121B	N46°29.779' E99°56.232'	Dolerite	Bayankhongor Ophiolite	Geochemistry	Yes	Table 3.1c	Table 3.1c	Not Measured	No	Yes
98M122	N46°29.779' E99°56.232'	Basalt	Bayankhongor Ophiolite	Geochemistry	Yes	Table 3.1c	Table 3.1c	Not Measured	No	Yes
98M123	N46°29.779' E99°56.232'	Basalt	Bayankhongor Ophiolite	Geochemistry	Yes	Table 3.1a	Table 3.1a	Not Measured	No	Yes
98M124	N46°29.779' E99°56.232'	Dolerite	Bayankhongor Ophiolite	Geochemistry	Yes	Table 3.1c	Table 3.1c	Not Measured	No	Yes
98M125	N46°29.779' E99°56.232'	Dolerite	Bayankhongor Ophiolite	Geochemistry	Yes	Table 3.1c	Table 3.1c	Not Measured	No	Yes
98M126	N46°29.684' E99°55.737'	Basalt	Burd Gol Mélange	Petrography	Yes	Not Measured	Not Measured	Not Measured	No	No
98M127	N46°29.684' E99°55.737'	Dolerite	Burd Gol Mélange	Petrography	Yes	Not Measured	Not Measured	Not Measured	No	No
98M128A	N46°29.684' E99°55.737'	Graphite Schist	Burd Gol Mélange	Kinematics	Yes	Not Measured	Not Measured	Not Measured	Parralel to lineation	No
98M128B	N46°29.684' E99°55.737'	Graphite Schist	Burd Gol Mélange	Kinematics	Yes	Not Measured	Not Measured	Not Measured	Parralel to lineation	No
98M200	N46°29.684' E99°55.737'	Phyllite	Burd Gol Mélange	Kinematics	Yes	Not Measured	Not Measured	Not Measured	Parralel to lineation	No

References:

Agar, S. M., 1990. The interaction of fluid processes and progressive deformation during shallow level accretion: Examples from the Shimanto Belt of SW Japan. *Journal of Geophysical Research* **95**, 9133-9147.

Alabaster, T., Pearce, J. A., and Malpas, J., 1982. The volcanic stratigraphy and petrogenesis of the Oman Ophiolite Complex. *Contributions to Mineralogy and Petrology* **81**, 168-183.

Alexander, R. J., and Harper, G. D., 1992, The Josephine ophiolite: an ancient analogue for slow- to intermediate-spreading oceanic ridges., *in* Parsons, L. M., and Murton, B. J., eds., Ophiolites and their Modern Ocean Analogues, London, UK, Geological Society of London, Special Publication No. 60, p. 3-38.

Allan, J. F., Chase, R. L., Cousens, B., Michael, P. J., Gorton, M. P., and Scott, S. D., 1993. The Tuzo Wilson volcanic field, NE Pacific: alkaline volcanism at a complex, diffuse, transform-trench-ridge triple junction. *Journal of Geophysical Research* **98**, 22367-22387.

Andreas, D., 1970, Geological sheet map (L-47-55E, 56, 67E, 68): Open file report in Geological Funds of Mongolia no. 1895.

Arawaka, Y., Naito, K., Takahashi, Y., Oyungerel, S., and Amakawa, H., 1998. Rb-Sr whole rock isochron age of Daltyn-am Complex in Bayankhongor area, central Mongolia. *Mongolian Geoscientist* **8**, 16-19.

Barr, S. R., Temperley, S., and Tarney, J., 1999. Lateral growth of the continental crust through deep level subduction-accretion: a re-evaluation of central Greek Rhodope. *Lithos* **46**, 69-94.

Barry, T. L., and Kent, R. W., 1998. Cenezoic magmatism in Mongolia and the origin of Central and East Asian Basalts. *Geodynamics* **27**, 347-364.

Barsbold, R., and Dorjnamjaa, D., 1991, Geological Map of the Khangay Highland: Mongolian Acadamy of Sciences.

Batiza, R., and Vanko, D., 1984. Petrology of young Pacific seamounts. *Journal of Geophysical Research* **89**, 11235-11260.

Ben-Avraham, Z., Nur, A., and Jones, D., 1982. The emplacement of ophiolites by collision. *Journal of Geophysical Research* **87**, 3861-3867.

Blevin, P. L., and Chappell, B. W., 1995. Chemistry, origin, and evolution of mineralised granites in the Lachlan Fold Belt, Australia: the metallogeny of I- and S- type granites. *Economic Geology* **90**, 1604-1619.

Boishenko, A. F., 1979, On age of rocks of the metamorphic complex in the Bayan-Khongor Zone (Ph.D. Thesis Abstract), Russian Acadamy of Sciences.

Bougalt, H., Joron, J. L., and Treuil, M., 1980. The primordial chondritic nature and large - scale heterogeneities in the mantle: evidence from high and low partitian coefficient elements in oceanic basalts. *Philosophical Transactions of the Royal Society of London* **A297**, 203-213.

Buchan, C., Cunningham, D., Windley, B. F., and Tomurhuu, D., 2001. Structural and lithological characteristics of the Bayankhongor ophiolite zone, Central Mongolia. *Journal of the Geological Society, London* **158**, 445-460.

Cameron, W. E., 1985. Petrology and origin of primitive lavas from the Troodos ophiolite, Cyprus. *Contributions to Mineralogy and Petrology* **89**, 239-255.

Cannat, M., Briais, A., Deplus, C., Escartin, J., Georgen, J., Lin, J., Mercouriev, S., Meyzen, C., Muller, M., pouliquen, G., Rabain, A., and Silva, P. d., 1999. Mid-Atlantic Ridge-Azores hotspot interactions: along-axis migration of a hotspot-derived event of enhanced magmatism 10 to 4 Ma ago. *Earth and Planetary Science Letters* **173**, 257-269.

Casey, J. F., and Dewey, J. F., 1984, Initiation of Subduction Zones Along Transform and Accreting Plate Boundaries, Triple-junction Evolution, and Forearc Spreading Centres-Implications for Ophiolite Geology and Obduction, *in* Gass, I. G., Lippard, S. J., and Shelton, A. W., eds., Ophiolites & Oceanic Lithosphere: Special Publication of the Geological Society, Oxford, Blackwell Scientific, p. 269-290.

Chappell, B. W., and White, A. J. R., 1974. Two contrasting granite types. *Pacific Geology* **8**, 173-174.

Chappell, B. W., and White, A. J. R., 1992. I- and S-type granites in the Lachlan Fold Belt. *Transaction of the Royal Society of Edinburgh: Earth Sciences* **83**, 1-26.

Cloos, M., 1993. Lithospheric boyancy and collision orogenesis: subduction of oceanic plateuas, continental margins, island arcs, spreading ridges and seamounts. *Geological Society of America Bulletin* **105**, 715-737.

Cocherie, A., Guerrot, C., and Rossi, P. H., 1992. Single-zircon dating by step-wise Pb evaporation: Comparison with other geochronological techniques applied to the Hercynian granites of Corsica, France. *Chemical Geology* **101**, 131-141.

Coleman, R. G., 1989. Continental Growth of Northwest China. *Tectonics* **8**, 621-635.

Collins, A. S., and Robertson, A. H. F., 1998. Processes of Late Cretaceous to Late Miocene episodic thrust-sheet translation in the Lycian Taurides, SW turkey. *Journal of the Geological Society* **155**, 759-772.

Corfield, R. I., Searle, M. P., and Green, O. R., 1999. Photang thrust sheet: an accretionary complex structurally below the Spontang ophiolite constraining timing environment of ophiolitic obduction, Ladakh Himalaya, NW India. *Journal of the Geological Society, London* **156**, 1031-1044.

Cousens, B. L., 1996, Depleted mantle and enriched upper mantle sources for basaltic rocks from diverse tectonic environments in the northeast Pacific Ocean: the generation of oceanic alkaline vs. tholeiitic basalts., *in* Basu, A., and Hart, S. R., eds., Earth processes: reading the isotopic code, Washinton DC, American Geophysical union.

Cox, K. G., and Hawkesworth, C. J., 1985. Geochemical stratigraphy of the Deccan Traps at Mahabaleshwar, Western Ghats, India, with impications for open system magmatic processes. *Journal of Petrology* **26**, 355-377.

Cunningham, W. D., 1998. Lithospheric controls on late Cenozoic construction of the Mongolian Altai. *Tectonics* **17**, 891-902.

Cunningham, W. D., 2001. Cenozoic normal faulting and regional doming in the southern Hangay region, Central Mongolia: implications for the origin of the Baikal rift province. *Tectonophysics* **331**, 389-411.

Davies, J. H., and vonBlanckenburg, F., 1995. Slab break-off: a model of lithosphere detachment and its test in the magmatism and deformation of collisional orogens. *Earth and Planetary Science Letters* **129**, 85-102.

Davis, E. E., and Karsten, J. L., 1986. On the cause of the asymmetric distribution of seamounts about the Juan de Fuca ridge: ridge-crest migration over a heterogeneous asthenosphere. *Earth and Planetary Science Letters* **79**, 385-396.

Delor, C., Deroin, J.-P., Maluski, H., and Tomurtogoo, O., 2000, Petrostructural constraints and Ar-Ar dating of the Bayankhongor ophiolites, *in* Badarch, G., and Jahn, B.-m., eds., IGCP 420 Continental Grouth in he Phanerozoic: Evidence from Central Asia, Second Workshop, Abstracts and Excursion Guidebook (Geotraverse through a terrane collage in Southern Hangay) July 25 - August 3, 1999, Ulaanbaatar, Mongolia., Rennes, Geosciences Rennes, Hors serie n. 2.

DePaolo, D. J., 1988. Age dependence of the composition of continental crust: evidence from Nd isotopic variations in granitic rocks. *Earth and Planetary Science Letters* **90**, 263-271.

DePaolo, D. J., Linn, A. M., and Schubert, G., 1991. The Continental crustal age distribution: methods of determining mantle separation ages from Sm-Nd isotopic data and application to the Southwestern United States. *Journal of Geophysical Research* **96**, 2071-2088.

Dergunov, A. B., Ryantsev, A. V., Luneva, O. I., and Rikhter, A. V., 1997. Structure and Geological History of the Bayan-Khongor Zone, Central Mongolia. *Geotectonics* **31**, 132-140.

Didenko, A. N., Mossakovsky, A. A., Pechersky, D. M., Ruzhentsev, S. V., Samygin, S. G., and Kheroskova, T. N., 1994. Geodynamics of the Central-Asian Paleozoic oceans. *Russian Geology and Geophysics* **35**, 48-61.

Dobretsov, N. L., Berzin, N. A., and Buslov, M. M., 1995. Opening and Tectonic Evolution of the Palaeo-Asian Ocean. *International Geology Review* **37**, 335-360.

Dorjnamjaa, D., Badarch, G., Badamgarov, J., Bat-ireedui, Y., Gerel, O., Cunningham, D., Windley, B., and Buchan, C., 1998, Geotectonic map of Mongolia: Mongolian Academy of Sciences, Palaeontological Centre.

Dosso, L., Bougault, H., Langmuir, C., Bollinger, C., Bonnier, O., and Etoubleau, J., 1999. The age and distribution of mantle heterogeneity along the Mid-Atlantic Ridge (31-41°N). *Earth and Planetary Science Letters* **170**, 269-286.

Einaudi, F., Pezard, P. A., Cocheme, J. J., Coulon, C., Laverne, C., and Godard, M., 2000. Petrography, geochemistry and physical properties of a continuous extrusive section from the Sarami Massif, Semail Ophiolite. *Marine Geophysical Researches* **21**, 387-407.

Ellis, S., Beaumont, C., and Pfiffner, O. A., 1999. Geodynamic models of crustal scale episodic tectonic accretion and underplating in subduction zones. *Journal of Geophysical Research* **104**, 15169-15190.

Ernst, W. G., 1999. Mesozoic petrotectonic development of the Sawers Bar suprasubduction-zone arc, central Klamath Mountains, northern California. *Geological Society of America Bulletin* **111**, 1217-1232.

Ewart, A., Collerson, K. D., Regelous, M., Wendt, J. I., and Niu, Y., 1998. Geochemical evolution within the Tonga-Kermadec-Lau Arc-Back-arc systems: the role of varying mantle wedge composition in space and time. *Journal of Petrology* **39**, 331-368.

Fitton, J. G., Saunders, A. D., Norry, M. J., Hardarson, B. S., and Taylor, R. N., 1997. Thermal and chemical structure of the Iceland plume. *Earth and Planetary Science Letters* **153**, 197-208.

Frey, F. A., Coffin, M. F., Wallace, P. J., Weis, D., Zhao, X., Jr., S. W. W., Wãhnert, V., Teagle, D. A. H., Saccocia, P. J., Reusch, D. N., Pringle, M. S., Nicolaysen, K. E., Neal, C. R., Müller, R. D., Moore, C. L., Mahoney, J. J., Keszthelyi, L., Inokuchi, H., Duncan, R. A., Delius, H., Damuth, J. E., Damasceno, D., Coxall, H. K., Borre, M. K., Boehm, F., Barling, J., Arndt, N. T., and Antretter, M., 2000. Origin and evolution of a submarine large igneous province: the Kerguelen Plateau and Broken Ridge, southern Indian Ocean. *Earth and Planetary Science Letters* **176**, 73-89.

Fryer, P., Ambos, E. L., and Hussong, D. M., 1985. origin and emplacement of Mariana forearc seamounts. *Geology* **13**, 774-777.

Geist, D., Naumann, T., and Larson, P., 1998. Evolution of Galapgos magmas: mantle and crustal fractionation without assimilation. *Journal of Petrology* **39**, 953-971.

Gillis, K. M., and Robinson, P. T., 1985. Low-Temperature Alteration of the Extrusive Sequence, Troodos Ophiolite, Cyprus. *Canadian Mineralogist* **23**, 431-441.

Godfrey, N. J., and Klemperer, S. L., 1998. Ophiolitic basement to a forearc basin and implications for continental growth: The Coast Range Great Valley ophiolite, California. *Tectonics* **17**, 558-570.

Goldstein, S. L., O'Nions, R. K., and Hamilton, P. J., 1984. A Sm-Nd isotopic study of atmospheric dusts and particulates from major river systems. *Earth and Planetary Science Letters* **70**, 221-236.

Hall, R., Ali, J. R., Anderson, C. D., and Baker, S. J., 1995. Origin and motion of history of the Philippine Sea Plate. *Tectonophysics* **251**, 229-250.

Hall, R., and Wilson, M. E. J., 2000. Neogene sutures in eastern Indonesia. *Journal of Asian Earth Sciences* **18**, 781-808.

Hanan, B. B., Blichert-Toft, J., Kingsley, R., and Schilling, J.-G., 2000. Depleted Iceland mantle plume geochemical signature: Artifact of multicomponent mixing? *Geochemistry Geophysics Geosystems* **1**.

Hannigan, R. E., Basu, A. R., and Teichmann, F., 2001. Mantle resevoir geochemistry from statistical analysis of ICP-MS trace element data of equitorial mid-Atlantic MORB glasses. *Chemical Geology* **175**, 397-428.

Hards, V. L., Kempton, P. D., Thompson, R. N., and Greenwood, P. B., 2000. The magmatic evolution of the Snaefell volcanic centre; an example of volcanism during incipient rifting in Iceland. *Journal of Volcanology and geothermal research* **99**, 97-121.

Harvey, P. K., Lovell, M. A., Brewer, T. S., Locke, J., and Mansley, E., 1996. Measurement of thermal neutron absorption cross section in selected geochemical reference materials. *Geostandards Newsletter* **20**, 79-85.

Hashimoto, Y., and Kimura, G., 1999. Underplating process from melange formation to duplexing: Example from the Cretaceous Shimanto Belt, Kii Peninsula, southwest Japan. *Tectonics* **18**, 92-107.

Hassanipak, A. A., and Ghazi, A. M., 2000. Petrology, geochemistry and tectonic setting of the Khoy ophiolite, northwest Iran: implications for Tethyan tectonics. *Journal of Asian Earth Sciences* **18**, 109-121.

Hauff, F., Hoernle, K., Bogaard, P. v. d., Avarado, G., and Garbe-Schönberg, D., 2000. Age and geochemistry of basaltic complexes in western Costa Rica: contributions to the geotectonic evolution of Central America. *Geochemistry, Geophysics, Geosystems* **1**, paper No. 1999GC000020.

Hekinian, R., Stoffers, P., Ackermand, D., Révillon, S., Maia, M., and Bohn, M., 1999. Ridge-hotspot interaction: the PAcific-Antarctic Ridge and the foundation seamounts. *Marine Geology* **160**, 199-223.

Helz, R. T., 1987, Differentiation behaviour of Kilauea Iki lava lake, Kilauea volcano, Hawaii: an overview of past and current work, *in* Mysen, B. O., ed., Magmatic processes: physiochemical principles, Geochemical Society.

Hendrix, M. S., Graham, S. A., Amory, J. Y., and Badarch, G., 1996. Noyon Uul Syncline, Southern Mongolia: Lower Mesozoic Sedimentary Record of the Tectonic Amalgamation of Central Asia. *Geological Society of America Bulletin* **108**, 1256-1274.

Höck, V., Frank, W., Hejl, E., and Furtmueller, G., 2000, Petrology and cooling history of the Mt. Ushgoeg Range (Central Mongolia)., *in* Badarch, G., and Jahn, B.-m., eds., IGCP 420 Continental Grouth in he Phanerozoic: Evidence from Central Asia, Second Workshop, Abstracts and Excursion Guidebook (Geotraverse through a terrane collage in Southern Hangay) July 25 - August 3, 1999, Ulaanbaatar, Mongolia., Rennes, Geosciences Rennes, Hors serie n. 2.

Hoernle, K., Werner, R., Morgan, J. P., Garbe-Schönberg, D., Bryce, J., and Mrazek, J., 2000. Existence of complex spacial zonation in the Galapogos plume for at least 14 m.y. *Geology* **28**, 435-438.

Hofmann, A. W., 1988. Chemical differentiation of the Earth: the relationship between mantle, continental crust, and oceanic crust. *Earth and Planetary Science Letters* **90**, 297-314.

Hsü, K. J., Qingcheg, W., Liang, L., and Jie, H., 1991. Geological evolution of the Neimonides: A Working Hypothesis. *Eclogae Geologicae Helvetiae* **84**, 1-31.

Jacobsen, S. B., and Wasserburg, G. J., 1980. Sm-Nd isotopic evolution of chondrites. *Earth and Planetary Science Letters* **50**, 139-155.

Jahn, B.-m., Griffin, W. L., and Windley, B. F., 2000. Continental Growth in the Phanerozoic; evidence from Central Asia. *Tectonophysics* **328**, 1-6.

Jaeckel, P., Kröner, A., Kamo, S. L., Brandl, G., and Wndt, J. I., 1997. Late Archaean to early Proterozoic granitoid magmatism and high-grade metamorphism in the central Limpopo belt, South Africa. *Journal of the Geological Society London* **154**, 25-44.

Jenner, G. A., Dunning, G. R., Malpas, J., Brown, M., and Brace, T., 1991. Bay of Islands and Little Port Complexes, Revisited - Age, Geochemical and Isotopic Evidence Confirm Suprasubduction-Zone Origin. *Canadian Journal of Earth Sciences* **28**, 1635-1652.

Kamenetsky, V. S., Crawford, A. J., Eggins, S., and Mühe, R., 1997. Phenocryst and melt inclusion chemistry of near-axis seamounts, Valu Fa Ridge, Lau Basin: insight into mantle wedge melting and addition of subduction components. *Earth and Planetary Science Letters* **151**, 205-223.

Kamenetsky, V. S., Crawford, A. J., Varne, R., Eggins, S. M., and Lanyon, R., 2000. Enriched end-member of primitive MORB melts: petrology and geochemistry of glasses from Macquarie Island (SW Pacific). *Journal of Petrology* **41**, 411-430.

Karabinos, P., 1997. An evaluation of the single-grain zircon evaporation method in highly discordant samples. *Geochimica Cosmochimica Acta* **61**, 2467-2474.

Keen, M. J., Salisbury, M., Burke, M., and Ishii, T., 1989. Serpentinite seamounts of Pacific fore-arcs drilled by the Ocean Drilling Program: Dr. Hess would be pleased. *Geoscience Canada* **16**, 177-182.

Kempton, P. D., Fitton, J. G., Saunders, A. D., Nowell, G. M., Taylor, R. N., Hardarson, B. S., and Pearson, G., 2000. The Iceland plume in space and time: a Sr-Nd-Pb-Hf study of the North Atlantic Rifted Margin. *Earth and Planetary Science Letters* **177**, 255-271.

Kepezhinskas, P. K., Kepizhinskas, K. B., and Pukhtel, I. S., 1991. Lower Plaeozoic Oceanic Crust in Mongolian Caledonides: Sm-Nd Isotope and Trace Element Data. *Geophysical Research Letters* **18**, 1301-1304.

Kerr, A. C., White, R. V., and Saunders, A. D., 2000. LIP reading: recognizing Oceanic Plateaux in the geological record. *Journal of Petrology* **41**, 1-16.

Kimura, G., Sakakibara, M., and Okamura, M., 1994. Plumes in central Panthalassa? Deductions from accreted ocean fragments in Japan. *Tectonics* **13**, 905-916.

Kober, B., 1986. Whole-grain evaporation for $^{207}Pb/^{206}Pb$-age-investigations on single zircons using a double-filament thermal ion source. *Contributions to Mineralogy and Petrology* **93**, 482-490.

Kober, B., 1987. Single-zircon evaporation combined with Pb^+ emitter bedding for $^{207}Pb/^{206}Pb$-age investigations using thermal ion mass spectrometry, implications to zirconology. *Contributions to Mineralogy and Petrology* **96**, 63-71.

Komarov, Y. V., Belogolvkin, A. A., Gladkov, B. G., and Chuluun, D., 1999, Structure and Gold mineralisation of black slates in Bayankhongor palaeorift zone (Mongolia): Problems of metallogeny of Mongolia., *in* Gerel, O., Bakhromeev, G. S., Dashdavaa, S., Ivanov, A. N., Chuluun, D., and Dandar, S., eds., Problems of Geology and Metallogeny of Mongolia (Scientific Transactions of the Kherlen Geological International Expedition), Ulaanbaatar, Mongolian Technical University, p. 16-28.

Kopteva, V., Kuz'min, M. I., and Tomurtogoo, O., 1984. Structure of the Upper Part of the Bayan-Khongor Ophiolite Zone, Mongolia. *Geotectonics* **18**, 481-491.

Kotov, A. B., Kozakov, I. K., Bibikova, E. V., Salnikova, E. B., Kirnozova, T. I., and Kovach, V. P., 1995. Duration of Regional Metamorphic Episodes in Areas of Polycyclic Endogenic Processes - a U-Pb Geochronological Study. *Petrology* **3**, 567-575.

Kovalenko, V. I., Pukhtel, I. S., Yarmolyuk, V. V., Zhuravlev, D. Z., Stosch, H., and Jagoutz, E., 1996a. The Sm-Nd Isotopic systematics of Ophiolites in the Ozernaya Zone (Mongolia). *Stratigraphy and Geological Correlation* **4**, 107-113.

Kovalenko, V. I., Yarmolyuk, V. V., Kovach, V. P., Kotov, A. B., Kozakov, I. K., and Sal'nikova, E. B., 1996b. Sources of Phanerozoic granitoids in Central Asia: Sm-Nd isotope data. *Geochemistry International* **34**, 628-640.

Kozakov, I. K., 1986, Precambrian infrastructures of Paleozoic complexes of Mongolia (Dokembriyskiye infrastukturnyye kompleksy paleozoid Mongolii): Leningrad, USSR, Izd. Nauka, Leningr. Otd., 144 p.

Kozakov, I. K., Kotov, A. B., Kovach, V. P., and Salnikova, E. B., 1997. Crustal growth in the geologic evolution of the Baidarik Block, Central Mongolia: Evidence from Sm-Nd isotopic systematics. *Petrology* **5**, 201-207.

Kozakov, I. K., Kotov, A. B., Salnikova, E. B., Bibikova, E. V., Kovach, V. P., Kirnozova, T. I., Berezhnaya, N. G., and Lykhin, D. A., 1999a. Metamorphic age of crystalline complexes of the Tuva-Mongolia Massif: The U-Pb geochronology of granitoids. *Petrology* **7**, 177-191.

Kozakov, I. K., Salnikova, E. B., Kotov, A. B., Kröner, A., and Zagornaya, N. Y., 1999b. Latest Neoproterozoic to Early Palaeozoic Crustal Accretion in Southern Siberia: A Reinterpretation of the Tuvino-Mongolian Massif. *Journal of Conference Abstracts, Terra Abstracts, European Union of Geosciences 1999* **4**, 109.

Kröner, A., Byerly, C. R., and Lowe, D. R., 1991. Chronology of early Archaean granite-greenstone evolution in the Barberton Mountain Land, South Africa, based on preciese dating by single zircon evaporation. *Earth and Planetary Science Letters* **103**, 41-54.

Kröner, A., and Hegner, E., 1998. Geochemistry, single zircon ages and Sm-Nd systematics of granitoid rocks from the Góry Sowie (Owl Mts), Polish West Sudetes: evidence for early Palaeozoic arc-prelated plutonism. *Journal of the Geological Society London* **155**, 711-724.

Kröner, A., and Todt, W., 1988. Single zircon dating constraining the maximum age of the Barberton greenstone belt, Southern Africa. *Journal of Geophysical Research* **93**, 15329-15337.

Kröner, A., Windley, B. F., Jaekel, P., Brewer, T. S., and Razakamanana, T., 1999. New Zircon ages and regional significance for the evolution of the Pan-African orogen in Madagascar. *Journal of the Geological Society, London* **156**, 1125-1135.

Kurimoto, C., Tungalag, F., Bayarmandal, L., and Ichinnorov, N., 1998. K-Ar ages of white micas from pelitic schists of the Bayankhongor area, west Mongolia. *Bulletin of the Geological Survey of Japan* **49**, 19-23.

Lagabrielle, Y., Goslin, J., Martin, H., Thirot, J.-L., and Auzende, J.-M., 1997. Multiple active spreading centres in the hot North Fiji Basin (Southwest Pacific): a possible model for Archaean seafloor dynamics? *Earth and Planetary Science Letters* **149**, 1-13.

Lallemand, S., Liu, C. S., Dominguez, S., Schnurle, P., and Malavieille, J., 1999. Trench-parallel stretching and folding of forearc basins and lateral migration of the accretionary wedge in the southern Ryukyus: A case of strain partition caused by oblique convergence. *Tectonics* **18**, 231-247.

Lamb, M. A., and Badarch, G., 1997. Palaeozoic Sedimentary Basins and Volcanic-Arc Systems of Southern Mongolia: New Stratigraphic and Sedimentologic Constraints. *international Geology Review* **39**, 542-576.

Lapierre, H., Bosch, D., Dupuis, V., Polvé, M., Maury, R. C., Hernandez, J., Monié, P., Yeghicheyan, D., Jaillard, E., Tardy, M., Lépinay, B. M. d., Mamberti, M., Desmet, A., Keller, F., and Sénebier, F., 2000. Multiple plume events in the genesis of the peri-Caribbean Cretaceous oceanic plateau province. *Journal of Geophysical Research* **105**, 8403-8421.

Leat, P. T., Livermore, R. A., Millar, I. L., and Pearce, J. A., 2000. Magma supply in back-arc spreading centre segment E2, East Scotia Ridge. *Journal of Petrology* **41**, 845-866.

Lee, T.-Y., and Lawver, L. A., 1995. Cenozoic plate reconstruction of Southeast Asia. *Tectonophysics* **251**, 85-138.

Leeman, W. P., Gerlach, D. C., Garcia, M. O., and West, H. B., 1994. Geochemical variations in lavas from Kahoolawe volcano, Hawaii: evidence for open system evolution of plume-derived magmas. *Contributions to Mineralogy and Petrology* **116**, 62-77.

LeMaitre, R. W., Bateman, P., Dudek, A., Keller, J., Bas, M. J. L. L., Sabine, P. A., Schmid, R., Sorenson, H., Streckeisen, A., Woolley, A. R., and Zanettin, B., 1989, A classification of igneous rocks and glossary terms: Oxford, Blackwell.

leRoex, A., Dick, H. J. B., and Watkins, R. T., 1992. Petrogenesis of anomalous K-enriched MORB from the Southwest Indian Ridge: 11°53'E to 14°38'E. *Contributions to Mineralogy and Petrology* **110**, 253-268.

Lundstrom, C. C., Gill, J., and Williams, Q., 2000. A geochemically consistent hypothesis for MORB generation. *Chemical Geology* **162**, 105-126.

Mahoney, J. J., Frei, R., Tejada, M. L. G., Mo, X. X., Leat, P. T., and Nägler, T. F., 1998. Tracing the Indian Ocean mantle domain through time: isotopic results from old west Indian, east Tethyan, and south Pacific seafloor. *Journal of Petrology* **39**, 1285-1306.

Malpas, J., 1990, Crustal accretionary processes in the Troodos ophiolite, Cyprus: evidence from field mapping and deep crustal drilling, *in* Malpas, J., Moores, E. M., Panayiotou, A., and Xenophontos, C., eds., Ophiolites oceanic crustal analogues. Proceedings of the symposium "Troodos 1987", Nicosia, Cyprus, The Geological Survey Department, Ministry of Agriculture and Natural Resources, p. 65-74.

Maltman, A., Byrne, T., Karig, D., and Lallemant, S., 1992. Structural geological evidence from ODP Leg 131 regarding fluid flow in the Nankai prism, Japan. *Earth and Planetary Science Letters* **109**, 463-468.

Mazzotti, S., Henry, P., Pichon, X. L., and Sagiya, T., 1999. Strain partitioning in the zone of transition from Nankai subduction to Izu-Bonin collision (Central Japan): implications for an extensional tear within the subducting slab. *Earth and Planetary Science Letters* **172**, 1-10.

McCaffrey, R., 1992. Oblique plate convergence, slip vectors, and forearc deformation. *Journal of Geophysical Research* **97**, 8905-8915.

Meschede, M., 1986. A method for discriminating between different types of mid-ocean ridge basalts and continental tholeiites with the Nb-Zr-Y diagram. *Chemical Geology* **56**.

Meschede, M., Zweigel, P., Frisch, W., and Völker, D., 1999. Mélange formation by subduction erosion: the case of the Osa mélange in southern Costa Rica. *Terra Nova* **11**, 141-148.

Millward, D., Marriner, G. F., and Saunders, A. D., 1984. Cretaceous tholeiitic volcanic rocks from the Western Cordillera of Columbia. *Journal of the Geoloigical Society, London* **141**, 847-860.

Mitrofanov, F. P., Bibikova, Y. V., Gracheva, T., Kozakov, I. K., Sumin, L. V., and Shuleshko, I. K., 1985. Isotope age of "grey" tonalites and gneisses of the Archean in Caledonian Structures of central Mongolia. *Doklady Akademii Nauk SSSR* **284**, 670-675.

Mitrofanov, F. P., Kozakov, I. K., and Palay, I. P., 1981, Precambrian of west Mongolia and South Tuva: Transactions of The Joint Soviet-Mongolian Scientific-Research Geological Expedition, v. 32: Leningrad, Nauka, 153 p.

Moore, J. C., and Byrne, T., 1987. Thickening of fault zones: A mechanism of melange formation in accreting sediments. *Geology* **15**, 1040-1043.

Moores, E. M., 1970. Ultramafics and orogeny, with models for the U. S. Cordillera and Tethys. *Nature* **228**, 837-842.

Moores, E. M., 1982. Origin and Emplacement of Ophiolites. *Reviews of Geophysics* **20**, 735-760.

Moores, E. M., and Vine, F. J., 1971. The Troodos Massif, Cyprus and other ophiolites as oceanic crust: evaluation and implications. *Philosophical Transactions of The Royal Society of London* **268**, 443-466.

Mossakovsky, A. A., and Derguno, A. B., 1985, The Caledonides of Kazakhstan, Siberis, and Mongolia: a review of structure, development history, and palaeotectonic environments, *in* Gee, D. G., and Sturt, B. A., eds., The Caledonian Orogen; Scandinavia and related areas, London, John Wiley & Sons Ltd., p. 1201-1215.

Mossakovsky, A. A., Ruzhentsev, S. V., Samygin, S. G., and Kheraskova, T. N., 1994. Central Asian Fold Belt: Geodynamic Evolution and Formational History. *Geotectonics* **27**, 445-474.

Nehlig, P., and Juteau, T., 1988a. Deep crustal seawater penetration and circulation at ocean ridges: Evidence from the Oman Ophiolite. *Marine Geology* **84**, 209-228.

Nehlig, P., and Juteau, T., 1988b. Low porosities, permeabilities and preliminary data on fluid inclusions and fossil thermal gradients in the crustal sequence of the Sumail ophiolite. *Tectonophysics* **151**, 199-222.

Nemcok, M., Pospisil, L., Lexa, J., and Donelick, R. A., 1998. Tertiary subduction and slab break-off model of the Carpathian-Pannonian region. *Tectonophysics* **295**, 307-340.

Niu, Y., and Batiza, R., 1997. Trace element evidence from seamounts for recycled oceanic crust in the Eastern Pacific mantle. *Earth and Planetary Science Letters* **148**, 471-483.

Niu, Y., Bideau, D., Hékinian, R., and Batiza, R., 2001. Mantle compositional control on the extent of mantle melting, crust production, gravity anomoly, ridge morphology, and ridge segmentation: a case study at the Mid-Atlantic Ridge 33-35°N. *Earth and Planetary Science Letters* **186**, 383-399.

Norman, M. D., and Garcia, M. O., 1999. Primitive magmas and source charecteristics of the Hawaiin plume: petrology and geochemistry of shield picrites. *Earth and Planetary Science Letters* **168**, 27-44.

Okamura, Y., 1991. Large -scale melange formation due to seamount subduction: an example from the Mesozoic accretionary complex in Central Japan. *Journal of Geology* **99**, 661-674.

Oxburgh, E. R., 1972. Flake tectonics and continental collision. *Nature* **239**, 202-204.

Oyungerel, S., 1998. Petrography of the granitoids in Bayankhongor area. *Mongolian Geoscientist* **8**, 4-15.

Oyungerel, S., and Takahashi, Y., 1999. New radiometric data of the granitoids in Bayankhongor area, central Mongolia. *Mongolian Geoscientist* **13**, 38-40.

Pearce, J. A., 1982, Trace element characteristics of lavas from destructive plate boundaries: Andesites, p. 525-548.

Pearce, J. A., and Cann, J. R., 1973. Tectonic setting of basic volcanic rocks determined using trace element analyses. *Earth and PLanetary Science Letters* **19**, 290-300.

Pearce, J. A., Lippard, S. J., and Roberts, S., 1984, Characteristics and tectonic significance of supra-subduction zone ophiolites, *in* Kokelaar, B. P., and Howells, M. F., eds., Marginal basin geology; volcanic and associated sedimentary and tectonic processes in modern and ancient marginal basins, London, UK, Geological Society of London Special Publication, p. 74-94.

Pearce, J. A., and Norry, M. J., 1979. Petrogenetic implications of Ti, Zr, Y and Nb variations in volcanic rocks. *Contributions to Mineralogy and Petrology* **69**, 33-47.

Pearce, J. A., and Parkinson, I. J., 1993, Trace element models for mantle melting: application to volcanic arc petrogenesis., *in* Prichard, H. M., Alabaster, T., Harris, N. B. W., and Neary, C. R., eds., Magmatic Processes and Plate Tectonics, London, UK, Geological Society of London Special Publication, p. 373-403.

Perfit, M., and Chadwick, W. W., 1998, Magmatism at mid-ocean ridges: constraints from volcanological and geochemical investigations, *in* Buck, R. W., Delaney, P. T., Karson, J. A., and Lagabrielle, Y., eds., Faulting and Magmatism at Mid-Ocean Ridges, Washington DC, American Geophysical Union, p. 59-115.

Perfit, M. R., Fornari, D. J., Smith, M. C., Bender, J. F., Langmuir, C. H., and Haymon, R. M., 1994. Samll-scale spatial and temporal variations in mid-ocean ridge crest magmatic processes. *Geology* **22**.

Pfänder, J., Jochum, K. P., Todt, W., and Kröner, A., 1999. Relationships between the mantle, lower crust and upper crust within the Agardagh-Tes Chem Ophiolite, Central Asia: Evidence from petrologic, trace element, and isotopic data. *Ofioliti* **24**, 151-152.

Pfänder, J. A., Jochum, K. P., Kozakov, I. K., Kröner, A., and Todt, W., 2001. Evolution of arc like mafic upper crust within the late Proterozoic Agardagh-Tes Chem ophiolite, Central Asia: evidence from trace element and Sr-Nd-Pb isotope data. *Contributions to Mineralogy and Petrology* .

Pidgeon, R. T., Furfaro, D., Kennedy, A., Nemchin, A. A., Bronswjk, W. v., and Todt, W., 1994. Calibration of the CZ3 zircon standard for the Curtin SHRIMP II. *US Geological Survey Circular* **1107**, 251.

Polat, A., and Kerrich, R., 1999. Formation of an Archean tectonic melange in the Schreiber-Hemlo greenstone belt, Superior Province, Canada: Implications for Archean subduction-accretion process. *Tectonics* **18**, 733-755.

Rampone, E., Hofmann, A. W., and Raczek, I., 1998. Isotopic contrasts within the Internal Liguride ophiolite (N. Italy): the lack of a genetic mantle-crust link. *Earth and Planetary Science Letters* **163**, 175-189.

Ranero, C. R., and Huene, R. v., 2000. Subduction erosion along the Middle America convergent margin. *Nature* **404**, 748-752.

Reynolds, J. R., Langmuir, C. H., Bender, J. F., Kastens, K. A., and Ryan, W. B. F., 1992. Spatial and temporal variability in the geochemistry of basalts from the East Pacific Rise. *Nature* **359**, 493-499.

Richardson, C. J., Cann, J. R., Richards, H. G., and Cowan, J. G., 1987. Metal-Depleted Root Zones of the Troodos Ore-Forming Hydrothermal Systems, Cyprus. *Earth and Planetary Science Letters* **84**, 243-253.

Roberts, S., Andrews, J. R., Bull, J. M., and Sanderson, D. J., 1993. Slow-spreading ridge-axis tectonics: evidence from the Lizard complex, UK. *Earth and Planetary Sceince Letters* **116**, 101-112.

Robertson, A. H. F., 2000, Formation of mélanges in the Indus Suture Zone, Ladakh Himalaya by successive subduction-related, collision and post-collisional processes during Late Mesozoic-Late Tertiary time, *in* Khan, M. A., Treloar, P. J., Searle, M. P., and Jan, M. Q., eds., Tectonics of the Nanga Parbat Syntaxis and the Western Himalaya, London, UK, Geological Society, London, p. 333-374.

Robertson, A. H. F., and Party, S. S., 1996, Role of the Eratosthenes seamount in collisional processes in the Eastern Mediterranean, *in* Emeis, K.-C., Robertson, A. H. F., and Richter, C., eds., Proceedings of the Ocean Drilling Program, Initial Reports, College Station, Texas, Ocean Drilling Program.

Robertson, A. H. F., and Xenophontos, C., 1993, Development of concepts concerning the Troodos ophiolite and adjacent units in Cyprus, *in* Prichard, H. M., Alabaster, T., Harris, N. B. W., and Neary, C. R., eds., Magmatic Processes and Plate Tectonics, London, UK, Geological Society of London Special Publication, p. 85-120.

Robinson, P. T., Zhou, M.-f., Hu, X.-F., Reynolds, P., Wenji, B., and Yang, J., 1999. Geochemical constraints on the origin of the Hegenshan Ophiolite, Inner Mongolia, China. *Journal of Asian Earth Sciences* **17**, 423-442.

Rollinson, H. R., 1993, Using Geochemical Data: Evaluation, Presentation, Interpretation: New York, Longman Scientific & Technical, 351 p.

Rubin, K. H., Smith, M. C., Bergmanus, E. C., Perfit, M. R., Sinton, J. M., and Batiza, R., 2001. Geochemical heterogeneity within mid-ocean ridge lava flows: insights into eruption, emplacement and global variations in magma generation. *Earth and Planetary Science Letters* **188**, 349-366.

Ryazantsev, A. V., 1994. Ophiolites of the Bayankhongor Zone in Palaeozoic Structure of Mongolia. *Doklady Acadamy Nauk* **336**, 651-654.

Saleeby, J. B., 1984, Tectonic significance of serpentinite mobility and ophiolitic melange, *in* Raymond, L. A., ed., Melanges : their nature, origin, and significance, Boulder, Colorado, Geological Society of America, p. 153-167.

Saleeby, J. B., 1992, Petrotectonic and palaeogeographic settings of U.S. Cordilleran ophiolites, *in* Burchfield, B. C., Lipman, P. W., and Zoback, M. L., eds., The Cordilleran Orogen: Conterminous U.S., Boulder, Colorado, Geological Society of America, p. 653-681.

Saunders, A. D., and Tarney, J., 1984, Geochemical characteristics and tectonic significance of back- arc basins: Marginal basin geology; volcanic and associated sedimentary and tectonic processes in modern and ancient marginal basins, p. 59-76.

Saunders, A. D., Tarney, J., Marsh, N. G., and Wood, D. A., 1980, ophiolites as oceanic crust or marginal basin crust: A geochemical approach., *in* Malpas, J., Moores, E. M., Panayiotou, A., and Xenephontos, C., eds., Ophiolites: Proceedings of the Intrnational Ophiolite Symposium, Nicosia, Cyprus, Geological Survey Department.

Schiffman, P., and Smith, B. M., 1988. Petrology and oxygen-isotope geochemistry of a fossil seawater hydrothermal system within the Solea graben, northern Troodos Ophiolite, Cyprus. *Journal of Geophysical Research* **93**, 4612-4624.

Schilling, J. G., Zajac, M., Evans, R., Johnston, T., White, W., Devine, J. D., and Kingsley, R., 1983. Petrologic and geochemical variations along the Mid-Atlantic Ridge from 29° N to 73° N. *American Journal of Science* **283**, 510-586.

Searle, M., and Cox, J., 1999. Tectonic setting, origin, and obduction of the Oman ophiolite. *Geological Society of America Bulletin* **111**, 104-122.

Şengör, A. M. C., Natal'in, B. A., and Burtman, V. S., 1993. Evolution of the Altaid tectonic collage and Palaeozoic crustal growth in Eurasia. *Nature* **364**, 299-307.

Shervais, J. W., 1982. Ti-V plots and the petrogenesis of modern and ophiolitic lavas. *Earth and Planetary Science Letters* **59**, 101-118.

Shervais, J. W., 2001. Birth, death, and resurrection: The life cycle of suprasubduction zone ophiolites. *Geochemistry, Geophysics, Geosystems* **2**.

Shreve, R. L., and Cloose, M., 1986. Dynamics of Sediment Subduction, Melange Formation, and Prism Accretion. *Journal of Geophysical Research* **91**, 10229-10245.

Sinton, C. W., Duncan, R. A., and Denyer, P., 1997. Nicoya Peninsula, Costa Rica: A single suite of Caribbean oceanic plateau magmas. *Journal of Geophysical Research-Solid Earth* **102**, 15507-15520.

Stein, M., and Hofmann, A. W., 1994. Mantle Plumes and episodic crustal growth. *Nature* **372**, 63-68.

Stern, R. J., and Bloomer, S. H., 1992. Subduction zone infancy: examples from the Eocene Izu-Bonin-Mariana and Jurassic California arcs. *Geological Society of America Bulletin* **104**, 1621-1636.

Strating, E. H. H., 1991, The evolution of the Piemonte-Ligurian ocean. A structural study of ophiolite complexes in Liguria (NW Italy).: Geologica Ultraiectina, v. 74: Utrecht, The Netherlands, Utrecht, 127 p.

Sun, S. S., and McDonough, W. F., 1989, Chemical and isotopic systematics of oceanic basalts: implications for mantle composition and processes., *in* Saunders, A. D., and Norry, M. J., eds., Magmatism in ocean basins., London, Geological Society of London Special Publication 42, p. 313-345.

Takahashi, Y., and Oyungerel, S., 1997. Chemical features of the granitic rocks in central Mongolia - magmatic activity in the Palaeozoic. *Mongolian Geoscientist* **4**, 6-15.

Takahashi, Y., and Oyungerel, S., 1998. The granitoid series in the Bayankhongor area, central Mongolia. *Mongolian Geoscientist* .

Takahashi, Y., Oyungerel, S., Naito, K., and Delgertsogt, B., 1998a. Geology and magnetic susceptibility of the granitoids in Bayankhongor area, central Mongolia. *Mongolian Geoscientist* **7**, 10-19.

Takahashi, Y., Oyungerel, S., Naito, K., and Delgertsogt, B., 1998b. The granitoid series in Bayankhongor area, central Mongolia. *Bulletin of the Geological Survey of Japan* **49**, 25-32.

Takahashi, Y., Oyungerel, S., Naito, K., and Delgertsogt, B., 1998c. Mineralogical charactersitics of feldspars of the granitoids in Bayankhongor area, central Mongolia. *Bulletin of the Geological Survey of Japan* **49**, 439-446.

Tankut, A., Dilek, Y., and Onen, P., 1998. Petrology and geochemistry of the Neo-Tethyan volcanism as revealed in the Ankara melange, Turkey. *Journal of Volcanology and Geothermal Research* **85**, 265-284.

Tarney, J., and Marsh, N. G., 1991, Major and trace element geochemistry of holes CY-1 and CY-4: implications for petrogenetic models., *in* Gibson, I. L., Malpas, J., Robinson, P. T., and Xenophontos, C., eds., Initial reports of the Cyprus Crustal Study., Geological Survey of Canada, p. 133-176.

Taylor, S. R., and McLennan, S. M., 1981. The composition and evolution of the continental crust: rare earth element evidence from sedimentary rocks. *Philosophical transactions of the Royal Society* **A301**, 381-399.

Temple, P. G., and Zimmerman, J., 1969. Tectonic significance of Alpine ophiolites in Greece and Turkey. *Geological Society of America, annual meeting abstracts* , 221-222.

Teraoka, Y., Suzuki, M., Tungalag, F., Ichinnorov, N., and Sakamaki, Y., 1996. Tectonic framework of the Bayankhongor area, West Mongolia. *Bulletin of the Geological Survey of Japan* **47**, 447-455.

Thompson, A. B., 1999, Some time-space relationships for crustal melting and granitic intrusion at various depths, *in* Castro, A., Fernández, C., and Vigneresse, J. L., eds., Understanding Granites: Integrating New and Classical Techniques, Geological Society Special Publication No. 168, London, Geological Society, London, p. 7-26.

Tomlinson, K. Y., Hall, R. P., Hughes, D. J., and Thurston, P. C., 1996. Geochemistry and assemblage accreation of metavolcanic rocks in the Beardmore-Geraldton Greenstone belt, Superior Province. *Canadian Journal of Earth Sciences* **33**, 1520-1533.

Tomurtogoo, O., 1989, Ophiolites and Formation of Folded belts in Mongolia, Russian Acadamy of Sciences 59 p.

Tomurtogoo, O., 1997, A New Tectonic Scheme of the Paleozoides in Mongolia: Proceedings of the 30th international geological Congress, p. 75-82.

Tomurtogoo, O., Nakajima, T., Takahashi, Y., Minjin, C., Ichinnorov, N., and Oyungerel, S., 1998, Geological map L-47-XVI: Mineral resources Authoroty of Mongolia, Office of Geology, Bureau of geological investigation C.

Tungalag, F., 1996. Stratigraphy and Structural Geology of Precambrian and Palaeozoic Strata in Bayankhongor Area. *Mongolian Geoscientist* **1**, 4-11.

Ueda, H., Kawamura, M., and Niida, K., 2000. Accretion and tectonic erosion processes revealed by the mode of occurrence and geochemistry of greenstones in Createceous accretionary complexes of the Idonnappu Zone, southern central Hokkaido, Japan. *The Island Arc* **9**, 237-257.

von Blanckenburg, F., and Davies, J. H., 1995. Slab breakoff: a model for syncollisional magmatism and tectonics in the Alps. *Tectonics* **14**, 120-131.

Whalen, J. B., Currie, K. L., and Chappell, B. W., 1987. A-type granites: geochemical characteristics, discrimination and petrogenesis. *Contributions to Mineralogy and Petrology* **95**, 407-419.

White, R. S., Minshull, T. A., Bickle, M. J., and Robinson, C. J., 2001. Melt generation at very slow-spreading oceanic ridges: constraints from geochemical and geophysical data. *Journal of Petrology* **42**, 1171-1196.

White, W. M., McBirney, A. R., and Duncan, R. A., 1993. Petrology and geochemistry of the Galapogos Islands: portrait of a pathalogical mantle plume. *Journal of Geophysical Research Letters* **98**, 19533-19563.

Wilson, M., 1989, Igneous Petrogenesis: London, UK, Chapman & Hall, 441 p.

Windley, B. F., and Allen, M. B., 1993. Mongolian Plateau - Evidence For a Late Cenozoic Mantle Plume Under Central-Asia. *Geology* **21**, 295-298.

Wood, D. A., 1980. The application of a Th-Hf-Ta diagram to problems of tectonomagmatic classification and to establishing the nature of crustal contamination of basaltic lavas of the Britich Tertiary volcanic province. *Earth and Planetary Science Letters* **50**, 11-30.

Yu, D., Fontignie, D., and Schilling, J.-G., 1997. Mantle plume-ridge interactions in the Central North Atlantic: a Nd isotope study of Mid-Atlantic Ridge basalts from 30°N to 50°N. *Earth and PLanetary Science Letters* **146**, 259-272.

Zabotkin, L. B., 1988, Geological sheet map (L-47-XXIII and XXIV): Open file report in Geological Funds of Mongolia no. 4276.

Zen, E.-a., 1986. Aluminium enrichment in silicate melts by fractional crystallization: some mineralogical and petrographic constraints. *Journal of Petrology* **27**, 1095-1117.

Zorin, A. Y., Belichenko, V. G., Turutanov, E. K., Kozhevnikov, V. M., Ruzhentsev, S. V., Dergunov, A. B., Filippova, I. B., Tumortogoo, O., Arvisbaatar, N., Bayasgalan, T., Biambaa, C., and Khosbayar, P., 1993. The South Siberia-Central Mongolia Transect. *Tectonophysics* **225**, 361-378.

Zorin, Y. A., 1999. Geodynamics of the western part of the Mongolia-Okhotsk collisional belt, Trans-Baikal region (Russia) and Mongolia. *Tectonophysics* **306**, 33-56.

Journal of the Geological Society, London, Vol. **158**, 2001, pp. 445–460. Printed in Great Britain.

Structural and lithological characteristics of the Bayankhongor Ophiolite Zone, Central Mongolia

CRAIG BUCHAN[1], DICKSON CUNNINGHAM[1], BRIAN F. WINDLEY[1] & D. TOMURHUU[2]
[1]*Orogenic Processes Group, Geology Department, University of Leicester, University Road, Leicester LE1 7RH, UK (e-mail: acb19@le.ac.uk)*
[2]*Institute of Geology and Mineral Resources, Mongolian Academy of Sciences, 63 Enkh Taivan Avenue, PO Box 118, Ulaanbaatar 210351, Mongolia*

Abstract: The mechanism of continental growth of Central Asia is currently debated between models invoking continuous subduction–accretion, or punctuated accretion due to closure of multiple ocean basins. Ophiolites in Central Asia may represent offscraped fragments in an accretionary complex or true collisional sutures. The Bayankhongor ophiolite, a NW–SE-striking sublinear belt 300 km long and 20 km wide, is the largest ophiolite in Mongolia and possibly Central Asia. We present results of the first detailed structural and lithological study of the ophiolite. The study area is divided into four zones: Baidrag complex, Burd Gol, Bayankhongor, and Dzag zones. The Archaean Baidrag complex comprises tonalitic granulites and metasediments. The Burd Gol zone is a metamorphosed sedimentary and igneous mélange. The Bayankhongor zone contains the dismembered ophiolite forming a serpentinite mélange. The Dzag zone consists of asymmetrically folded chlorite–mica schists resembling meta-turbidites. The structure is dominated by steeply dipping, NE directed thrusts and NE-vergent folds. We suggest the Bayankhongor ophiolite marks the closure of an ocean separating two microcontinents: the Baidrag complex with the Burd Gol accretionary complex to the south, and a northern continent that forms the basement for the Hangai region. Subduction was towards the SW with NE-directed ophiolite obduction onto a passive margin represented by the Dzag zone.

Keywords: Mongolia, ophiolites, plate tectonics, Central Asian orogenic belt.

Central Asia is a collage of continental blocks, ancient island arc terranes, subduction complexes and fragments of oceanic crust that amalgamated during the late Precambrian, Palaeozoic and Mesozoic. Şengör *et al.* (1993) produced a regional tectonic synthesis of the basement geology of Western China, Kazakhstan, Mongolia and parts of Russia utilizing existing published information, and proposed a mechanism for continuous continental growth through subduction accretion and arc collision. They suggested that a subduction zone existed along the southern margin of the Angara craton (Fig. 1, inset) throughout the Palaeozoic era and that a vast complex of arc and subduction–accretion material including offscraped ophiolitic fragments accumulated in front of seaward-migrating magmatic fronts. In contrast, Coleman (1989) and Hsü *et al* (1991) identified distinct ophiolite belts in northwestern China, which they interpreted as discrete suture zones separating different Palaeozoic blocks. These models differ in that the former invokes steady state subduction–accretion over a prolonged period of time, whereas the latter favours punctuated accretion by collision and closure of multiple ocean basins now marked by ophiolitic sutures. Mossakovsky *et al.* (1994) proposed a model for Central Asia whereby the early stages of continental growth were dominated by arc development and accretion and the late stages by collision of accreted continents. In order to understand how the bulk of the continent of Asia was formed, it is essential to work out the tectonic significance of the Central Asian ophiolites and their role in the continental accretion process.

Mongolia presents an exceptional opportunity to examine this problem because it lies centrally within this collage (Fig. 1, inset) and contains some of the best preserved Palaeozoic ophiolitic rocks in Central Asia with over 60 reported separate occurrences (Fig. 2). Despite their abundance, few Mongolian ophiolites have been studied using modern structural techniques and important questions remain regarding their internal structures, mechanism of emplacement and overall tectonic significance. Here we present results of a detailed structural study of the Bayankhongor ophiolite, the longest continuously exposed ophiolite belt in Mongolia and possibly all of Central Asia.

Regional geology

The basement geology of Mongolia comprises tectonostratigraphic terranes between the major Precambrian cratonic blocks of Angara, North China and Tarim (Fig. 1; Şengör *et al.* 1993; Zorin *et al.* 1993; Mossakovsky *et al.* 1994; Dobretsov *et al.* 1995). These terranes form gently curving, NW-SE striking belts in the west and south of Mongolia and a less ordered mosaic pattern in the central and northern provinces around the Hangai region (Fig. 1; Mossakovsky *et al.* 1994; Zorin *et al.* 1993). A generally accepted concept is that accretion progressed southwards through time (Mossakovsky & Dergunov 1985; Şengör *et al.* 1993; Mossakovsky *et al.* 1994; Dobretsov *et al.* 1995). This interpretation has traditionally led to the basement geology being divided into three belts according to their time of accretion: the Baikalian, Caledonian and Variscan (Mossakovsky & Dergunov 1985; Mossakovsky *et al.* 1994). However, some workers are reluctant to use divisions that refer to European orogenic events and which are poorly constrained by existing age data. Another problem is

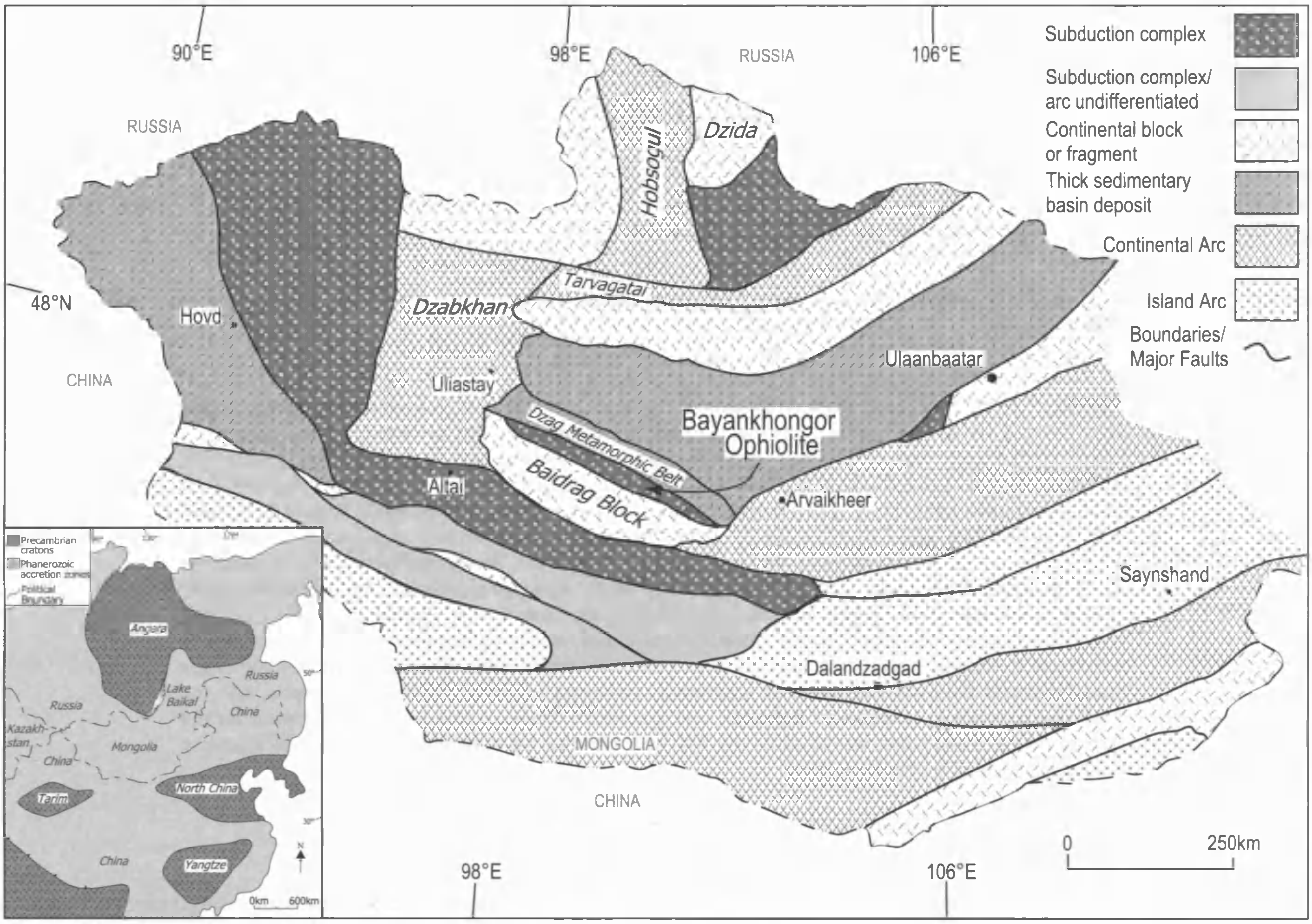

Fig. 1. Major terranes of central and western Mongolia from Dorjnamjaa *et al.* (1998). Position of the Bayankhongor ophiolite zone is indicated. Inset map shows Mongolia's position in Central Asia and locations of major Precambrian cratons.

that past studies have tended to identify all high-grade metamorphic terranes in Mongolia as Precambrian without supporting isotopic evidence (e.g. Barsbold & Dorjnamjaa 1993). Thus some authors have interpreted disparate regions containing crystalline basement (Baidrag, Dzabkhan, Tarvagatai, Hobsogul and Dzida blocks) to be part of a larger Precambrian terrane called the Tuva–Mongolian microcontinent (Fig. 1; Mossakovsky & Dergunov 1985; Şengör *et al.* 1993; Zorin *et al.* 1993; Mossakovsky *et al.* 1994; Dobretsov *et al.* 1995; see Lamb & Badarch 1997 for more discussion). However, Didenko *et al.* (1994) suggested that these blocks are separate units which were brought together during the Palaeozoic and this model is partly supported by recent U–Pb zircon dating of samples from the northern section of the Tuva–Mongolian microcontinent located in Tuva, south Siberia by Kozakov *et al.* (1999*a*, *b*) who showed that the earliest deformation in the basement rocks here occurred in the early Cambrian around 536 ± 6 Ma rather than in the Precambrian as previously assumed. However, despite these results, there are some proven Precambrian continental blocks in Central Mongolia such as the Baidrag massif which lies to the SW of the Bayankhongor ophiolite zone (Fig. 1) and which has yielded U–Pb zircon ages of 2646 ± 45 Ma and 1854 ± 5 Ma (Mitrofanov *et al.* 1985; Kozakov 1986; Kotov *et al.* 1995). From cross-sections compiled from a geological and geophysical transect across Central Mongolia, Zorin *et al.* (1993) suggested that continental crust, probably Precambrian in age, is also present below the thick sedimentary cover of the Hangai region to the NE of the Bayankhongor ophiolite. Kovalenko *et al.* (1996) published an array of Sm–Nd model ages from Phanerozoic granites in the Hangai region, which range from T_{DM}=1058 Ma to T_{DM}=2154 Ma. Because the granites have negative ε_{Nd} values, Kovalenko *et al.* (1996) argue that they are sourced from melting of continental crust below the Hangai region whose minimum age is given by the model ages.

The Bayankhongor ophiolite zone (Figs 1 & 2) is situated on the southern side of the Hangai mountains which formed during regional Cenozoic doming (Windley & Allen 1993; Barry & Kent 1998; Cunningham 1998). The ophiolite forms a NW–SE-striking sub-linear zone approximately 300 km long and up to 20 km wide (Figs 1 & 2) exposed continuously from just west of the town of Dzag to just east of Bayankhongor City (Fig. 2b). Uplift and erosion along the southern flank of the dome has resulted in good exposure of the ophiolite belt. Previous lithological mapping enables a four-fold tectonic subdivision of the region from south to north: the Baidrag complex, Burd Gol mélange, Bayankhongor zone and Dzag zone (Fig. 1; Teraoka *et al.* 1996; Tomurtogoo *et al.* 1998).

The Archaean Baidrag complex, composed of tonalitic gneiss, granulite and amphibolite, with minor marble and quartzite, has been interpreted as a microcontinental block (Mitrofanov *et al.* 1985; Kozakov 1986; Kozakov *et al.* 1997).

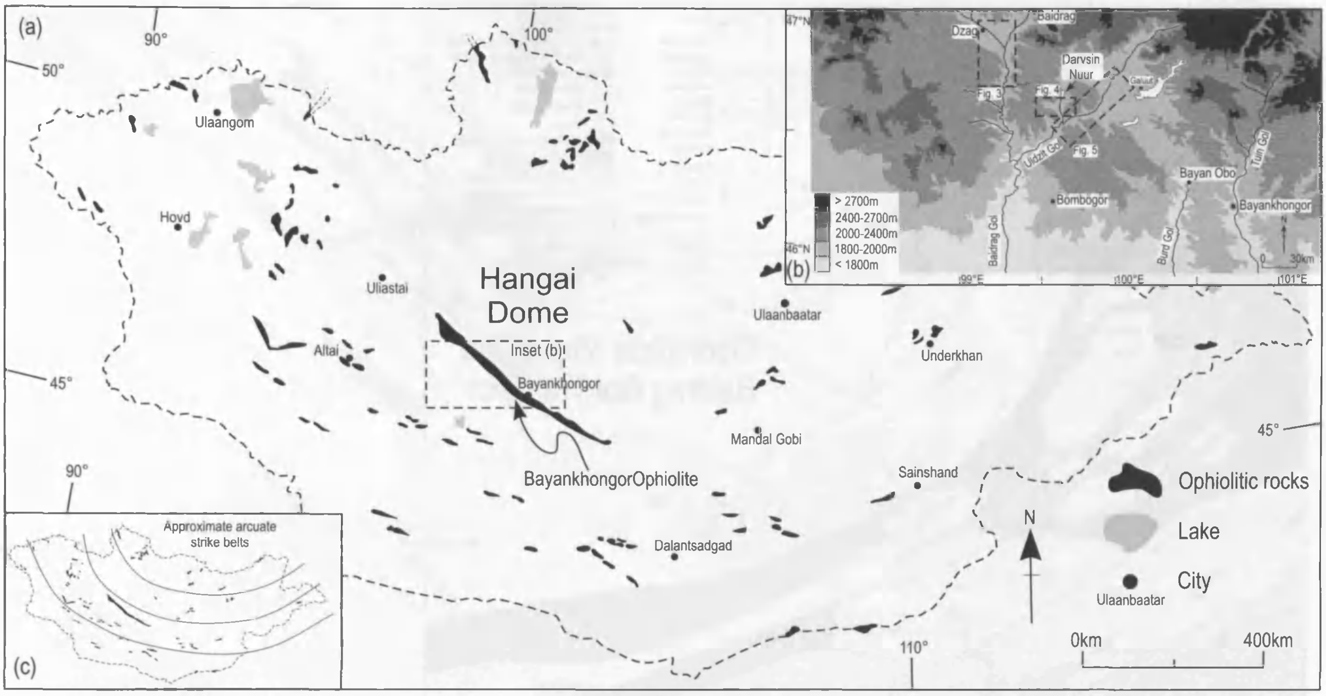

Fig. 2. (**a**) Ophiolite occurrences in Mongolia. The Bayankhongor ophiolite is the largest in the region. (**b**) Topography of the Bayankhongor area. Locations of transects and Figures 3–5 shown. (**c**) Map showing general structural trends of basement rocks in Mongolia.

The Burd Gol zone is a tectonic mélange containing lenses of sedimentary and igneous rocks cut by abundant quartz veins. From palaeontological dating of stromatolites in limestone lenses, Mitrofanov *et al.* (1981) suggested that the Burd Gol mélange has a late Precambrian age. Within the mélange, metamorphic grade increases towards the north. North of the Burd Gol zone there is a small area of interbedded marine mudstone and limestone which reportedly contain Carboniferous fossils (Dergunov *et al.* 1997).

The Bayankhongor zone contains three sub-units, here named the Delb Khairkhan mélange, ophiolite mélange and Haluut Bulag mélange. The Delb Khairkhan mélange lies to the south of the ophiolite and contains sedimentary and volcanic rocks of Precambrian to Ordovician age (Ryantsev 1994; Dergunov *et al.* 1997). The ophiolite mélange is composed of a complete ophiolite stratigraphy (Moores 1982), dated at 569 ± 21 Ma (Sm–Nd hornblende and whole-rock isochron on gabbro; Kepezhinskas *et al.* 1991) dismembered into blocks enclosed within a serpentinite matrix. The Haluut Bulag mélange is dominantly sedimentary with lenses of bedded limestone, sandstone, siltstone, and locally vesicular basalt, enclosed in a matrix of pelitic schist.

The Dzag zone consists of asymmetrically folded chlorite–mica schists that locally contain relict sedimentary features suggesting they are meta-turbidites.

Transect data

In the summers of 1997 and 1998, three cross-strike geological transects were carried out through the Bayankhongor ophiolite (including Delb Khairkhan and Haluut Bulag mélanges) and adjacent Dzag and Burd Gol zones (Figs 3–5). The transects along the Baidrag Gol south of Darvsin Nuur and along the Uldzit Gol, were chosen because of the deep incision and excellent exposure created by these river systems (Fig. 2b). Fieldwork focused on documenting stratigraphic and metamorphic relations, internal structures and structural evolution of the ophiolite and adjacent lithological units. Reconnaissance was also carried out in other areas within the Bayankhongor Zone in order to gain a wider understanding of along-strike variations and to fully characterize the Dzag and Burd Gol zones.

Major lithotectonic units

The study area is divided into six major lithotectonic units: Burd Gol mélange, Carboniferous sedimentary rocks and volcanic sequence, Delb Khairkhan mélange, ophiolitic rocks, Haluut Bulag mélange, and Dzag Zone which are juxtaposed along NE–SW-trending, NE-vergent thrust faults (Figs 3–5). In this section we describe the important lithological characteristics of each unit.

Burd Gol mélange

The contact of the Burd Gol mélange with the Baidrag block to the south is observed SW of the town of Bömbögör (Fig. 2b, N46°16.962′, E99°32.360′), where granitic gneisses of the Baidrag block are overlain unconformably by a series of thick quartzites and sandstones which comprise the southernmost section of the Burd Gol mélange. The foliation in the Baidrag gneisses dips steeply NW and the Burd Gol mélange rocks dip shallowly NE. Detailed descriptions of the Archaean Baidrag complex can be found in Kozakov (1986) and Kozakov *et al.* (1997). A few kilometres NE of the contact, the Burd Gol mélange becomes more mixed with lenses of sedimentary and igneous lithologies enclosed in a black schist matrix. Andesitic dykes, which cut the foliation are dismembered and surrounded by a matrix of graphitic schists. A more detailed study

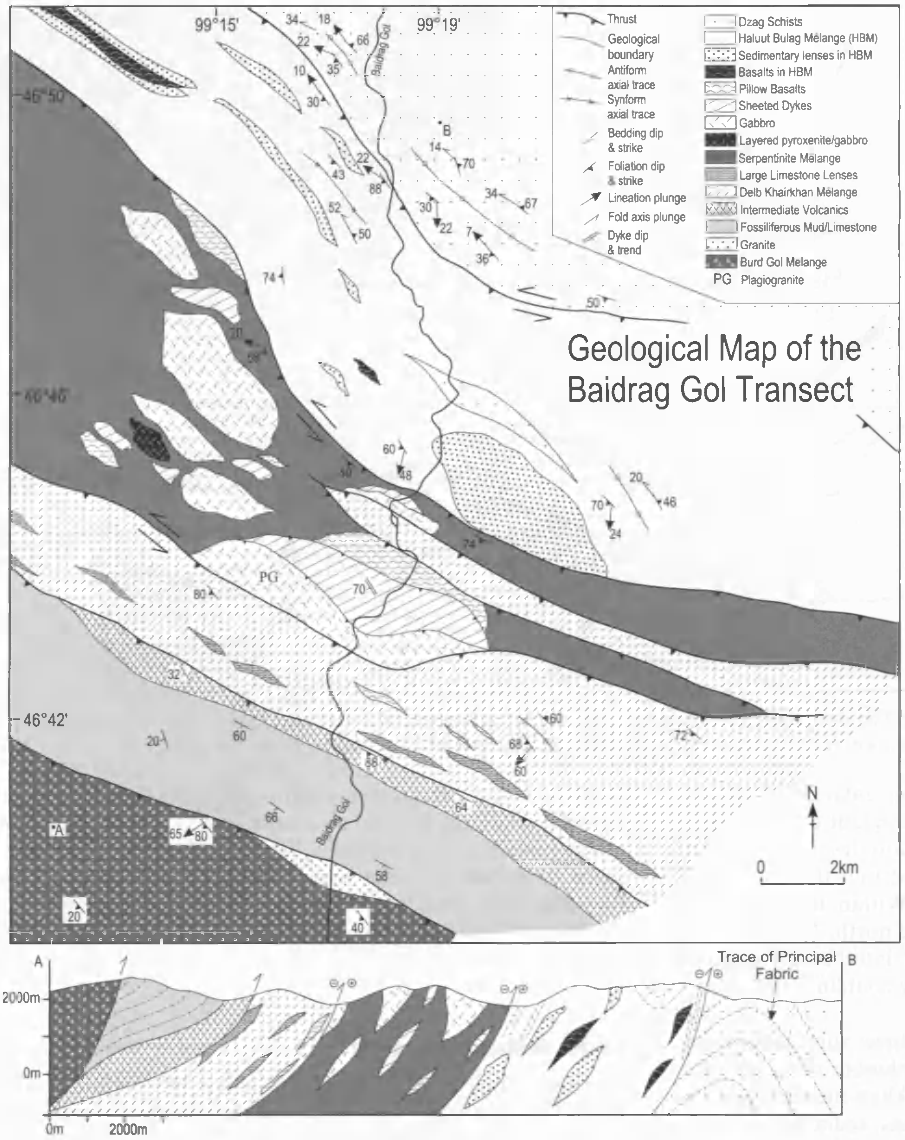

Fig. 3. Geological map and cross section of the Baidrag Gol (*River*) transect. See Figure 2b for location.

of the Burd Gol mélange was carried out to the NW of Bömbögör (Fig. 2b, N46°19.785′ E99°36.017′) where numerous, variably oriented quartz veins up to 4 m wide cut the mélange. The veins are locally gold-bearing (Komarov *et al.* 1999). Teraoka *et al.* (1996) obtained a K–Ar age of 699 ± 35 Ma from muscovite from the black schists. To the north of these black schists, many igneous and sedimentary lenses several hundred metres across are enclosed in a black schist matrix. The sedimentary lenses are composed of limestone, sandstone, siltstone, mudstone, shale, chert and well-bedded calci-turbidite. These lenses contain internal deformation which appears to have formed before incorporation into the mélange matrix, because proximal blocks of the same lithology contain dismembered folds. Igneous lithologies include basalt, gabbro, dolerite, andesite and rare rhyolite.

The Uldzit Gol transect contains particularly good exposures of the Burd Gol mélange that demonstrate that the mélange matrix is metamorphically zoned with classic Barrovian facies (Fig. 5). Over a distance of approximately 6 km, grades increase northwards reaching amphibolite facies at the thrusted contact with the Carboniferous sedimentary rocks. This is indicated by metamorphic assemblages that contain cleavage forming biotite and biotite porphyroblasts up to 1 cm in size in the south whereas northwards, the schists become garnet–biotite–muscovite-bearing with abundant euhedral, syntectonic garnets (5 mm), and then staurolite–muscovite–biotite schists. The staurolites form 1 cm wide and up to 3 cm long euhedral porphyroblasts. These are the highest-grade assemblages observed in this study, but Dergunov *et al.* (1997) reported sillimanite and Komarov *et al.* (1999) reported kyanite and sillimanite from the same unit. Possible kyanite pseudomorphs were observed, but contact metamorphism, caused by a local granite intrusion, may have overprinted any higher-grade metamorphic assemblage. Takahashi & Oyungerel (1997, 1998) determined K–Ar ages ranging from 551 Ma to 467 Ma on biotite and muscovite from granite plutons in the Uldzit Gol area, which they interpreted to represent the crystallization age. However, because these granites are tectonically foliated, we suggest that the younger ages may be due to younger metamorphic events. Local amphibolite bodies and mélange schists near the granite intrusion, contain a contact overprint texture with 5–10 cm acicular

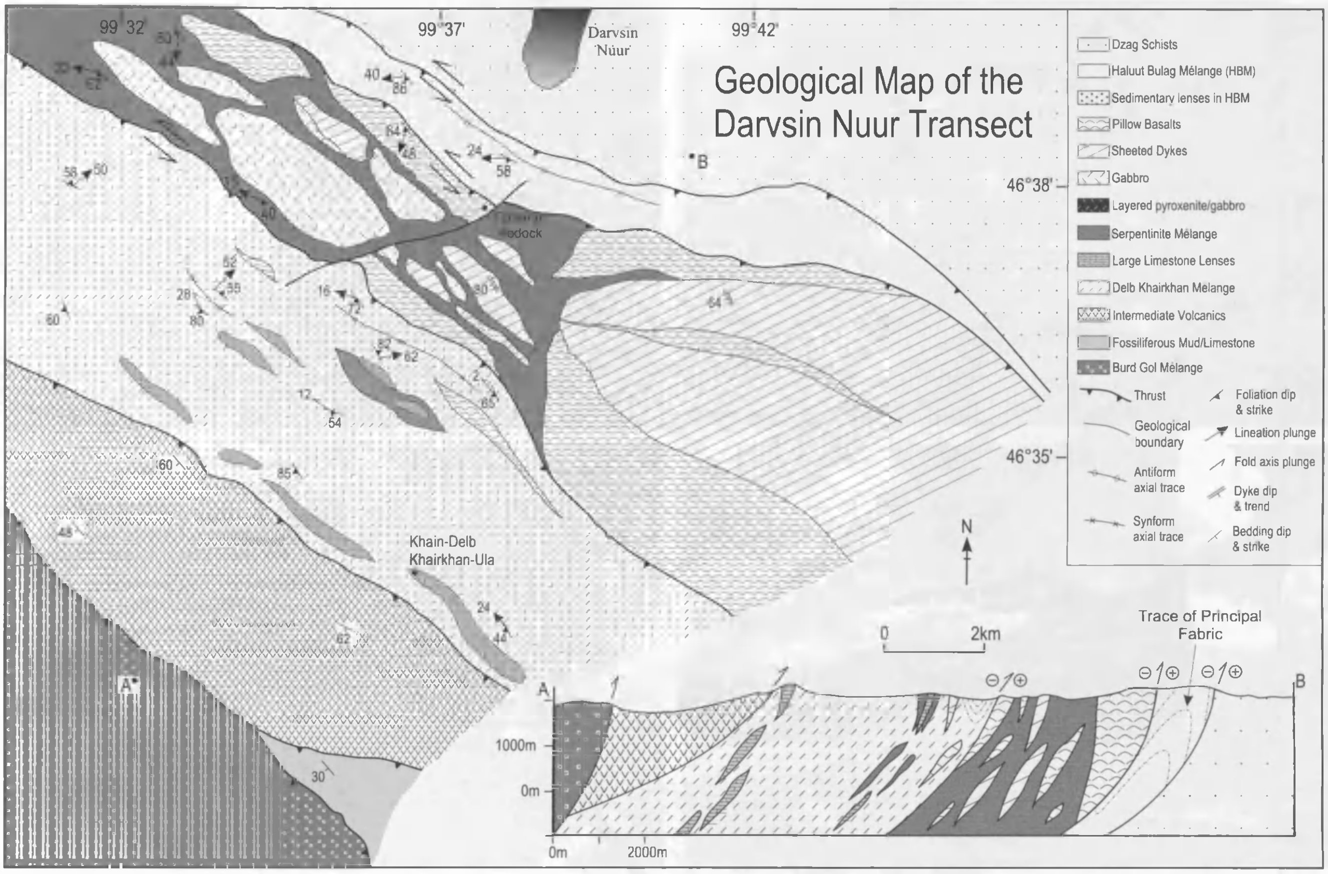

Fig. 4. Geological map and cross section of the Darvsin Nuur (*Lake*) transect. See Figure 2b for location.

bow-tie hornblende crystals overprinting the primary schistosity. The amphibolites form sheet-like bodies but it is unclear whether they were originally lava flows or dykes since they are dismembered and surrounded by the pelitic schists of the mélange.

Carboniferous sedimentary rocks and volcanic sequence

To the north and NE of the Burd Gol mélange, there are interbedded green Carboniferous fossiliferous marine mudstones and limestones (Figs 3–5), which contain abundant, well-preserved brachiopods, bryozoans, crinoids and corals (Tungalag 1996; Dergunov *et al.* 1997). The sedimentary rocks are well bedded and dominated by mudstones with beds 2–5 m thick. The limestone beds vary from a few centimetres to about 3 m thick and occur locally and discontinuously. These are the youngest known rocks in the study area.

The Carboniferous sedimentary rocks lie unconformably on (Fig. 3), or in thrust contact with (Figs 4 & 5), a sequence of extrusive volcanic rocks and minor sedimentary rocks which have been variously assigned to the Ordovician (Dergunov *et al.* 1997) or Devonian periods (Tungalag 1996) based on palaeontological evidence and correlation with similar units elsewhere. The volcanic strata consist of sheet-like flows of andesite, dacite, basalts, and trachybasalts that are interbedded with agglomerates and tuffs. There are also small intrusive bodies of quartz–plagioclase porphyry. Dacites and agglomerates are the most abundant lithologies. The agglomerates contain 2–5 cm angular fragments of nearly all other volcanic rocks, enclosed in a fine groundmass dominated by plagioclase. Individual flows vary in thickness from about 1 m to 15 m. Stratigraphically above these volcanic and plutonic rocks is a thin conformable sequence (5–10 m) of volcanogenic conglomerate and sandstone.

Delb Khairkhan mélange

The Delb Khairkhan mélange contains mixed lenses of igneous and sedimentary rocks enclosed in a matrix of pelitic schist. Along the southern boundary of the mélange in the Baidrag Gol and Uldzit Gol transects, igneous rocks seemingly derived from the volcanogenic sequence to the south, consisting of quartz–plagioclase porphyry, dacite and volcanogenic conglomerates and sandstones are included in the mélange. On the north side of the mélange near its contact with the ophiolitic sequence, lenses of gabbro, dolerite and pillow basalts several hundred metres long and 20–30 m wide resemble those in the ophiolite (Figs 3 & 4). In addition to the volcanogenic sedimentary rocks, there are lenses of limestone, quartzite, shale and sandstone. Along the contact with the volcanic rocks there is a prominent ridge of limestone that continues in en-echelon segments along strike to the east for several hundred kilometres (Figs 3–5). The ridge limestone is interbedded with shales and mudstones, bedding dips SW and the unit has a maximum thickness of around 1 km. Similar limestones occur as smaller lenses throughout the mélange.

The ridge limestones contain abundant well-preserved stromatolites. These stromatolites have been identified as *Conofiton gargantuous* by Boishenko (1979) and interpreted as late Precambrian in age (Riphean stage in Russian terminology).

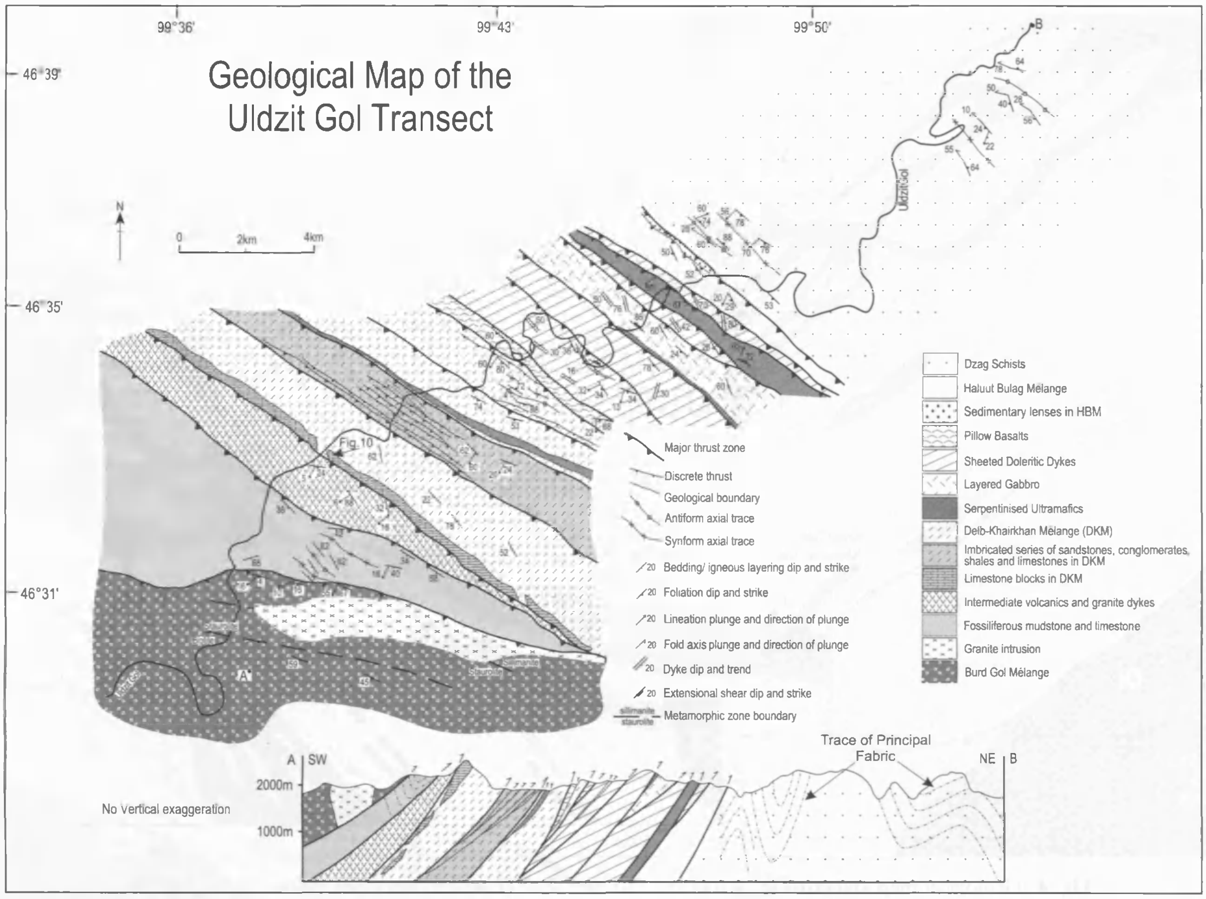

Fig. 5. Geological map of the Uldzit Gol transect. See Figure 2b for location. Note that the Delb Khairkhan mélange is subdivided into smaller lithological groups to highlight the imbricate structure that occurs where mechanically weak matrix is subordinate to rigid coherent blocks. This structural relationship is unique to this transect.

Ophiolitic rocks

The ophiolitic rocks comprise a complete ophiolite stratigraphy (Moores 1982): i.e. ultramafic cumulates, gabbro, sheeted dykes, pillow lava and local chert and limestone. However, the ophiolite is dismembered into blocks, which vary in the completeness of their internal stratigraphy (Figs 3–5). These blocks are enclosed in a matrix of sheared, serpentinized ultramafic rocks and thus the entire sequence constitutes another mélange. The composition of the mélange varies along strike. In the NW, the sequence is dominated by blocks of gabbro, poorly preserved pyroxenite and pillow basalt surrounded by serpentinite, whereas in the SE it is dominated by pillow basalt and sheeted dyke lenses (Figs 3–5). In the east of the Darvsin Nuur transect and throughout the Uldzit Gol section, the mélange has less serpentinite matrix and is dominated by thrust imbricated blocks of upper ophiolite stratigraphy (Figs 4 & 5).

Gabbro blocks (Fig. 6a) have metre-scale compositional layering (pyroxenite to leucogabbro) and crystal size layering on tens of metre scale. Generally (with the exception of local pyroxenite-dominated bodies; Fig. 3) gabbro lenses are derived from the top of the cumulate section near the sheeted dyke transition because numerous doleritic dykes and sills crosscut cumulate layering. The dykes consistently strike between 280° and 300° and dip steeply NE. One gabbro block (PG on Fig. 3) located on the southern boundary with the Delb Khairkhan mélange in the Baydrag Gol transect contains several plagiogranite dykes 1–1.5 m thick discordant to the cumulate layering of the gabbro.

On the eastern bank of the Uldzit Gol, a gabbro block has graded layers that become particularly leucocratic reaching near-anorthositic compositions. Kepezhinskas *et al.* (1991) produced a Sm–Nd whole rock and mineral isochron age of 569 ± 21 Ma for this unit, which they interpreted to be the crystallization age.

The sheeted dyke complex is very well preserved and demonstrates clear dyke-in-dyke relationships (Fig. 6b). There are two different types of dykes in the study area, plagiophyric and aphyric (Ryantsev 1994; Dergunov *et al.* 1997). The plagiophyric dykes are on average 2–3 m wide and are characterized by large (3–5 cm) plagioclase phenocrysts, which are concentrated in the centre of the dykes. The aphyric variety are around 1 m wide and have a more typical doleritic composition and texture. In addition, the aphyric dykes are often slightly discordant to the plagiophyric ones suggesting that they may be derived from a different generation of magma.

The boundary between the sheeted dykes and pillow lavas is tectonic (Figs 3–5), and because of shearing, the pillow basalts are locally poorly preserved. Aphyric (Fig. 6c) and plagiophyric pillow basalts are present and are mineralogically and texturally similar to the sheeted dykes. These similarities suggest that dykes intruding the pillow section represent the feeding conduits for successive flows. Multiple flows are

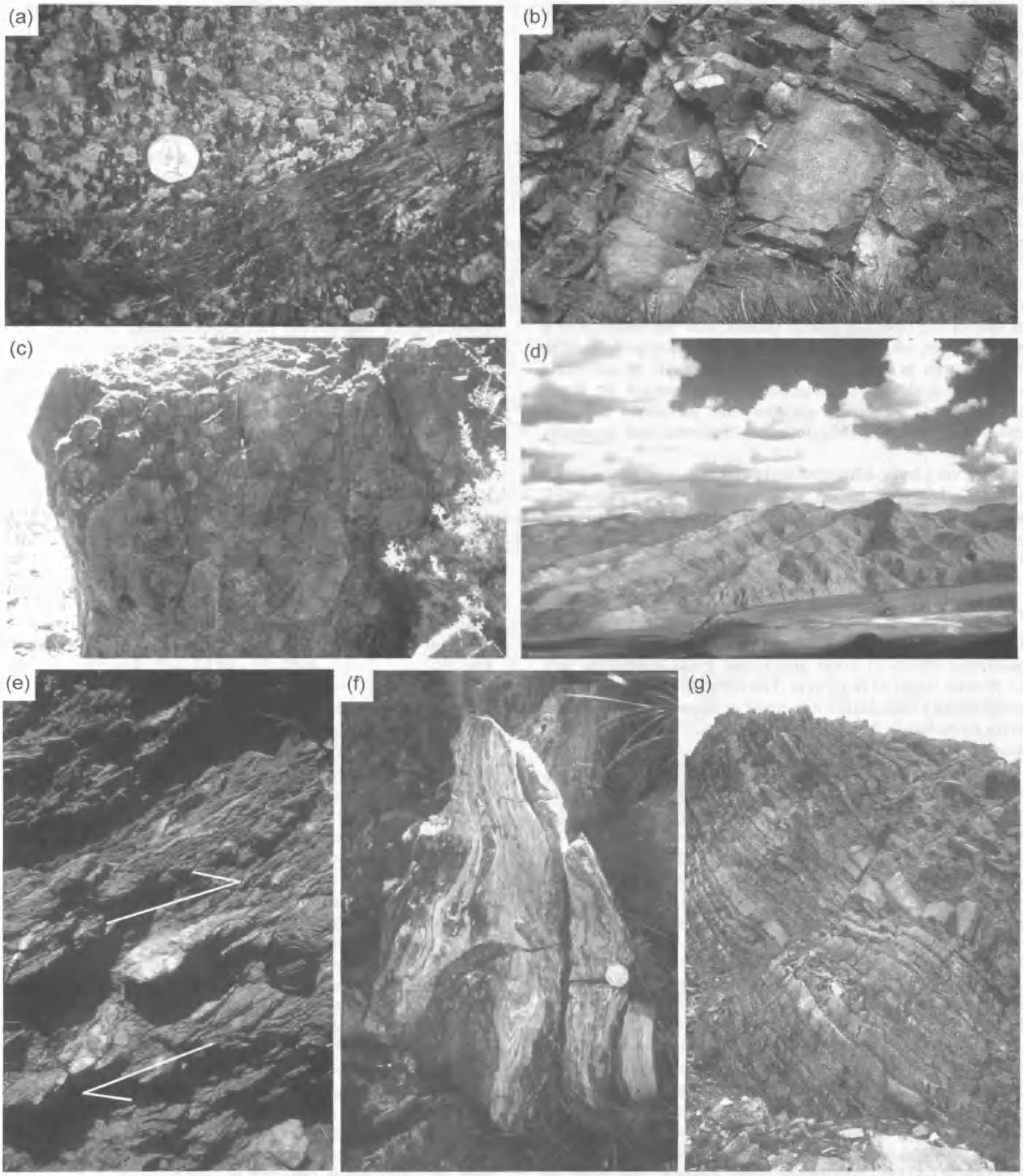

Fig. 6. Photographs illustrating typical lithologies of major tectonic units. (**a–c**) Ophiolitic rocks: (**a**) gabbro with a small ductile shear zone, (**b**) sheeted dykes (**c**) aphyric pillow basalt, (**d**) View looking east of bedded sedimentary rocks in the Haluut Bulag mélange. The darker rocks in the centre are interbedded basaltic lavas, (**e**) View looking NW of asymmetric calcite boudin in the Dzag zone suggesting top-to-the-NE shear. (**f–g**) Burd Gol mélange: (**f**) SE view of deformed limestone surrounding fragments of basalt, (**g**) calc-turbidite beds looking SE.

separated by zones of pillow breccia. The pillow lavas show considerable hydrothermal alteration with epidote veining and epidotization of some pillows.

On the western bank of the Uldzit Gol (Fig. 5; N46°33.640′, E99°43.625′) outcrops of well-preserved pillow basalts contain inter-pillow limestone and chert, and are locally overlain by bedded black chert and limestone. This is the only location where bedded sedimentary rocks were observed to be in direct contact with the pillow basalts. Neither the cherts nor the limestones were found to contain fossils, but Ryantsev (1994) reported lower Cambrian sponge spicules from the same unit.

Haluut Bulag mélange

The Haluut Bulag mélange is dominated by sedimentary lithologies. However, these lithologies are different from those of the Delb Khairkhan mélange, suggesting that the constituent lithologies of the two mélanges formed in different environments. The Haluut Bulag mélange contains lenses of limestone, sandstone, chert, tuff, minor acid volcanic material, and vesicular basalt. The basalts have a different composition to that of the ophiolite pillow basalts, that are enclosed in a pelitic matrix, which is itself lithologically heterogeneous. The matrix varies in composition from black shale to carbonate mudstone and quartzose siltstone. The matrix is metamorphosed to low-grade phyllite that surrounds coherent lenses that are commonly intensely fractured and internally brecciated.

Some very large kilometre-scale blocks within the mélange in the Baidrag Gol transect, contain interbedded basalt, mudstone and limestone, with a shallow NE dip (Fig. 6d). These large blocks dominate the NW margin of the mélange for 12 km along strike at the contact zone with the Dzag zone.

Dzag zone

The Dzag zone is composed of highly deformed pelitic and psammitic schists of lower greenschist grade containing rare 0.5 m wide layers of limestone. The composition of the schists varies slightly with higher muscovite contents occurring in the south immediately below the thrusted contact with the Haluut Bulag mélange.

Less metamorphosed fine-grained interbedded siltstones, sandstones and shales contain rounded quartz grains and preserved sedimentary structures and resemble slightly metamorphosed turbidites. Cleavage generally overprints and obscures primary bedding. However, approximately 5 km to the north of the town of Dzag (Fig. 2b), outcrops of the Dzag schists contain reasonably preserved pebbles of sandstone and siltstone despite penetrative cleavage development. Reconnaissance to the north of Dzag showed that the Dzag schists continue northeastwards over a cross-strike width of at least 10 km consisting of chlorite–muscovite schists in which the amount of chlorite relative to muscovite increases, in a northwards direction, away from the thrust contact to the south.

Kurimoto *et al.* (1998) obtained a K–Ar date of 453.9 ± 9.1 Ma on white mica from a locality on the east side of the Baidrag Gol (N46°45.93′, E99°26.98′) close to the contact between the Dzag zone and the Haluut Bulag mélange and produced a second date of 447.4 ± 9.0 Ma from a second sample of Dzag schists near Bayan Obo village (N46°19.88′, E100°14.50′). They interpreted these dates to represent an Ordovician regional metamorphic event.

Structural characteristics

Despite the general continuity of lithotectonic units in the study area, the structural architecture of the Bayankhongor zone is complex and changes along strike. In this section we describe detailed structural observations from each of the three transects from west to east followed by observations made during reconnaissance mapping in areas to the east near Bayankhongor City.

Baidrag Gol transect

Burd Gol mélange. The foliation in the matrix of the Burd Gol mélange dominantly dips shallowly (between 20° and 40°) south to SW but is locally folded into gentle NE-vergent asymmetric folds. The folding becomes more intense and foliation in the matrix dips more steeply (80°) towards the unit's northern contact which is a thrust fault that places the mélange over Carboniferous marine mudstones to the north (Fig. 3).

Carboniferous sedimentary rocks and volcanic sequence. Bedding in the Carboniferous rocks dips moderately to the SW (40–60°; Fig. 3) and contains evidence of brittle fracturing and brecciation. In this transect, the contact between the Carboniferous strata and the volcanic sequence appears to be an unconformable sedimentary contact (Fig. 3).

The dip of flows in the volcanic sequence varies from about 60°SW to sub-vertical close to the contact with the Delb Khairkhan mélange to the north (Fig. 3). A weak shear fabric occurs preferentially along the chilled margins between successive flows and is most strongly developed near the thrusted contact between the volcanic rocks and the Delb Khairkhan mélange to the north. The foliation dips steeply to the SW, has a down-dip lineation, and C–S fabrics suggest top-to-the-NE shearing i.e. the volcanic sequence has been transported over the Delb Khairkhan mélange to the north (see cross section in Fig. 3).

Delb Khairkhan mélange. The structure of the Delb Khairkhan mélange is very complex. Foliation in the matrix generally dips between 40° and 80°SW, but locally is vertical or dips steeply NE. Foliation generally strikes NW–SE, but is locally deflected around more competent lenses that are elongate parallel to strike. Small-scale folds of the foliation with fold axes trending NW and axial planes dipping SW occur locally (Figs 3 & 7).

Quartz and chlorite stretching lineations show two major trends, either down dip to the SW or sub-horizontal plunge to the west or NW, i.e. along strike (Fig. 7). SW lineations are most common. Asymmetric quartz boudins and rotated lithic clasts observed parallel to SW-trending lineations suggest top-to-the-NE movement, whereas shear sense where sub-horizontal lineations predominate is top-to-the-SE or sinistral sense. Within the pervasively sheared mélange matrix, there are discrete zones of more concentrated shearing and brittle crushing. These high strain zones are marked by 20–30 m wide belts in which the matrix rocks have been fractured to form gouge-like clay, which contains a sub-vertical fabric. Slickensides trend around 285° with a near horizontal plunge. C–S fabrics parallel to the slickensides again suggest top-to-ENE movement. The boundary of the Delb Khairkhan mélange with the ophiolite is complex in this transect; it has an 'S' shaped map view (Fig. 3), reflecting repetition caused by thrust imbrication.

Ophiolitic rocks. The ophiolitic mélange in the Burd Gol transect contains many large blocks and some near complete sections of ophiolite stratigraphy (Fig. 3). The largest blocks are at least 4 km long, and 2 km wide (Fig. 3) and the smallest are centimetre scale. Most of the larger blocks are composed of

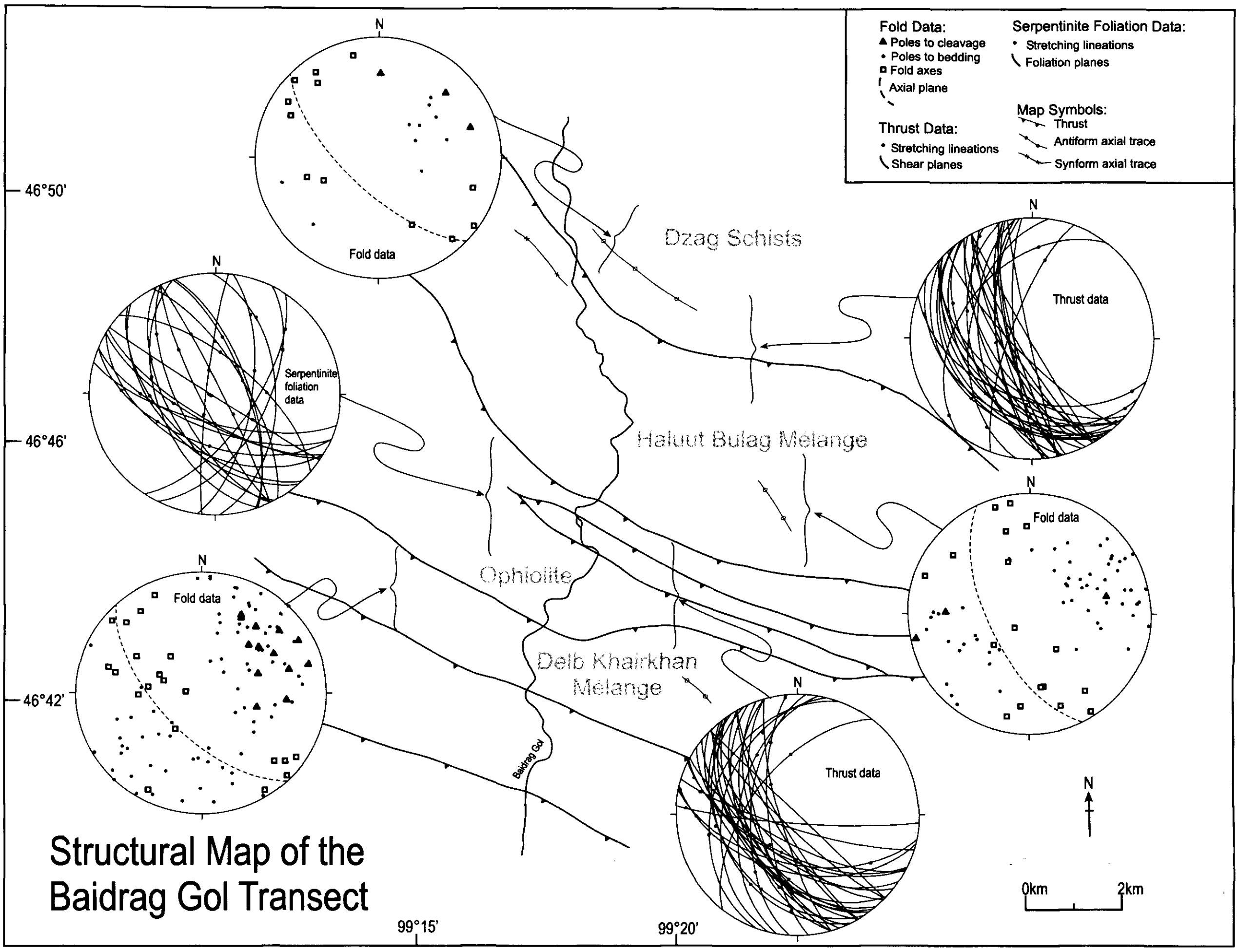

Fig. 7. Structural data from the Baidrag Gol transect. Fold data indicate SW-dipping axial planes consistent with NE-vergent thrusting. Shallow stretching lineations to WNW or NW, shown on thrust data plots, are consistent with shear sense criteria which suggest a sinistral strike slip component to the deformation. Foliation in the serpentinite mélange dips SW and ENE dips about a vertical axis due to fabric divergence around rigid lenses in the mélange, rather than folding. Lower hemisphere, equal area stereoplots. Refer to Figure 3 for lithological relations.

gabbro with cumulate layering dipping gently to the SW, but the dip direction is inconsistent in smaller blocks suggesting that these have been rotated during shearing.

A more complete ophiolite section crosses the Baidrag Gol (Fig. 3), the lowest unit is gabbro which contains an increasing number of doleritic dykes towards the north, culminating in local occurrences of sheeted dykes. However, the boundary between the gabbro–dyke unit and the sheeted dyke complex is tectonic (dipping SW) with the gabbro thrust over the sheeted dykes (Fig. 3). Although the general stratigraphic sequence has remained intact, the boundaries between units are sheared.

The sheeted dykes have trends consistent with dykes in the gabbro of between 280° and 300°, and dip to the SW (Fig. 3). Local shearing, with a SW dipping foliation, along the chilled margins of some individual dykes has produced internal breccias distorting the dyke-in-dyke relationships.

The serpentinite matrix forms low-lying easily eroded topography. The foliation in the serpentinite matrix dips steeply (60–90°) to the SW or NE fanning around a vertical axis along strike. We interpret this to be due to the foliation diverging around rigid lenses as no evidence for folding was observed (Figs 3 & 7). Lineations are difficult to detect; the few that were observed are generally expressed by chlorite accumulations on shear surfaces and record variable directions (Fig. 7).

The overall width of the serpentinite mélange is variable along strike in the Baidrag Gol transect. Towards the west, the width of the belt increases to more than 15 km (Fig. 3). However, to the east the width narrows to about 1–2 km.

The contact between the serpentinite mélange and the Haluut Bulag mélange to the north is not well exposed due to low topography and grass cover. However, it is probably tectonic because foliation intensity increases towards the contact.

Haluut Bulag mélange. The matrix structure of the Haluut Bulag mélange is dominated by a well-developed SW-dipping shear fabric (Fig. 7) that is locally folded into NE-vergent asymmetric folds (Fig. 7), and a second weak cleavage is developed axial planar to these folds. Locally, the fold hinges become rotated due to development of minor orthogonal shears in the matrix causing it to be broken into blocks. Chlorite and biotite stretching lineations on the foliation planes trend either down-dip to the SW or oblique to the west and NW. C–S fabrics, rotated quartz clasts and asymmetric boudins in shear zones suggest top-to-the-NE shear sense consistent with that documented previously in the Delb Khairkhan mélange.

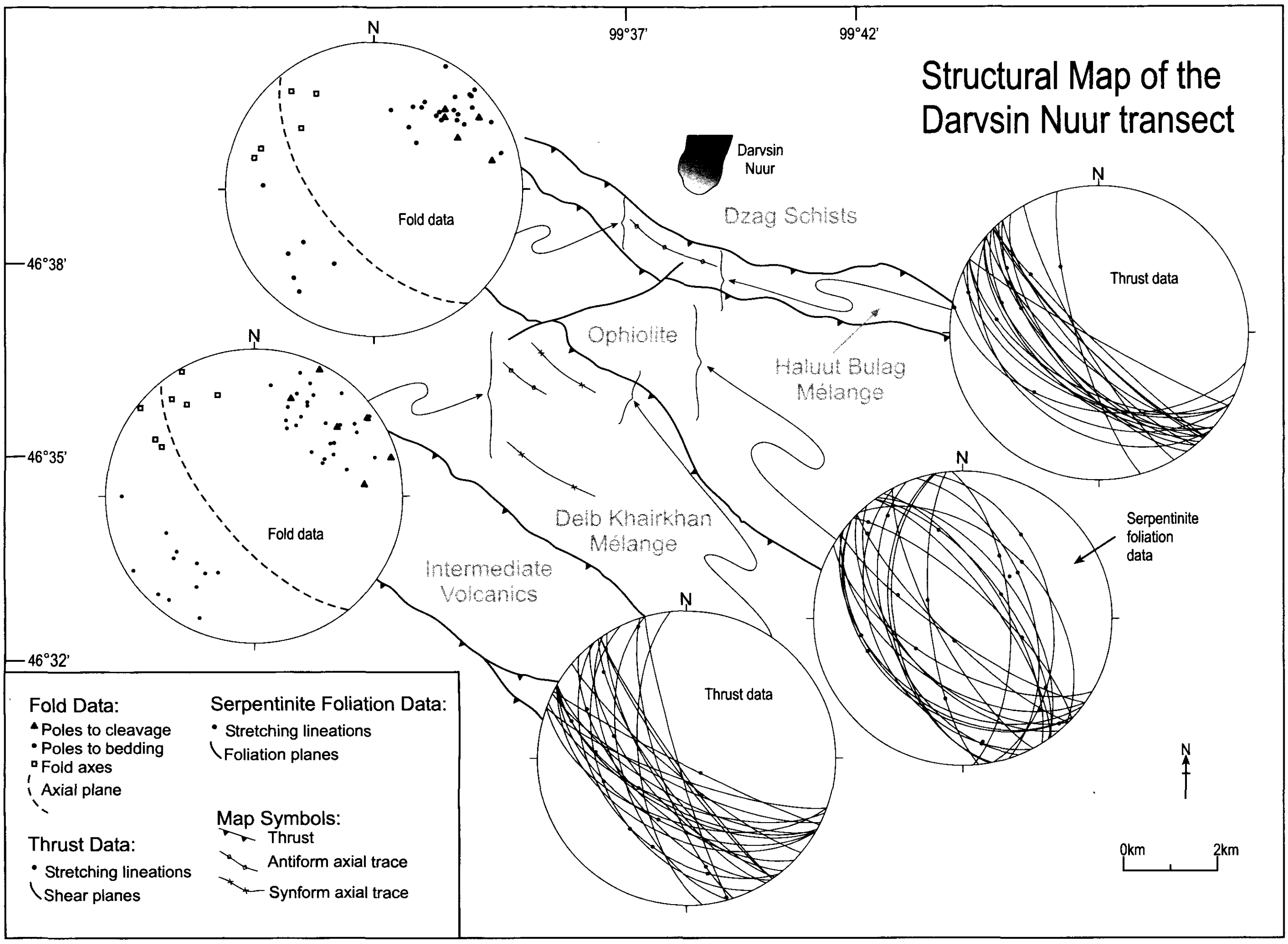

Fig. 8. Structural data from the Darvsin Nuur transect. SW-dipping thrust fabric and axial planes of folds are consistent with NE-vergence. Foliation in the serpentinite mélange is steep and fans about a NW–SE vertical axis. Lower hemisphere, equal area stereoplots. Refer to Figure 4 for lithological relations.

Dzag zone. The contact between the Haluut Bulag mélange and the Dzag zone to the north is exposed in only one locality on the western bank of the Baidrag Gol near its junction with the Dzag Gol (Fig. 3, N46°49.688′, E99°16.989′). There, the rocks of the Haluut Bulag mélange are thrust over the Dzag zone along a thrust fault which dips between 50° and 80° to the SW (Figs 3 & 7). The fault zone is about 20 m thick and contains internally imbricated slices of the Dzag schists. The cleavage is deformed into asymmetric NE-vergent folds (Fig. 7). Minor fold axes have consistent shallow plunges to the NW, and a weak SW-dipping second cleavage is axial planar to the hinge zones. Abundant thin calcite and quartz veins cut the schists, and have been boudinaged and rotated parallel to the first cleavage. Lineations are not well developed in the contact thrust zone with the Haluut Bulag mélange, but those that are detectable suggest slightly oblique slip in a WSW–ENE direction. Shear sense indicators such as boudinaged veins (Fig. 6e) suggest top-to-the-NE shearing which is consistent with the NE vergence of folds of the first cleavage. Immediately to the north of this locality, outcrop exposure ends and grass covered plains obscure the geology around the town of Dzag (Fig. 2b).

Darvsin Nuur transect

Burd Gol mélange. The Darvsin Nuur transect is located approximately 40 km SE along strike from the Baidrag Gol transect (Fig. 2). In the Darvsin Nuur transect, the Burd Gol mélange is poorly exposed due to grass cover. However, the rocks that are exposed are dominated by pelitic schists with a penetrative schistose foliation that dips SW at approximately 40–60°. The northern margin of the mélange is marked by a thrust contact with both the Carboniferous sedimentary rocks and extrusive volcanic sequence (Fig. 4).

Carboniferous sedimentary rocks and volcanic sequence. The Carboniferous sedimentary rocks crop out in the SW of the transect area and increase in thickness towards the SW (Fig. 8). Bedding dips about 30°SW. The contact between the Carboniferous rocks and the volcanic sequence is unexposed.

The volcanic sequence is poorly exposed over a 5 km width but extends along strike to the NW and SE. Flows of basalt and dacite strike NW–SE and have a variable dip between 40° and 60°S or SW (Fig. 4). Locally developed sub-vertical ENE–WSW striking shear zones record dextral shear sense based on asymmetry of boudinaged calcite veins. These shear zones have a maximum width of 10 cm and are confined to the volcanic units. Near the contact of the volcanic series with the Delb Khairkhan mélange, to the north, a pervasive shear fabric is developed in the volcanic units with shear zones dipping approximately 50° to the SW. Quartz stretching lineations in the shear zones are down-dip and rotated clasts in the agglomerates suggest top-to-the-NE shearing or thrusting of the volcanic series over the Delb Khairkhan mélange (Fig. 4).

Delb Khairkhan mélange. The principal fabric in the Delb Khairkhan mélange becomes gradually steeper from 50° at the thrust contact to approximately 80° near the limestone at the summit of the Khain–Delb Khairkhan-Ula ridge (Fig. 4). The limestone is highly fractured and contains abundant calcite and quartz veins. Thin interbeds of shale dipping approximately 60°SW within the limestone have accommodated local shearing. On the north side of the ridge, there is a 300 m wide zone of shale that is deformed into NE vergent open folds with minor fold axes plunging consistently 10–30°NW (Figs 4 & 8). The area to the south of the contact with the ophiolitic rocks is a broad valley with only a few small isolated hills providing exposure of the mélange.

On the north side of the mélange there is a small block of brecciated dolomite surrounded by foliated serpentinite forming a broadly sigmoidal outcrop pattern (Fig. 4). As well as the serpentinite outcrops, there are also some pillow basalt blocks in variable states of preservation near the contact of the Delb Khairkhan mélange with the ophiolitic rocks (Fig. 4) which contain a heavily sheared phacoidal texture, with individual phacoids forming rod-like structures. The long axes of the rods have variable orientations in individual blocks suggesting rotation between blocks. The matrix schists around these blocks have a more consistent foliation that dips approximately 70–85° to the SW and in some places locally to the NE (Fig. 8). Amphibole and calcite stretching lineations on the foliation planes plunge shallowly WNW and asymmetric minor folds suggest thrust movement with a sinistral component. The contact of the Delb Khairkhan mélange with the ophiolitic sequence is not exposed, but is assumed to be tectonic due to well-developed shear fabric close to the contact zone in both the pillow lava blocks and the matrix schists.

Ophiolitic Rocks. The large gabbro block on the west side of the area in Fig. 4 (N46°37.000′ E99°35.000′), has well-developed reticulate vein networks associated with local normal-sense shear zones. Other small shear zones with ductile characteristics (Fig. 6a) are not associated with veining but are also normal sense. The normal-sense shears are confined to the gabbro block and may represent relict ocean floor faulting.

In the easternmost section, there is a very large block of pillow basalt and sheeted dyke rocks that extends into the Uldzit Gol section and has a more thrust-imbricate style of deformation (Fig. 4). The contact between the pillow basalt block and the sheeted dykes is sheared and is almost vertical but reliable indicators of shear sense were not found. The strike and dip of the dykes in this transect, and in the Baidrag Gol transect are similar, i.e. they strike NW–SE and dip 60–80°SW (Figs 3 & 4). Flows in the pillow basalts dip steeply to the SW at around 60° to 80°.

Within the serpentinite matrix, small sheeted-dyke lenses approximately 5 m in length have their long axes orientated NW–SE parallel to the strike of the serpentinite foliation, which clearly diverges around and envelops the blocks. The dominant foliation dip is to the SW consistent with that observed throughout the transect (Figs 4 & 8). Serpentine and talc stretching lineations are either down-dip, or plunge shallowly to the NE or SW. Deviations from southwesterly dips occur in zones where there are large expanses of serpentinite without coherent blocks. The foliation in such areas generally has a near vertical to NE dip, possibly related to foliation fanning around vertical (Fig. 8) Generally, it is difficult to measure foliation planes because the serpentinite contains small phacoidal bodies rather than parallel cleavage planes.

At the contact zone between the serpentinite mélange and the Haluut Bulag mélange (Fig. 4), there are highly sheared pillow basalts on the south side and highly sheared limestones and pelitic rocks on the north side. On both sides of the contact a strong penetrative foliation that dips 30–50° to the SW (Fig. 8). Chlorite and quartz stretching lineations plunge in a SW or WSW direction. C–S fabrics and asymmetric quartz boudins parallel to these lineations suggest top-to-the-NE or top-to-the-east directed shear consistent with the general directions observed in the Baidrag Gol Transect.

Haluut Bulag mélange. The Haluut Bulag mélange is significantly thinner in the area of Darvsin Nuur than in the Baidrag Gol transect, reaching less than 2 km maximum outcrop thickness.

Cleavage planes in the mudstone, dip shallowly SW near the contact with the serpentinite mélange, but steeply NE towards the Dzag zone in the north. It appears therefore that the foliation is folded into a large NE-vergent open fold (Figs 4 & 8). Foliation is more strongly developed in the mudstones near the contact with the Dzag zone, suggesting a tectonic contact (Figs 4 & 8) but the actual contact is unexposed.

Dzag zone. There is very poor exposure of the Dzag lithologies in this transect area due to low topography around Darvsin Lake.

Uldzit Gol transect

Burd Gol mélange. The overall structure of the Burd Gol mélange is extremely complex with variable foliation strike and dip. As well as pervasive shearing within the matrix there are local areas of more concentrated shear. In the high strain zones, a near vertical penetrative foliation strikes NW–SE, and rocks have suffered intense brittle deformation and internal brecciation producing 5 m wide zones of clay gouge material. In one high strain zone, shearing has produced ductile mylonitic fabrics in limestone surrounding fragments of basalt (Fig. 6f). Away from the high strain zones large lenses of undeformed sedimentary rocks (Fig. 6 g) are enclosed within the pelitic schist matrix. Near to the contact with the Carboniferous rocks to the north, the foliation in the mélange matrix becomes more uniform dipping to the SW. The contact is a thrust fault (Fig. 5) marked by a clear topographic break striking NE–SW. The pelitic schists and amphibolites in the Burd Gol mélange above the fault have a well developed cleavage dipping 4°–20°SW (Figs 5 & 9). Biotite and amphibole lineations on the cleavage plane plunge consistently SW or WSW (Figs 5 & 9). C–S fabrics and rotated staurolite porphyroblasts within the matrix schists suggest top-to-the-NE movement.

Carboniferous sedimentary rocks and volcanic sequence. Directly beneath the thrust contact with the Burd Gol mélange in the footwall, Carboniferous limestones are mylonitized and the mylonitic fabric is folded into tight isoclinal folds inclined slightly to the NE. Fold axes plunge shallowly NW. The degree of mylonitization diminishes to the north of the contact, where after 30 m the rocks lack shear fabrics and folds are more open in character (Figs 5 & 9).

Near the northern contact with the volcanic sequence, the Carboniferous sedimentary rocks have a weak cleavage that

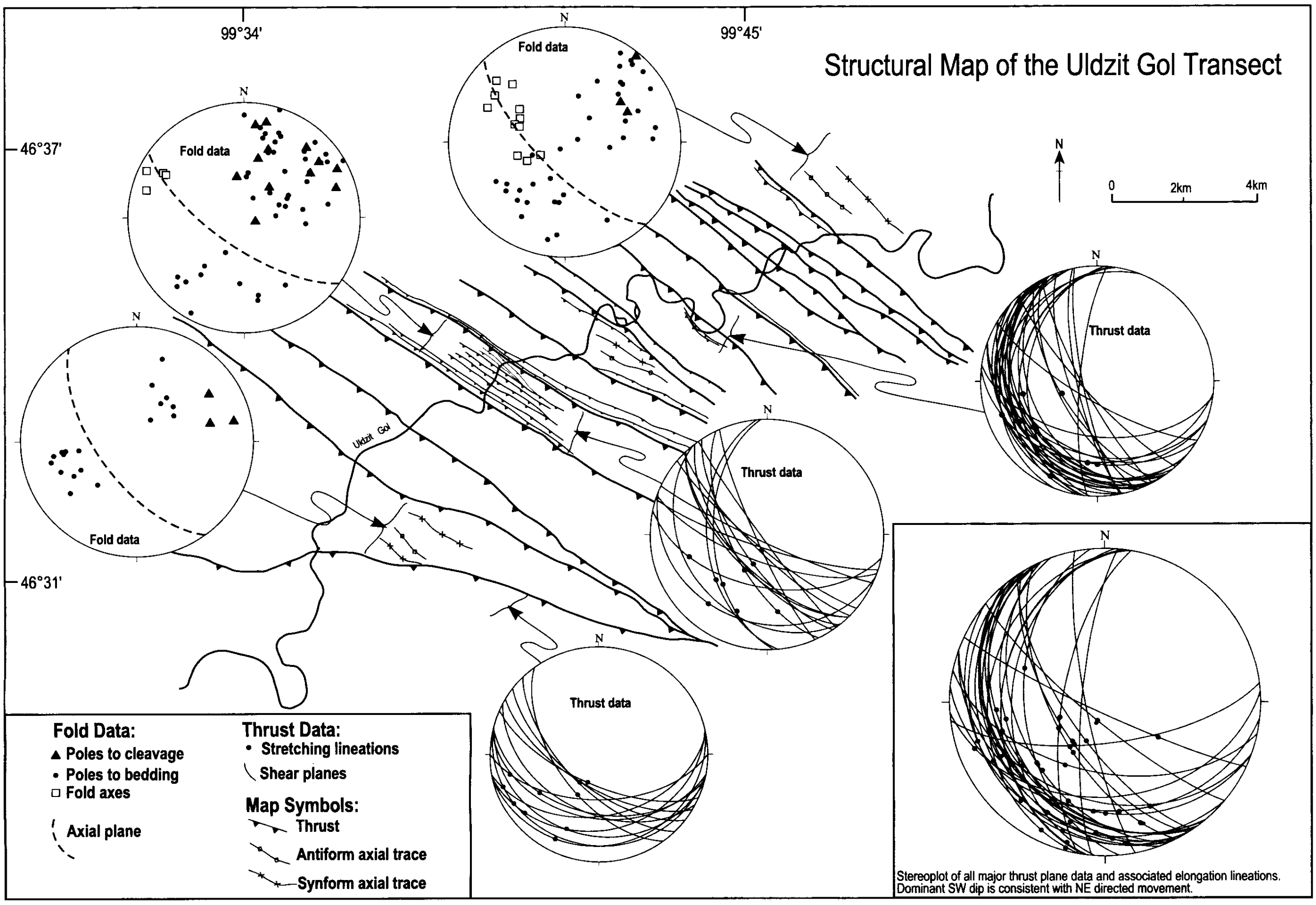

Fig. 9. Structural data from the Uldzit Gol transect. SW-dipping axial planes of folds and dominant SW-dipping thrust fabric suggest NE-vergent thrusting in the area. Lower hemisphere, equal area stereoplots. Refer to Figure 5 for lithological relations.

dips steeply SW and is accompanied by brecciation of the mudstones. The volcanic rocks immediately on the north side of the contact are also foliated with the same dip and strike. The actual contact is not exposed and there are no reliable shear sense indicators, but it appears likely that the Carboniferous rocks have been thrust over the volcanic units based on the evidence for NE transport of the Burd Gol mélange and the NE-vergent folding within the Carboniferous rocks (Figs 5 & 9).

On the northern side of the volcanic sequence, the rocks are weakly foliated with foliation dipping to the south or SW (Fig. 5). Down-dip quartz stretching lineations and C–S fabrics suggest top-to-the-north or NE, or thrusting of the volcanic and Carboniferous rocks over the Delb Khairkhan mélange to the north (see cross-section Fig. 5).

Delb Khairkhan mélange. In this transect, the mélange is divided into two compositional and structural zones. The southern zone is lens-dominated and highly imbricated by thrusting with very little pelitic matrix (Fig. 5, cross-section), whereas the northern section near the ophiolite is dominated by a pelitic matrix. Figure 10 shows a view across the imbricate zone looking NW. The northern and southern zones are separated by a zone of concentrated shearing (Fig. 5, N46°34.000′, E99°39.000′), in which the matrix rocks have suffered intense brittle deformation and internal brecciation. This shear zone marks a metamorphic divide because the matrix rocks on the north side are more recrystallized with a greater abundance of muscovite and sericite defining the principal foliation. The dominant dip of the foliation is to the SW and there are some minor folds with axial planes that dip SW and quartz stretching lineations also plunge SW consistent with overall NE transport (Figs 5 & 9). Near the contact between the Delb Khairkhan mélange and the ophiolite, the foliation is more strongly developed suggesting a non-exposed tectonic contact.

Ophiolitic rocks. Immediately to the north of the Delb Khairkhan mélange is a block of aphyric pillow basalt that has pervasive SW dipping foliation. Small, locally developed shears dip north and contain C–S fabrics and offset veins that suggest normal shear sense. Surrounding these shears are zones of carbonate alteration and copper mineralization. Since the normal-sense shears are confined to the pillow basalts we suggest that these structures may be relicts of ocean floor faulting.

SW-dipping foliation becomes more pervasive to the north, close to the contact with a block of sheeted dykes, suggesting a sheared contact. Sub-horizontal chlorite stretching lineations plunge WSW or ESE, and rotated plagioclase phenocrysts parallel to the WSW lineation suggest top-to-ENE shearing. The sheeted-dyke complex to the north has a total thickness of approximately 2.5 km but is actually composed of two sheeted-dyke blocks juxtaposed along a large thrust fault which has caused the dyke rocks to have a strong shear fabric throughout an area 100 m wide (Fig. 5). The dykes strike NW, consistent

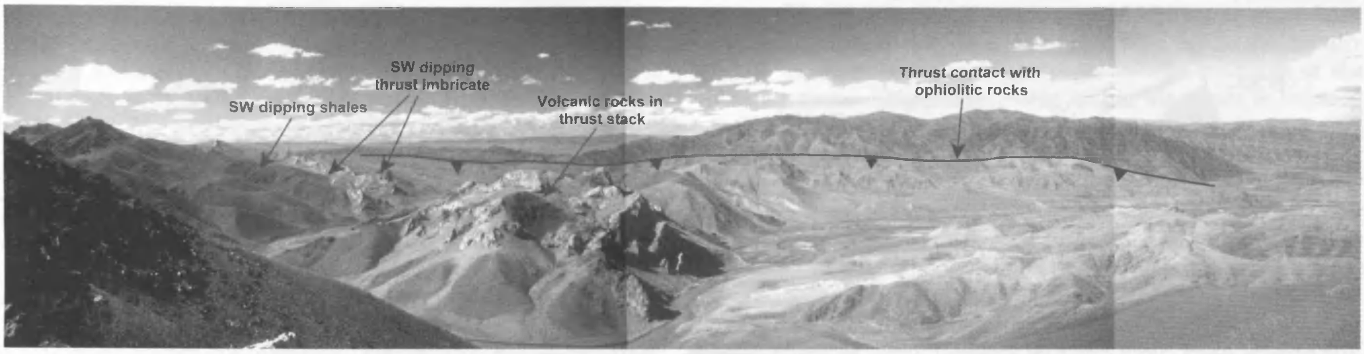

Fig. 10. Composite panoramic photograph looking NW across the Delb Khairkhan mélange to the thrust contact with the ophiolitic rocks in the Uldzit Gol Transect. Note that topography at the thrust contact with the ophiolitic rocks reflects resistance to erosion (see Fig. 3 for viewpoint location).

with those observed in the other two transects, but in contrast they dip NE.

A large gabbro body to the north contains several dykes intruded along NNE dipping shears in the gabbro body. The dykes have been boudinaged into a series of sigmoidal lenses enclosed in mylonitized gabbro. Rotation of phenocrysts in the gabbro and C–S fabrics in the dykes suggests that the shears are normal sense. Locally dykes form complex reticulate networks, which end abruptly in shear zones that offset the dykes suggesting normal shear sense. The normal shears are confined to the gabbro block and do not extend into the surrounding serpentinite mélange.

The northernmost section of sheeted dykes at the contact with the Haluut Bulag mélange has a prominent foliation which dips steeply to the SW.

Haluut Bulag mélange. On the west side of the Uldzit Gol, the Haluut Bulag mélange is very thin and is composed of only a single massive limestone block. On the eastern side of the Uldzit Gol, the mélange widens and is dominated by pelitic schists with small lenses of sandstone and siltstone. Foliation in the schists dips variably to the SW (Fig. 9). Near the contact with the Dzag zone, schistosity becomes steeper (up to 80° to the SW) and more pervasive (Fig. 9).

Dzag zone. The foliation of the schists in the Dzag zone immediately north of the contact, is folded and kinked into open, NE vergent asymmetric folds (Figs 5 & 9). Chlorite stretching lineations on the foliation plane plunge SW (Figs 5 & 9) and asymmetric boudinaged calcite veins viewed parallel to the lineation direction suggest top-to-the-NE shearing, consistent with the general shear directions recorded throughout the transect (see cross-section Fig. 5).

Reconnaissance observations near Bayan Obo and Bayankhongor City

Reconnaissance studies were carried out to assess whether the structural observations made in the three transect areas continue along strike to the SE.

Near Bayan Obo village (Fig. 2b) the same lithotectonic units of the Delb Khairkhan mélange, ophiolite zone and Haluut Bulag mélange were found but without the Carboniferous sedimentary rocks or volcanic sequence. The structures in the three mélange units are consistent with those observed in the transect zones, i.e. a SW-dipping foliation and top-to-the-NE shear sense. However, the sub-linear arrangement of units breaks down near Bayankhongor City, where it becomes difficult to discern individual mélange units. Sporadic outcrops of ophiolite lithologies are surrounded by shale and limestone. Unfortunately, the degree of exposure is very poor making it impossible to carry out detailed structural investigations. Delor *et al.* (2000) produced an Ar/Ar age of 484 ± 5.9 Ma of hornblende from a foliated pillow basalt collected just SW of Bayankhongor City which was interpreted as the age of metamorphism.

The Dzag schists to the north of Bayankhongor City have slightly different structural characteristics with foliation commonly dipping steeply NE. However this is variable along strike and because the average dip value is approximately 80° this variation could simply be the result of steep cleavage fanning.

Discussion

The above data show that all three transects share structural and lithological similarities that can be extrapolated over the entire 300 km strike length of the ophiolite zone. The main subdivisions of the Burd Gol and Delb Khairkhan mélanges, ophiolitic rocks, Haluut Bulag mélange and Dzag zone can be traced continuously along strike (Fig. 11). In contrast, the Carboniferous marine sedimentary rocks and the volcanic series are less continuous and occur only locally in the transect areas (Fig. 11), but not along strike to the east as shown by reconnaissance investigations. Moreover, the Carboniferous sedimentary rocks are discontinuous within the individual transect areas (Fig. 11) and have experienced less intense deformation than the other lithological units as the beds have only been tilted to the SW or gently folded without penetrative cleavage development.

Mitrofanov *et al.* (1985) and Komarov *et al.* (1999) suggested that the Burd Gol mélange represents a passive margin sequence. Although bedded sedimentary rocks in unconformable contact with the Baidrag block could constitute a passive margin environment, we believe that the highly mixed and structurally complex rocks adjacent to the ophiolite zone constitutes a subduction accretion complex. The Burd Gol mélange is also the most highly metamorphosed unit locally containing amphibolite grade staurolite and kyanite schists. The increase in metamorphic grade towards the contact with the ophiolite could be because deeper sections of the accretionary wedge are exposed along the thrust contact, or that the contact itself represents the site of the original subduction zone and locus of highest pressure metamorphic assemblages. The

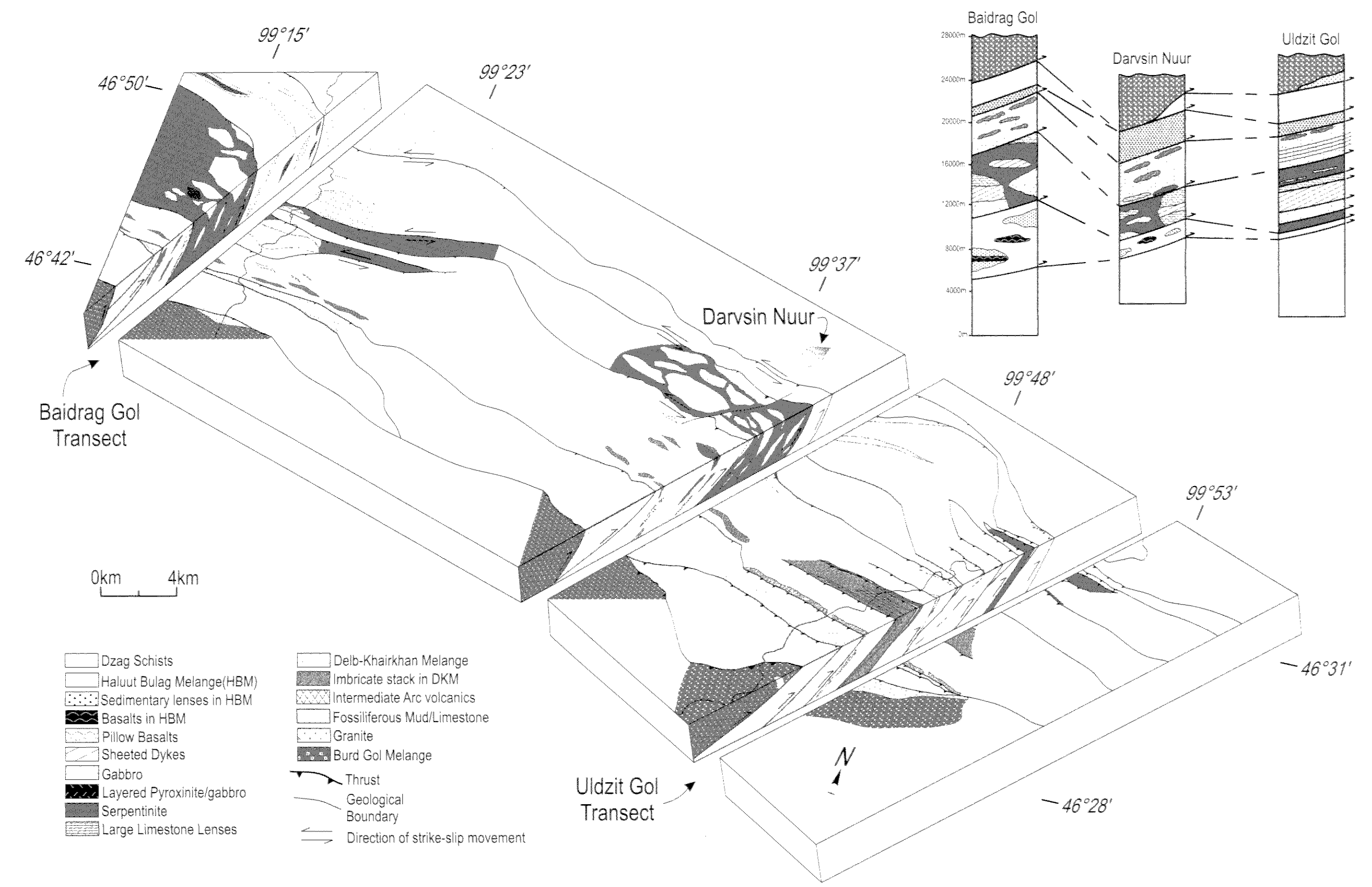

Fig. 11. Block diagram illustrating interpreted along-strike linkage of lithological units and major faults within the Bayankhongor ophiolite belt. Continuity of units and structures in unmapped areas is interpreted from geomorphic relations and aerial photograph analysis. Schematic columns represent correlation of tectonic stratigraphy between transect areas. Dotted tie lines represent interpreted correlations between boundaries along strike. Note discontinuous nature of the Carboniferous mudstones and the changes in thickness of other units.

abundant quartz veins within the mélange are probably products of dewatering of sedimentary rocks and dehydration of subducting oceanic crust similar to those described from modern accretionary environments such as Nankai in Japan (Agar 1990; Maltman *et al.* 1992).

All three mélanges that make up the Bayankhongor ophiolite zone (Delb Khairkhan, ophiolite, and Haluut Bulag mélanges) contain similar lithologies, in which lenses of competent rocks are enclosed within a less competent matrix. Generally, the lenses are largely undeformed, whereas the matrix has absorbed most of the strain and consequently has a well-developed foliation. The foliation consistently dips steeply (50–80° on average) to the SW (Figs 7–9). In addition, stretching lineations developed within the foliation plane trend uniformly to the SW or WSW–ESE (Figs 7–9), and shear sense indicators consistently suggest top-to-the-NE or ESE. It is possible that thrusting was directed first to the NE and then there was a change in stress field conditions to produce the ESE-directed strike-slip movement indicated by the shallow lineations. However, both lineation orientations are defined by chlorite and quartz which deform ductiley at low temperatures (<400°C), thus both directions of movement may have been synchronous and deformation may have been partitioned between NE-directed thrusting and sinistral strike-slip displacements in an overall transpressional regime. However, with the present data it is impossible to conclude definitively whether this is the case or if deformation was partitioned in time. The fact that folding in the Dzag zone is consistently NE-vergent might suggest that the ESE strike-slip zones are a more localized feature within the ophiolite zone. We suggest that combining the overall thrust movement with a strike-slip component is a mechanism by which mélanges can be created that have complexly mixed lithological lenses, but within clearly defined boundaries i.e. only ophiolitic rocks in the serpentinite mélange. Thus internal divisions are mixed, but original facies boundaries are commonly retained (Fig. 11). An exception to this is within the Delb Khairkhan mélange where ophiolitic lenses such as pillow basalts and serpentinite (Figs 3 & 4) are included in the sediment-dominated mélange, presumably due to localized mixing along the contact where a sinistral strike-slip component of deformation has occurred. There are some slight differences in the style of deformation of the mélange units along strike. The most notable example is in the Uldzit Gol Transect where the Delb Khairkhan and serpentinite mélanges contain an imbricate thrust stack instead of a pervasively sheared mélange (Fig. 5). This is probably because where imbrication has occurred, the mélanges contain less mechanically weak matrix and accommodate shortening by discrete thrust motion between more rigid lenses.

Lithological variations within the Delb Khairkhan mélange suggest that the mélange is derived from different tectonic environments. The large limestone lenses that locally contain stromatolites, and sandstone and conglomerates suggest a shallow water environment, whereas the fine muds and siltstones which comprise the protolith for the matrix schists suggest deeper water environments. Together, these rocks may represent sediments from the trench of a subduction zone with the limestones and sandstones being shed from the top of the accretionary wedge and the pelitic rocks of the mélange matrix representing pelagic mudstone scraped from the ocean floor.

The Dzag schists to the north of the ophiolite zone have previously been interpreted as part of an accretionary wedge (Dergunov *et al.* 1997). We believe that thick and lithologically monotonous chlorite mica schists, may have once been clastic turbidites and more likely represent a deep-water passive margin or more specifically continental rise sequence than an accretionary wedge. In addition, the Haluut Bulag mélange which is composed dominantly of limestone lenses in a pelagic matrix also contains vesicular basalts suggesting subaerial eruption. These rocks may have been shed from a continental margin to the north onto the continental rise as debris flows and subsequently incorporated into the mélange during obduction of the ophiolite.

Previously, there has been disagreement over the direction of obduction of the ophiolite and the vergence of structures. Tomurtogoo (1989, 1997) suggested that the ophiolite was thrust to the SW based mostly on inferred dip of stratigraphic units, whereas Kopteva *et al.* (1984), Ryantsev (1994) and Dergunov *et al.* (1997) recognized SW-dipping faults and suggested NE-directed thrusting based on the palaeontological age of the units available. We agree with the latter opinion based on the evidence presented here of consistent SW-dipping structures and shear sense indicators which suggest NE or ENE movement.

The ophiolite contains a complete igneous stratigraphy of serpentinized ultramafics, gabbro, sheeted dykes and pillow lavas, as described by Moores (1982). We interpret the rocks to have formed at a spreading centre based on the stratigraphic relations, presence of sheeted dykes, and relict normal faults that presumably formed during sea-floor spreading. What remains unclear is whether the rocks formed in an open ocean or a marginal back-arc basin associated with a subduction zone. The discovery of limestone in spaces between pillow basalts suggests that the ophiolite formed in an environment above the carbonate compensation depth, but conversely, local occurrences of chert suggest a deeper water environment. As there are no other sedimentary rocks in direct contact with the ophiolite and since dismemberment makes it difficult to determine how thick the ocean crust was, we cannot draw any more substantive conclusions. The only current published geochemical data available on the ophiolitic lithologies are in Kepezhinskas *et al.* (1991) which ambiguously show some MORB characteristics together with indications of a modified source, possibly a plume. The evidence for a shallow water environment shown by the interpillow limestones suggests that this was not a normal Atlantic-type ocean basin. A more detailed environmental model requires a better geochemical database.

The chronology of deformation in the area is complex and the age of obduction of the ophiolite remains controversial. Deformation occurred in the Burd Gol mélange as early as 699 Ma (Teraoka *et al.* 1996) which implies that subduction was occurring from at least this time, well before the obducted ophiolitic rocks were formed at 569 ± 21 Ma (Sm–Nd mineral and whole rock isochron; Kepezhinskas *et al.* 1991). Dates relating to metamorphism of the Dzag schists cluster around 450 Ma (K–Ar method on white micas; Kurimoto *et al.* 1998) and combined with the Ar/Ar age of 484 Ma (Delor *et al.* 2000) from the ophiolite itself suggests that obduction may have occurred around this time. However, this age could equally relate to post obduction metamorphism. The inclusion of the Carboniferous sedimentary rocks within the thrust imbricated succession may suggest that deformation was continuous until post Carboniferous times. However, since the sediments are less penetratively deformed than the other units, we suggest that these represent an overlap assemblage, deposited after major deformation associated with ophiolite obduction and mélange deformation in the Bayankhongor area. Post-Carboniferous reactivation of the Bayankhongor zone may be related to late Palaeozoic tectonic events in southern Mongolia (Hendrix *et al.* 1996; Lamb & Badarch 1997; Höck *et al.* 2000), but the actual extent of these deformational events in the Southern Hangay region is poorly resolved. Work in progress will hopefully lead to more precise dating and will allow a more detailed evolutionary history to be developed.

Because the area is dominated by sedimentary mélanges, it could be suggested that Şengör *et al.*'s (1993) model of a vast accretion complex applies to this area. Moreover, the occurrence of andesitic dykes intruding the Burd Gol mélange and the intermediate volcanic sequence to the north (Fig. 11), could be interpreted to represent incipient arc formation, built on top of the accretionary wedge which is a prominent feature of the Şengör *et al.* (1993) model. However, an implicit part of their model is that the accretion zone has a continuous history, therefore ophiolites represent offscraped fragments within the complex rather than discrete sutures. It seems unlikely that an ophiolite fragment 300 km long would remain intact and unmixed with the rest of the rocks in an accretionary wedge. In addition, other small ophiolite occurrences less than 300 km to the east and west suggest that the ophiolite extends further along-strike (Fig. 2). Moreover, current work in Tuva (southern Siberia) by Pfänder *et al.* (1999) has identified ophiolite occurrences also dated at 569 ± 1.0 Ma (Pb/Pb on single zircon) suggesting that these ophiolites may be genetically related to the Bayankhongor ophiolitic rocks. Also, growing evidence for a continental block beneath Hangai (e.g. Sm–Nd model ages of Kovalenko *et al.* 1996) suggests that the Bayankhongor ophiolite marks a collisional suture between the Baidrag and Hangai continents.

Our preferred interpretation is that the Bayankhongor ophiolite represents a suture marking the position of a now inactive subduction zone between the Baidrag block to the south, and the Dzag zone to the north. Subduction was to the SW based on the dominant polarity of thrusting with the Burd Gol mélange representing an accretionary wedge built up against the Baidrag continental block to the south. The ophiolite was obducted in a northeasterly direction over the Dzag zone which may have been part of a passive margin of a continent located beneath the sedimentary cover of the Hangai region. Future work along strike is needed to establish whether the ophiolite belt can be traced into neighbouring regions and therefore constitutes one of the major suture belts of Central Asia.

We thank the Institute for Geology and Mineral Resources (Mongolia) for their help in organizing fieldwork and providing mapping materials. Critical reviews by M. Lamb and V. Höck led to improvement of the manuscript. Craig Buchan is especially grateful to G. Badarch and O. Tomurtogoo for useful discussions and for providing mapping assistance. C. Buchan is supported by a NERC PhD studentship no. GT04/97/145/ES. B. F. Windley acknowledges NERC grant no. GR9/01881.

References

AGAR, S.M. 1990. The interaction of fluid processes and progressive deformation during shallow level accretion: Examples from the Shimanto Belt of SW Japan. *Journal of Geophysical Research*, **95**, 9133–9147.

BARRY, T.L. & KENT, R.W. 1998. Cenozoic magmatism in Mongolia and the origin of Central and East Asian Basalts. *Geodynamics*, **27**, 347–364.

BARSBOLD, R. & DORJNAMJAA, D. 1993. *Geological Map of the Khangay Highland*. Mongolian Acadamy of Sciences, Ulaanbaatar.

BOISHENKO, A.F. 1979. *[On age of rocks of the metamorphic complex in the Bayan-Khongor Zone]*. PhD thesis. Russian Acadamy of Sciences, Moscow, [in Russian].

COLEMAN, R.G. 1989. Continental growth of northwest China. *Tectonics*, **8**, 621–635.

CUNNINGHAM, W.D. 1998. Lithospheric controls on late Cenozoic construction of the Mongolian Altai. *Tectonics*, **17**, 891–902.

DELOR, C., DEROIN, J.-P., MALUSKI, H. & TOMURTOGOO, O. 2000. Petrostructural constraints and Ar–Ar dating of the Bayankhongor ophiolites. *In:* BADARCH, G. & JAHN, B. (eds) *IGCP 420 Continental Grouth in the Phanerozoic: Evidence from Central Asia, Second Workshop, Abstracts and Excursion Guidebook (Geotraverse through a terrane collage in Southern Hangay) July 25–August 3, 1999, Ulaanbaatar, Mongolia*. Geosciences Rennes. Hors serie, **2**, 21.

DERGUNOV, A.B., RYANTSEV, A.V., LUNEVA, O.I. & RIKHTER, A.V. 1997. Structure and geological history of the Bayan-Khongor Zone, Central Mongolia. *Geotectonics*, **31**, 132–140.

DIDENKO, A.N., MOSSAKOVSKY A.A. *et al.* 1994. Geodynamics of the Central-Asian Paleozoic oceans. *Russian Geology and Geophysics*, **35**, 48–61.

DOBRETSOV, N.L., BERZIN, N.A. & BUSLOV, M.M. 1995. Opening and tectonic evolution of the Palaeo-Asian Ocean. *International Geology Review*, **37**, 335–360.

DORJNAMJAA, D., BADARCH, G., BADAMGARAV, J., BAT-IREEDUI, YA., WINDLEY, B.F., CUNNINGHAM, D. & BUCHAN, C. 1998. *Geotectonic map of Mongolia*. Mongolian Academy of Sciences, Palaeontological Centre, Ulaanbaatar.

HSÜ, K.J., QINGCHEG, W., LIANG, L. & JIE, H. 1991. Geological evolution of the Neimonides: a working hypothesis. *Eclogae Geologicae Helvetiae*, **84**, 1–31.

HENDRIX, M.S., GRAHAM, S.A., AMORY, J.Y. & BADARCH, G. 1996. Noyon Uul Syncline, Southern Mongolia: Lower Mesozoic sedimentary record of the tectonic amalgamation of Central Asia. *Geological Society of America Bulletin*, **108**, 1256–1274.

HÖCK, V., FRANK, W., HEJL, E. & FURTMUELLER, G. 2000. Petrology and cooling history of the Mt. Ushgoeg Range (Central Mongolia). *In:* BADARCH, G. & JAHN, B. (eds) *IGCP 420 Continental Grouth in he Phanerozoic: Evidence from Central Asia, Second Workshop, Abstracts and Excursion Guidebook (Geotraverse through a terrane collage in Southern Hangay) July 25–August 3, 1999, Ulaanbaatar, Mongolia*. Geosciences Rennes. Hors serie, **2**, 35–37.

KEPEZHINSKAS, P.K., KEPEZHINSKAS, K.B. & PUKHTEL, I.S. 1991. Lower Palaeozoic oceanic crust in Mongolian Caledonides: Sm–Nd isotope and trace element data. *Geophysical Research Letters*, **18**, 1301–1304.

KOMAROV, Y.V., BELOGOLVKIN, A.A., GLADKOV, B.G. & CHULUUN, D. 1999. Structure and gold mineralisation of black slates in Bayankhongor palaeorift zone (Mongolia): problems of metallogeny of Mongolia. *In:* GEREL, O. *et al.* (ed.) *Problems of Geology and Metallogeny of Mongolia (Scientific Transactions of the Kherlen Geological International Expedition)*. Mongolian Technical University, Ulaanbaatar, 16–28.

KOPTEVA, V., KUZ'MIN, M.I. & TOMURTOGOO, O. 1984. Structure of the upper part of the Bayan-Khongor ophiolite zone, Mongolia. *Geotectonics*, **18**, 481–491.

KOTOV, A.B., KOZAKOV, I.K. *et al.* 1995. Duration of regional metamorphic episodes in areas of polycyclic endogenic processes—a U-Pb Geochronological Study. *Petrology*, **3**, 567–575.

KOVALENKO, V.I., YARMOLYUK, V.V., KOVACH, V.P., KOTOV, A.B., KOZAKOV, I.K. & SAL'NIKOVA, E.B. 1996. Sources of Phanerozoic granitoids in Central Asia: Sm–Nd isotope data. *Geochemistry International*, **34**, 628–640.

KOZAKOV, I.K. 1986. *Precambrian infrastructures of Paleozoic complexes of Mongolia (Dokembriyskiye infrastukturnyye kompleksy paleozoid Mongolii)*. Izdvestya Akadamiya Nauk Otdelenie fiziko-matematicheskikh, Leningrad.

KOZAKOV, I.K., KOTOV, A.B., KOVACH, V.P. & SALNIKOVA, E.B. 1997. Crustal growth in the geologic evolution of the Baidarik Block, Central Mongolia: evidence from Sm–Nd isotopic systematics. *Petrology*, **5**, 201–207.

KOZAKOV, I.K., KOTOV, A.B., SALNIKOVA, E.B., BIBIKOVA, E.V., KOVACH, V.P., KIRNOZOVA, T.I., BEREZHNAYA, N.G. & LYKHIN, D.A. 1999*a*. Metamorphic age of crystalline complexes of the Tuva-Mongolia Massif: The U–Pb geochronology of granitoids. *Petrology*, **7**, 177–191.

KOZAKOV, I.K., SALNIKOVA, E.B., KOTOV, A.B., KRÖNER, A. & ZAGORNAYA, N.Y. 1999*b*. Latest Neoproterozoic to Early Palaeozoic crustal accretion in Southern Siberia: A Reinterpretation of the Tuvino-Mongolian Massif. *Terra Abstracts, European Union of Geosciences 1999*, **4**, 109.

KURIMOTO, C., TUNGALAG, F., BAYARMANDAL, L. & ICHINNOROV, N. 1998. K–Ar ages of white micas from pelitic schists of the Bayankhongor area, west Mongolia. *Bulletin of the Geological Survey of Japan*, **49**, 19–23.

LAMB, M.A. & BADARCH, G. 1997. Palaeozoic sedimentary basins and volcanic-arc systems of Southern Mongolia: new stratigraphic and sedimentologic constraints. *International Geology Review*, **39**, 542–576.

MALTMAN, A., BYRNE, T., KARIG, D. & LALLEMANT, S. 1992. Structural geological evidence from ODP Leg 131 regarding fluid flow in the Nankai prism, Japan. *Earth and Planetary Science Letters*, **109**, 463–468.

MITROFANOV, F.P., BIBIKOVA, Y.V., GRACHEVA, T., KOZAKOV, I.K., SUMIN, L.V. & SHULESHKO, I.K. 1985. Isotope age of 'grey' tonalites and gneisses of the Archean in Caledonian Structures of central Mongolia. *Doklady Akademii Nauk SSSR*, **284**, 670–675.

MITROFANOV, F.P., KOZAKOV, I.K. & PALAY, I.P. 1981. *Precambrian of west Mongolia and South Tuva*. Transactions of The Joint Soviet–Mongolian Scientific–Research Geological Expedition, **32**. Nauka, Leningrad.

MOORES, E.M. 1982. Origin and emplacement of ophiolites. *Reviews of Geophysics and Space Physics*, **20**, 735–760.

MOSSAKOVSKY, A.A. & DERGUNOV, A.B. 1985. The Caledonides of Kazakhstan, Siberia, and Mongolia: a review of structure, development history, and palaeotectonic environments. *In:* GEE, D.G. & STURT, B.A. (eds) *The Caledonian Orogen; Scandinavia and Related Areas*. John Wiley & Sons Ltd, London, 1201–1215.

MOSSAKOVSKY, A.A., RUZHENTSEV, S.V., SAMYGIN, S.G. & KHERASKOVA, T.N. 1994. Central Asian Fold Belt: geodynamic evolution and formational history. *Geotectonics*, **27**, 445–474.

PFÄNDER, J., JOCHUM, K.P., TODT, W. & KROENER, A. 1999. Relationships between the mantle, lower crust and upper crust within the Agardagh-Tes Chem ophiolite, Central Asia: evidence from petrologic, trace element, and isotopic data. *Ofioliti*, **24**, 151–152.

RYANTSEV, A.V. 1994. [Ophiolites of the Bayankhongor Zone in Palaeozoic structure of Mongolia]. *Doklady Acadamiiy Nauk*, **336**, 651–654, [in Russian].

ŞENGÖR, A.M.C., NATAL'IN, B.A. & BURTMAN, V.S. 1993. Evolution of the Altaid tectonic collage and Palaeozoic crustal growth in Eurasia. *Nature*, **364**, 299–307.

TAKAHASHI, Y. & OYUNGEREL, S. 1997. Chemical character of the granitic rocks in the Bayankhongor area, central Mongolia; reconstructing magmatic activity in the Palaeozoic. *Mongolian Geoscientist*, **4**, 6–15.

TAKAHASHI, Y. & OYUNGEREL, S. 1998. The granitoid series in the Bayankhongor area, Central Mongolia. *Bulletin of the Geological Survey of Japan*, **49**, 25–32.

TERAOKA, Y., SUZUKI, M., TUNGALAG, F., ICHINNOROV, N. & SAKAMAKI, Y. 1996. Tectonic framework of the Bayankhongor area, West Mongolia. *Bulletin of the Geological Survey of Japan*, **47**, 447–455.

TOMURTOGOO, O. 1989. *[Ophiolites and formation of folded belts in Mongolia]*. PhD Thesis. Russian Academy of Sciences, Moscow, [in Russian].

TOMURTOGOO, O. 1997. A new tectonic scheme of the Paleozoides in Mongolia. *In:* ZHIQIN, X., YUFENG, R. & XIAOPING, Q. (eds) *Proceedings of the 30th International Geological Congress*. VSP, 75–82.

TOMURTOGOO, O., NAKAJIMA, T., TAKAHASHI, Y., MINJIN, CH., ICHINNOROV, N. & OYUNGEREL, S. 1998. *Geological map L-47-XVI 1: 200 000*. Mineral Resources Authority of Mongolia Office of Geology Bureau of geological investigation C, Ulaanbaatar.

TUNGALAG, F. 1996. Stratigraphy and structural geology of Precambrian and Palaeozoic strata in Bayankhongor Area. *Mongolian Geoscientist*, **1**, 4–11.

WINDLEY, B.F. & ALLEN, M.B. 1993. Mongolian plateau—evidence for a Late Cenozoic mantle plume under Central Asia. *Geology*, **21**, 295–298.

ZORIN, Y.A. 1999. Geodynamics of the western part of the Mongolia-Okhotsk collisional belt, Trans-Baikal region (Russia) and Mongolia. *Tectonophysics*, **306**, 33–56.

ZORIN, A.Y., BELICHENKO V.G. *et al.* 1993. The South Siberia-Central Mongolia transect. *Tectonophysics*, **225**, 361–378.

Received 19 May 2000; revised typescript accepted 12 November 2000.
Scientific editing by Ray Burgess.